GEOCHEMISTRY AND TECTONIC SETTING OF THE 1700 Ma ALDER AND RED ROCK GROUPS FROM TONTO BASIN, ARIZONA

by
Phillip D. Noll, Jr.

Submitted in partial fullfilment
of the requirements for the degree of
Master of Science in Geology

New Mexico Institute of Mining and Technology
Socorro, New Mexico

November 28, 1988

ACKNOWLEDGEMENTS

As always, in any modest scientific endeavor, many people besides the principle investigator are involved. My sincerest thanks go out to all who helped me better understand the ways and means of the academic/scientific community.

In particular I would like to thank Dr. Kent C. Condie for suggesting the problem, providing financial support in the form of a Research Assistantship and for being my principal advisor. I would also like to thank Dr. Antonius Budding and Dr. Jamie Robertson for being on my advisory committee and for their constructive criticisms of my thesis. Conversations with numerous graduate students (M.K., C.C., D.W., and J.R.R.) improved my understanding of Precambrian geology and igneous and sedimentary geochemistry. I would also like to thank Monica Schumer who helped with the typing.

Chris McKee of the New Mexico Bureau of Mines and Mineral Resources' X-ray Fluorescence (XRF) Laboratory is thanked for his help with analytical procedures and sample preparation. For instrumental neutron activation analysis (INAA) samples were irradiated at the nuclear reactor at Sandia National Labs, Albuquerque, New Mexico. The reactor staff is gratefully acknowledged for their assistance.

This thesis was supported by National Science Foundation Grant EAR-8313735 to K.C. Condie.

ABSTRACT

Early Proterozoic (1700Ma) supracrustal rocks in Tonto Basin include from oldest to youngest, the Alder Group (submarine volcanics and volcaniclastic and cratonic sediments), Red Rock Group (chiefly subaerial felsic ash flows), and Mazatzal Group (shallow marine to terrestrial quartzites and pelites). Basalts and andesites occur as flows and as dikes and sills. Felsic volcanics (dacite-rhyolite) are chiefly ash flow tuffs. Alder sediments include graywacke, quartz wacke, conglomerates, quartz arenite, and pelites.

The Alder-Red Rock succession has been metamorphosed to the lower greenschist facies (chlorite zone) but probably did not attain equilibrium. Primary textures are well preserved and include cross- and graded bedding, ripple marks, pillows, and flow structures. The succession was deformed during the Mazatzal Orogeny-a NW-SE compressional event resulting in the formation of a NE-SW trending foreland fold/thrust belt.

Volcanic rocks tend to have mixed tholeiitic and calc-alkaline affinities. Unlike most other early Proterozoic successions in the southwestern U.S., the Alder-Red Rock volcanics are not bimodal but comprise a continuous (dominantly tholeiitic) suite. Volcanics of all compositions plot in subduction zone related fields on geochemical tectonic discriminant diagrams (Hf-Ta-Th, Zr-Nb-Y, NMORB-normalized plots) and have incompatible element and element ratio distributions similar to corresponding rocks from continental margin arcs. Mafic rocks are slightly light REE enriched and may have small negative Eu anomalies. Felsic rocks have moderate to strong negative Eu anomalies and slightly enriched heavy REE and HFSE similar to rhyolites from continental back-arc basins and from rifts. Mafic igneous rocks can be related by variable degrees of batch melting of a chemically and mineralogically heterogeneous garnet lherzolite source which is similar to primitive mantle. Alder volcanics can be produced by shallow closed system fractional crystallization of basalt and Red Rock felsic volcanics by either fractional crystallization of dacitic liquids or by partial melting of the lower crust.

Alder sediments consist of two populations. One population (quartz arenite, quartz wacke, and some pelites) have detrital mode and geochemical affinities to cratonic sediments whereas the other population (graywackes, conglomerates, and pelites) are arc related. Geochemistry, field relations and paleocurrent analysis suggests that these two populations entered a shallow, narrow basin from opposing sides. Some mixing of sediment from the two source areas may have occurred in the basin.

The geochemistry of the volcanics and sediments along with the rock package and field relations suggest that the Alder-Red Rock Groups were deposited in a back-arc basin associated with a continental margin arc.

TABLE OF CONTENTS

Acknowledgments i

Abstract ii

Table of Contents iv

List of Figures vi

List of Tables x

Introduction 1

Summary 3

Stratigraphy 12

Structure 17

Relationship of "Pre-Alder" and Alder Group Rocks to the Slate Creek Shear Zone 19

Metamorphism 21

Alteration 23

Igneous Rocks 29

Field Relationships 29

Petrography 29

Geochemistry 31

Major Elements 31

Trace Elements 37

Petrogenetic Modeling 40

Batch Melting and Fractional Crystallization Equations 40

Batch Melting 40

Fractional Crystallization 43

Mantle Source 44

Batch Melting Model 50

Fractional Crystallization Models 57

Melting of the Lower Crust 63
Tectonic Discriminant Diagrams 71
Sedimentary Rocks 84
Field Relationships 84
Petrography 85
Geochemistry 86
Provenance 98
Discussion 101
Tectonic Setting 102
Regional Implications 109
Relation of the Mazatzal Terrane to the Yavapai Terrane 109
Relation of the Mazatzal Terrane to the Dos Cabezas and Pinal Terranes 111
Conclusions 113
Appendix A: Sample Locations and Access 114
Appendix B: Chemical Data and CIPW Normative Minerals for Igneous Rocks 127
Appendix C: Chemical Data for Sedimentary Rocks 159
Appendix D: Analytical Procedures 181
Appendix E: Analytical Precision and Accuracy 183
Appendix F: Petrographic Descriptions of Sedimentary Rocks 194
References 198
Acceptance Form 207

LIST OF FIGURES

Figure 1 Map of Arizona Showing Location of Field Area 4

Figure 2 Stratigrphic Column 5

Figure 3 Photo of Graded and Cross Bedding in the Breadpan Formation 7

Figure 4 Photo of Graded Beds in the Flying W Formation 7

Figure 5 Photo of Herring-bone Cross-bedding in the Houdon Formation 8

Figure 6 Photo of Ripple Marks in the Houdon Formation 8

Figure 7 Photo of Graded Beds in the Board Cabin Formation 9

Figure 8 Photo of Pillow Basalts in the Flying W Formation 9

Figure 9 Photo of Hyaloclastic breccia in the Flying W Formation 10

Figure 10 Geologic Map of Field Area 13

Figure 11 Alteration Screen 24

Figure 12 Alteration Screen 25

Figure 13 Alteration Screen 26

Figure 14 Alteration Screen 27

Figure 15 Zr/TiO_2 vs. Nb/Y Classification Diagram for Igneous Rocks 32

Figure 16 Jensen Cation Plot 33

Figure 17 AFM Plot 34

Figure 18 Increase in K_2O/K_2O+Na_2O Content with Stratigraphic Height for Felsic Rocks 36

Figure 19 Chondrite Normalized REE Plot of Tonto Basin Mafic Rocks 38

Figure 20 Chondrite Normalized REE Plot of Tonto Basin Felsic Rocks 39

Figure 21 Y vs. Hf Diagram for the Geochemical Modeling of the Mafic Rocks 45

Figure 22 Yb vs. Nb Diagram for the Geochemical Modeling of the Mafic Rocks 46

Figure 23 NMORB-normalized Diagram for Tonto Basin Mafic Rocks 49

Figure 24 Pressure-temperature Diagram for Peridotite Melting 52

Figure 25 TiO_2 vs. Zr Diagram Showing Modeling Trends 54

Figure 26 Zr/Y vs. Zr Diagram Showing Modeling Trends 55

Figure 27 La/Yb vs. Yb Diagram Showing Modeling Trends 56

Figure 28a REE Plot of Average Tonto Basin Basalt and Calculated Basalt 59

Figure 28b REE Plot of Average Tonto Basin Andesite and Calculated Andesite 59

Figure 29a REE Plot of Average Tonto Basin Dacite and Calculated Dacite 61

Figure 29b REE Plot of Average Tonto Basin Rhyolite and Calculated Rhyolite (FXL Model) 61

Figure 30 REE Plot of Average Tonto Basin Rhyolite and Calculated Rhyolite (Crustal Melting Model) 66

Figure 31 TiO_2 vs. Zr Diagram Showing Melting and FXL Trajectories for Lower Crust Model 68

Figure 32 Zr/Y vs. Zr Diagram Showing Melting and FXL Trajectories for Lower Crust Model 69

Figure 33 La/Yb vs. Yb Diagram Showing Melting and FXL Trajectories for Lower Crust Model 70

Figure 34 Th/Yb vs. Ta/Yb Tectonic Discriminant Diagram 73

Figure 35 Zr-Nb-Y Tectonic Discriminant Diagram 74

Figure 36 NMORB-normalized Diagram of Tonto Basin Mafic Volcanic rocks 75

Figure 37 Th-Hf-Ta Tectonic Discriminant Diagram 77

Figure 38 Th-Hf Tectonic Discriminant Diagram 78

Figure 39 Rb vs. Yb+Ta Tectonic Discriminant Diagram 80

Figure 40 Rb vs. Y+Nb Tectonic Discriminant Diagram 81

Figure 41 Hf-Rb-Ta Tectonic Discriminant Diagram 82

Figure 42 NMORB-normalized Diagram for Tonto Basin Felsic Rocks 83

Figure 43 Al_2O_3/SiO_2 vs. Fe_2O_3T+MgO Tectonic Discriminant Diagram for Sandstones 87

Figure 44 K_2O/Na_2O vs. SiO_2 Tectonic Discriminant Diagram for Sandstones and Pelites 88

Figure 45 Th-La-Sc Tectonic Discriminant Diagram for Sandstones 90

Figure 46 Co-Th-Zr Tectonic Discriminant Diagram for Sandstones 91

Figure 47 Ti/Zr vs. La/Sc Tectonic Discriminant Diagram for Sandstones 92

Figure 48 Companion Diagram to Figure 48 93

Figure 49 Chondrite-normalized REE Distribution of Tonto Basin Pelites 95

Figure 50 Th-La-Sc Tectonic Discriminant Diagram for Pelites 96

Figure 51 Hf-Th-Co Tectonic Discriminant Diagram for Pelites 97

Figure 52 Schematic Diagram of Proposed Arc During Alder Time 106

Figure 53 Schematic Diagram of Proposed Arc During Red Rock Time 107

Figure 54 Schematic Diagram of Proposed Arc During Mazatzal Orogeny 108

Figure 55 Map of ARizona Showing Geographic Relationships of the Yavapai, Mazatzal, Pinal, and Dos Cabezas Terrances 110

LIST OF TABLES

Table I	Compilation of Results of Diagrams Used to Distingiush Calc-alkaline from Tholeiitic Trends	35
Table II	Distribution Coefficients Used	41
Table III	Mode and Melt Proportions for Batch Melting Model	47
Table IV	Chemical Composition of the Calculated Mantle Source	51
Table V	Modes and Amounts of FXL for Closed System FXL Models	58
Table VI	Mode and Melt Proportions for Batch Melting of the Lower Crust; Mode and Amount of FXL Used to Produce Tonto Basin Rhyolites	65
Table VII	Compilation of Results of Tectonic Discrimination Diagrams	79
Table VIII	Source Directions for Sedimentary Samples	99
Table A1	Sample Locations	114
Table B1	Chemical Composition of Igneous Rocks	127
Table B2	CIPW Normative Minerals for Igneous Rocks	151
Table C1	Chemical Composition of Sedimentary Rocks	159
Table E1	Number of Analyses for Standards Using XRF	185
Table E2	Summary of Precision and Accuracy for Standards Analyzed by XRF	186
Table E3	Number of Analyses for Standrads Using INAA	191
Table E4	Summary of Precision and Accuracy for Standards Analyzed by INAA	191

INTRODUCTION

The origin and growth of continents is a subject that has received much attention during the past several years. Many models of crustal growth have been proposed, most of which involve either accretion of allochthonous terranes to a stable Archean craton or tectonic reworking of Archean continental crust.

According to Karlstrom and Bowring (1988) more than 50% of the present crust of North America was assembled in the period 2000-1600Ma. The continental crust in the northern United States and Canada appears to have formed by the reworking of Archean crust with little addition of juvenile crust, whereas in the southwestern United States, large volumes of juvenile crust (in the form of allochthonous terranes) was added to North America during the early and middle Proterozoic (Karlstrom and Bowring, 1988). The Proterozoic of the southwestern United States is similar to Phanerozoic orogenic belts in North America (i.e. the Cordilleran and Appalachian orogenic belts) that also formed by accretion of allochthonous terranes (Condie, 1988). In central Arizona a transition zone occurs between the Colorado Plateau and the Basin and Range Province and within this transition zone, parts of the aforementioned Proterozoic orogenic belt are well exposed. Study of the rocks exposed in central Arizona provides information on the mechanisms by which the North American continent grew during the Proterozoic.

The main focus of this thesis is to determine the tectonic setting of early Proterozic rocks in central Arizona. In the Tonto Basin area the early Proterozoic consists of the Alder, Red Rock, and Mazatzal Groups. These three groups are part of the Mazatzal terrane--an allochthonous terrane that accreted to the stable North American Continent during the so-called "Mazatzal Orogeny" between 1695 and 1630Ma (Karlstrom and Bowring, 1988). Study of the Proterozoic in the Tonto Basin area of central Arizona is facilitated by a relatively large data base including extensive and detailed geologic mapping (Gastil, 1958; Conway, 1985), several studies relating to geologic interpretations of the area, U-Pb zircon ages from felsic volcanics and granitic rocks, (Karlstrom et al., 1987), and relatively easy access to outcrops. The main objectives of this study are as follows:

1) Determine the nature of the Slate Creek Shear Zone by comparing the field relations and geochemistry of the Alder Group rocks on either side;
2) Chemically analyze a representative suite of rocks from the Alder and Red Rock Groups;
3) Geochemically model the metaigneous rocks in order to constrain the nature of the mantle source and\or the parental liquids;
4) Determine field relations and obtain provenance data for the metasedimentary rocks;
5) Geochemically compare Proterozoic rocks from Tonto Basin to younger rocks a variety of tectonic settings to constrain the tectonic setting of the Alder and Red Rock Groups;
6) Propose a model for the origin of the Alder and Red Rock Group rocks based on field relations, geochemical, petrographic, and provenance data; and
7) Discuss regional implications of the Alder and Red Rock Groups.

Studies of this kind are necessary in order to better understand the mechanisms of continental growth responsible for the formation of the North American continent. The data contained within this thesis is presented as a contribution to this goal.

SUMMARY OF THE PRECAMBRIAN GEOLOGY OF TONTO BASIN

Conway and Silver (1986a) have proposed the name Pinal Supergroup to include the ≈1700 Ma Alder, Red Rock, Mazatzal, and Hess Canyon Groups in central Arizona and the Pinal schist and other sequences in central to southeastern Arizona. More recently, Conway et al. (1987) have reassigned the Alder, Red Rock, and Mazatzal Groups to the Tonto Basin Supergroup. These three Groups are well exposed in the Tonto Basin area of central Arizona (Fig. 1). The field area of this study is located below the Mogollon rim approximately 9.5 km east of Young, Arizona. Outcrops of the supracrustal rocks are limited to the more deeply eroded parts of the basin in and along canyons particularly Spring and Tonto Creeks and their tributaries.

The Alder Group (Fig. 2) consists of submarine volcanics and volcaniclastic and cratonic sediments. The Red Rock Group is comprised almost entirely of rhyolite and dacite/rhyodacite ash flow tuffs with assoicated epiclastic sediments (mainly rhyolite conglomerates). The Mazatzal Group consists of shallow marine to terrestrial quartzites and pelites. This study focuses on the Alder and Red Rock Groups. For information on the Mazatzal Group the reader is referred to Conway et al. (1981, 1982), Ludwig (1973), Wilson (1922), and Trevena (1979, 1981).

The early Proterozoic supracrustal rocks are intruded by mafic and felsic hypabyssal rocks, the Young granite to the east and possibly by the Payson granite. Basalts and andesites occur as flows (some pillowed) and as dikes and sills. They occur mainly in the Flying W and Board Cabin Formations of the Alder Group (Fig. 2). Felsic volcanics, largely ash flow tuffs, occur sporadically throughout the Alder succession and dominate in the Red Rock Group. Dacite/rhyodacite ash flows comprise the base of the Red Rock Group. Most of the Alder Group (≈70%) is composed of volcaniclastic sediments including graywackes and pelites which are intimately interbedded with quartz arenites, quartz wackes, and pelites. The apparent thickness of the succession is approximately 7400m (Conway, 1976; Gastil, 1958).

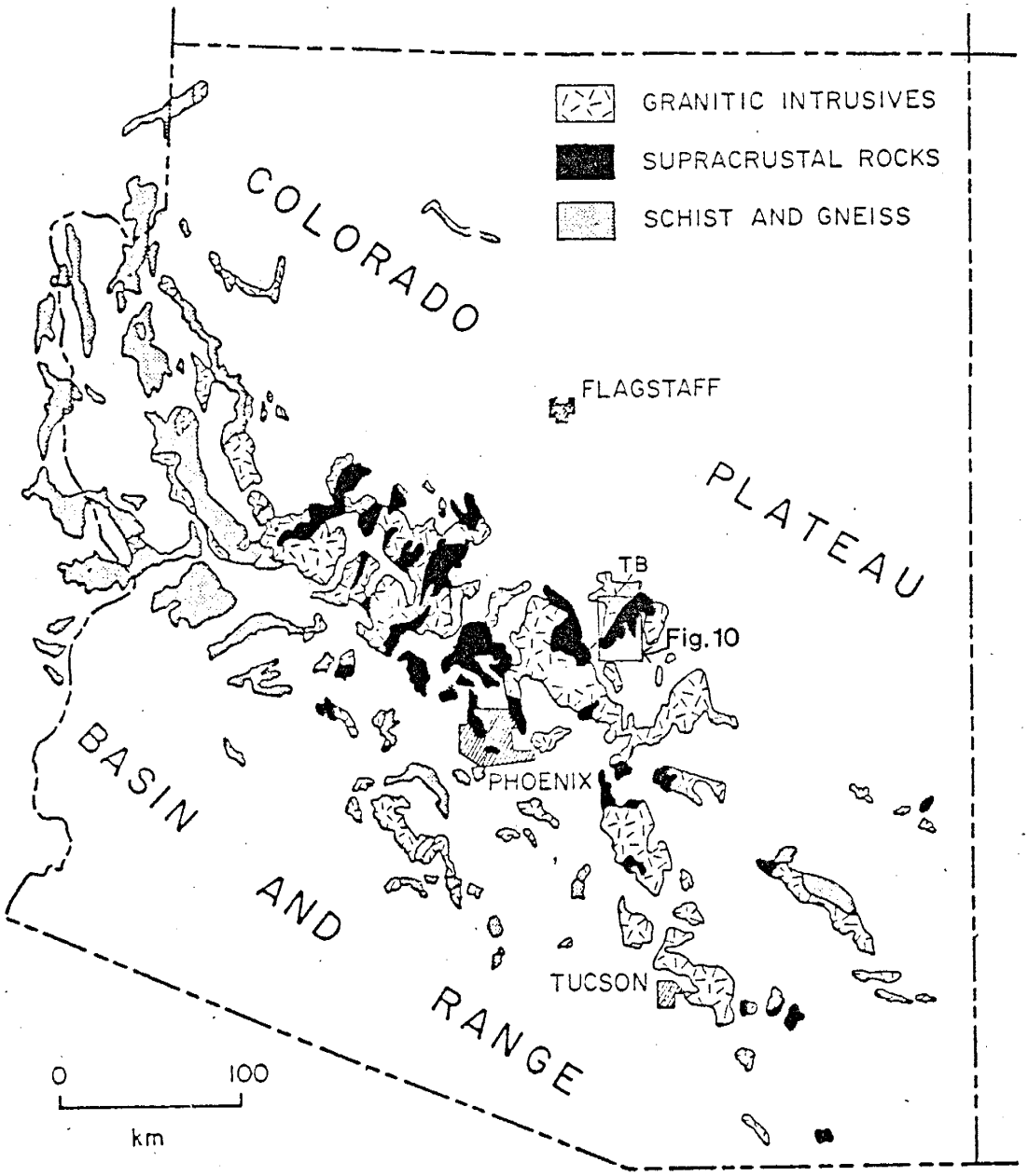

Figure 1. Generalized map of the Precambrian of Arizona showing the location of Tonto Basin (TB, Fig. 10).

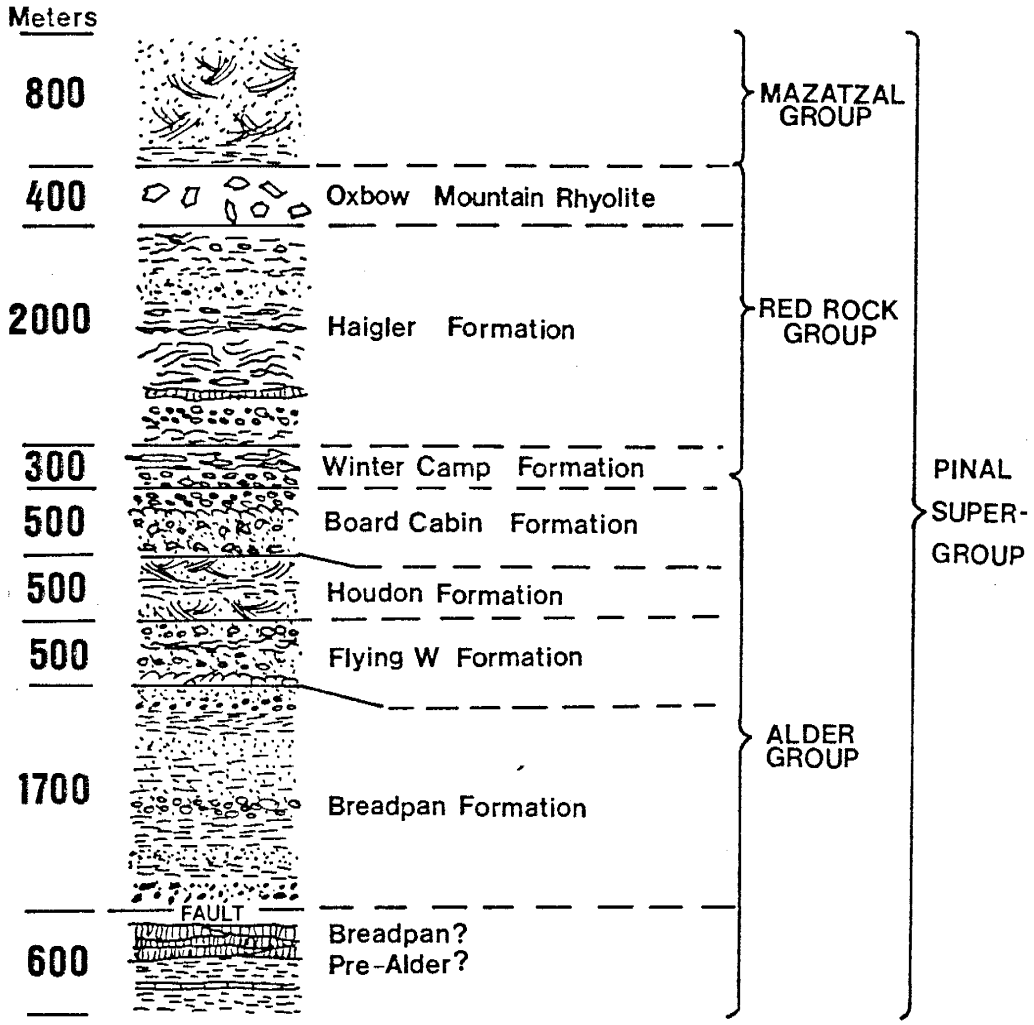

Figure 2. Stratigraphic column of the Alder and Red Rock Groups (modified after Conway, 1976).

No basement rocks have yet been identified in the area. U-Pb zircon ages from felsic volcanics and intrusive granites fall in the range 1700-1710 Ma and suggest that volcanism, deposition and intrusion occurred in a relatively short period of time (Conway and Silver, 1986a, 1986b; Karlstrom et al., 1987).

The supracrustal sequence trends southwest-northeast and is folded into an asymmetrical synclinorium (Conway, 1976). Following the folding event the rocks were subjected to thrust and reverse faulting and finally left lateral to normal faulting (Conway, 1976). Tonto Basin is cut by the Slate Creek shear zone which also trends southwest-northeast through Breadpan Canyon (Plate 1, Fig. 10). This shear zone was first described by K. Karlstrom and co-workers in the Reno Pass area of the Mazatzal Mountains (Roller and Karlstrom, 1986; K. Karlstrom, pers. comm., 1987). In the Flying W ranch area (Plate 1, Fig. 10) the shear zone is approximately 4 km wide the supracrustal rocks are metamorphosed to the lower greenshist facies. Despite deformation and metamorphism primary textures are well preserved. Sedimentary rocks display cross-bedding, graded bedding, herring-bone cross-bedding, and ripple marks (Figs. 3-7). volcanic rocks exhibit flow structures, pillows (Figs. 8-9), and porphyritic textures.

Early work in the area (Gastil, 1954, 1958) is limited mainly to mapping and geologic descriptions. Conway (1973, 1976) and Conway and Silver (1976, 1986a, 1986b), using mainly field relations, proposed that the Alder-Red Rock succession formed in either a continental rift or continental hotspot setting comparable to the Yellowstone rhyolite plateau, the Rio Grande and Keweenawan rifts, late Proterozoic continental rifts in the Appalachians, and possibly to the anorogenic felsic igneous complex of the St. Francois Mountains, Missouri. Other proposed tectonic settings include accreted arc terrances (Condie, 1982, 1986; Karlstrom et al., 1987) and continental margin arc back-arc-basins (Reed et al., 1987).

Sample locations and access to the study area are outlined in Appendix A. Of the 165 samples collected, 49 metasedimentary and 50 metaigneous rocks were chosen for detailed chemical analysis. Analytical procedures are discussed in Appendix D, accuracy and precision of these procedures are discussed in Appendix E, chemical compositions and

Figure 3. Photo of graded and cross-bedding in the Breadpan Formation.

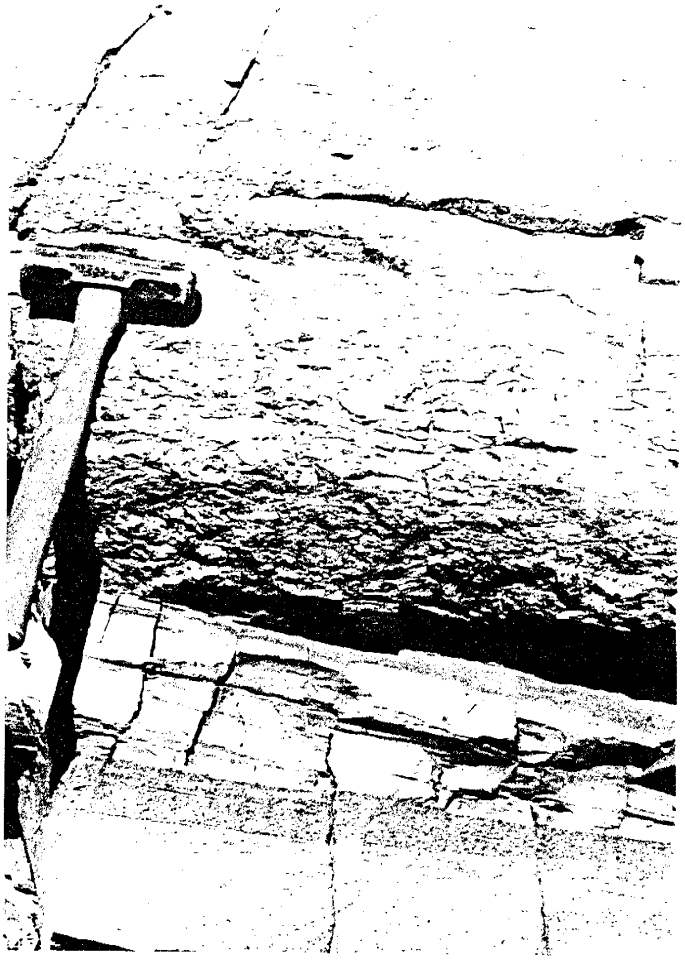

Figure 4. Photo of graded beds in the Flying W Formation.

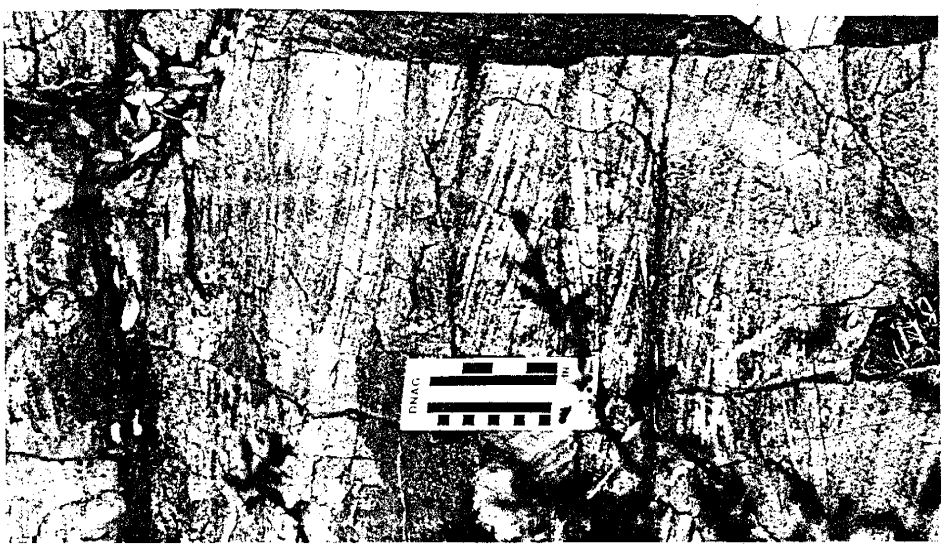

Figure 5. Photo of herring-bone cross-bedding in the Houdon Formation.

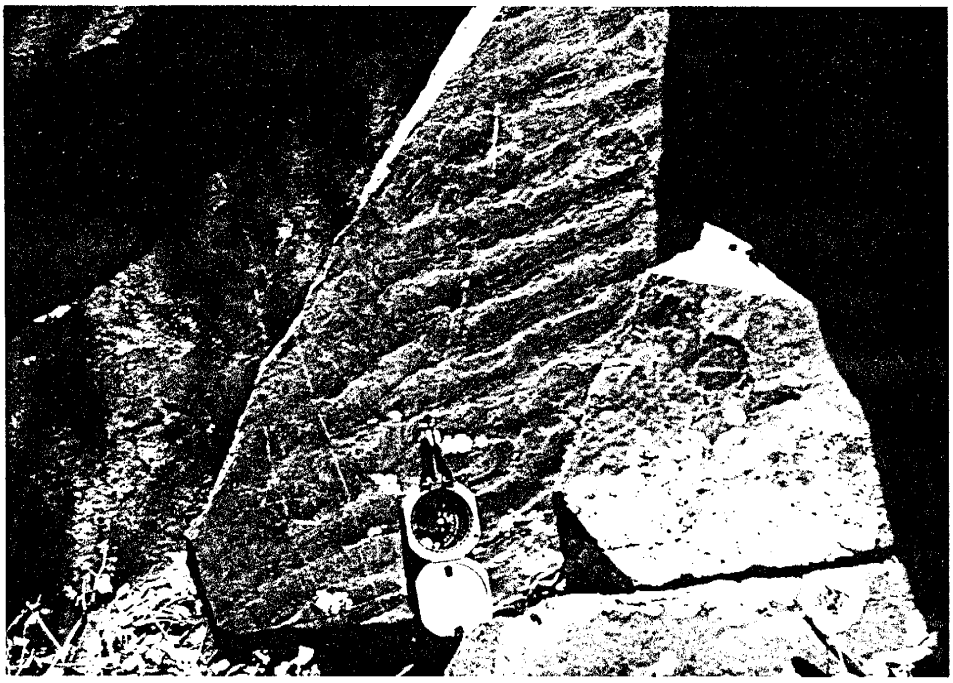

Figure 6. Photo of ripple marks in the Houdon Formation.

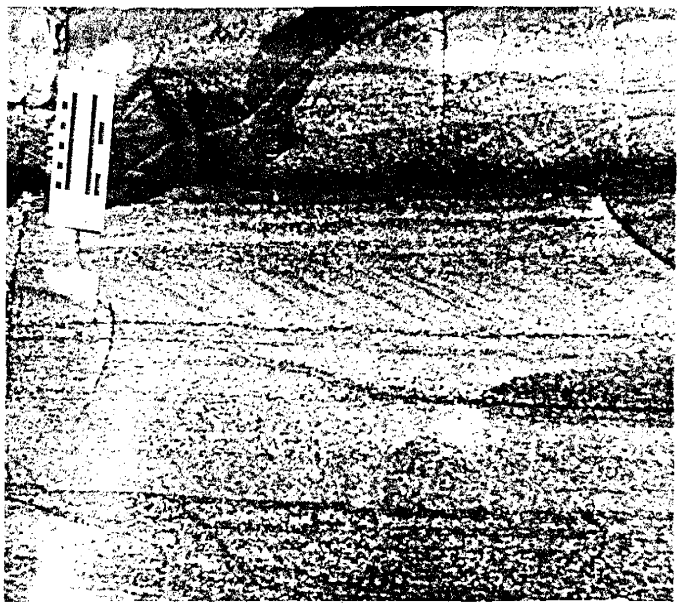

Figure 7. Photo of graded beds in the Board Cabin Formation.

Figure 8. Photo of pillow basalts in the Flying W Formation.

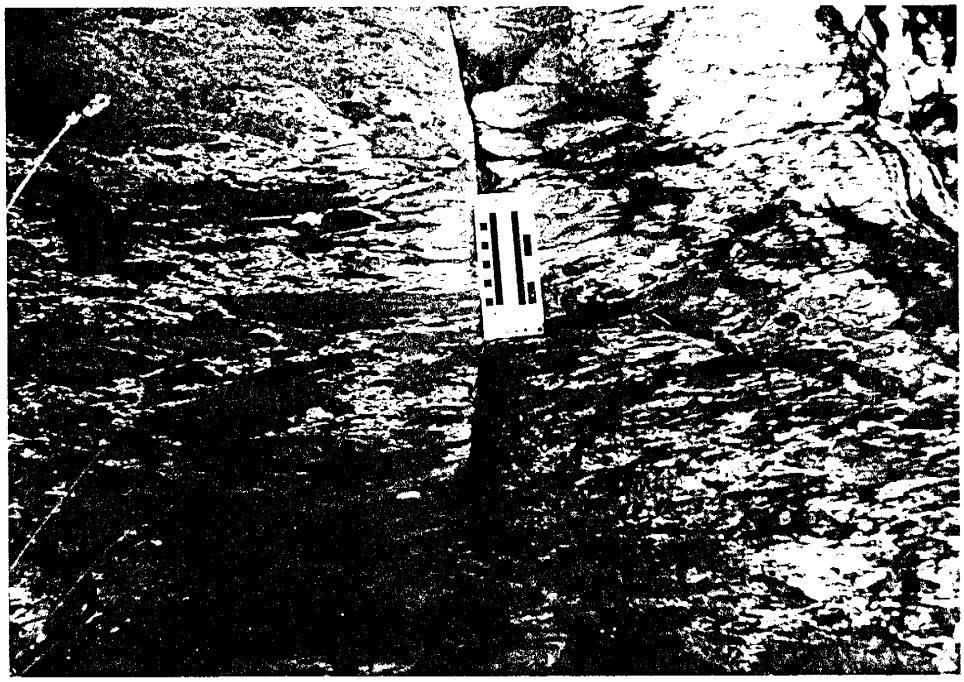

Figure 9. Photo of deformed hyaloclastic breccia in the Flying W Formation.

element ratios of volcanic rocks appear in Appendix B, chemical composition and element ratios of sedimentary rocks appear in Appendix C, and petrographic descriptions of selected samples are in Appendix F.

STRATIGRAPHY

The general stratigraphy of the area is shown in Figure 2. The following descriptions are brief and based in part of the work of Gastil (1958), Conway (1976), and Conway and Silver (1986b).

Pre-Alder Rocks

No crystalline basement rocks have been identified in the Tonto Basin area. Conway and Silver (1986a) propose that the Pinal Supergroup rests unconformably on rocks of the Yavapai Series and that the Yavapai Series and associated batholiths constitute the "basement" within the Tonto Basin area. This, however, has not been proven. Conway and Silver (1986b) suggest that pendants of metamorphosed volcanic and sedimentary rocks within the Gibson Creek Complex near Gisela, Arizona (Fig. 10) are equivalent to rocks of the East Verde River Sequence to the west and that the East Verde River Sequence is equivalent to the Yavapai Series. This presents the possibility that the pendants at Gisela are the oldest rocks in the Tonto Basin area and, with the Gibson Creek Complex, may constitute a "basement" some 40-50 million years older than the stratified and hypabyssal rocks of the area (Conway and Silver, 1986b).

The oldest preserved rocks in Tonto Basin are rocks that have been termed "Pre-Alder" by Gastil (1958). Conway (1976) and Conway and Silver (1986a, 1986b) also suggest that these rocks may be the oldest and termed them "Alder Group Undivided". They consist of slate with minor beds of carbonate, chert, metavolcanics, and pyroclastic rocks. The rocks are highly sheared and metamorphosed to lower greenschist facies. They occur immediately south of what Gastil (1958) and Conway (1976) call the Breadpan Canyon fault in the vicinity of the Flying W ranch (Fig. 10). In this area the Breadpan Canyon fault is the northern boundary of the Slate Creek shear zone which is approximately 4 km wide. In the opinion of this author, the highly sheared rocks are not "Pre-Alder" as suggested by previous workers but rather are lower Breadpan Formation rocks that have been sheared and repeated during high angle reverse faulting.

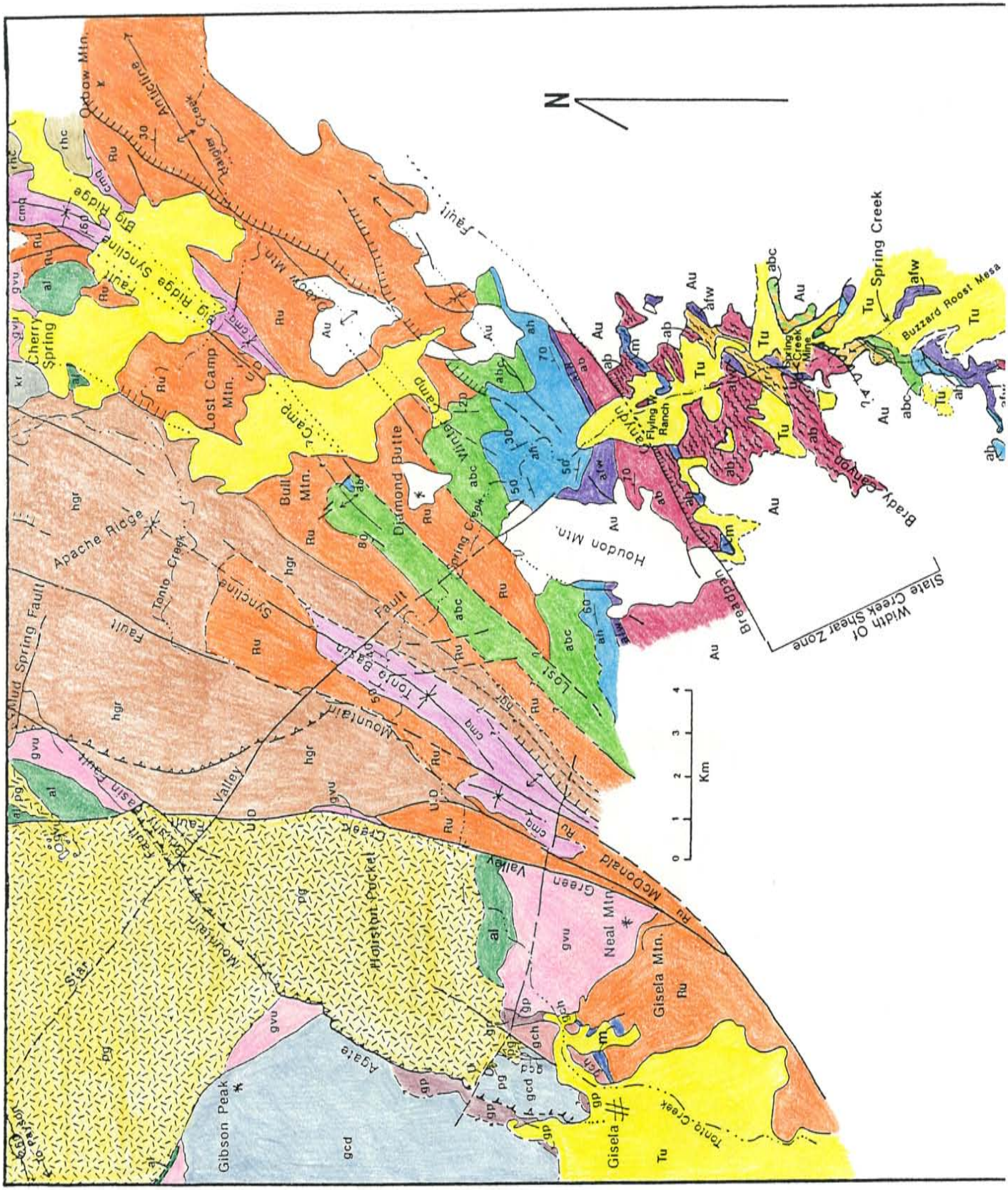

Figure 10. Generalized geologic map of Tonto Basin (after Conway, 1976, and Gastil, 1958). Reinterpretation of rocks in the Slate Creek shear zone as Breadpan Formation from this study. Location shown in Fig. 1. Field area of this study includes the eastern half of Tonto Basin.

The Alder Group

The Breadpan Formation consists of a lower section (≈1200m thick) of interbedded shale, graywacke, pebble conglomerate, and coarse feldspathic and lithic arenite; a middle section (90-300m thick) composed of quartz arenite, and an upper section (180m thick) of shale with interbeds of chert and feldspathic graywacke (Conway and Silver, 1986b). Graded bedding and cross-bedding are locally preserved.

The Flying W Formation (100-400m thick) is composed of mafic to felsic volcanic rocks, pebble to boulder conglomerate with clasts of the same volcanic rocks, quartz arenites, lithic arenites and shales and lies conformably upon the Breadpan Formation (Gastil, 1958). Most mafic rocks are basalt to basaltic andesite and some flows are pillowed. Conway (1976) reports that the felsic flows which Gastil (1958) termed rhyolite and keratophyre are alkali rhyodacite. This is partly true in that the keratophyres are dacite/rhyodacites. However, rocks termed rhyolite by Gastil are not rhyodacites but are, in fact, rhyolites. Sandstones and shales are interbedded and usually occur near the middle of the section between the volcanic rocks and an upper conglomerate and cross-bedding is locally present in the sandstones.

The Houdon Formation consists of a lower basal conglomerate (0-30m), a lower quartzite unit (100-400m) a central shale unit (0-100m) and an upper quartzite unit (100-150m) (Conway, 1976, Gastil, 1958). There is a slight angular unconformity between the Houdon and Flying W Formations (Gastil, 1958). The basal conglomerate contains clasts of vein quartz, banded red chert and volcanic rocks. Both quartzite units display cross-bedding with herring-bone cross-bedding more prevalent in the upper quartzite. The middle shale unit varies from shale, siltstone, and argillaceous quartzite near the base to shale and graywacke near the top (Conway and Silver, 1986b). The shale is finely laminated and free from cross-bedding. The coarse grained portions of the middle unit display asymmetrical ripple marks, graded bedding, and cross-bedding.

The Board Cabin Formation consists of basaltic to andesitic volcanic rocks, dikes, and sills; conglomerate and agglomerate; quartzose, feldspathic, and volcanic sandstones; tuffaceous wackes and minor shales and lies conformably on the Houdon Formation (Gastil,

1958). The formation ranges in thickness from 250-600m (Conway and Silver, 1986b). Gastil (1958) and Conway (1976) report pillows in the basic flows in Board Cabin Draw, though none were seen by this investigator. The most conspicuous rock type in the formation is porphyritic andesite. This rock is dark green with large (up to 2cm in length) yellowish-white plagioclase phenocrysts and numerous amygdules, some filled with secondary carbonate, epidote, quartz, and hematite. Some of the porphyritic units have zoned plagioclase phenocrysts implying that these rocks formed by fractional crystallization. Sandstones locally display graded- and cross-bedding. Conglomerates consist dominantly of clasts of the aforementioned volcanic rocks and the clasts are usually well rounded.

The Red Rock Group

At the base of the Red Rock Group is the Winter Camp Formation (≈300m thick) which consists of dacite/rhyodacite ash flows, tuff breccias, and conglomerate. Gastil (1958) reports that there may be a slight angular unconformity between the Winter Camp Formation and the Board Cabin Formation. The dacite/rhyodacite occurs as strongly laminated flows, pumice breccias, and pyroclastic to epiclastic beds (Conway and Silver, 1986b). The flows are porphyritic with phenocrysts of albite. The pumice breccias are non-porphyritic and clasts are rounded and poorly defined (Gastil, 1958). The conglomerates are composed predominantly of rock types that immediately underlie them and also occasionally contain clasts probably derived from the Board Cabin Formation. These clasts are sub-rounded and well sorted (Gastil, 1958).

The Haigler Formation (≈2000m thick) is comprised of chiefly rhyolitic ash flow tuffs. Also present are conglomerates (composed mainly of rhyolite clasts), rare shale and feldspathic quartz wackes, and basic lava flows. The shales are finely laminated and the wackes display graded bedding in intervals of 1mm or less (Gastil, 1958). The basic lavas are amygdaloidal, aphanitic andesites. The shales, wackes, and basic lavas occur as lenses within the upper part of the formation (Conway and Silver, 1986b). The rhyolite flows contain phenocrysts of quartz and alkali feldspar (1-4mm) and often exhibit laminar flow foliation (Conway, 1976).

The Oxbow Mountain Rhyolite overlies the Haigler Formation and is the uppermost unit in the Red Rock Group. This rhyolite is approximately 100-700m thick. The rhyolite is, for the most part, massive, structureless and porphyritic with quartz (1-6mm) and alkali feldspar (1-3mm) phenocrysts accounting for about 20 percent of the rock (Conway and Silver, 1986b). Flow structures and fiamme are present in the Oxbow Mountain Rhyolite exposed along Haigler Creek near the Alderwood campground. Conway and Silver (1986b) state that the pumice fragments become less distinct upward. This, along with the limited lateral extent, and rapid change in thickness led Conway and Silver (1986b) to suggest that the Oxbow Mountain Rhyolite may have originated as a dome or if an ash flow, it must have been ponded by a barrier or in a depression.

STRUCTURE

The supracrustal succession in the Tonto Basin area (and in the Mazatzal Mountains to the west) was folded and faulted during the Mazatzal Orogeny. The general structural trend is NE-SW (Fig. 10) and is similar to that found regionally in Precambrian rocks of central Arizona. Conway (1976) has shown that the Tonto Basin area is underlain by an asymmetrical synclinorium with the Tonto Basin syncline as the major synclinal element. The Alder Group rocks are exposed in the southeastern limb of the synclinorium which is composed of two anticlines and two synclines. The following description of the structural elements of the Tonto Basin area is taken largely from Conway (1976). In addition, data from more recent studies (Puls and Karlstrom, 1985, 1986; Karlstrom and O'Hara, 1984; Karlstrom and Puls, 1984; Karlstrom et al., 1987; Conway and Silver, 1986a, 1986b) is also included.

Folds

Folding appears to be the first manifestation of deformation. The style and degree of folding is largely a function of rock type (competency). The lower parts of the succession (the "Pre-Alder" and lower Alder Group) are comprised of dominantly incompetent shales, wackes and mafic volcanic rocks. As a result the rocks of the lower Alder Group tend to be isoclinally folded, highly foliated, and penetratively deformed. In contrast, the rocks of the upper Alder, Red Rock, and Mazatzal Groups (dominantly competent rhyolites, andesites, conglomerates, and quartzites) tend to be openly folded and weakly foliated.

All folds are generally shallow, trend NE-SW, and axial planes are nearly vertical. The Tonto Basin syncline (Fig. 10) plunges southwestward at approximately 10-15°. South of the Lost Camp fault (Fig. 10), folds generally plunge shallowly northeastward. Amplitudes of the major folds are estimated at $\geq$ 1-2 km and the amplitude of the Tonto Basin syncline may be 4-5 km.

Conway also reports numerous, steeply dipping minor folds mostly in the less competent sedimentary and tuffaceous rocks in the lower parts of the succession. They are small (amplitudes less than 100m) with their axes parallel to a set of lineations and stretched

pebbles, which generally plunge steeply to the northeast. Conway terms these minor folds incongruous drag folds and suggests that they formed under a different, later stress field than did the large shallow folds-perhaps following folding and thrusting and concomitantly with late NE-SW strike-slip faults.

Faults

Conway has divided the faulting episodes into three stages. Stage I faults are thrust and high angle reverse faults, Stage II are left-lateral strike-slip and east-side-down normal faults, and a single right-lateral strike-slip fault represents Stage III.

The Agate Mountain fault (Fig. 10) dips towards the southeast at approximately 15-20°. Offset is estimated at a minimum of 4.8 km but may be as great as 11 km. The Buttes fault (Fig. 10) is the only other thrust fault in the area. It dips about 30° southeastward and offset is less than a few hundred meters. Due to the consistent NE trend of all the folds, thrust faults, and reverse faults, Conway concludes that the direction of thrusting is most likely towards the NW. Working in the Mazatzal Mountains to the southwest, Karlstrom and Puls (1984) have identified several thrust faults in the Mazatzal Group quartzites and rocks of the underlying Red Rock Group are also involved in thrusting (Puls and Karlstrom, 1985). A NW direction of thrusting is substantiated by NW-verging asymmetrical folds, minor thrusts, slickensides, and quartz fibers in movement plains (Karlstrom and Puls, 1984).

High angle reverse faults are also present and are interpreted to be of the same generations as the two thrust faults. Conway bases this interpretation on the common implication for NW-SE compression. These faults apparently dip southeastward and the southeast side is up.

Stage II faults are interpreted to be younger than the thrust and reverse faults and have both left-lateral strike-slip and east-side-down vertical components of offset. According to Conway, the faults are vertical or near vertical and frequently have 1-20 km wide zones of brecciation and silicification. Conway has subdivided the Stage II faults into Subset I faults which are earlier, trend NE-SW, and have left-lateral offset, and Subset II faults which are late, arcuate, NE-SW to N-S trending, and have vertical east-side-down

offset. These faults are post-Mazatzal Orogeny and may have formed in response to a regional left-lateral couple with strain distributed over a broad region in the crust (Conway and Silver, 1986a).

The Brushy Basin Canyon fault (Fig. 10) is the only Stage III fault present. It is nearly vertical and has about 400m of right-lateral offset. This fault may represent the latest episode of Precambrian faulting in the area.

The Slate Creek Shear Zone

The Slate Creek shear zone, first described by Roller and Karlstrom (1986), extends from the Reno Pass area of the Mazatzal Mountains, (northeast of Sunflower, Arizona), northeastward for ≈34 km across most of Tonto Basin and is lost under the cover of younger rocks in the Spring Creek area ≈5 km northeast of the Flying W Ranch (Plate 1). The tectonic significance of the shear zone is unresolved. In the Tonto Basin area the shear zone is ≈4 km wide (Fig. 10). The northern boundary of the shear zone is marked by an abrupt change from highly sheared and foliated slates and volcaniclastic rocks, to relatively unfoliated quartzites and slates. This abrupt change has been mapped as the Breadpan Canyon Fault (Gastil, 1958). The Southern margin of the shear zone, as a result of the author's mapping is marked by a gradual decrease in the amount of shearing south of the Spring Creek Mine (Fig. 10) where the Alder rocks are relatively unfoliated. Although Conway (1976) was unable to assign the Breadpan Canyon fault to one of his three stages, the author believes that it is a high angle reverse fault of stage one with shearing developed in the upper plate. This is also indicated by Karlstrom et al. (1987) in their Figure 5.

Relationship of "Pre-Alder" and Alder Group Rocks to the Slate Creek Shear Zone

The southernmost exposure of Alder Group rocks is in Rock Creek just west of Buzzard Roost Mesa (Fig. 10). These rocks are part of the Breadpan Formation (Gastil, 1958). Between this outcrop and the southern margin of the shear zone the entire Alder section is exposed (Gastil, 1958). The entire Alder section is again exposed starting at the northern boundary of the shear zone and extending towards the N-NW (Gastil, 1958).

Gastil (1958) has mapped "Pre-Alder", Breadpan, and Flying W Formations within the shear zone--all of which are so intensely sheared that assigning these rocks to formations is difficult. The author believes that some (if not all) of the "Pre-Alder" is lower Breadpan. Evidence for this includes: 1) contacts between "Pre-Alder" and Breadpan rocks (Fig. 10) (as mapped by Gastil, 1958) within the shear zone are usually gradational; 2) at the southern edge of the shear zone near the Spring Creek Mine along Spring Creek, the Breadpan Formation ranges from intensely sheared to unsheared (shearing decreases gradually as one passes to the south and out of the shear zone) and the sheared rocks have a striking resemblance to the purple slates of the "Pre-Alder" rocks; and 3) the Brady Canyon area (west of Spring Creek) mapped by Gastil (1958) as "Pre-Alder" basic volcanics consists dominantly of purple slates with interbeds of more competent quartzites. These slates and quartzites are identical to those in the Breadpan Formation in the vicinity of the Spring Creek Mine along Spring Creek ≈3.5 km south of the Flying W ranch (Fig. 10).

It is possible that several high angle reverse faults or minor thrust faults (in addition to the Breadpan Canyon fault) are present within the Slate Creek shear zone accounting for repeated sections of the Breadpan Formation. Two fragments or "slivers" of the Flying W Formation are faulted into the Breadpan Formation within the shear zone (Fig. 10). Although these faults are mapped as normal faults (Conway, 1976) they could possibly be high angle reverse or thrust faults. There also must be a major thrust fault south of the Slate Creek shear zone to account for repetition of the Alder section. A possible candidate for this fault is present ≈1 km south of the Spring Creek Mine on Spring Creek (Fig. 10). Again, this fault has been mapped as a normal fault (Gastil, 1958), but limited outcrop and lack of fault movement indicators such as slickensides make determinations of fault movement difficult.

Puls and Karlstrom (1985) and Karlstrom and Puls (1984) have suggested that the belt of folds and thrust faults present in the Mazatzal and Red Rock Groups is a foreland fold-thrust belt with compressional forces oriented NW-SE. It is difficult to envisage normal faulting occurring in such an environment. However, a NW-SE compressional regime is consistent with the observed structural repetitions.

METAMORPHISM

In addition to folding and faulting, the Alder and Red Rock Groups bare the effects of greenschist facies metamorphism. It is probable that the metamorphism accompanied the deformation but at present it is not possible to make a certain correlation (Conway, 1976). All Proterozoic terranes in the southwestern United States (i.e. the Dos Cabezas Mountains (Bowling, 1987), the Pinal Schist (Copeland, 1986; Copeland and Condie, 1986), the Mazatzal Mountains (Reed, 1988), the San Andres Mountains (Alford, 1987)) have been metamorphosed to some extent but few are as well preserved in terms of textures, and chemical compositions as that of Tonto Basin (Conway, 1976). Thus, the Tonto Basin rocks are referred to in terms of their protoliths throughout this thesis.

Although the term "greenschist" implies that the rocks impart a schistose texture, the Tonto Basin rocks are nearly devoid of schistosity. Were present, schistosity is confined to fine grained pelites and matrix material in coarse grained sandstones. The best developed schistosity occurs in or near shear zones or near intrusive dikes and sills and is secondary.

The rocks display mineral assemblages characteristic of lower greenschist facies metamorphism. The absence of biotite in all rock types and the nearly ubiquitous presence of chlorite indicates that temperatures and pressures probably did not exceed those of the chlorite-zone. Plagioclase is converted to albite (An_{2-10})though Conway (1976) reports the presence of more calcic plagioclase in some rocks. Conway also reports that pyroxene and hornblende are not preserved in volcanic rocks. However, amphiboles and pyroxenes are observed in a mafic intrusive mapped by Gastil (1958) as pyroxenite. This rock is not a pyroxenite as it has the mineralogy of a gabbro (see section on petrography of igneous rocks). The amphibole has characteristics of both actinolite and hornblende and the author feels that it was a primary hornblende that did not completely revert to actinolite.

Some characteristic metamorphic mineral assemblages of the Tonto Basin rocks are:

Sandstones

1. quartz-muscovite (sericite)-chlorite-albite-epidote±calcite
2. quartz-muscovite-chlorite-albite
3. quartz-muscovite-chlorite

Basalts and Andesites

1. "actinolitic" hornblende-albite-chlorite-muscovite-epidote-calcite
2. chlorite-albite-muscovite-epidote-quartz-calcite
3. chlorite-muscovite-epidote-calcite

Felsic Volcanics

1. quartz-microcline-albite-muscovite
2. quartz-microcline-albite-muscovite-chlorite
3. quartz-microcline-albite-muscovite-calcite
4. quartz-albite-muscovite-chlorite-epidote-calcite

The presence of"actinolitic" hornblende and the range in plagioclase compositions combined with the characteristic greenschist facies mineral assemblages suggests that the Tonto Basin rocks were subjected to the conditions of lower greenschist facies metamorphism (chlorite-zone) but did not attain equilibrium.

ALTERATION

Since this study calls upon the use of tectonic discrimination and classification diagrams employing trace and major elements, the effects of alteration and element mobility must be considered.

The use of trace elements in determining tectonic setting (for both igneous and sedimentary rocks) and for distinguishing between different magma types has been well established (Pearce, 1982, 1983; Pearce and Cann, 1973; Pearce and Norry, 1979; Meshede, 1986; Winchester and Floyd, 1977; Wood, 1980; Bhatia, 1983; Bhatia and Crook, 1986; Roser and Korsch, 1986). However, there is a growing opposition to the use of these diagrams based partly on element mobility. Even so, many studies (Davies and Whitehead, 1979; Finlow-Bates and Stumpfl, 1981; Ludden et al., 1982; Campbell et al., 1984; Vance and Condie, 1987) have shown that the high field strength elements (HRSE) (i.e. Ti, Zr, Nb, Y, Hf, etc.) and the rare earth elements (REE) (La-Lu) are relatively immobile under conditions of low grade metamorphism, hydrothermal alteration events, and weathering. It appears that only under very specialized conditions (i.e. extreme hydrothermal alteration, CO_2 and K metasomatism) are these elements mobilized (Hynes, 1980; Campbell et al., 1984; Ludden et al., 1982).

Alteration can generally be considered as any process that modifies the original state of a rock, either mineralogically, texturally, or chemically. There are a number of processes that can impart one or more of these affects including diagenesis, weathering, halmyrolysis (deep sea alteration), hydrothermal alteration, contact metamorphism (including metasomatism), and regional metamorphism (including heating, deformation, and recrystallization). In most cases it is impossible to distinguish and separate which processes have occured. As a result, any interpretations based on the assumption that the present state of the Tonto Basin rocks reflects their primary state must be regarded with extreme caution.

In an attempt to determine which samples analyzed for the present study are significantly altered, a series of alteration screens are employed (Figs. 13-16)(Beswick and

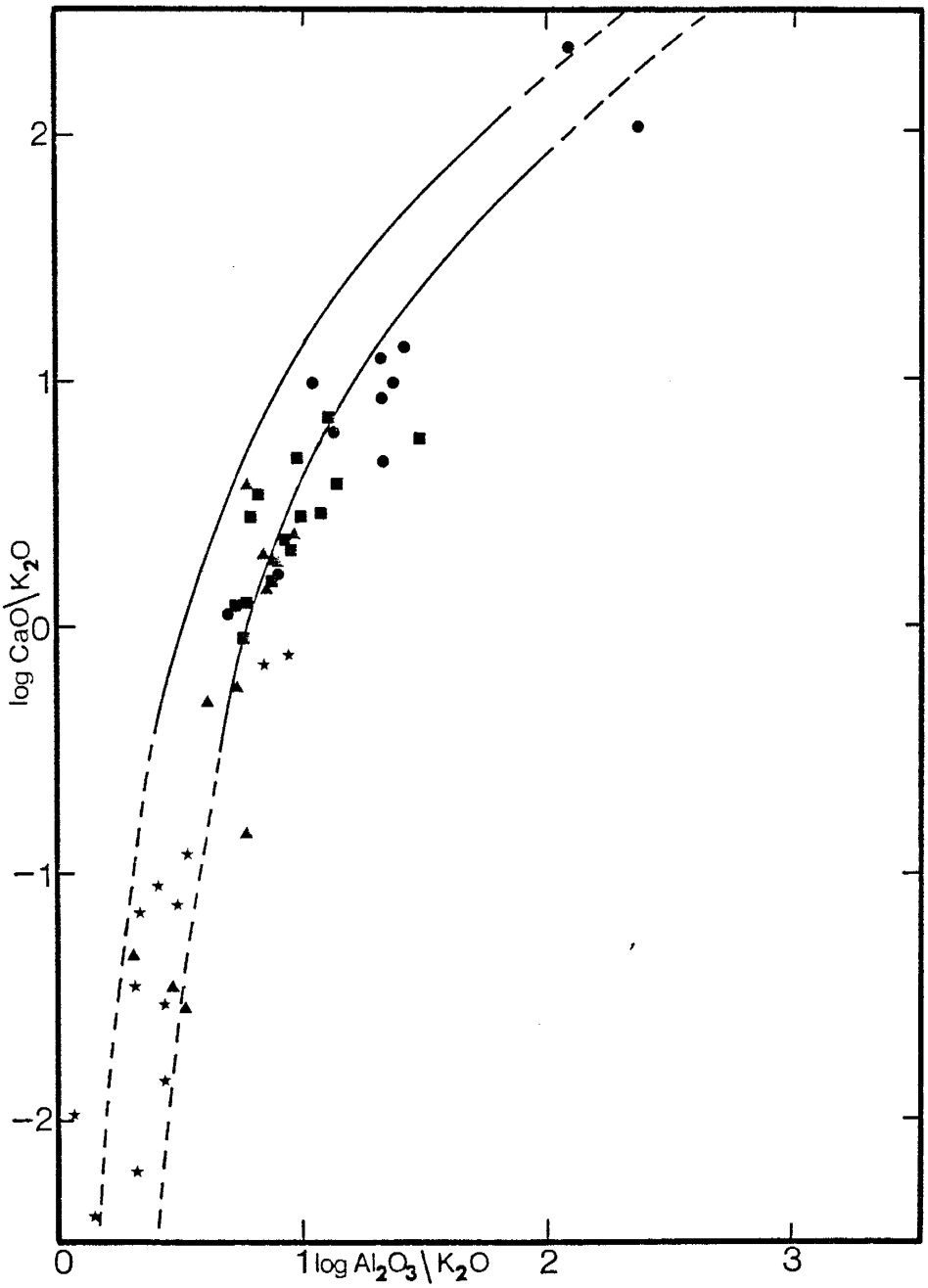

Figure 11. Log CaO/K_2O-log Al_2O_3/K_2O alteration screen after Beswick and Soucie (1978). Unaltered samples plot between the two lines. Basalts and basaltic andesites-circles, andesites-squares, dacite/rhyodacite-triangles, and rhyolites-stars.

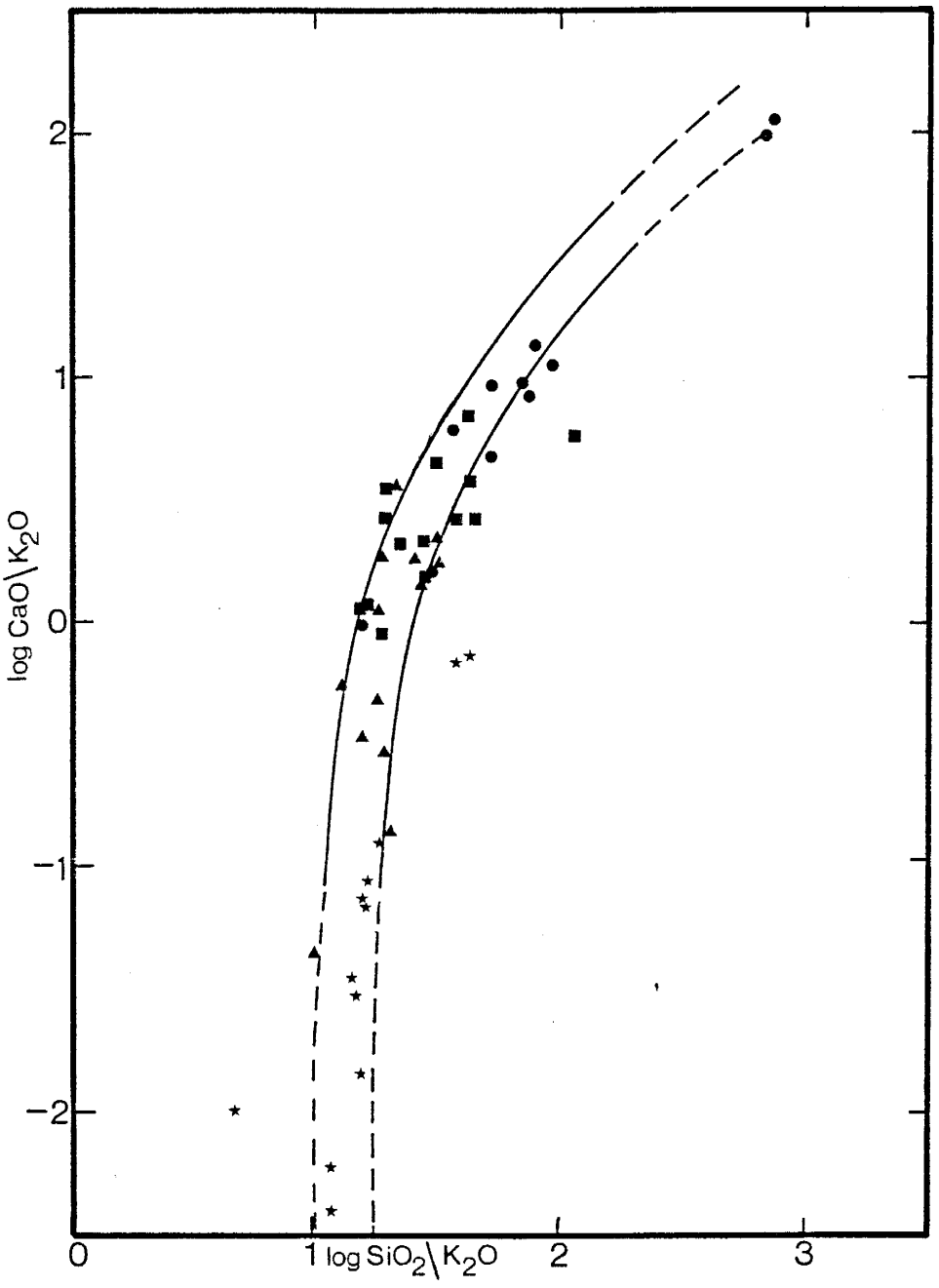

Figure 12. Log CaO/K_2O-log SiO_2/K_2O alteration screen after Beswick and Soucie (1978). Unaltered samples plot between the two lines. Symbols as in Figure 11.

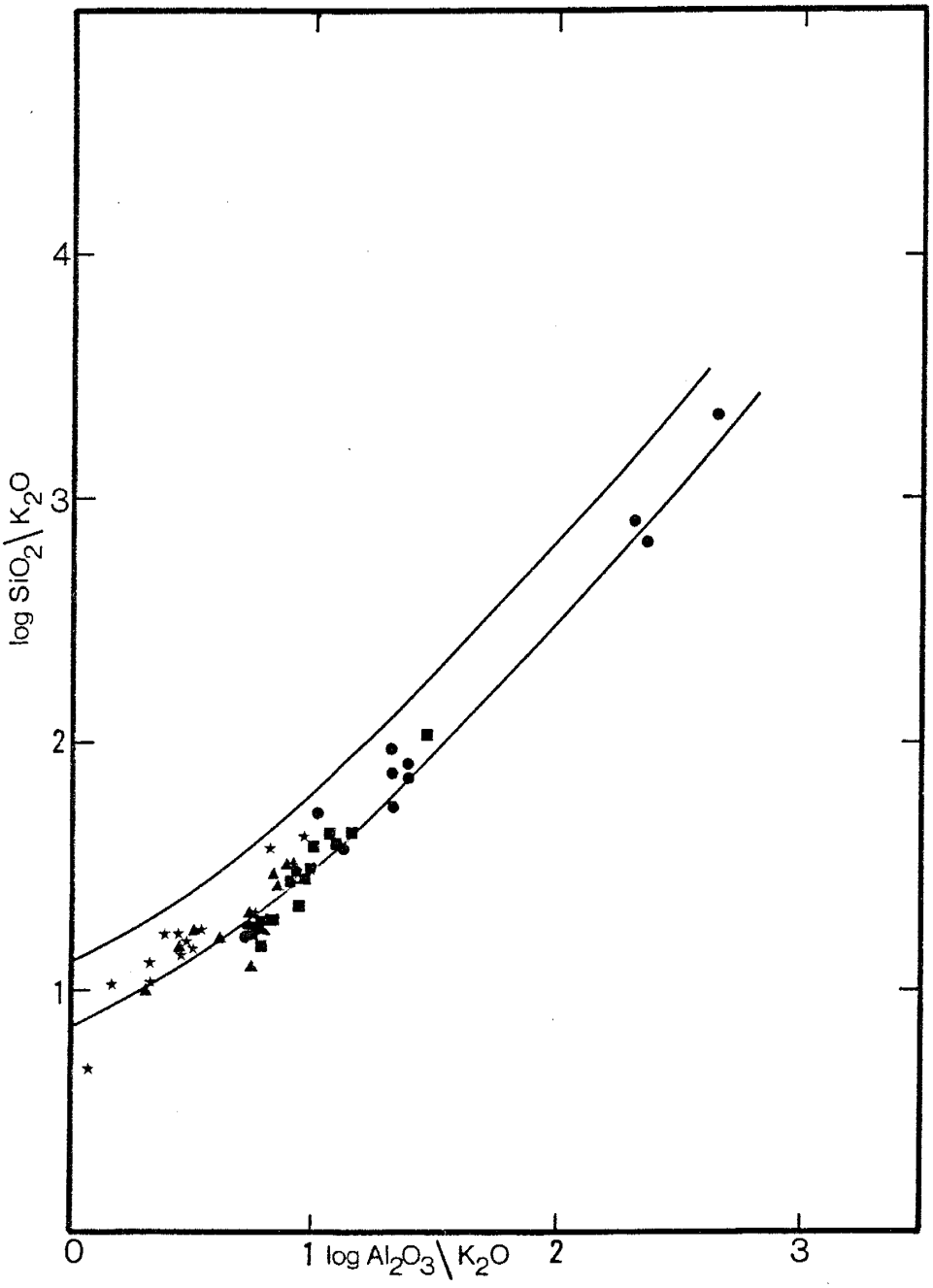

Figure 13. Log SiO_2/K_2O-log Al_2O_3/K_2O alteration screen after Beswick and Soucie (1978). Unaltered samples plot between the two lines. Symbols as in Figure 11.

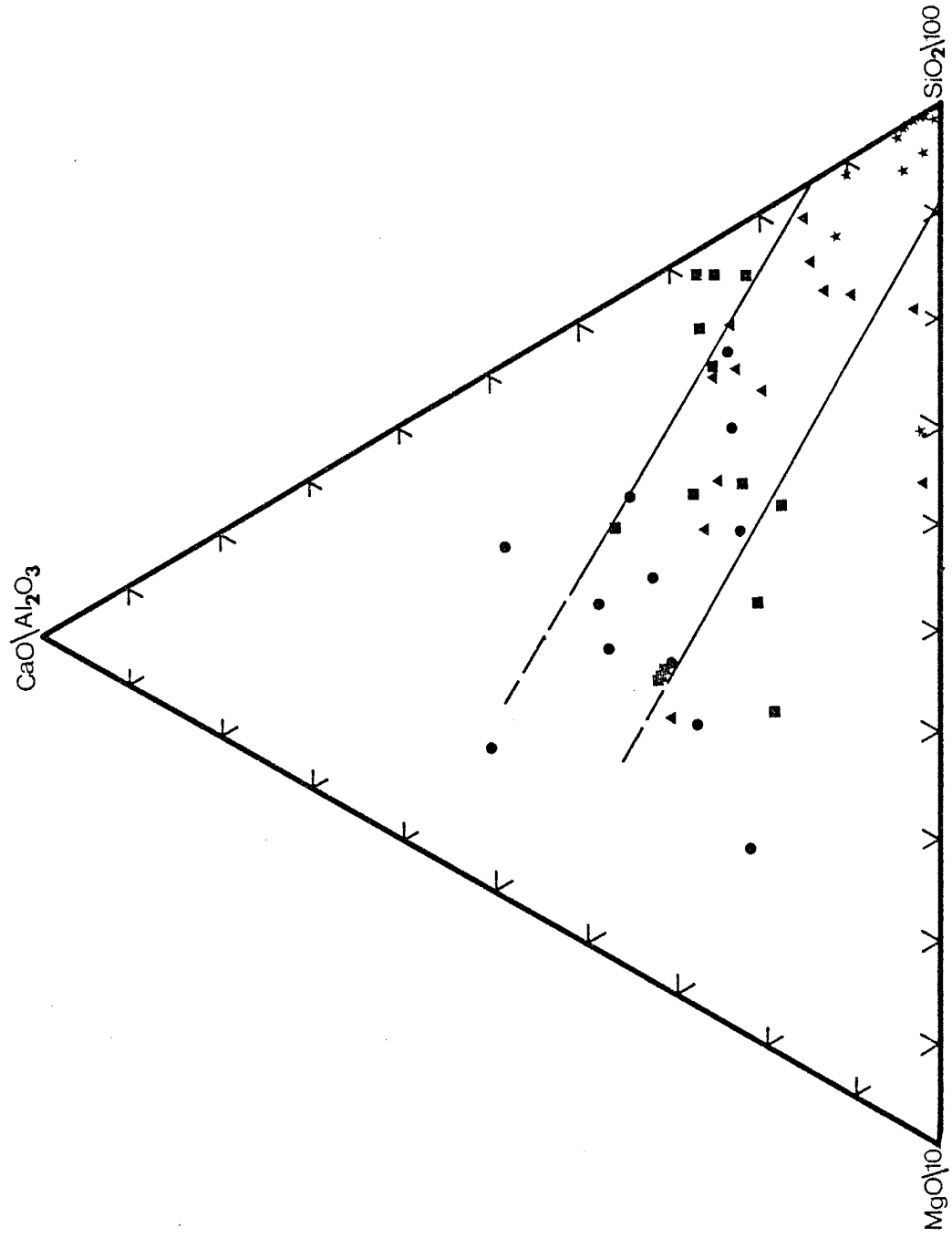

Figure 14.Mgo/10-CaO/Al_2O_3-SiO_2/100alteration screen after Davis et al. (1979). Unaltered samples plot between the two lines. Symbols as in Figure 11.

Soucie, 1978; Davis, 1979). In conjunction with these alteration screens various other indicators of alteration such as high loss on ignition (L.O.I., $\geq$2.5%), abnormal normative minerals, and unusual REE patterns are also considered. The results indicate that 17 out of 51 igneous samples have been classified as significantly altered. These samples are not used for chemical classification or geochemical modeling purposes. The geochemistry of the remaining samples is used in the classsification of the igneous rocks and, combined with field relations and interpretations, the determination of the tectonic setting.

Due to the low grade of metamorphism and the excellent state of preservation of the Tonto Basin supracrustal succession, the probability that these rocks experienced significant element mobility is low. Consequently, interpretations based on the compositions of the samples classified as not being significantly altered are assumed to be adequately reliable.

IGNEOUS ROCKS

Field Relationships

Mafic volcanic rocks typically occur as lava flows (some pillowed), dikes, and sills. Basalt flows are usually amygdaloidal and some have vesicles. Amygdules are usually filled with epidote±calcite±hematite. Most basalt flows are very fine grained and appear green to black on weathered surfaces and black on fresh surfaces. Hyaloclastic breccias are present in association with pillowed basalt flows.

Intermediate rocks occur dominantly as lava flows and sills. Some flows are pillowed (Gastil, 1958) and most contain prominent large (up to 2 cm) plagioclase phenocrysts although aphanitic andesites are present in some areas. Sills also contain large plagioclase phenocrysts that are sometimes oriented parallel to the contacts. Distinguishing between andesite flows and sills is difficult. Chilled margins are very small (<.5 cm) or non-existent. The orientation of plagioclase laths parallel to intrusive contacts and the truncation of plagioclase phenocryst in underlying andesites are two criteria used to distinguish sills from flows.

Dacitic and rhyolitic rocks occur chiefly as ash-flow tuffs showing variable degrees of welding. Flow structures, pumice fragments, and relict glass shards are locally preserved. Granophyric rocks that intrude the middle Alder and Red Rock Groups are chemically similar to the felsic volcanics.

Petrography

The mafic igneous rocks rarely display original mineralogy. Pyroxenes and amphiboles are replaced by chlorite+epidote±calcite. Albite is replaced by sericite±calcite±epidote and sieve textures are common. Late calcite and quartz veins are also common. Opaque minerals (i.e. magnetite±hematite) are also present in the mafic rocks. Amphiboles and pyroxenes are preserved in a gabbroic intrusive rock mapped by Gastil (1958) as pyroxenite. Gastil reports that this rock contains 31% primary augite, 42% actinolite (after augite), 10% epidote, 18% chlorite, 2% leucoxene, 1% hornblende and trace amounts of opaques. In contrast to Gastil's modal analysis the author found abundant, plagioclase and

minor augite, and the amphiboles have characteristics of both actinolite and hornblende. It appears that most actinolite is derived from hornblende - not augite, thus, this rock is better classified as a gabbro.

Despite metamorphic recrystallization, some primary textures are preserved. Diabasic (ophitic-subophitic) textures are preserved in many dikes and basalt flows display both aphanitic and porphyritic textures with phenocrysts typically $\leq$ 1mm in size.

Andesite sills and flows contain albite+epidote+ sericite+quartz+chlorite±calcite. Albite is highly sericitized and no primary amphiboles or pyroxenes are present. Both sills and flows are usually porphyritic with plagioclase phenocrysts up to 2 cm long and quartz phenocrysts up to 2 mm in diameter. Most plagioclase is twinned and occasional zoned plagioclase crystals are present.

Dacitic to rhyolitic rocks are porphyritic ash-flow tuffs. Rocks of more intermediate compositions contain quartz, plagioclase+opaques±chlorite (after hornblende?)± epidote±calcite. K-feldspar is rare and plagioclase is the only phenocryst phase. Rocks of rhyolitic composition contain quartz+plagioclase+K-feldspar+muscovite+zircon+opaques± chlorite±sericite±epidote±calcite. Plagioclase and K-feldspar vary from well preserved to highly sericitized and K-feldspar is usually Fe-oxide stained giving the grains a reddish color. Quartz and zircon crystals are usually euhedral. Epidote+calcite+sericite and some quartz are derived from the breakdown of plagioclase. Devitrified fiamme are present in some units and the glass is replaced by either quartz or K-feldspar. One sample of Haigler rhyolite has a matrix composed almost entirely of devitrified glass. The glass is
replaced by "rosettes" of microcline and is similar to that observed in the San Andres Mountains in south-central New Mexico (Condie and Budding, 1979). Phenocrysts in the rhyolites include quartz which ranges up to 5 mm in diameter, plagioclase up to 4-5 mm long and K-feldspar up to 10 mm across. In some units the phenocrysts have been rotated clockwise.

Geochemistry

The igneous rocks of the Alder and Red Rock Groups from the Tonto Basin area have been chemically classified according to the Zr/TiO_2 vs. Nb/Y diagram (Fig. 15) proposed by Winchester and Floyd (1977). This diagram is favored over other classification schemes due to its employment of ratios of relatively immobile elements. From this diagram it can be seen that the rocks are subalkaline and form a continuous suite from basalt to rhyolite. The suite is not bimodal which is in contrast to most suites of Proterozoic rocks from the southwestern United States (Condie, 1986). However, Reed (1988) indicates that the Alder plus Red Rock succession in the Mazatzal Mountains is bimodal with a sparsity of andesites. This may be due to a sampling bias.

The Jensen Cation plot (Fig. 16) and the AFM plot (Fig. 17) show that the suite has mixed tholeiitic and calc-alkaline affinities. A compilation of results from various other diagrams devised to distinguish calc-alkaline from tholeiitic fractionation trends is given in Table I. The Alder-Red Rock suite is dominantly tholeiitic, especially the mafic to andesitic compositions. The felsic end of the suite tends to be more calc-alkaline in nature. It is interesting to point out that volcanic rocks with mixed tholeiitic and calc-alkaline affinities are also typical of modern arc systems (Knoper and Condie, 1987). Rocks that fall in the "dacite/rhyodacite" field (Fig. 15) are referred to in this thesis as dacite/rhyodacite.

Major Elements

Mafic rocks (basalts through andesites) tend to have high Al_2O_3 and moderate to high CaO and show a slight to moderate Fe enrichment trend. These features are characteristic of young arc basalts or incipient back-arc basins respectively (Knoper and Condie, 1987). Variable K_2O and high TiO_2 and P_2O_5 are also characteristic of the mafic rocks.

Felsic rocks (dacites through rhyolites) display variable Na_2O, CaO, MgO, and high TiO_2, K_2O and Fe. The $K_2O/K_2O + Na_2O$ ratio seems to increase with increasing stratigraphic height (Fig. 18). This feature was first recognized by Gastil (1953) and may indicate compositional polarity in a developing arc system.

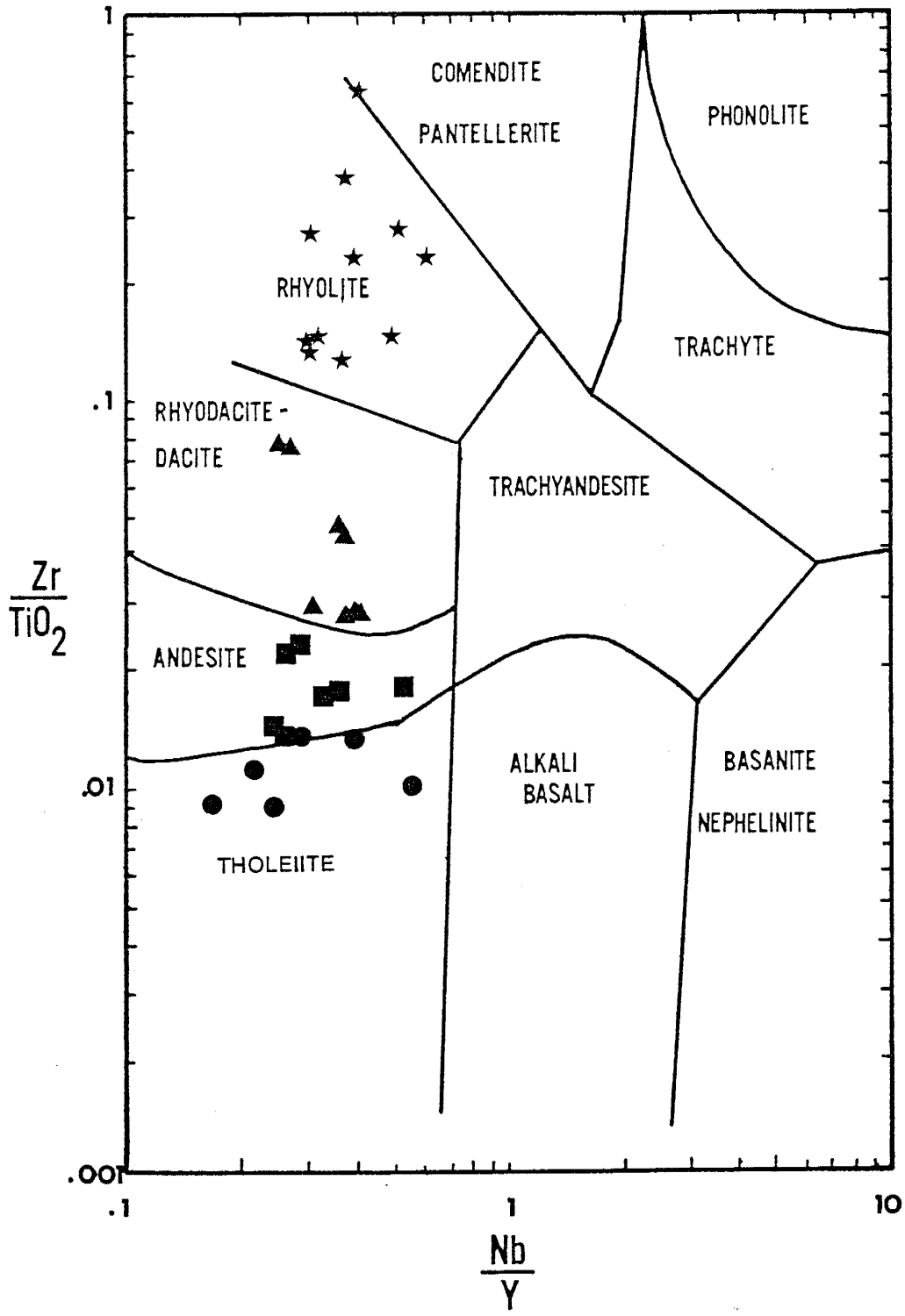

Figure 15. Geochemical classification of Tonto Basin igneous rocks using the Zr/TiO_2-Nb/Y diagram of Winchester and Flotd (1977). Symbols as in Figure 11.

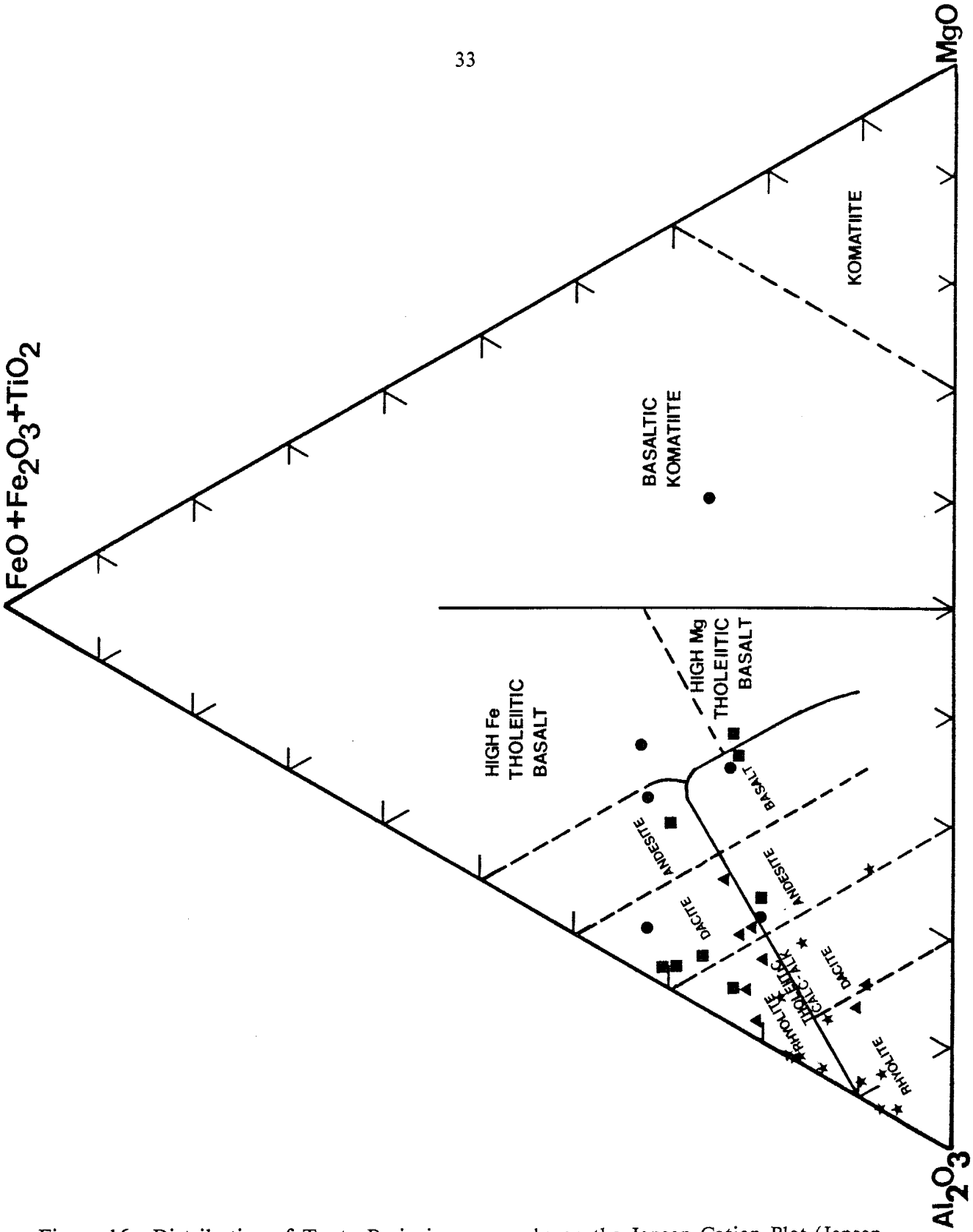

Figure 16. Distribution of Tonto Basin igneous rocks on the Jensen Cation Plot (Jensen, 1976). Symbols as in Figure 11.

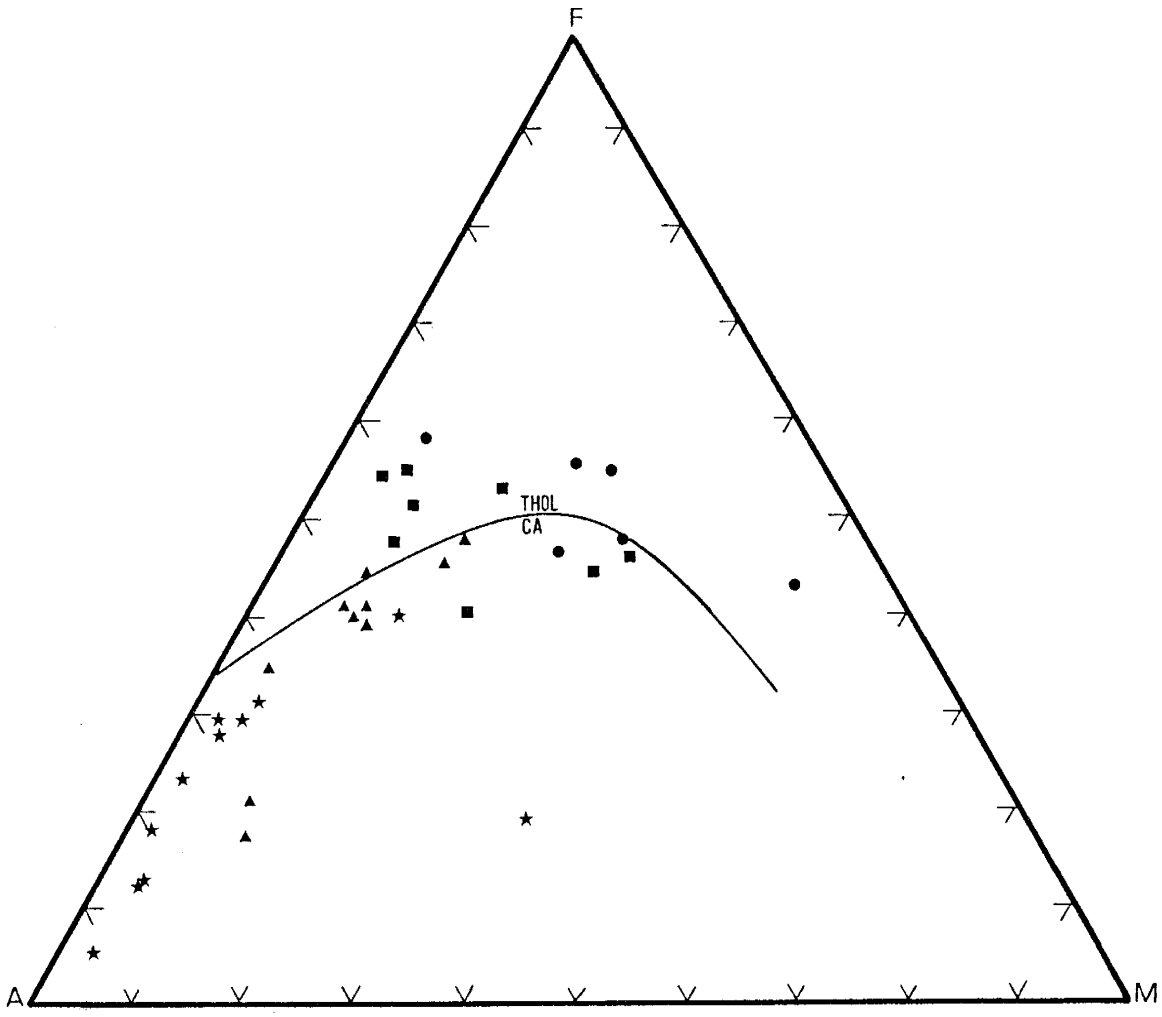

Figure 17. Distribution of the Tonto Basin igneous rock on an AFM plot. Symbols as in Figure 11. A=Na_2O+K_2O, M=MgO, F=$FeO+Fe_2O_3$, Thol=tholeiitic, CA=calc-alkaline.

Table I

Compilation of results of various diagrams devised to distinguish Calc-Alkaline from Tholeiitic trends in mafic rocks.

Diagram	Calc-alkaline	Tholeiitic	Mixed	Reference
FeO vs. FeO/MgO	31	50	19	Miyashiro (1974)
MgO vs. FeO	41	18	41	Jolly (1975)
SiO2 vs. FeO/MgO	18	58	24	Miyashiro (1974)
Jensen	33	67	0	Jensen (1976)
SiO2 vs. Cr	6	94	0	Miyashiro (1974)

Number indicates % of rocks plotting in each field.
FeO as total Fe.

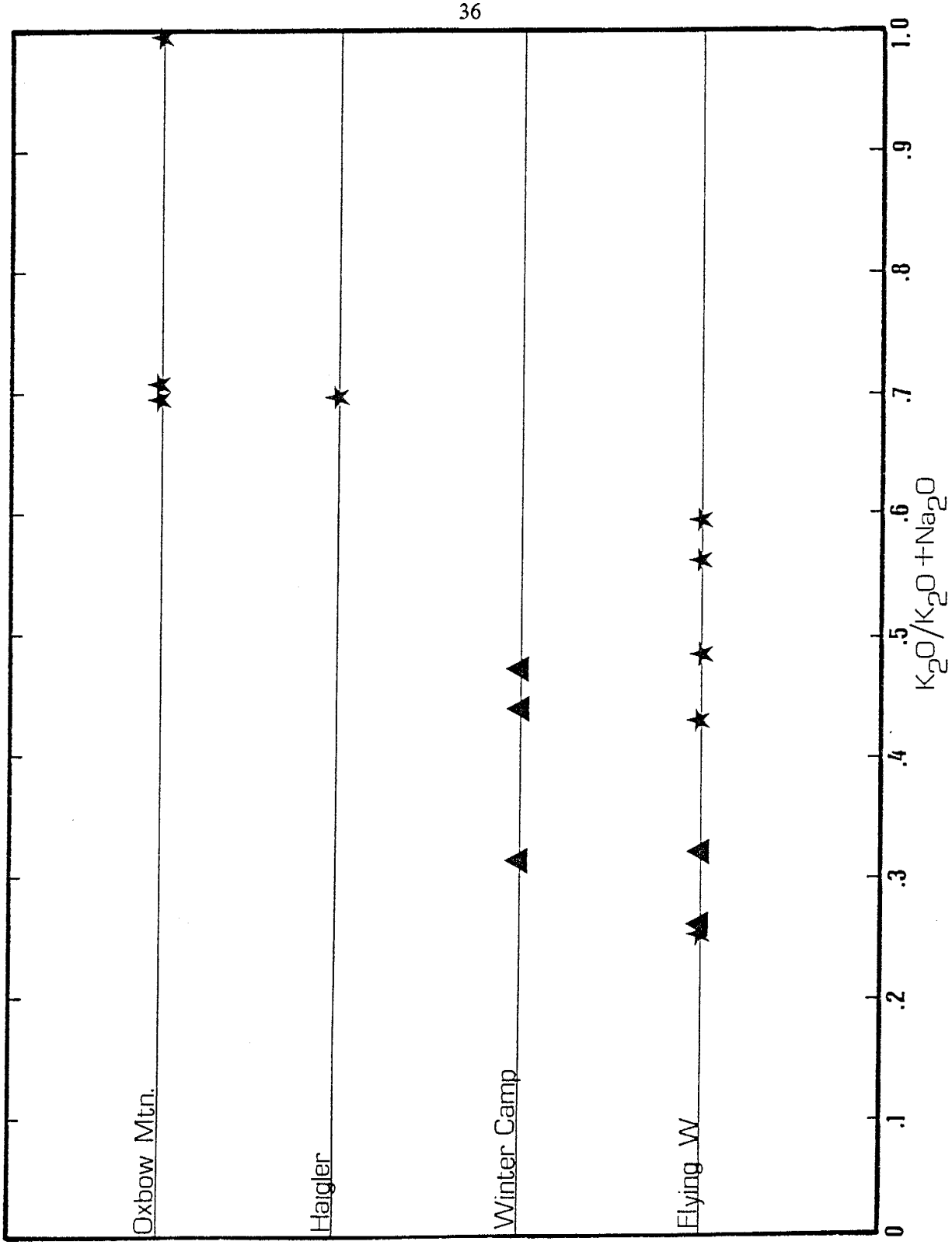

Figure 18. Diagram showing the increase in K_2O/K_2O+Na_2O with stratigraphic height in the felsic rocks. Symbols as in Figure 11.

Trace Elements

Large-ion lithophile element (LILE) concentrations are enriched but somewhat variable in all igneous rocks (Appendix B). This variability is due to the high mobility of these elements during alteration and metamorphism. As a result, the LIL elements are generally avoided in classification and modeling.

All igneous rocks were analyzed for seven rare earth elements (REE). On a chondrite normalized diagram (Fig. 19) mafic rocks are light REE enriched (≈100 x chondrites), have small negative to positive Eu anomalies (indicating the removal or accumulation of plagioclase, respectively), and have slightly depleted heavy REEs. Felsic rocks are also light REE enriched (100-300 x chondrites), have moderate to strong negative Eu anomalies, and have flat heavy REEs (Fig. 20).

High field strength elements (HFSE) are present in very low concentrations in the mafic rocks (Appendix B). According to Pearce (1983) this is a characteristic of volcanics from modern arc systems. In the felsic rocks, Zr increases compared to the concentrations of Nb, Ta, and Hf (which remain more or less constant) indicating that zircon played a role in the genesis of the felsic volcanics.

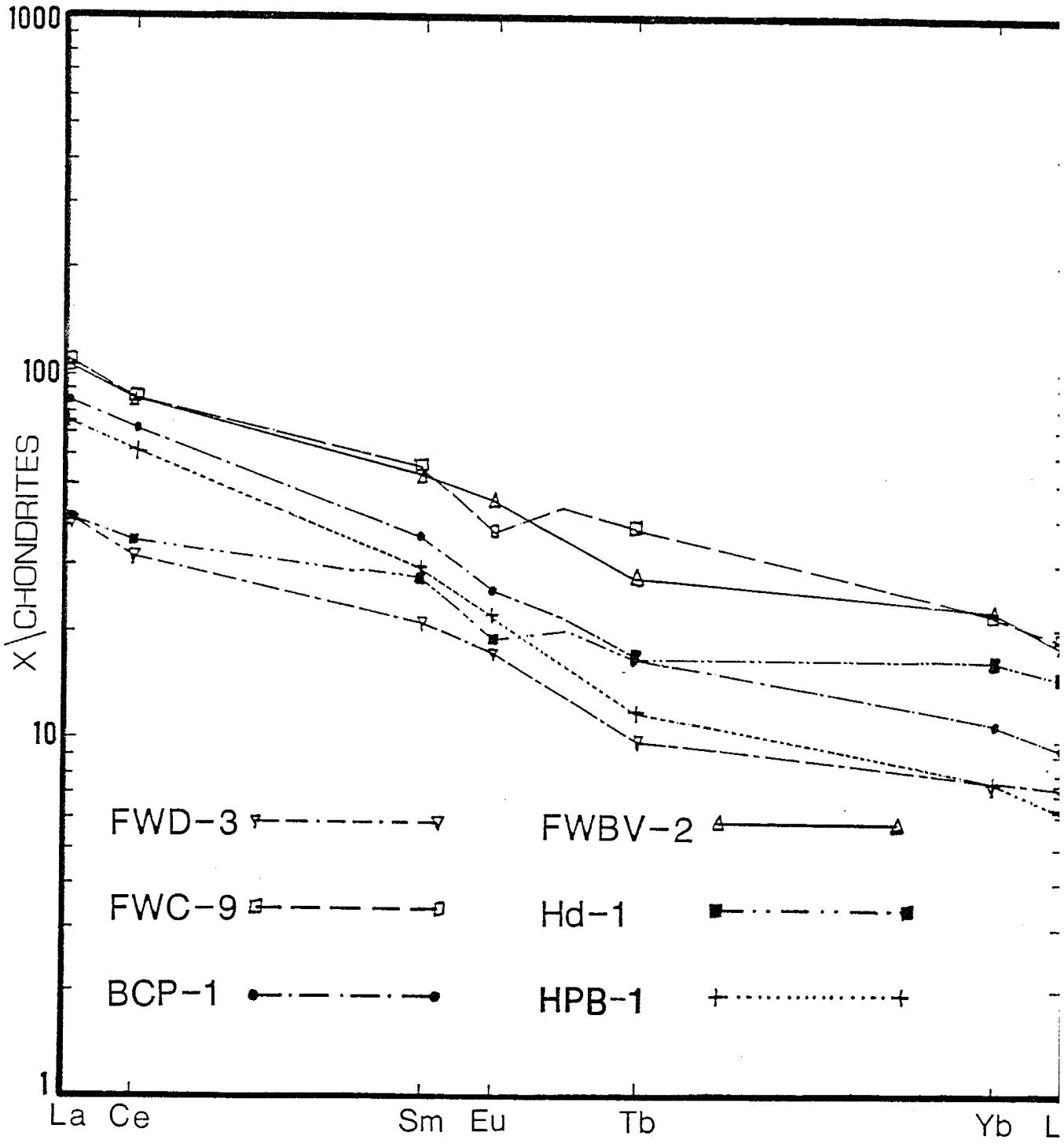

Figure 19. Chondrite normalized REE plots of Tonto Basin mafic rocks.

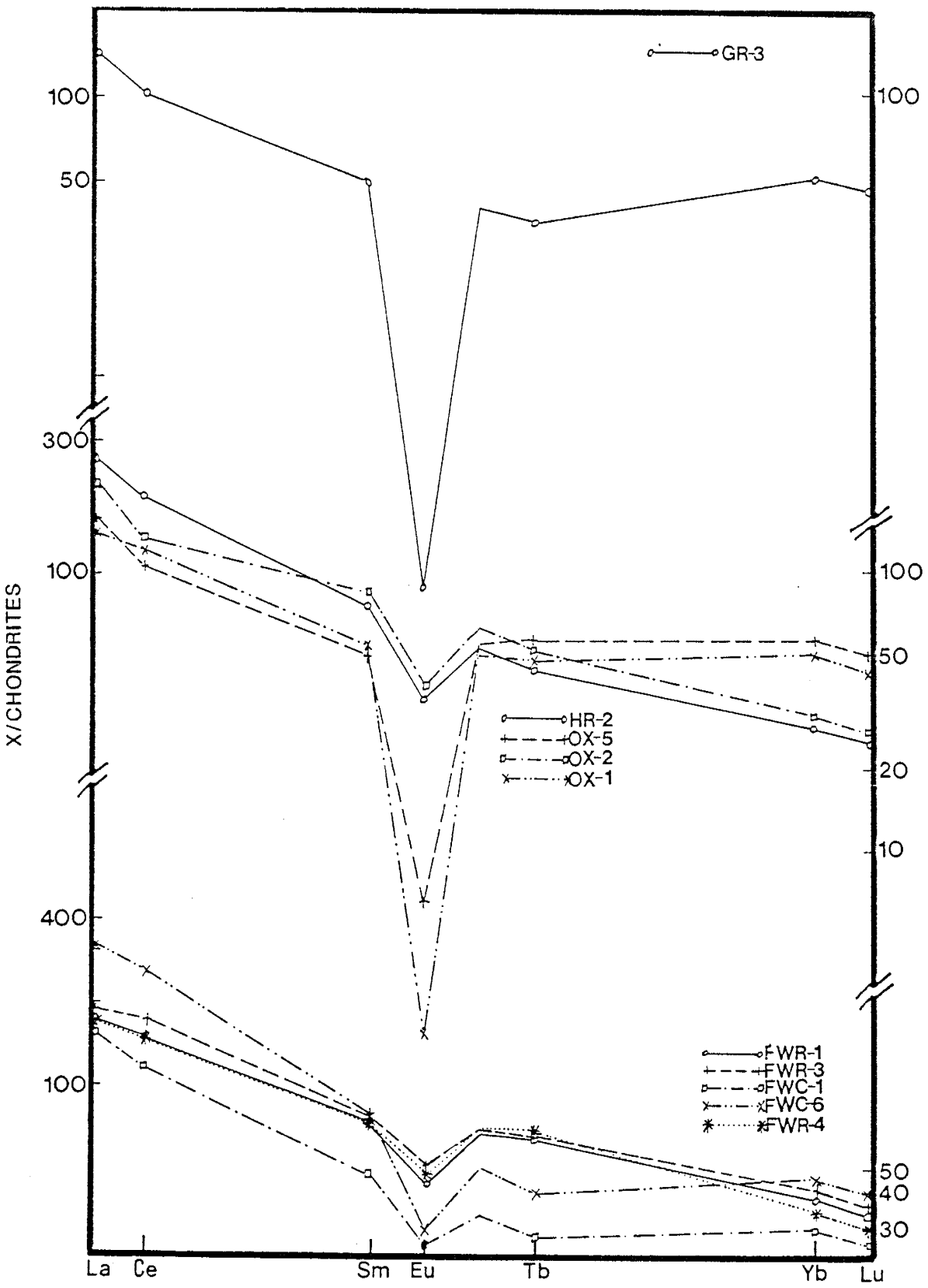

Figure 20. Chondrite normalized REE plots of Tonto Basin felsic rocks.

PETROGENETIC MODELING

Petrogenetic trace element modeling is presented here in order to characterize the mantle source and the genetic relationships of the volcanic rocks from the Alder and Red Rock Groups. The modeling of the trace element abundances was accomplished by using a computer program (MODULUS) developed by Knoper (1988). This program uses well established melting and crystallization relationships (O'Hara, 1977; Allegre and Minster, 1978) and published mineral-liquid distribution coefficients (Kds) and allows the user to test a large number of models in a relatively short time. The Kds used are listed in Table II.

BATCH MELTING AND FRACTIONAL CRYSTALLIZATION EQUATIONS

Batch Melting

Batch melting (also called partial melting) is the simplest model for the partial melting of a complex mineral assemblage. In this model it is assumed that the liquid remains at the site of melting and is in chemical equilibrium with the solid residue until mechanical conditions allow it to escape as a single "batch" of primary magma (Cox et al., 1979). The concentration of an element in the liquid (C_l) is related to the concentration of that element in the original unmelted source (C_0) by:

$$\frac{C_l}{C_o} = \frac{1}{F + D - FD}$$

Where F is the weight fraction of melt and D is the bulk distribution coefficient for the residual solids at the moment the melt is removed from the system (Cox et al., 1979; Allegre and Minster, 1978). The bulk distribution coefficient (D) is calculated from the weighted proportions of each mineral in the assemblage (w) times the Kd for that mineral:

$$\sum_{i=1}^{n} w_i K d_i$$

Table II

List of Kd values used in geochemical modeling.

	MAFIC Kds					
	Ni	Zr	Y	Yb	La	Ti
Olivine	*	0.01	0.01	0.02	0.00001	0.02
Clinopyroxene	*	0.1	0.5	0.6	0.07	0.4
Orthopyroxene	*	0.03	0.2	0.15	0.007	0.1
Plagioclase	0	0.01	0.03	0.07	0.15	0.15
Magnetite	30	0.1	0.2	0	0	7.5
Biotite	-	-	-	-	-	-
Ilmenite	-	-	-	-	-	-
Quartz	-	-	-	-	-	-
Zircon	0.01	-	60	138	0.08	0
Allanite	-	-	-	-	-	-
Garnet	*	0.3	2.0	5.0	0.03	0.3
	INTERMEDIATE Kds					
	Ni	Zr	Y	Yb	La	Ti
Olivine	-	-	-	-	-	-
Clinopyroxene	*	0.25	1.5	2.0	0.2	0.4
Orthopyroxene	*	0.08	0.45	0.85	0.1	0.25
Plagioclase	0	0.03	0.06	0.08	0.08	0.05
Magnetite	30	0.2	0.5	0	0	25
Biotite	-	1.2	0.03	0.03	0.03	1.5
Ilmenite	-	0.6	-	0	0	50
Quartz	-	-	-	-	-	-
Zircon	0.01	1000	60	200	2.0	50
Allanite	-	2	100	100	2500	50
Garnet	*	0.5	11	40	0.35	0.5
	FELSIC Kds					
	Ni	Zr	Y	Yb	La	Ti
Olivine	-	-	-	-	-	-
Clinopyroxene	-	0.6	4.0	1.5	0.3	0.7
Orthopyroxene	-	0.2	1.0	0.85	0.1	0.4
Plagioclase	-	0.1	0.1	0.05	0.3	0.05
Magnetite	-	0.8	2.0	0.1	0	35
Biotite	-	2.0	0.03	0.44	0.11	2.5
Ilmenite	-	1.0	-	0.1	0	50
Quartz	-	-	-	-	-	-
Zircon	-	1000	60	200	2	50
Allanite	-	2.0	100	100	2500	50
Garnet	-	1.2	35	40	0.35	1.2

An*indicates temperature dependent Kds.

The above equations are for modal batch melting. This means that the mass fractions of the minerals entering the melt are equal to the observed mass fractions of the minerals in the source rock. Since very few source rocks undergo modal melting it is necessary to modify the batch melting equation to account for non-modal melting. This is done by introducing the bulk distribution coefficient of melting (P) into the batch melting equation. The bulk distribution coefficients (P) expresses the relative contributions of phases entering the melt as follows:

$$P = \sum_{i=1}^{n} P_i K d_i$$

where P_i is the mass fraction of a phase entering the melt and Kd_i is the distribution coefficient of that phase. Thus the equation for non-modal batch melting is:

$$\frac{C_l}{C_o} = \frac{1}{D + F(1 - P)}$$

Depending on the modal and melt proportions of individual minerals in the assemblage undergoing melting, different minerals may be exhausted with increasing degrees of melting. This will cause discontinous changes in the value of D and thus affect incompatible element concentrations in the liquid. For example, when melting a garnet lherzolite, garnet will be the first mineral to be consumed (provided it is present in minor quantities - 5-15%). When garnet is completely melted the Yb concentration of the melt will drastically increase. Since the Kd for Yb in garnet is relatively high (4.0, Cox et al., 1979) most Yb is concentrated in garnet until all garnet has completely melted. Since incompatible elements are concentrated in the liquid (melt) it follows that the smaller the degree of melting-- the higher the concentration of incompatible elements in the melt. Thus, the degree of partial melting and the consumption of phases in the source control the chemical composition of the melt.

Fractional Crystallization (FXL)

If the phases crystallizing out of a magma remained in equilibrium with the magma this would be the reversal of batch melting. Instead, it is more likely that the phases crystallizing out of a magma are not in equilibrium with the melt. As Cox et al. (1979) point out, the growth of zoned crystals would probably proceed faster than they could re-equilibrate with the changing composition of the liquids. Also, gravity settling could effectively remove certain phases from the melt by sinking or floating. Thus, the model developed for closed system fractional crystallization assumes that the crystals are removed from the melt as soon as they are formed and also that the magma chamber remains a closed system (i.e. there can be no injections of new magma). The equation which relates the concentration of an element in the initial liquid (C_o) to the concentration of that element in the liquid after the removal of a certain amount of crystals (C_l) is as follows:

$$\frac{C_l}{C_o} = F^{(D-1)}$$

where F is the mass fraction of the liquid and D is the bulk distribution coefficient (Allegre and Minster, 1978; Cox et al., 1979).

Fractional crystallization has the opposite effect, on the chemical composition of the liquid, of batch melting. For low degrees of fractional crystallization, the liquid becomes severly depleted in compatible elements. The incompatible element concentration of the magma, however, does not rise greatly until very high degrees of fractional crystallization are reached. By this time, removal of the liquid from the crystals is ineffective (Cox et al., 1979).

Open system fractional crystallization (O'Hara, 1977) allows for the magma chamber to be periodically replentished with new batches of magma. This effectively changes the bulk composition of the liquid by allowing the melt to be greatly increased in incompatible elements. Thus, open system fractional crystallization can enrich a magma in incompatible elements much faster than closed system fractional crystallization.

Mantle Source

According to Wood (1979) the Earth's mantle consists of three broad reservoirs--primitive mantle (PM), depleted mantle (DM), and enriched mantle (EM). Primitive mantle is defined as mantle that has not undergone a melt extraction event thus depleting the mantle in incompatible elements (i.e. it is undepleted). Depleted mantle is defined as primitive mantle that has undergone a melt extraction event, resulting in a mantle reservoir depleted in incompatible elements. Enriched mantle is defined as primitive mantle that has been enriched in incompatible elements by some process (i.e. mantle metasomatism or mixing of two mantle components, etc.). The estimated compositions of these three mantle components (Wood, 1979) are used here for comparison purposes in order to help constrain the nature of the mantle source for the Tonto Basin volcanics.

Reed (1988) has shown that mafic samples fron the Alder-Red Rock succession in the Mazatzal Mountains are probably derived from a mantle source similar to PM and that this source has variable amounts of modal garnet (5-15%). By plotting the Tonto Basin mafic samples on diagrams which use elements that are compatible with garnet it can be determined if garnet was a residual phase during melting. The Y vs. Hf (Fig 21) and Yb vs. Nb (Fig.22) diagrams are used for this purpose. On the Y vs. Hf diagram the Tonto Basin samples are plotted along with the estimated compositions of EM and PM. The Tonto Basin samples are also plotted on the Yb vs. Nb diagram along with PM and DM. Batch melting curves for PM, EM, and DM (calculated using the mode and melt proportions in TableIIIA) are also drawn on these diagrams.

Like the Mazatzal mafic rocks (Reed, 1988) most of the Tonto Basin rocks appear to be evolved (i.e. they have low Mg numbers-20 to 56, and low Ni contents-6 to 68 ppm). This means the parent liquid of the mafic rocks must have undergone extensive fractional crystallization. In order to relate the Tonto Basin volcanics to the batch melting curves, closed system fractional crystallization trajectories are also plotted (Figs. 21 and 22). Approximately 55% fractional crystallization of olivine and clinopyroxene in a 4:1 ratio covers the spread in the basalts. From these two diagrams it can be seen that the mantle

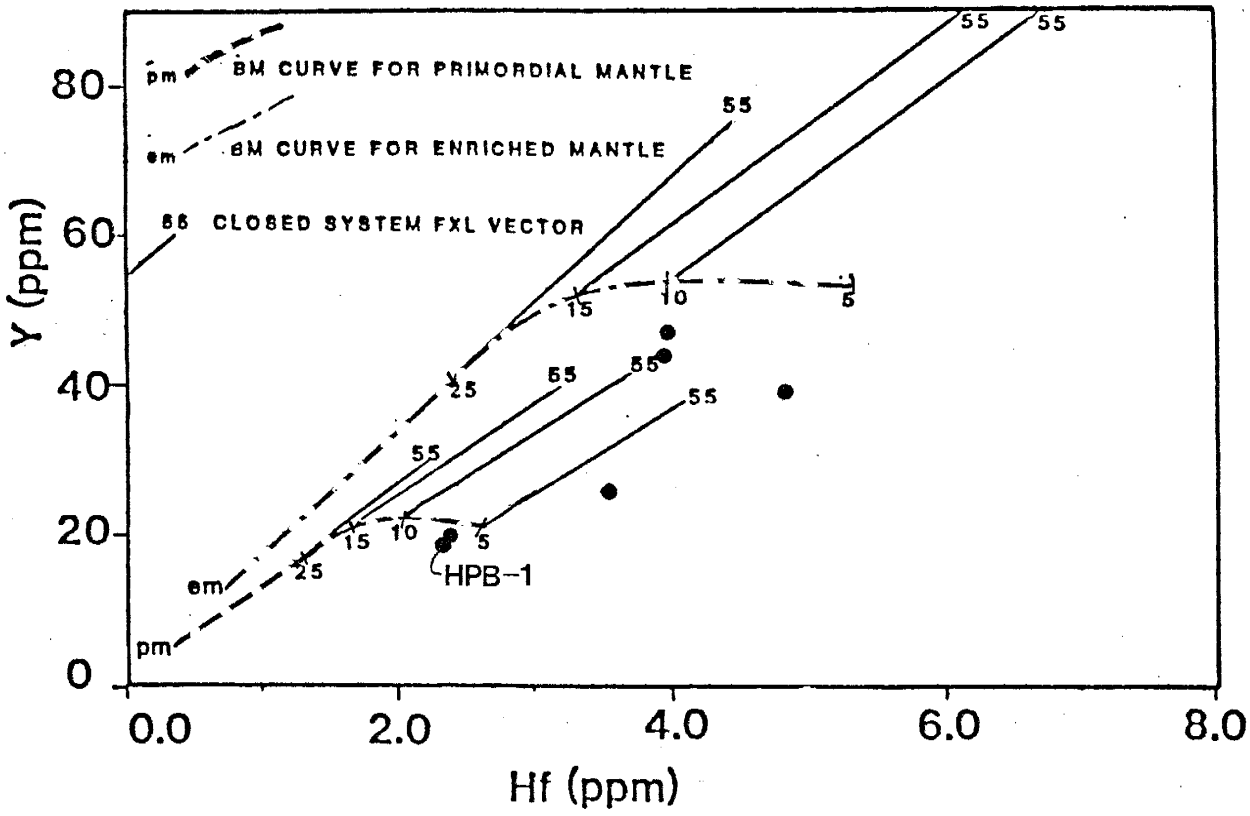

Figure 21. Distrubtion of the Tonto Basin mafic rocks on the Y vs. Hf diagram. BM=batch melting, FXL=fractional crystallization, numbers on FXL vectors indicated percent crystallization, numbers on BM curves indicate percent melting, pm=primitive mantle, em=enriched mantle. Mantle compositions from Wood (1979). Filled circle=basalt.

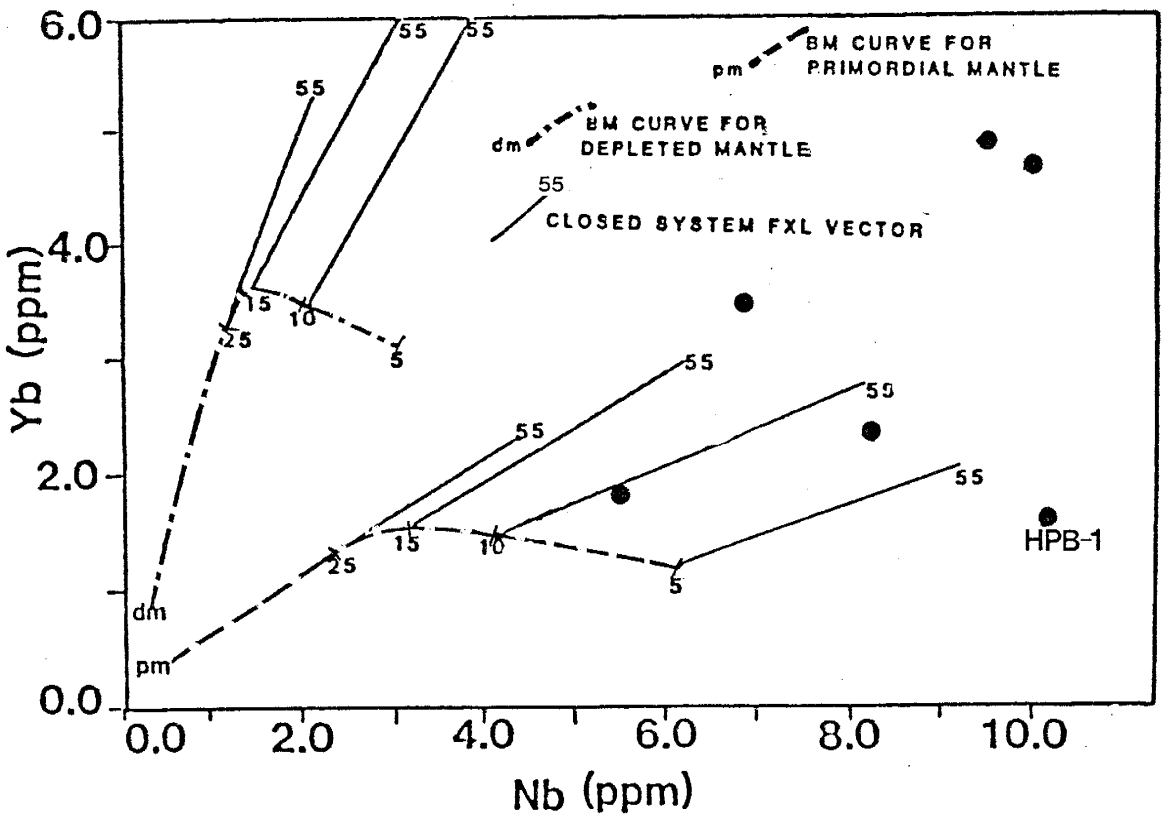

Figure 22. Distribution of the Tonto Basin mafic rocks on the Yb vs. Nb diagram. BM=batch melting, FXL=fractional crystallization, numbers on FXL vectors indicate percent crystallization, numbers on batch melting curves indicate percent melting, pm=primitive mantle, dm=depleted mantle. Filled circles=basalt.

TABLE III

Mode and melt proportions for batch melting models.

A: Garnet Lherzolite

Mineral	Mode	Melt
Olivine	0.60	0.05
Orthopyroxene	0.15	0.05
Clinopyroxene	0.20	0.45
Garnet	0.05	0.45

B: Garnet Lherzolite

Mineral	Mode	Melt
Olivine	0.60	0.05
Orthopyroxene	0.15	0.05
Clinopyroxene	0.10	0.45
Garnet	0.15	0.45

Mineral proportions in melts and parent rocks were estimated from experimental petrologic data and available modal data for garnet lherzolite nodules.

source of the Tonto Basin mafic rocks most closely resembles primitive mantle. It is also apparent that garnet must be present as a residual phase in the mantle. If garnet were not a residual phase the melts generated would be too enriched in Y and Yb and the Tonto Basin mafic rocks cannot be derived from such melts.

Some of the samples plot close to the partial melting trajectory (Figs. 21 and 22). One of theses samples, HPB-1, is the most primitive mafic rock found during this study. It has a Mg number of 70 and a Ni content of 528 ppm and may have formed directly from a partial melt. The other samples, especially the ones plotting close to the batch melting trajectories cannot be derived by partial melting alone but require some FXL to account for their low Ni content and Mg numbers. Variable amounts of garnet in the mantle source can move the melting trajectories to higher (less garnet) or lower (more garnet) Y and Yb values and explain the spread in the samples along the trajectories.

Further characterization of the mantle source can be made from NMORB-normalized incompatible element distribution plots of basalts (Pearce, 1983). Figure 23 shows several Tonto Basin basalts and basaltic andesites plotted on such a diagram. The enrichment of the large ion lithophile elements (LILE)(Sr, K, Rb, Ba, Th) and REE relative to Ta and Nb has been interpreted by Pearce (1983) to indicate a subduction zone component. Many workers (Best, 1975; Gill, 1981; Pearce, 1983) have suggested that these selective enrichments are caused by transport of the enriched elements by aqueous fluids derived from the descending slab by devolatilization. Ta and Nb are apparently retained in the descending slab in some refractory phase such as rutile (Saunders et al., 1980). It appears that the mantle source for the Tonto Basin volcanics was located in a subduction zone environment and has been enriched in LILE and REE. Variable enrichments of the mantle wedge in the LILE and REE and possible variations in th mineralogy of the mantle wedge (i.e. variations in modal garnet) may be responsible for the scatter in the data.

A mantle source composition is calculated using the most primitive mafic sample (HPB-1) and assuming a garnet lherzolite mode (Table IIIB) and 10% melting. Elemental abundances for this rock were considered to represent the composition of a basaltic liquid

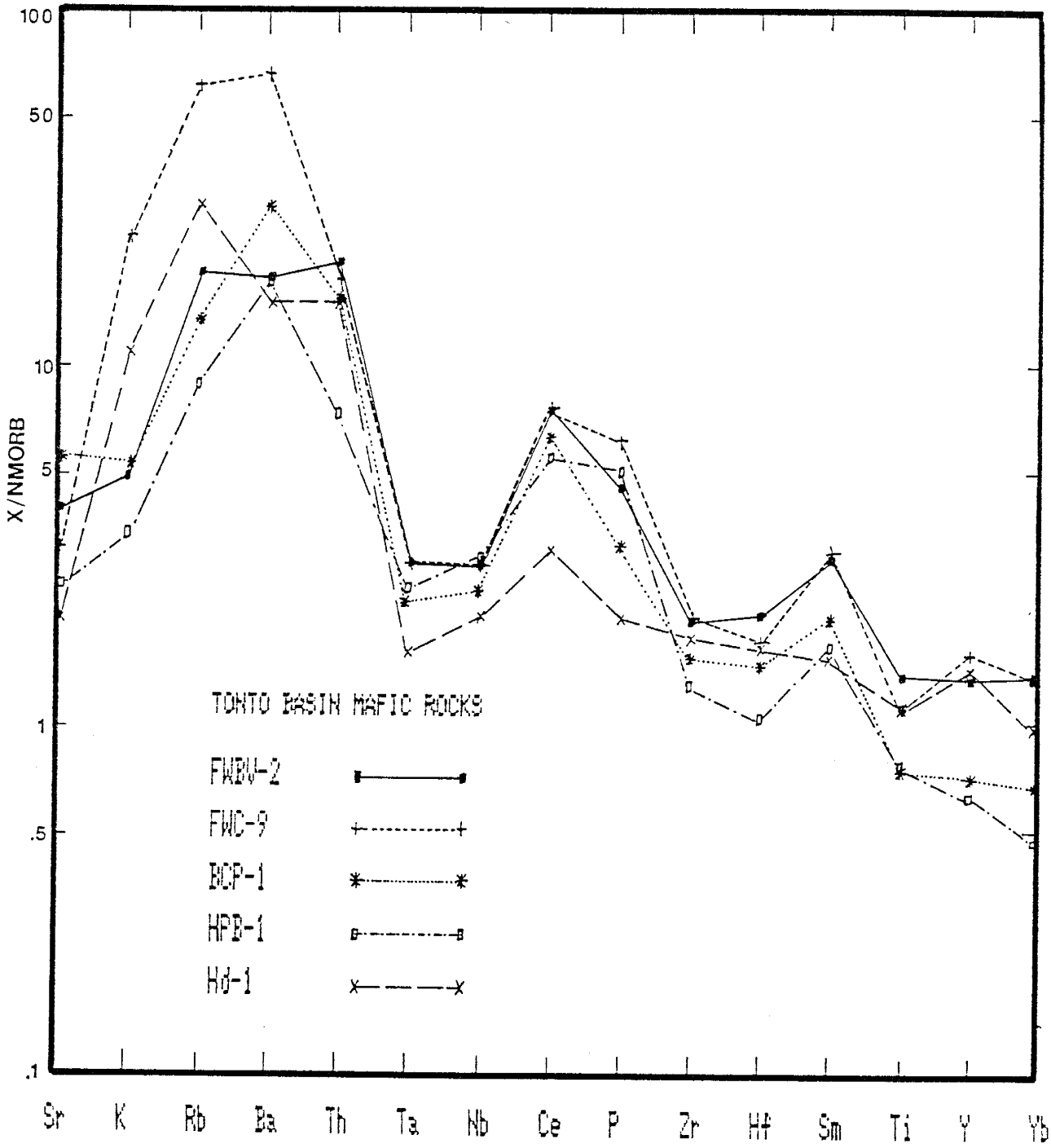

Figure 23. NMORB-normalized diagram showing the distribution of the Tonto Basin mafic rocks. Normalizing values from Pearce (1983).

derived from some source. By solving for C_0 in the batch melting equation, the composition of this source was calculated. This source is enriched in K, Rb, Sr, Cs, Ba,Th, U, La, Ce, Sm, Tb, Yb, P, Y, Zr, Nb, Ta, and Hf compared to PM and DM and depleted in Ti, Ni, and V compared to PM (Table IV).

Batch Melting Model

Jaques and Green (1980) have shown that pressure, temperature, degree of partial melting, and source composition all play important roles in generating basalts of different compositions. Figure 24 shows that, depending on the temperature and pressure, partial melting of spinel peridotite can generate akalic or tholeiitic basalts. For instance, at 15 Kb pressure, <15% melting will generate akalic magmas, 20-30% will form olivine tholeiite and 40-60% can produce komatiitic liquids (Hall, 1987). Likewise, Mysen and Kushiro (1977) determined that at 20 Kb pressure, <16% partial melting of a garnet peridotite will generate alkali basalt magma and from 16 to 44%-tholeiitic magma. It appears that under the same P-T conditions, the same type of magmas will be produced by similar degrees of partial melting of either garnet or spinel peridotite.

To determine if the calculated mantle source can produce the Tonto Basin basalts, melting and crystallization relationships have been modeled geochemically. Since most basaltic magmas erupted today are at temperatures of 1000-1200°C (McDonald, 1972), it is assumed that eruption temperatures were the same for the Tonto Basin basalts. An assumed temperature of melting of 1300°C is used in the non-modal equilibrium batch melting equation (for temperature dependent Kds). The system is assumed to be closed (i.e. no contamination, magma mixing, or injections of new magma into the chamber). At 1300°C the solidus is reached at 15 Kb pressure (≈50 km depth) (Fig. 24). Comparison of vertical cross sections of hypocenter distributions beneath modern arc-trench systems (Condie, 1982b pp. 108-110) suggests that the volcanic fronts of many arcs correspond to a subducted plate depth of ≈100-150 km. Most subducted slabs lose their water by 80-150 km depth. If this devolatilization at 80-150 km is responsible for lowering the melting temperature of the

TABLE IV

Chemical composition of calculated mantle source.

Element	Calc. Source	PM	DM	EM
K	476	252	216	106
Rb	2.1	0.86	0.1	0.39
Sr	36.4	23	13.2	17.9
Cs	0.5	0.019	0.0013	0.007
Ba	38.6	7.56	1.2	4.77
Th	0.21	0.096	0.02	0.06
U	0.08	0.027	0.01	0.015
La	2.9	0.71	0.31	0.66
Ce	6.5	1.9	0.95	1.68
Sm	0.91	0.385	0.32	0.42
Eu	0.38	--	--	--
Tb	0.27	0.099	0.08	0.08
Yb	1.09	0.38	0.6	--
Lu	0.16	--	--	--
P	193	90.4	73.3	61.6
Sc	21.3	16	--	--
Ti	1376	1526	1177	1044
Y	7.4	4.87	4.1	2.7
Zr	17.4	11	11.4	11.3
Nb	1.6	0.62	0.31	0.72
Hf	0.43	0.36	0.34	0.26
Ta	0.07	0.043	0.022	0.062
V	57.5	50	--	--

Values for PM, DM, and EM from Wood (1979).

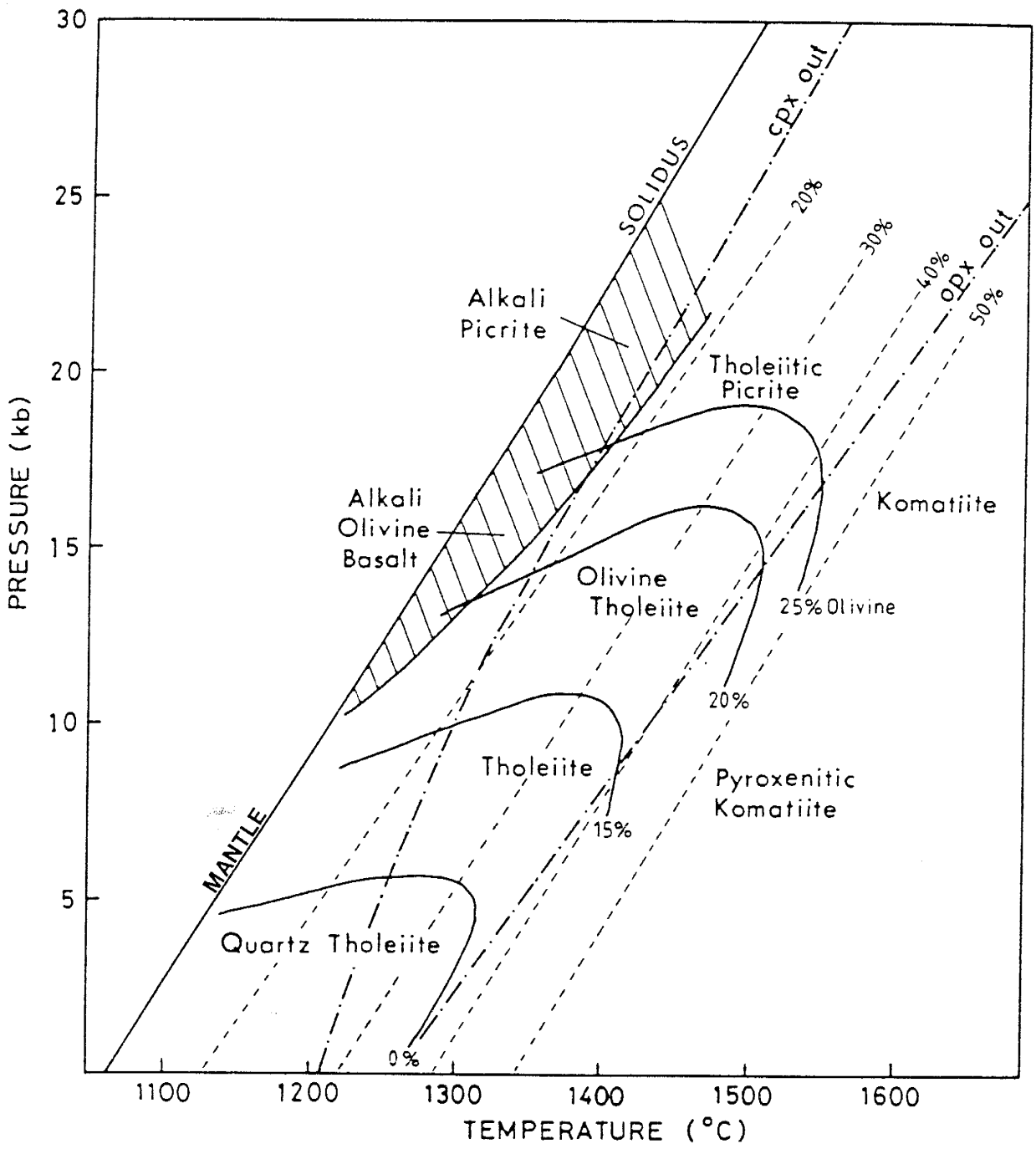

Figure 24. Pressure-temperature relationships for melting of spinel peridotite (after Jaques and Green, 1980). Dashed lines indicate degree of melting in percent. Solid lines indicate percent modal olivine. Diagonally ruled area indicates pressure-temperature regime where alkali basalt magmas are generated.

mantle, 50 km depth (15 Kb) would be a reasonable depth of generation of the parental magma to the Tonto Basin basalts.

Inspection of Figure 24 shows that at 15 Kb and 1300°C a partial melt of <15% will generate an alkali basalt. In direct agreement with this, a 5% melt of the calculated mantle source at 1300°C produces an akali basalt (as classified on the Zr/TiO_2 vs. Nb/Y diagram of Winchester and Floyd, 1977). However, 15% melting generates a tholeiitic basalt that is herein assumed to be the parental magma of the Tonto Basin volcanics. Thus, it appears that in terms of experimental petrology and volcanic arc geometry the composition of the calculated source for the Tonto Basin basalts is reasonable.

The calculated mantle source and the batch melting trajectory are plotted on Figures 25, 26, and 27. On these figures a few basalts plot close to the melting curve while others do not. Some of these evolved samples however, can be related to the batch melting curve by 55% closed systen fractional crystallization of olivine (80%) and clinopyroxene (20%) of the assumed parental magma (sample HPB-1). The others can be explained by invoking variable degrees of batch melting followed by FXL.

In Figure 25 it can be seen that a 15% melt of the calculated mantle source produces a liquid within the range of basalts but is relatively low in TiO_2 and Zr with respect to the evolved basalts. The 55% FXL vector (Stage 1 of the fractional crystallization model-see Table V) brings the liquid closer to some of the basalts. Figures 26 and 27 show similar relationships. From these three diagrams it appears that the Tonto Basin mafic rocks can best be explained by 15-30% partial melting of the calculated mantle source followed by the aforementioned amount of FXL. Also, a variable source composition may contribute to some of the scatter in the data. It can also be seen from Figure 27 that during partial melting of the calculated mantle source, La increases greatly with respect to Yb. This provides further evidence that Yb is retained in garnet in the residue.

Figure 28A shows the REE pattern of a calculated model basalt compared to an average of six Tonto Basin basalts. The match is fairly good. Compared to the average, the calculated basalt is slightly enriched in REE but falls within the range of Tonto Basin basalts.

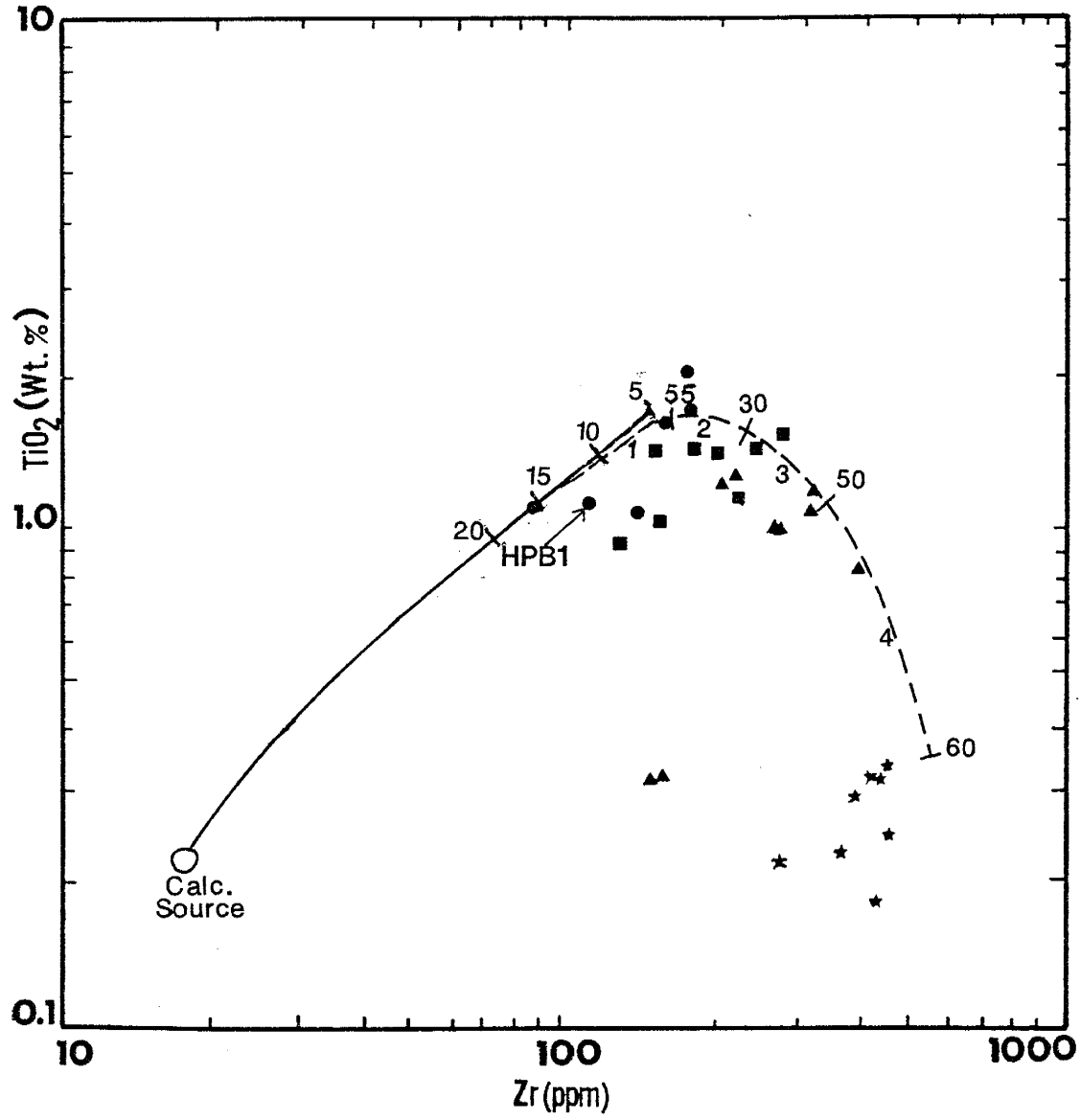

Figure 25. Distribution of Tonto Basin igneous rocks on the TiO_2 vs. Zr diagram. Solid line represents batch melting curve. Dashed line represents FXL curve. Numbers indicate degree of melting and FXL, repectively. Numbers 1,2,3, and 4 correspond to the four stage FXL model. Circles=basalts, squares=andesites, triangles=dacites, and stars=rhyolites.

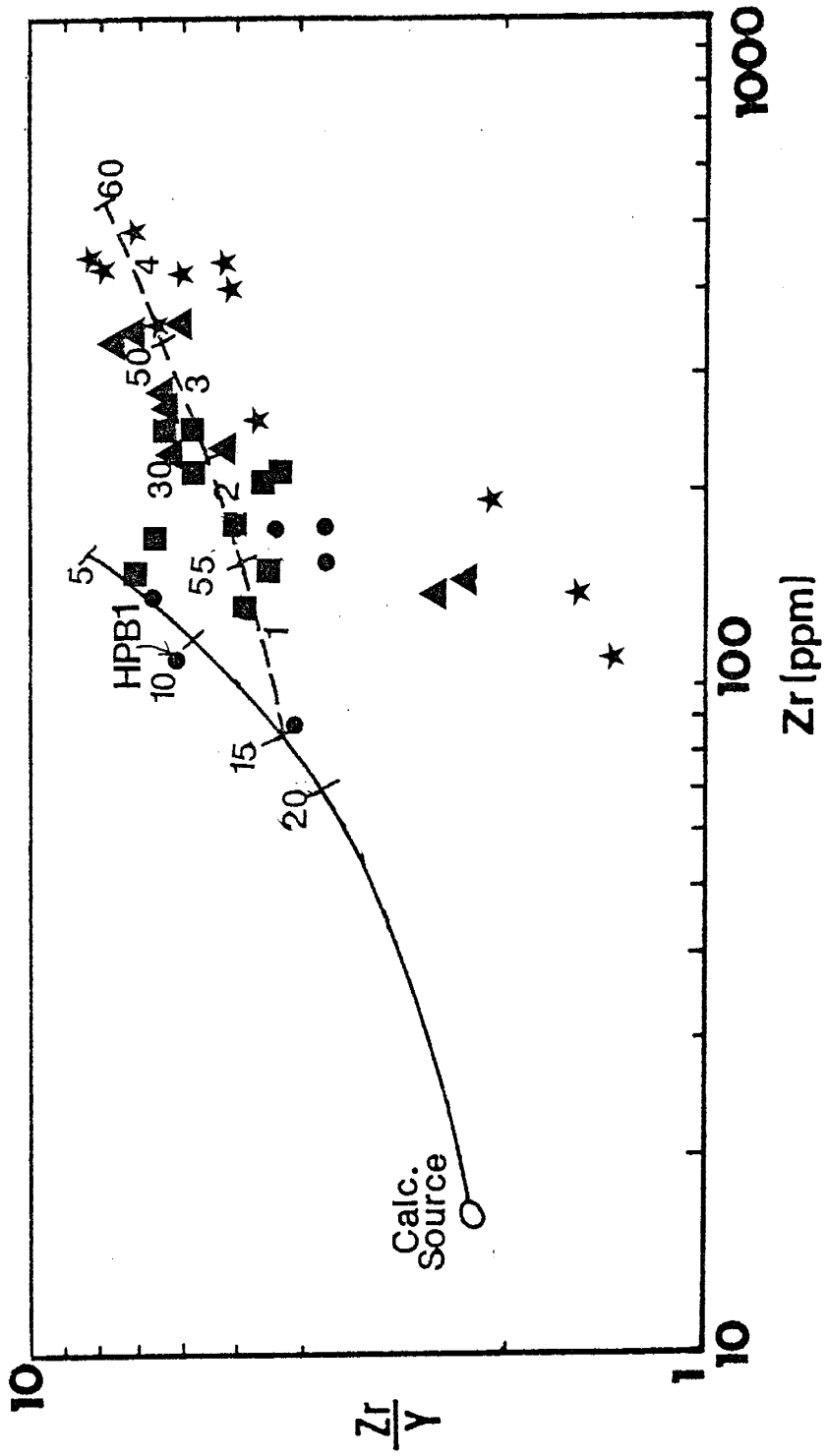

Figure 26. Distribution of Tonto Basin igneous on the Zr/Y vs. Zr diagram. Solid line represents batch melting curve. Dashed line represents FXL curve. Numbers represent percent of batch melting and FXL, respectively. Numbers 1,2,3, and 4 correspond to the four stage FXL model. Symbols as in figure 25.

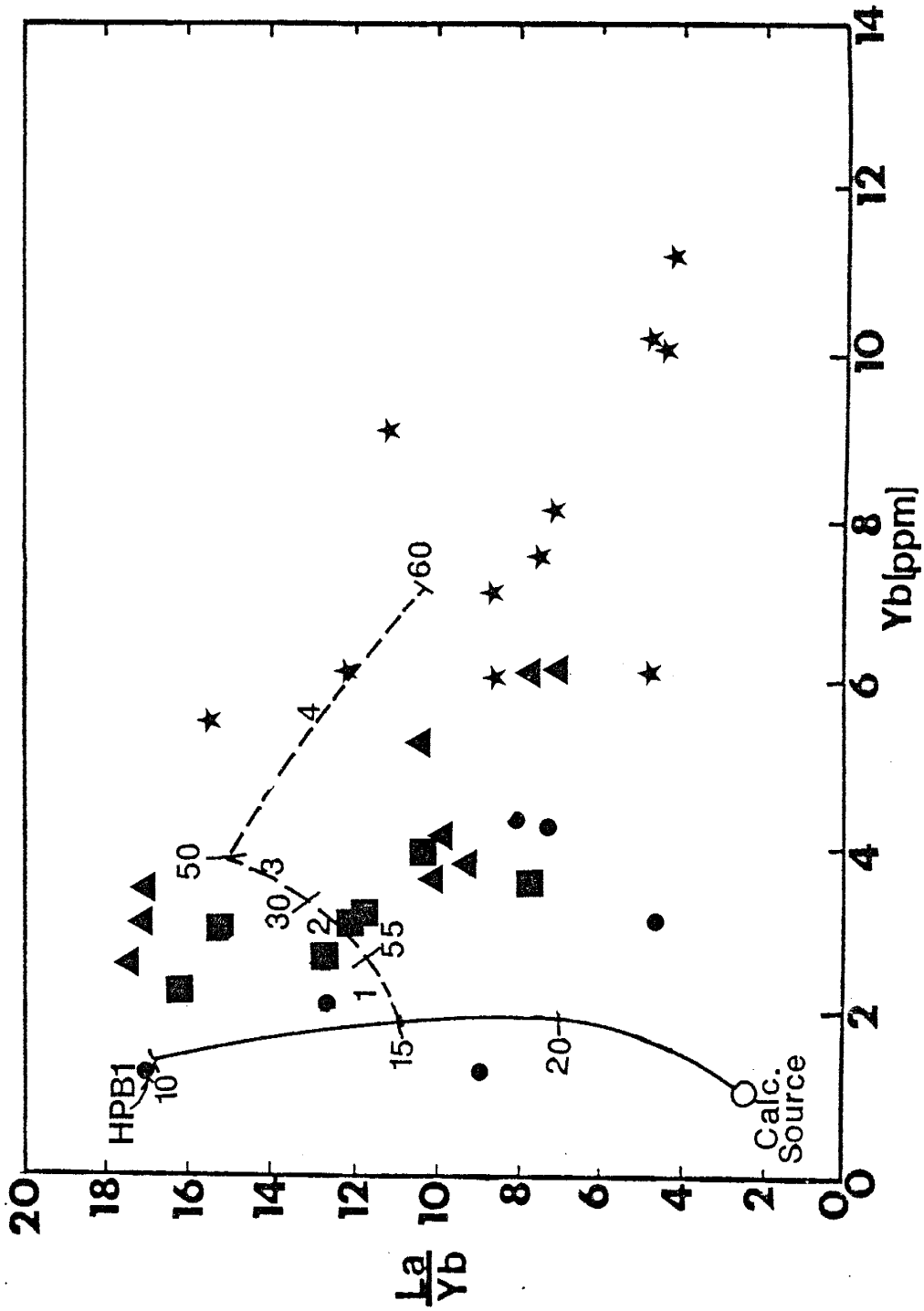

Figure 27. Distribution of the Tonto Basin igneous rocks on the La/Yb vs. Yb diagram. Solid line represents batchmelting curve. Dashed line represents FXL curve. Numbers indicate percent batch melting and FXL, respectively. Numbers 1,2,3, and 4 correspond to the four stage FXL model. Symbols as in figure 25.

Fractional Crystallization Models

Volcanic rocks of intermediate to felsic composition in Tonto Basin can be derived from associated basalts by shallow closed system fractional crystallization. The geochemical modeling presented here is divided into four stages (Table V). Stage 1 involves the production of the basalts from the parental magma and has already been discussed.

Stage 2 involves the production of andesitic liquids from the basalt produced in Stage 1. Approximately 30% FXL of olivine, clinopyroxene, plagioclase, and magnetite (Table V) is required. From Figures 25, 26, and 27 it can be seen that Stage 2 of the FXL model effectively covers the range of andesites though the calculated andesite is slightly high in TiO_2. Figure 28B shows the REE pattern of the calculated andesite compared to an average of 8 Tonto Basin andesites. The calculated andesite has an identical pattern to the average but is slightly enriched in all REE. The high field strength element concentrations of the calculated andesite also compare well with the measured concentrations of these elements (Nb is slightly high). LIL elements are variable but typically low compared to measured concentrations.

Overall the match of the trace element concentrations of the calculated andesite with Tonto Basin andesites is good. Major element mixing calculations between basalts and andesites from the Mazatzal Mountains (Reed, 1988) yield squared residuals of 0.12 to 0.14 indicating that formation of andesite by FXL of basalt is a statistically valid model for the Alder Group rocks. The presence of zoned plagioclase phenocrysts in the Tonto Basin andesites may also support and FXL origin.

In Stage 3, dacitic liquids are modelled as derivatives of the andesitic liquids produced in Stage 2. By crystallizing an assemblage of orthopyroxene, clinopyroxene, plagioclase, and magnetite with traces of zircon and allanite (Table V) until the mass fraction of crystals reaches 50% a dacitic liquid is produced (Figs.25, 26, and 27). LIL element concentrations of the calculated dacite are variable but generally slightly low. HFSE are in good agreement with measured concentrations in Tonto Basin dacites except for Zr and Nb which are slightly enriched and Sc which is low. LREE are slightly enriched and HREE slightly

TABLE V

Modes and amounts of FXL for closed system FXL models.

Stages	1	2	3	4
Mineral	Basalt 1-F=55%	Basalt to Andesite 1-F=30%	Andesite to Dacite 1-F=50%	Dacite to Rhyolite 1-F=60%
Olivine	0.8	0.122		
Orthopyroxene			0.15	0.08
Clinopyroxene	0.2	0.23	0.27	0.10
Plagioclase		0.61	0.53	0.71
Magnetite		0.05	0.05	0.06
Quartz				0.05
Zircon			0.0003	0.0003
Allanite			0.0002	0.0002

1-F = Degree of fractional crystallization in %. Numbers at top of column keved to trajectory segments on Figures 25, 26, and 27. Modes are based on typical FXL modes for liquids of these compositions from modern volcanics.

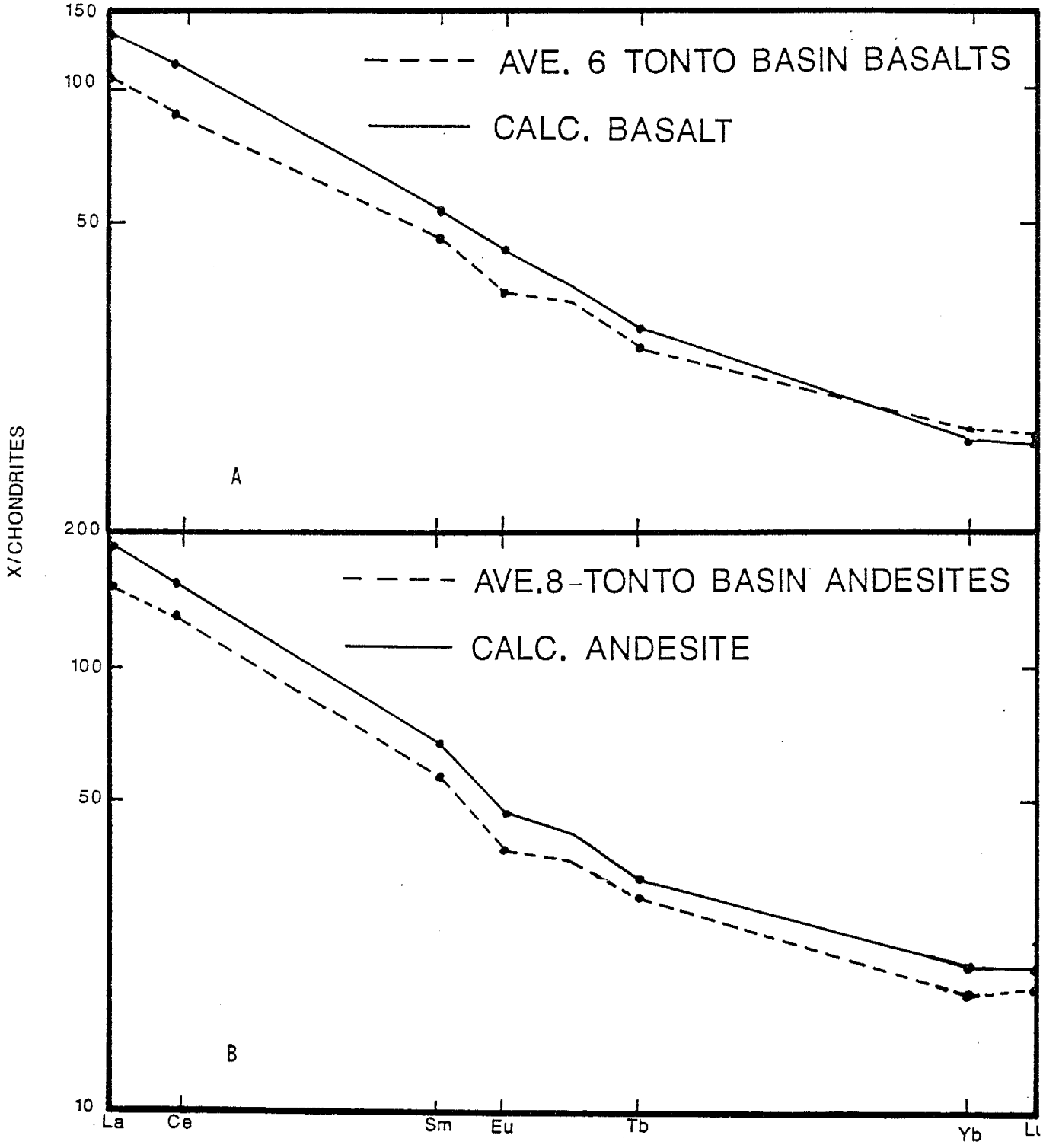

Figure 28. A.) REE plot of calculated basalt and average basalt. B.) REE plot of calculated andesite and average andesite.

depleted compared to an average of 9 Tonto Basin dacites (Fig. 29A). Again, the REE content of the calculated dacite falls within the range of observed REE concentrations of the Tonto Basin dacites. Major element mixing calculations (Reed, 1988) were unsuccessful in relating dacite to any of the andesites from the Mazatzal Mountains. However, only one dacitic sample was analyzed by Reed (1988) and it is possible that it was altered. The agreement of trace element concentrations of the calculated dacite with the Tonto Basin dacites suggests that the model is possible. Trace amounts of zircon and allanite are needed to produce a better fit of the LREE and Zr and a high Kd for Ti in magnetite (25) is required to lower the Ti content of the dacites.

The origin of the Tonto Basin rhyolites is problematical. Reed (1988) showed that major element mixing calcultions are unsuccessful in relating the rhyolites to associated dacites, suggesting that a FXL origin for the Alder and Red Rock rhyolites is unlikely. When plotted on tectonic discriminant diagrams (see next section) data give mixed results. Both within-plate (suggesting a lower crustal melting origin for the rhyolites) and arc (suggesting either FXL or partial melting of the lower crust, or both) settings for the Tonto Basin rhyolites are indicated.

Stage 4 of the FXL models (Table V) evaluates FXL as an origin for Tonto Basin rhyolites. The dacitic liquid obtained in Stage 3 is allowed to crystallize 60% of an assemblage of orthopyroxene, clinopyroxene, plagioclase, magnetite, and quartz with traces of zircon and allanite. The resulting composition is similar to the Tonto Basin ryholites but the match is not as good as that obtained for the basalts, andesites, and dacites in terms of REE contents (Fig. 29B). LREE are enriched and HREE are depleted compared to an average of 10 Tonto Basin rhyolites (Fig. 29B). LIL elements are generally enriched compared to measured concentrations. HFSE show adequate agreement but Zr is enriched by a factor of 1.3 and Nb by a factor of 1.8 when compared to measured concentrations.

Stage 4 of the FXL model only brings the composition of the liquid to the edge of the range of rhyolites in Figure 25. Open system FXL could effectively move the composition of the liquid in Stage 4 to cover the entire range. Three late stage high silica+alkalies

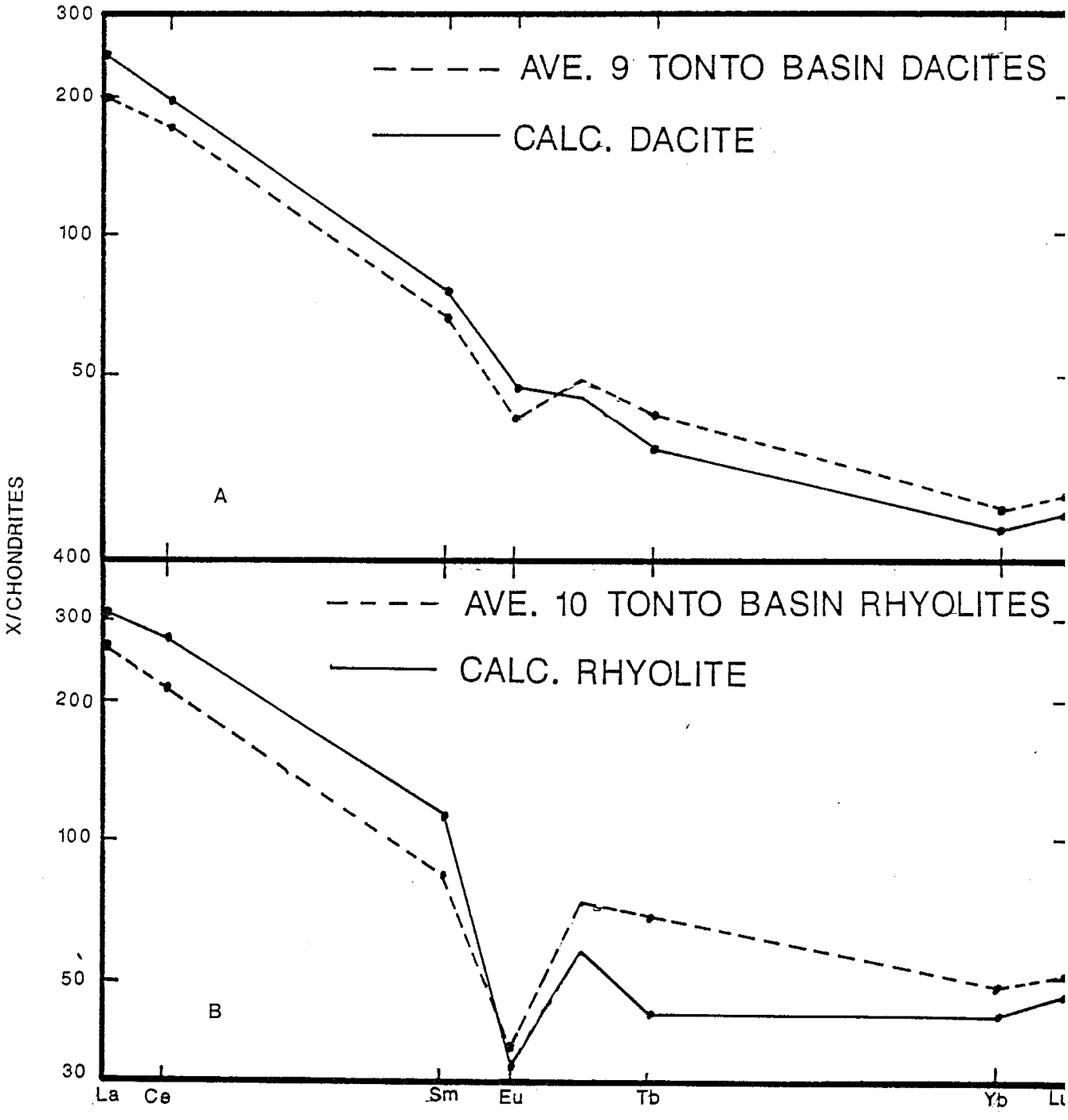

Figure 29. A.) REE plot of calculated dacite and average dacite. B.) REE plot of calculated rhyolite and average rhyolite.

rhyolites (GR-3, OX-2, and OX-5) plot below the graph at low TiO_2 values. GR-3 is a hypabyssal intrusive rhyolite and OX-2 and OX-5 are rhyolites from the last stage of felsic volcanism during Red Rock time (i.e. the Oxbow Mountain Rhyolite). Due to their highly differentiated nature these three rhyolites plot away from the main group of rhyolites.

In figure 26, Stage 4 of the FXL model covers most of the range of the rhyolites. This suggests that open system FXL is not required and thus the variability in the data must be explained without calling upon open system FXL. The three late stage rhyolites plot at low Zr and Zr/Y values attesting to their highly differentiated nature.

The "kink" in the FXL trajectory at Stage 4 (Fig. 27) is due to the substitution of felsic Kds for intermediated Kds into the fractional crystallization equation. This results in La being preferentially incorporated into zircon and allanite to a higher degree than for Stage 3 and thus the La/Yb ratio drops. Here again, Stage 4 cannot cover the spread in the rhyolite data and it seems that either the rhyolites did not form by FXL of dacitic liquids or that open system FXL is required. If open system FXL is called upon then much more zircon must fractionate out of the magma in order to control the Zr contents (see Figures 25 and 26).

The trace amounts of zircon and allanite are required to produce a better match for the LREE and Zr abundances. The Kd for Ti in magnetite has to be increased to 35 in order to lower the Ti content of the calculated rhyolite to a value compareable to measured concentrations. Due to the relatively poor match of the trace element distributions between modelled and measured rhyolite and the failure of major element mixing calculations (Reed, 1988) a FXL origin seems unlikely, but cannot be ruled out.

It must be noted that most rhyolites modelled here are from the Flying W Formation. Most samples of dacites and rhyolites collected from the Red Rock Group plot is the same area as the Alder dacites and rhyolites with the exception of the three late stage rhyolites. The limited data from the Red Rock Group suggests that the Winter Camp and Haigler Formation volcanics may be genetically related to Alder Group volcanics. The Oxbow Mountain Rhyolite, however, may have originated from a seperate magma chamber since most of these rhyolites plot away from the Flying W and Haigler rhyolites. Obviously, much

more data is needed to constrain the origin of the Red Rock Group and its relation to the Alder Group.

Several possibiliteis exist to explain the variability of the Tonto Basin volcanics. A mantle source with a variable composition could move the batch melting trajectory. For example, a mantle source with slightly less TiO_2 and Zr would move the batch melting trajectory in such a way that the FXL vectors would be centered through most of the data points. Also, by starting FXL at a higher degree of melting of the mantle source, the FXL vectors could be moved so as to pass through most of the data points. In other words, a variable source composition, variable degrees of partial melting of the source, variability in the crystallizing modes in the FXL models, crustal contamination, and open system FXL as opposed to closed system FXL could be called upon to explain the variation in the data.

These models were presented to help constrain possible genetic relationships of the volcanic rocks in Tonto Basin. It is possible, and quite likely, that the basalts, andesites, and dacites are related by closed system FXL. The rhyolites may be related to the dacites by FXL but this cannot be determined with any degree of certainty. Due to the high variability of the data and the numerous processes that can affect melting and crystallization relationships, these models merely suggest that genetic relationships are possible and should not considered as evidence that the Tonto Basin volcanic rocks formed by FXL.

Melting of the Lower Crust

Although the Tonto Basin rhyolites may be related to the dacites by FXL, there is some evidence that this is not the case (i.e. the failure of major element mixing calculations to relate the dacites to the rhyolites and the fact that some tectonic discriminant diagrams suggest a within-plate origin for the rhyolites). Is is possible that the rhyolites formed by partial melting of the lower crust. Reed (1988) carried out major element mixing calculations between the composition of the lower crust (Weaver and Tarney, 1984) and a Red Rock Group rhyolite. The sum of the squared residuals ranges from 0.08 to 0.16 which suggests that the formation of the rhyolites by partial melting of the lower crust is statistically viable.

A 10% melt of the lower crust produces a rhyolitic liquid which is similar in major element contents to the least differentiated Tonto Basin rhyolites. In order to generate rhyolites that are more differentiated (i.e. more enriched in HFSE, HREE and depleted in compatible elements) it is proposed that the magma generated during the melting event underwent fractional crystallization (mode given in table VI). REE plots of the calculated rhyolite (10% melting of the lower crust followed by 30% closed system FXL) and an average of 10 Tonto Basin rhyolites is shown in figure 30. Light REE are enriched by a factor of ≈1.2 and heavy REE by a factor of ≈2 compared to the average. The addition of trace amounts of allanite to the crystallizing assemblage can decrease the concentration of the LREE. Since HREE are concentrated in zircon (and to a lesser extent allanite) and clinopyroxene, smaller amounts of these minerals in the mode may cause the liquid to be more enriched in these elements. Also, if garnet is present in the lower crust (i.e. garnet granulite), the melting of garnet will enrich the liquid in HREE.

Figures 31, 32, and 33 show the lower crustal melting model followed by 30% closed system FXL. In figure 31 it can be seen that a 10% melt of the lower crust produces a rhyolitic liquid but this liquid is too enriched in TiO_2 and slightly depleted in Zr compared to the Tonto Basin rhyolites. Thirty percent closed system FXL of this liquid (involving ilmenite) can bring the TiO_2 contents down somewhat. Zr contents are affected by the amount of zircon crystallizing. Since the composition of the lower crust is not well constrained, variations in lower crustal compositions could effectively change the composition of the 10% melt so as to produce a liquid closer to the compostion of the Tonto Basin rhyolites. Of course, the resulting liquid after 30% FXL would likewise be affected. Crustal contamination may also play a role. It does not appear that open system FXL is required. An increase in the proportion of ilmenite in the FXL mode could deplete the liquid in TiO_2 to the degree seen in the Tonto Basin rhyolites.

Figure 32 shows that the 10% melt followed by 30% closed system FXL provides a fairly good match to the Tonto Basin rhyolites in terms of Zr and Y contents. Again,

TABLE VI

Mode and melt proportions for batch melting of the lower crust; mode and amount of FXL used to produce the Tonto Basin Rhyolites.

	Lower Crust		Felsic FXL Assemblage
Mineral	Mode	Melt	Mode (1-F=30%)
Orthopyroxene	0.05	0.02	0.12
Clinopyroxene	0.02	0.02	0.05
Plagioclase	0.65	0.42	0.72
Biotite	0.05	0.11	0
Quartz	0.18	0.42	0.07
Ilmenite	0.05	0.01	0.04
Zircon	0.0004	0.001	0.001
Allanite	0.0001		0

Composition of the lower crust from Weaver and Tarney (1984). Mode and melt proportions and FXL mode from Reed (1988).

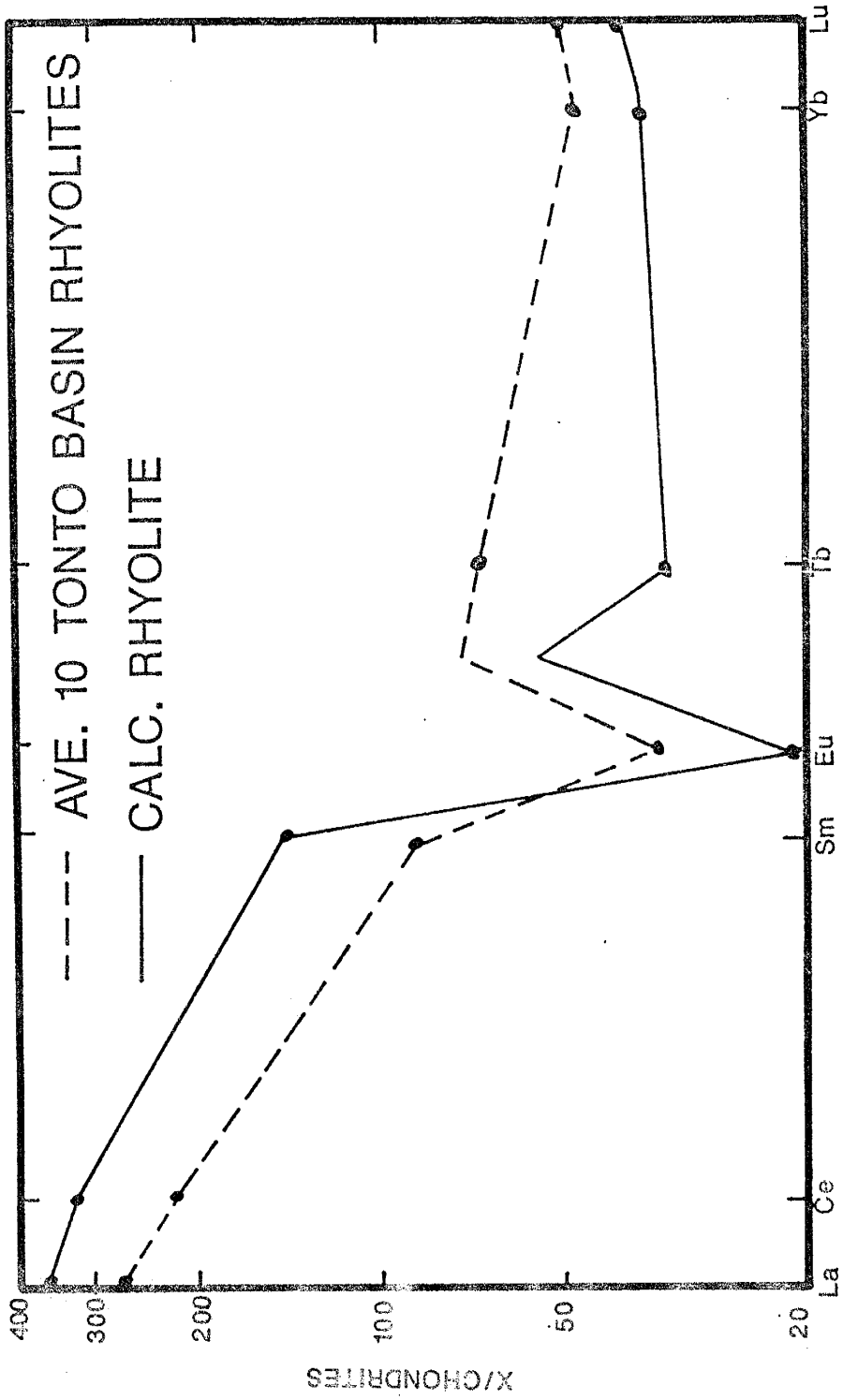

Figure 30. REE plot of calculated rhyolite (lower crustal melting model) and average Tonto Basin rhyolite.

variations in lower crustal composition or crustal contamination could account for the slight variation in the Zr/Y ratio observed in the rhyolites.

In Figure 33 the lower crustal partial melting vector approaches the Tonto Basin rhyolites at 10% melting. The 30% closed system FXL of the melt can account for some of the rhyolites. An increase in the amount of FXL to ≈50% effectively covers the range of Yb concentrations in the Tonto Basin rhyolites (except for the three late stage rhyolites). The range in the La/Yb ratio can be explained by source composition variations, crustal contamination, and/or by variable amounts of trace minerals (zircon and allanite) in the residue.

Due to the uncertainties in estimated lower crustal compositions, an accurate model for the generation of the Tonto Basin rhyolites by lower crustal melting is difficult to produce. In fact, most data suggests that rhyolite cannot be produced by melting of basalt and the lower crust is probably composed of basaltic material. Perhaps a middle or upper crustal melting model would be a more realistic approach. However, the data presented above suggests that it is possible to produce the Tonto Basin rhyolites by partial melting of the lower crust. Major element mixing calculations (Reed, 1988) support a partial melting of the lower crust origin for the Alder-Red Rock rhyolites and variations in the data can be explained in a number of ways including variable source composition, variable mode-melt proportions, variable FXL modes, and crustal contamination. It is not possible to determine whether the Tonto Basin rhyolites formed by FXL from dacitic liquids or by partial melting of the lower crust with the available data. An isotopic study of the Tonto Basin igneous rocks may help in determining the origin of the rhyolites.

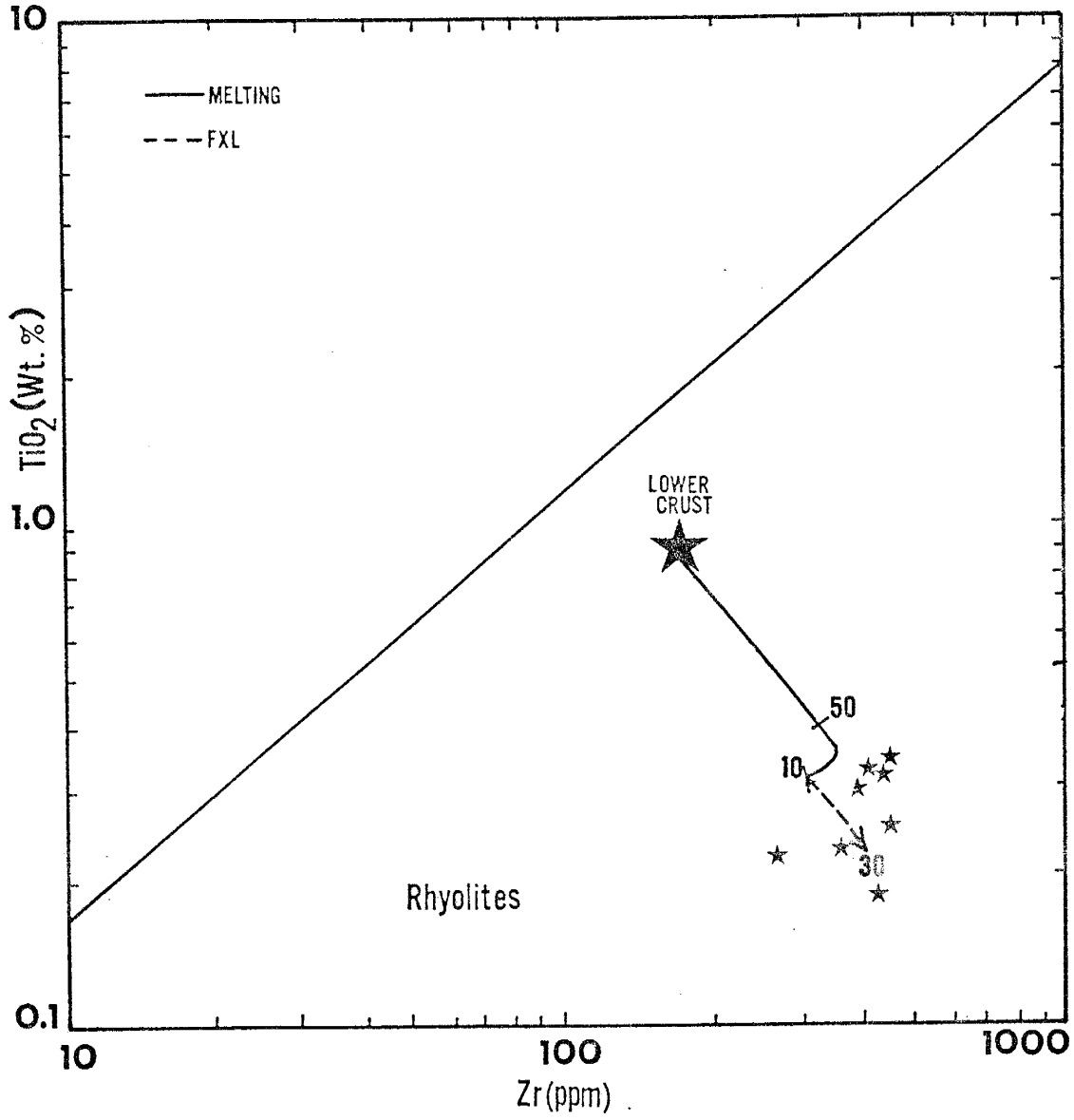

Figure 31. Distribution of Tonto Basin rhyolites on the TiO_2 vs. Zr diagram. Solid line represents batch melting curve and dashed line represents FXL curve for lower crustal melting model. Numbers indicate degree of melting and FXL in percent, respectively. Rhyolites represented as stars. Large star is the composition of the lower crust after Weaver and Tarney (1984).

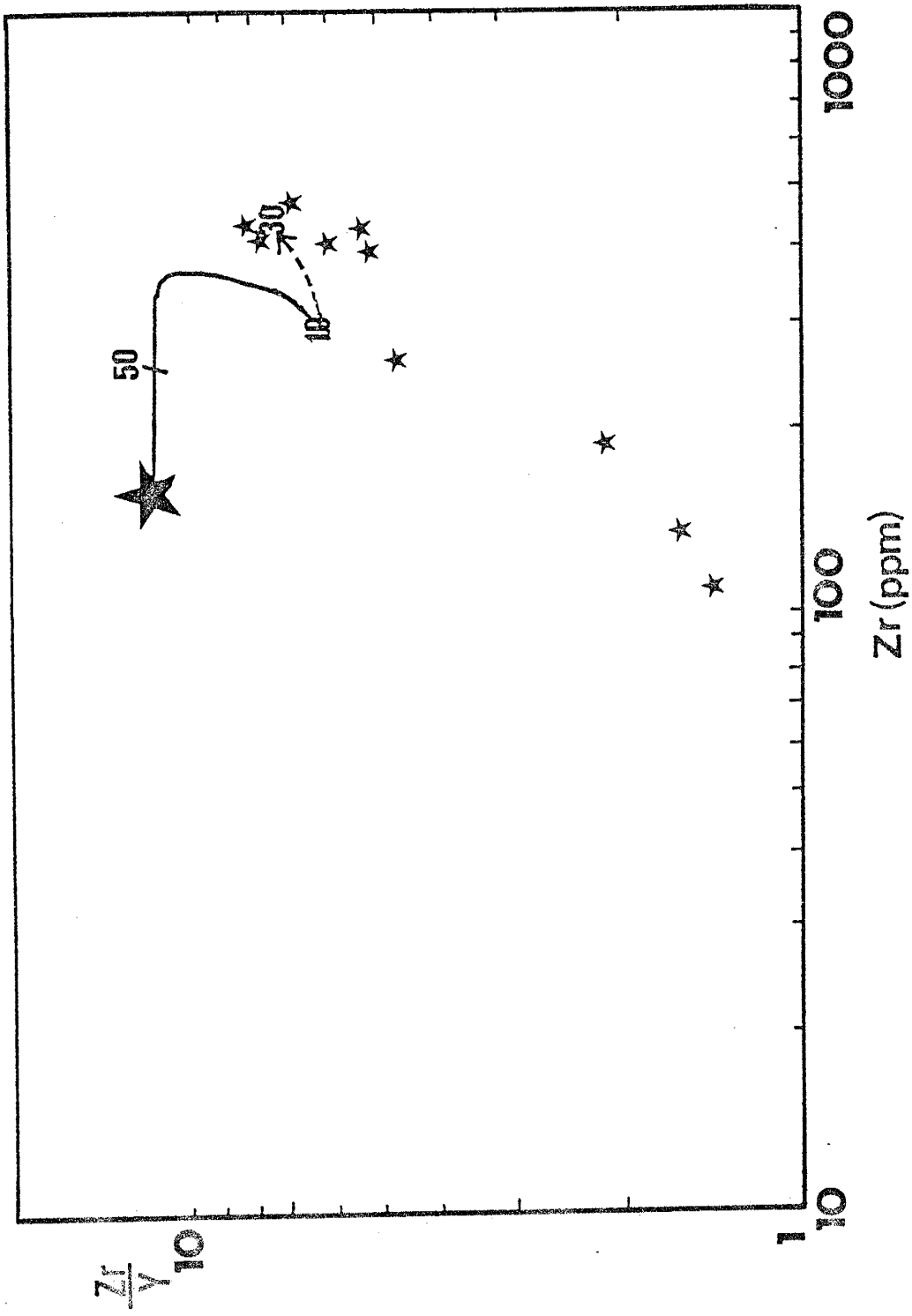

Figure 32. Distribution of Tonto Basin felsic rocks on the Zr/Y vs. Zr diagram. Solid line represents batch meltin curve and dashed line represents FXL curve for the lower crustal melting model. Numbers indicate degree of melting and FXL in percent, respectively. Large star represents composition of the lower crust after Weaver and Tarney (1984). Small stars represent rhyolites.

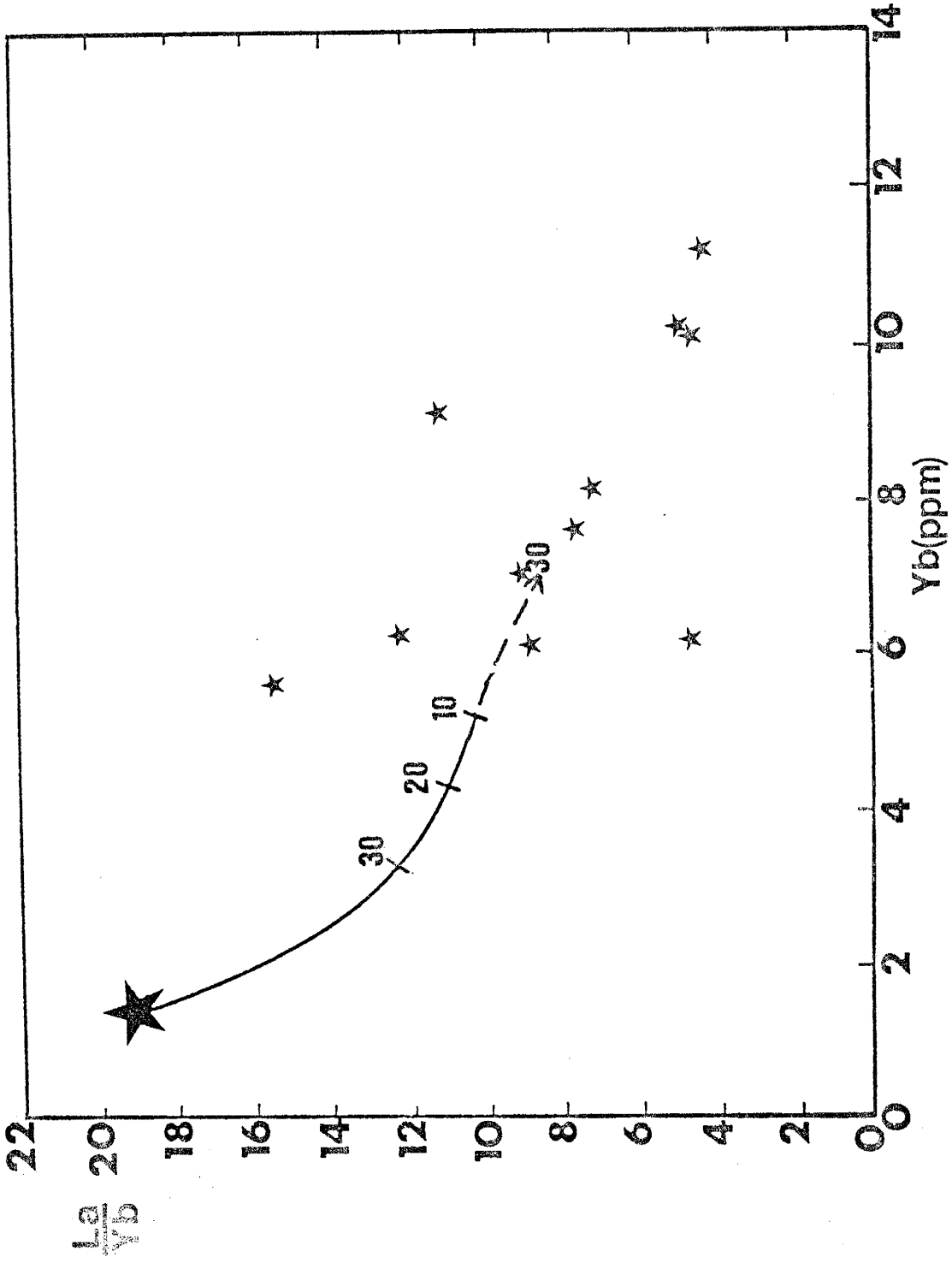

Figure 33. Distribution of the Tonto Basin felsic rocks on the La/Yb vs. Yb diagram. Solid line represents batch melting curve and dashed line represents FXL curve for the lower crustal melting model. Numbers indicate degree of partial melting and FXL in percent, respectively. Large star represents the composition of the lower crust after Weaver and Tarney (1984). Small stars represent rhyolites.

TECTONIC DISCRIMINANT DIAGRAMS

Over the past 15 years, many researchers have demonstrated that volcanic rocks erupted within specific tectonic settings carry with them distinctive trace and major element signatures (Pearce and Cann, 1973; Wood, 1980; Pearce 1982, 1983; Meschede, 1986). As a result of this, many tectonic discrimination diagrams have appeared in the literature. The application of these diagrams to Precambrian rocks is somewhat limited. This is due to the assumption that the relationships between the element distributions and tectonic setting has not changed with time and that element distributions are characteristic of only one tectonic setting.

There are several examples where rocks of a known tectonic setting (determined by methods other than geochemistry) plot incorrectly on geochemical tectonic discriminant diagrams (Arculus, 1987; Duncan, 1987; and Marsh, 1987). Arculus (1987) has shown cases of arc-related basalts plotting in ocean floor fields, and within-plate volcanics plotting in arc-related fields. Duncan (1987) demonstrates that some of the Karoo flood basalts of South Africa (which are clearly within-plate volcanics) also plot in arc-related fields. Marsh (1987) has shown that many continental flood basalts do not plot in within-plate fields but rather have geochemical signatures similar to ocean floor basalts and sometimes arc basalts. Clearly the assumption that certain element distributions are characteristic of only one tectonic setting is not valid.

The enrichment of LIL elements with respect to HFSE and REE and the depletion of Nb and Ta with respect to other HFSE and REE has been interpreted as being unique to arc settings. These enrichments and depletions are usually attributed to devolatilization of the subducted slab and retention of Nb and Ta in the slab, respectively. However, Arculus (1987) points out that similar element distributions can occur in within-plate settings by reactions of high-SiO_2 melts with mantle peridotite, crustal contamination involving the lower crust, or by mantle metasomatism. Duncan (1987) also suggests that mantle metasomatism may be responsible for arc signatures in within-plate volcanics. Another possibility is that

subduction occurred at some place and time in the past and that the observed enrichments and depletions are characteristic of arcs and the mantle retained these element enrichments and depletions. Subsequent plate motions could result in this portion of the mantle being located underneath, and well within a plate. Later rifting of this plate could tap this mantle containing the subduction zone component resulting in within-plate volcanics with a subduction zone signature (Duncan, 1987).

It is apparent that detailed petrogenetic interpretations of data from tectonic discriminant diagrams is severely limited. However, when used in conjunction with field relations (i.e. structural, metamorphic and deformational interpretations, and relationships of volcanic rocks to sedimentary rocks, etc.) tectonic discriminant diagrams can, and often do, provide useful information.

The following series of tectonic discriminant diagrams is presented in an attempt to compare the Tonto Basin volcanics to volcanics from modern tectonic settings.

Figure 34 shows that Tonto Basin mafic rocks have a striking similarity to modern basalts from continental margin arc systems. In Figure 35 the mafic rocks plot in the volcanic arc field. When the altered Tonto Basin basalts and basalts from the Mazatzal Mountains are included on this diagram the samples plot in a trend that is transitional from the EMORB field to the arc field. According to Tarney et al. (1981) and Pearce (1985) some volcanic rocks from incipient back-arc or intra-arc basins may show a similar trend and this may characterize marginal basins that form within or near continental crust (Knoper and Condie, 1987).

As mentioned earlier, NMORB-normalized diagrams showing incompatible element distributions of Tonto Basin mafic volcanics (Fig. 36) suggest a subduction zone component. The enrichment in LIL elements relative to Nb-Ta is characteristic of arc rocks. Also on Figure 36, average Phanerozoic basalts from various tectonic settings are also shown (Knoper and Condie, 1987). The Tonto Basin mafic volcanics appear to be most similar to modern basalts erupted within back-arc basins.

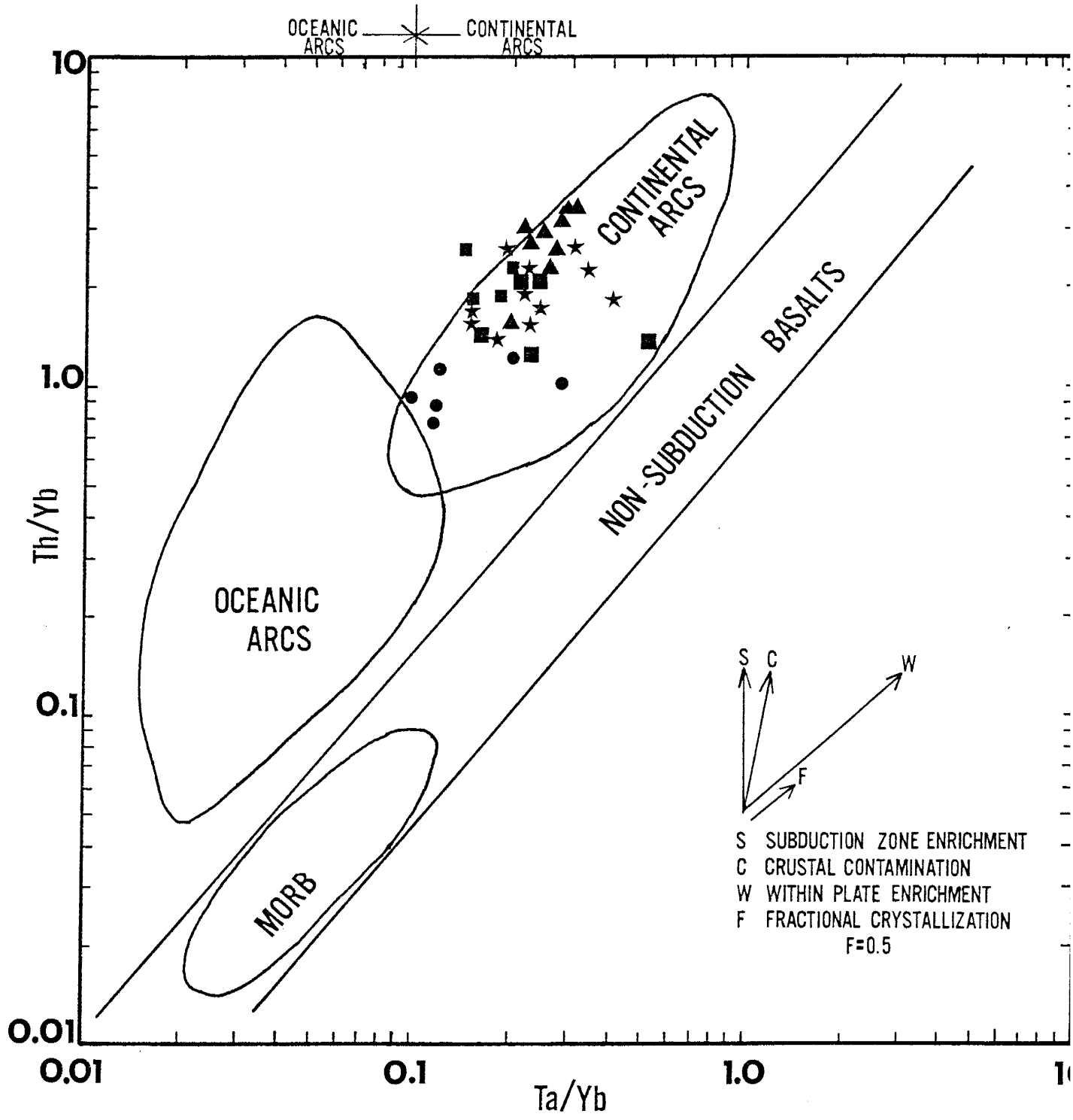

Figure 34. Distribution of Tonto Basin igneous rocks on the Th/Yb vs. Ta/Yb tectonic discriminant diagram of Pearce (1982). Symbols as in Figure 25.

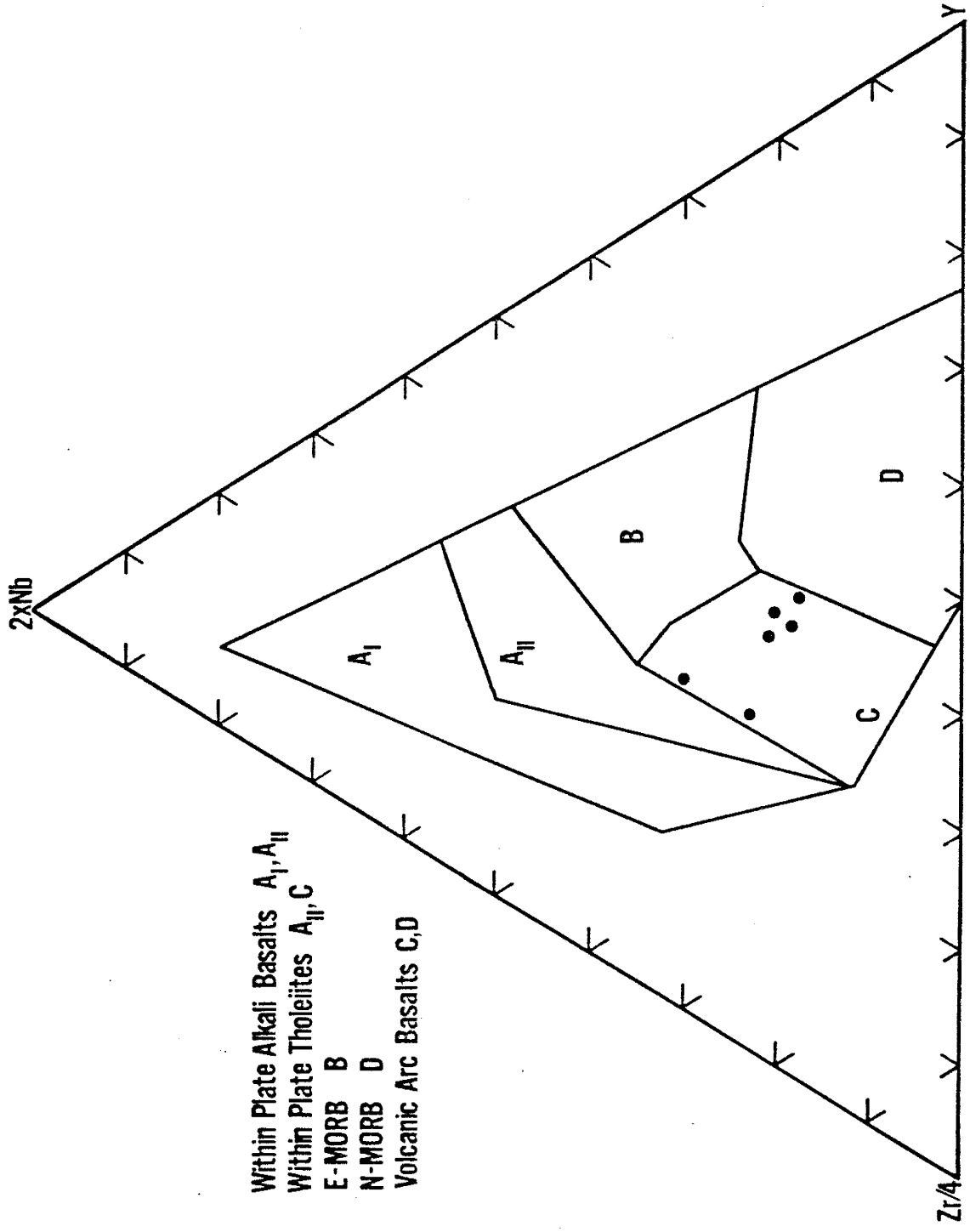

Figure 35. Distribution of Tonto Basin mafic rocks on the Zr-Nb-Y tectonic discriminant diagram of Meschede (1986).

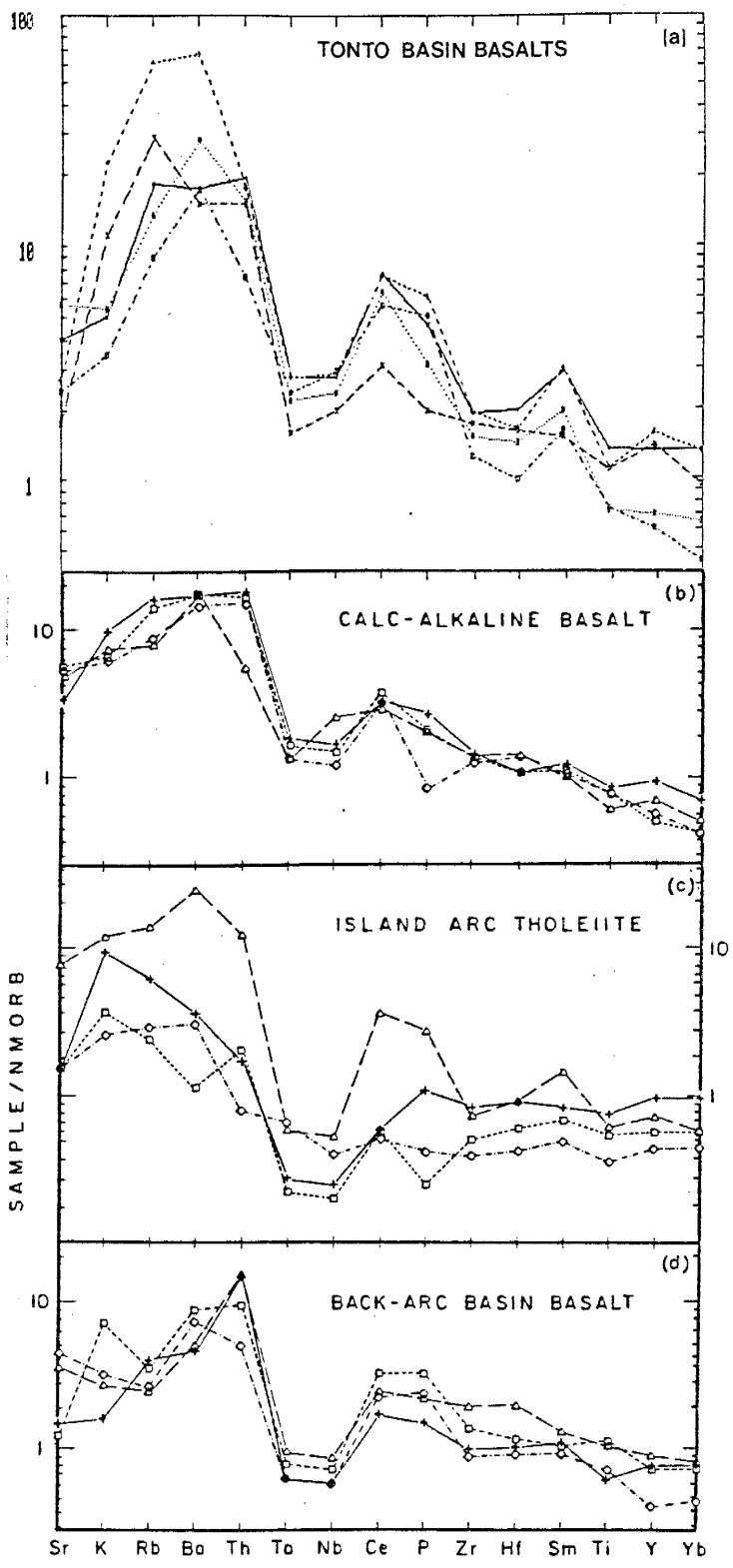

Figure 36. a. NMORB-normalized plot of Tonto Basin mafic rocks. b.-d. Average Phanerozoic basalts from various tectonic settings (Knoper and Condie, 1987). Normalizing values from Pearce (1983).

In Figure 37 volcanics of all compositions plot nearly exclusively in the volcanic arc field. Note that there is no apparent trend from the EMORB field to the arc field as in Figure 35. However, in Figure 38 (and on the NMORB-normalized diagrams) the Tonto Basin mafic volcanics appear to be enriched in Th. This enrichment displaces the mafic rocks closer to the Th apex on the Th-Hf/3-Ta diagram removing the apparent trend.

Results of other tectonic discrimination diagrams are summarized in Table VII. The data suggest that the Tonto Basin mafic to intermediate rocks are most similar to modern volcanics from continental margin arcs whereas the felsic rocks have both within-plate and arc signatures.

On most discriminant diagrams for felsic rocks the Tonto Basin samples display an unusually high degree of scatter. For the most part felsic rocks tend to plot dominantly in within plate fields (Figures 39 and 40). In contrast, Figure 41 indicates that the felsic rocks are arc related. NMORB-normalized diagrams for the Tonto Basin felsic volcanics (Fig. 42) also show an arc affinity. One possible explanation for this apparent contradiction is that the felsic volcanic rocks originated in a back-arc basin. Perhaps the back-arc basin underwent rifting giving the felsic volcanics a within-plate character but the magmas retained or inherited a subduction zone signature from the arc proper. Subduction zone signatures have been identified in volcanic rocks from within-plate settings (e.g. the Karoo basalts, Duncan, 1987; Marsh, 1987).

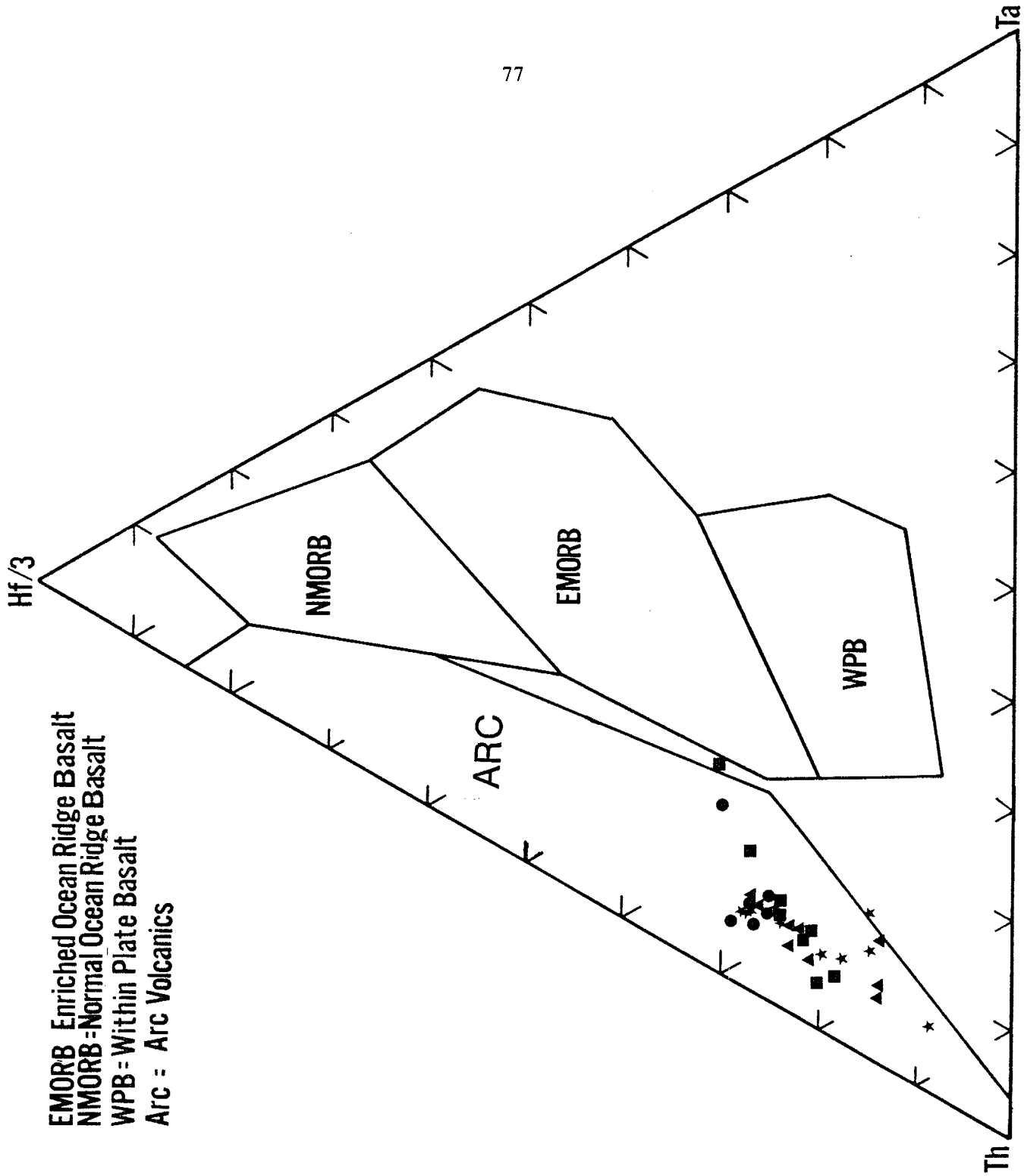

Figure 37. Distribution of Tonto Basin igneous rocks on the Th-Hf-Ta tectonic discriminant diagram of Wood (1980). Symbols as in Figure 25.

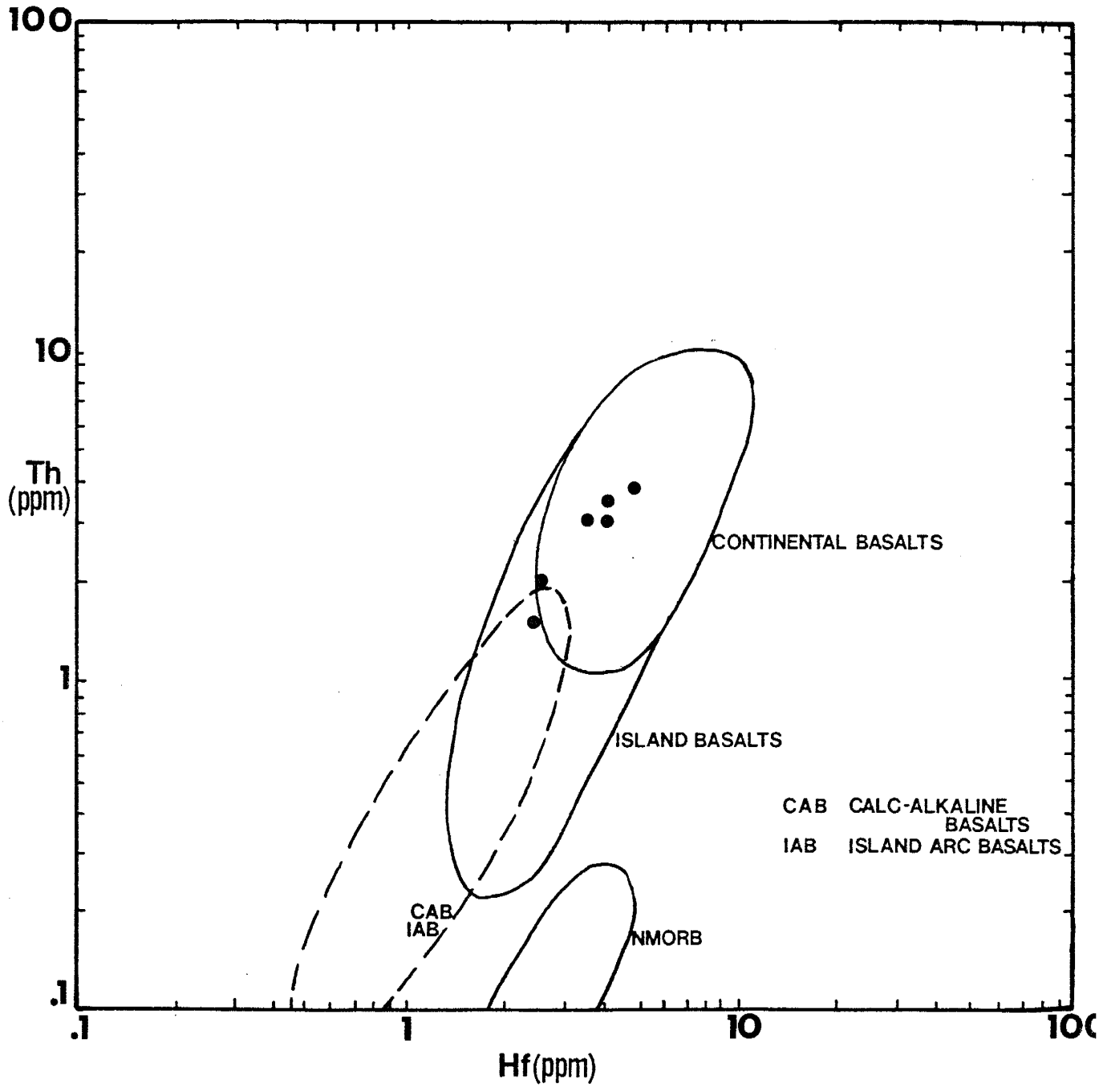

Figure 38. Distribution of Tonto Basin mafic rocks on the Th vs. Hf tectonic discriminant diagram of Wood et.al. (1979).

TABLE VII

Compliation of results of tectonic discrimination diagrams.

Diagram	Mixed	WPB	Cont. Arc	Oceanic Arc	Reference
Th/Yb vs. Ta/Yb	0	0	100	0	Pearce (1982)
TiO_2 vs. Zr	0	68	32	0	Pearce (1982)
Zr-Nb-Y	100	0	0	0	Meschede (1986)
Zr-Ti-Y	0	35	65	0	Pearce and Cann (1973)
V vs. TiO_2	0	100	0	0	Hodder (1985)
Th vs. Ta	100	0	0	0	Drury (1983)
La vs. Ta	0	0	100	0	Drury (1983)
Th-Hf-Ta	0	0	100	0	Wood (1980)
Ti vs. Cr	0	0	85	(MORB=15%)	Garcia (1978)
MnO-TiO_2-P_2O_5	0	0	100	0	Mullen (1983)
Th vs. Hf	17	83	0	0	Wood et al. (1979)
La/Yb-Yb	0	100	0	0	Condie (1986)
Zr/Y-Zr	0	0	50	(MORB=50%)	Pearce and Cann (1973)

Number equals % of samples plotting in each field.
WPB=Within Plate Basalt
Cont. Arc=Continental Arc

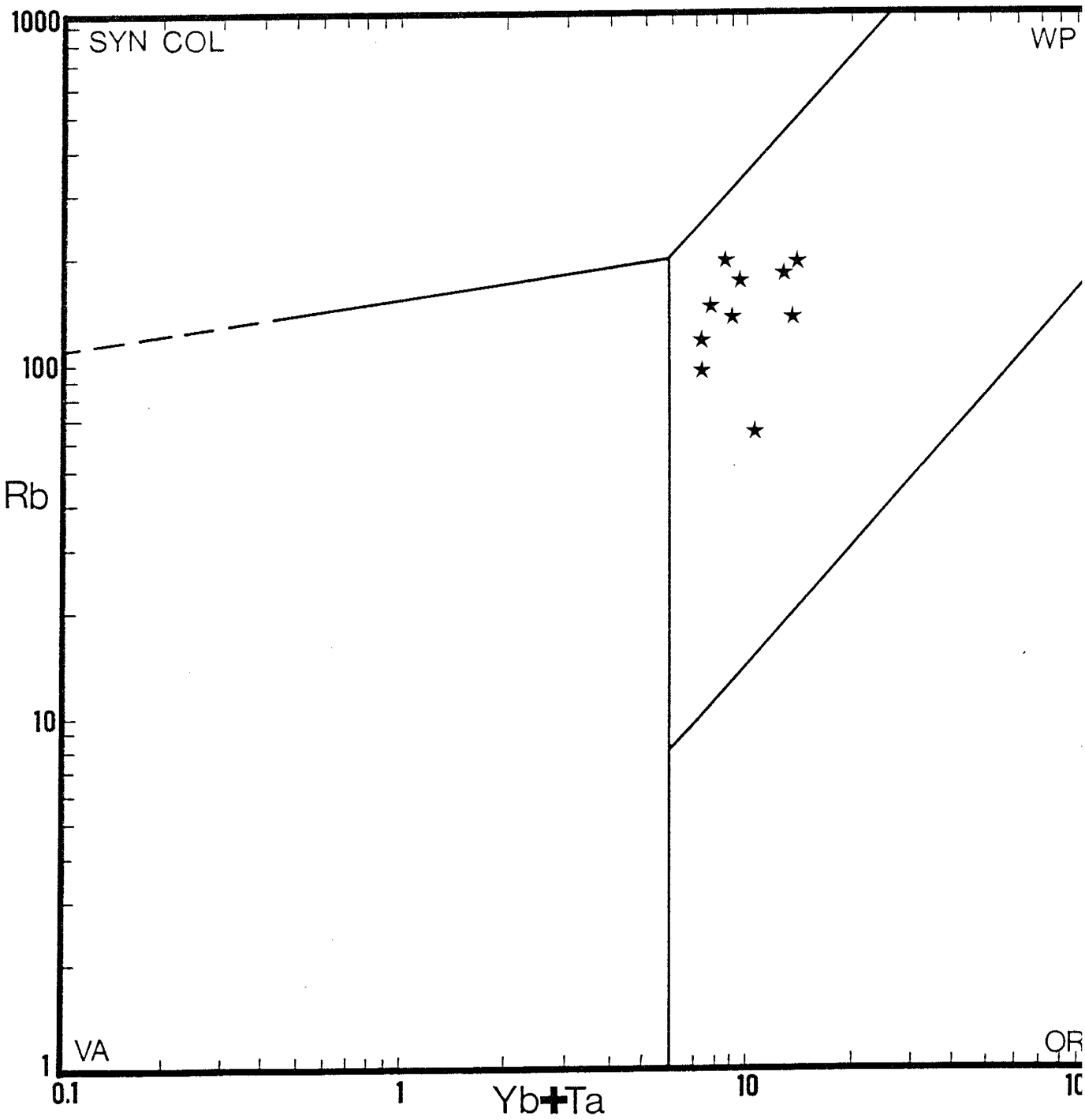

Figure 39. Distribution of Tonto Basin rhyolites on the Rb vs. Yb+Ta tectonic discrimination diagram of Pearce et al. (1984). WP=within-plate, OR=ocean ridge, VA=volcanic arc, and SYN COL=syncollisional.

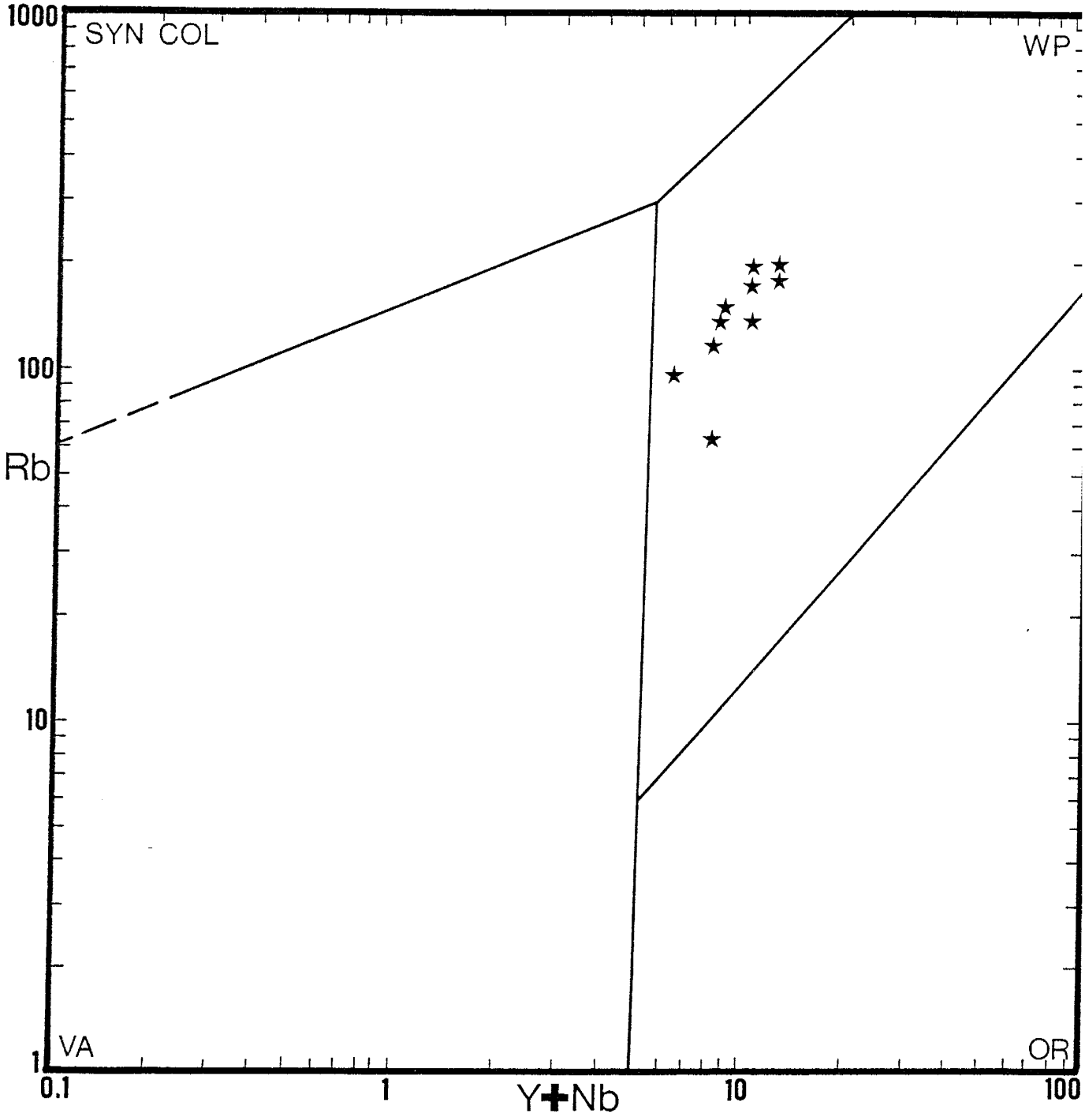

Figure 40. Distribution of Tonto Basin rhyolites on the Rb vs. Yb+Nb tectonic discrimination diagram of Pearce et al. (1984). WP=within-plate, OR=ocean ridge, VA=volcanic arc, and SYN COL=syncollisional.

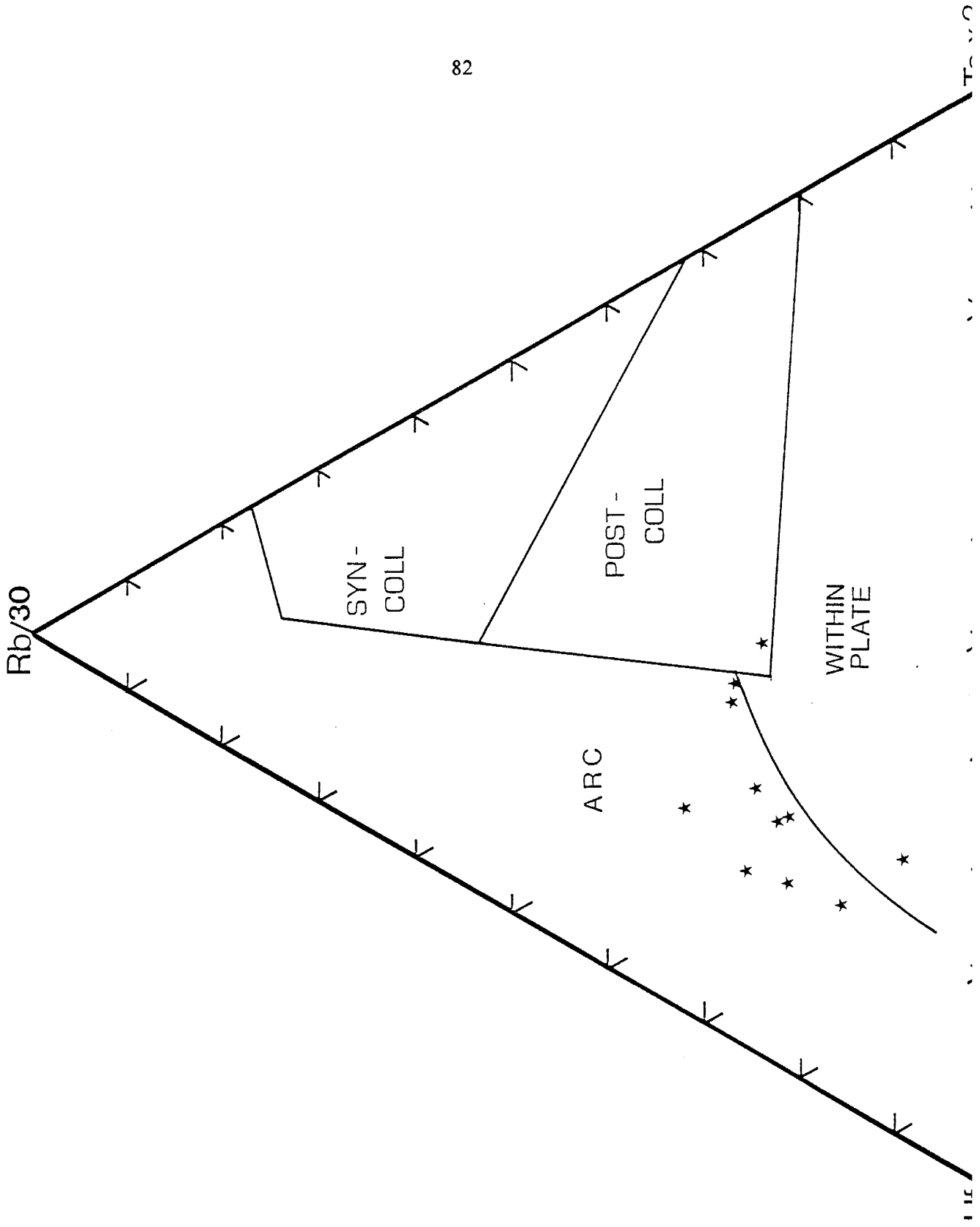

Figure 41. Distribution of Tonto Basin rhyolites on the Hf-Rb-Ta tectonic discrimination diagram of Harris et al. (1986).

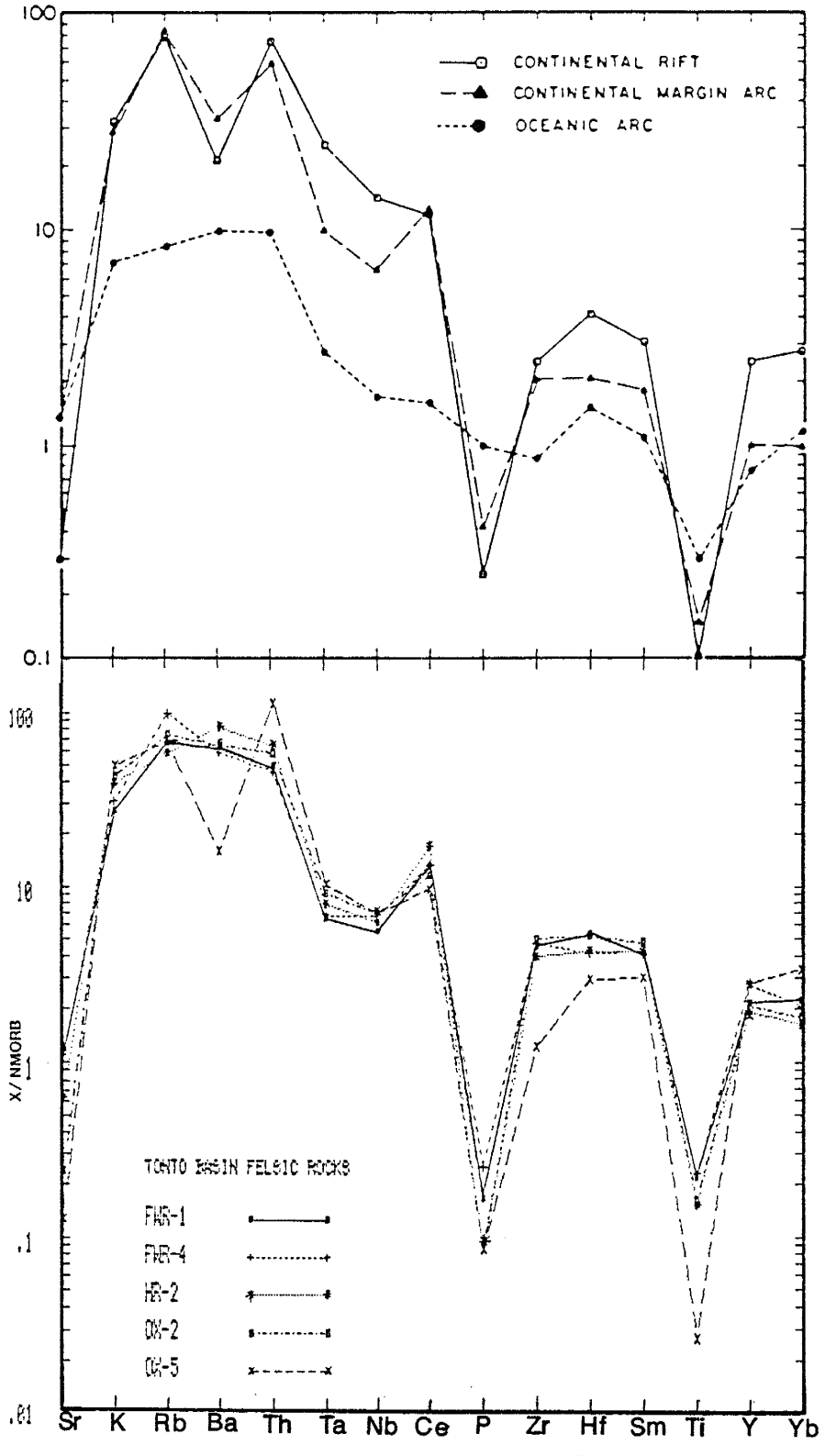

Figure 42. a. NMORB-normalized diagram showing the distribution of Tonto Basin rhyolites. b. Average Phanerozoic rhyolites from various tectonic settings (Condie, 1986).

SEDIMENTARY ROCKS

A variety of sediments is present in the Alder Group. Sediment types include: quartz wackes, graywackes (lithic arenites and lithic wackes), quartz arenites, pelites, conglomerates, and minor cherts and carbonates (limestones?). Detailed petrographic studies of Alder sandstones by Reed (1988) using QFL and QmFl diagrams of Dickinson and Suzcek (1979) suggest that the quartz wackes and quartz arenites reflect recycled orogen or craton provenance while the graywackes reflect arc provenance. Based on geochemistry, the pelites also have two origins--an arc-related provenance and a craton-related provenance. The arc provenance greatly dominates.

Field Relationships

Cherts and carbonates occur as approximately one inch thick beds alternating with purple slates. The bedded nature of the cherts and carbonates led Gastil (1958) to believe they were true sedimentary rocks. However, the possibility exists that they may be hydrothermal in nature and not sedimentary. Reed (1988) reports the existence of jasper beds in the Cornucopia member of the Alder Group in the Mazatzal Mountains. The jasper is interbedded with volcanics and volcaniclastics and hydrothermal carbonate. This carbonate is interbedded with purple slates much like those in Tonto Basin. Reed (1988) suggests that the presence of red jasper beds below the carbonate implies that the carbonate is hydrothermal and not a clastic sedimentary rock. The interbedded nature of the cherts and carbonates in Tonto Basin suggests that they are of sedimentary origin--not hydrothermal. Although the color of chert is usually not definitive, the bedded cherts in Tonto Basin are tan in color-not the red jasperoid commonly associated with hydrothermal vents. The only occurence of red jasper in Tonto Basin is as clasts in conglomerates and minor small fragments in lithic wackes in the formations of the Alder Group. Further studies are needed to determine the origin of these two rock types.

Conglomerates occur in all Alder Group rocks and in the Winter Camp and Haigler Formations of the Red Rock Group. They are almost always composed of clasts of volcanic

rocks, usually from pebble to cobble size and usually rest on volcanic rocks of the same composition as the clasts. Conglomerates can occur at any stratigraphic position within a formation.

Graywackes (lithic arenites and lithic wackes) usually occur interbedded with shales, conglomerates, and volcanics and sometimes with quartz arenites. Gradded bedding is common and cross-bedding is present locally.

Quartz arenites and quartz wackes are usually interbedded with shales and sometimes represent a transgression-regression sequence such as the Houdon Formation. They can also be interbedded with graywackes and volcanics. Cross-bedding and herring-bone cross-bedding is common and graded bedding is present locally.

Pelites (shales) usually occur between volcanics and sandstones or between two sandstone layers. In the coarse grained pelites, cross-bedding is observed and ripple marks are present on some surfaces. Pelites are usually foliated and have a slaty texture. Fissility depends on the degree of metamorphism.

Petrography

Quartz arenites are typically fine to medium grained, moderately well sorted, and grain shapes range from angular to subrounded. Quartz arenites are composed chiefly of quartz, both mono- and polycrystalline (>80%), rock fragments (10%), and <5% matrix. Opaque Fe minerals are present as accessories and highlight cross-bedding in some units. These rocks are typically unfoliated but in some cases a faint foliation is detected in thin section. Matrix consists of sericite and chlorite and in most cases distinction between rock fragments and matrix is difficult. This is particularly true for the quartz wackes and graywackes.

Quartz wackes usually contain 40-45% quartz grains (mono- and polycrystalline), 35-50% rock fragments (chiefly volcanic), and 5-10% matrix. They are moderately well sorted, medium to coarse grained, and grain shapes are typically angular to subrounded. Matrix consists of chlorite and sericite. Plagioclase is sometimes present as isolated grains in the matrix and are well preserved. Rock fragments are highly altered to sericite and chlorite.

The term graywacke is used in this study to refer to lithic arenites and lithic wackes. Lithic arenites typically consist of 5-10% mono- and polycrystalline quartz (mostly monocrystalline), plagioclase (up to 3%), ≈75% rock fragments, and <10% matrix. Lithic arenites range from fine to coarse grained, are moderately to well sorted, and grain shapes range from angular to rounded. Rock fragments are chiefly volcanic and are highly altered to sericite and chlorite. Some sedimentary rock fragments display bedding and graded bedding. Matrix consists of chlorite and sericite with minor amounts of opaques.

Lithic wackes contain <20% quartz (mostly monocrystalline), 55 to 70% rock fragments, 8-12% matrix, and some plagioclase grains. These rocks range from fine to coarse grained, are poorly sorted, and grains are typically subangular to rounded. Rock fragments include fine grained porphyritic volcanic rocks, vein quartz, chert, sedimentary rocks, and granitic rocks. Matrix consists of sericite and chlorite with minor amounts of calcite, chert quartz, and opaques.

Geochemistry

All sedimentary rocks were analyzed for the same spectrum of elements as the igneous rocks. Element concentrations and element ratios for each sample are given in Appendix C. Results are plotted on a series of major and trace element tectonic discriminant diagrams (Figs. 43 through 47).

Figure 43 shows that the total Alder Group sedimentary package forms an almost complete continuum from oceanic arc type sediments to cratonic basin type sediments. For the most part the graywackes tend to be derived from an arc related source whereas the quartz arenites and quartz wackes are derived from a cratonic source--an observation in direct agreement with the petrographic studies.

The K_2O/Na_2O vs. SiO_2 diagram of Roser and Korsch (1986) (Fig. 44) shows basically the same features as the previous figure. Graywackes are arc related and quartz wackes and quartz arenites are similar to sandstones from passive margin settings; however the two pelite populations are less distinct. According to Roser and Korsch, sandstone and associated pelites from the same unit can be treated as a sandstone-pelite "pair". When lines drawn between

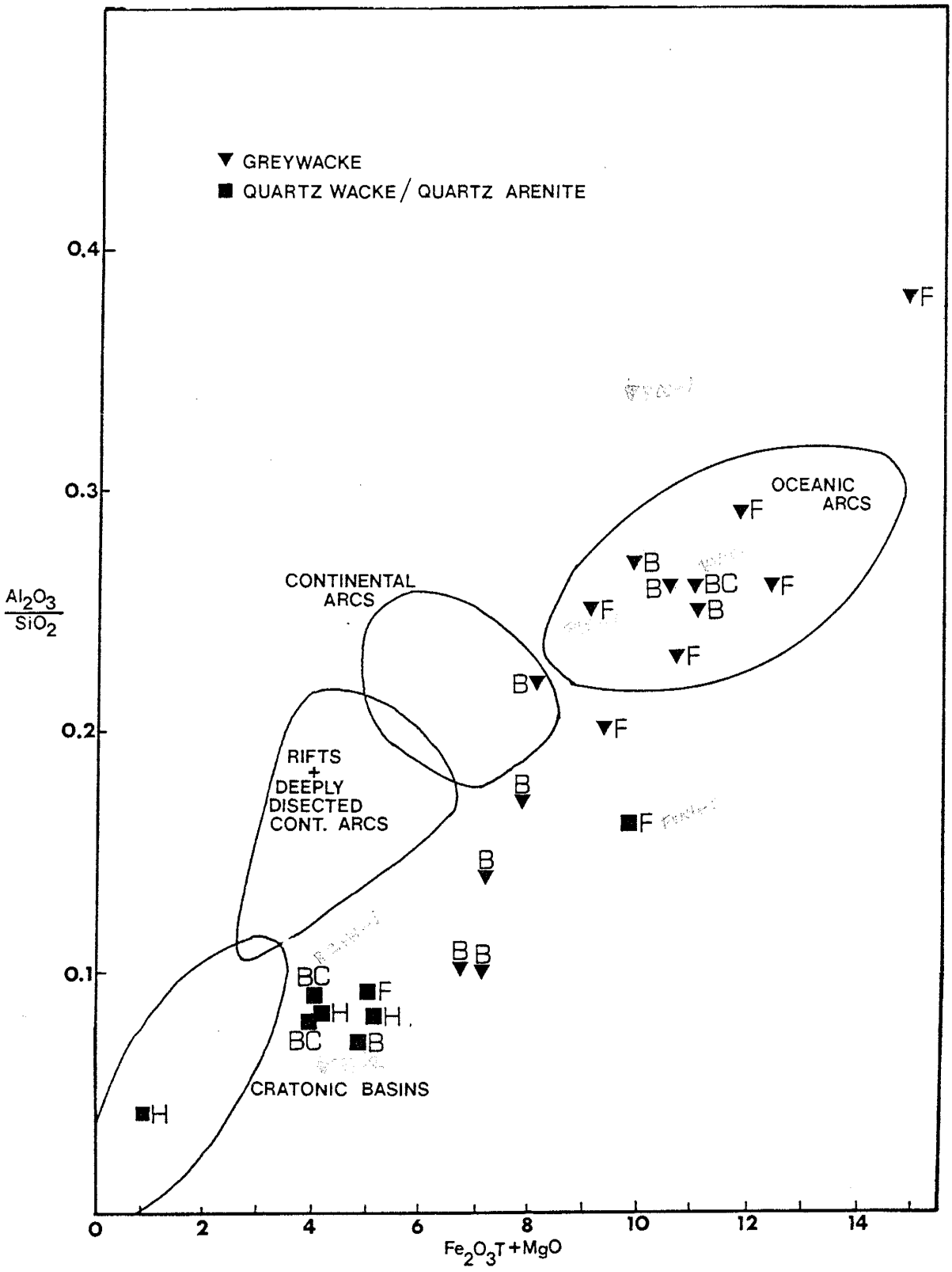

Figure 43. Distribution of Tonto Basin sandstones on the Al_2O_3/SiO_2 vs. Fe_2O_3+MgO tectonic discriminant diagram of Bhatia (1983). B=Breadpan Formation, F=Flying W Formation, H=Houdon Formation, and BC=Board Cabin Formation.

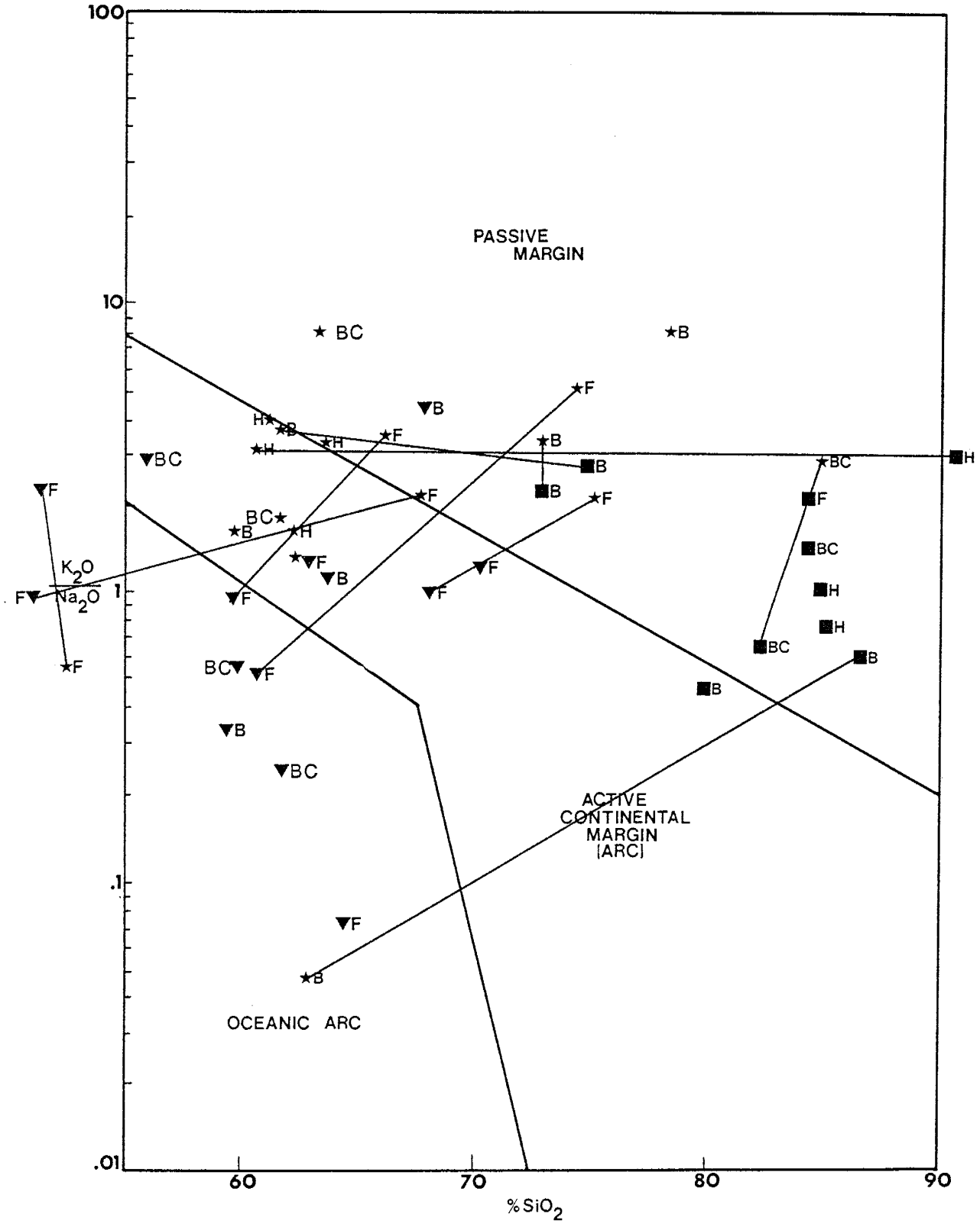

Figure 44. Distribution of Tonto Basin sandstones and pelites on the K_2O/Na_2O vs. SiO_2 tectonic discriminant diagram of Roser and Korsch (1986). Symbols as in Figure 43. Stars represent pelites.

pairs define intersecting trends, as the do here (Fig. 44), deposition in a back-arc basin is suspected.

Trace element discriminant diagrams for sediments also distinguish two populations with distinct provenances. Although the separation of the two populations is less obvious, Figures 45, 46, and 47 all show that graywackes tend to plot in and near arc related fields and quartz arenites and quartz wackes tend to plot in or near passive margin fields, supporting the major element geochemistry. Most of the sandstones plot in continental arc or active margin fields, a feature characteristic of back-arc basin sediments (Reed, 1988).

Figure 47 is a "ratio-ratio" plot. According to Langmuir et al. (1978) mixing lines on ratio-ratio plots are hyperbolic. Reed (1988) showed that sandstones from the Alder Group in the Mazatzal Mountains area plot in a roughly hyperbolic pattern on this diagram which is suggestive of end member mixing. To test the mixing hypothesis Reed (1988) plotted the Mazatzal Mountains sandstones on a "companion" diagram to the Ti/Zr vs. La/Sc diagram. A companion diagram plots one of the ratios of the original diagram against the ratio of the denominators. If the sandstones plot linearly on the companion diagram there is strong evidence for chemical mixing of sediment end members. The Mazatzal Mountains samples do plot linearly on the companion diagram lending support to the mixing hypothesis. However, from Figure 47 it can be seen that the Alder Group sandstones from the Tonto Basin area do not plot in a hyperbolic pattern and also do not plot linearly on the companion diagram (Fig. 48) which suggests that chemical mixing of sediment endmembers was not as extensive in the Tonto Basin area.

Tonto Basin pelites have variable major element concentrations, but SiO_2/Al_2O_3 and K_2O/Na_2O ratios are similar to NASC (North American Shale Composite). K_2O/Na_2O ratios are >1 suggesting a cratonic source as opposed to a volcanic dominated source (Wronkiewicz and Condie, 1987). However, SiO_2 values range from 40-85% and low silica pelites (40-65 wt. % SiO_2) have high alkali contents whereas high silica pelites (66-85 wt.% SiO_2) have low alkali contents suggesting two source areas for the pelites. The low silica pelites are probably derived from mafic to intermediate volcanic rocks associated with a volcanic arc whereas the

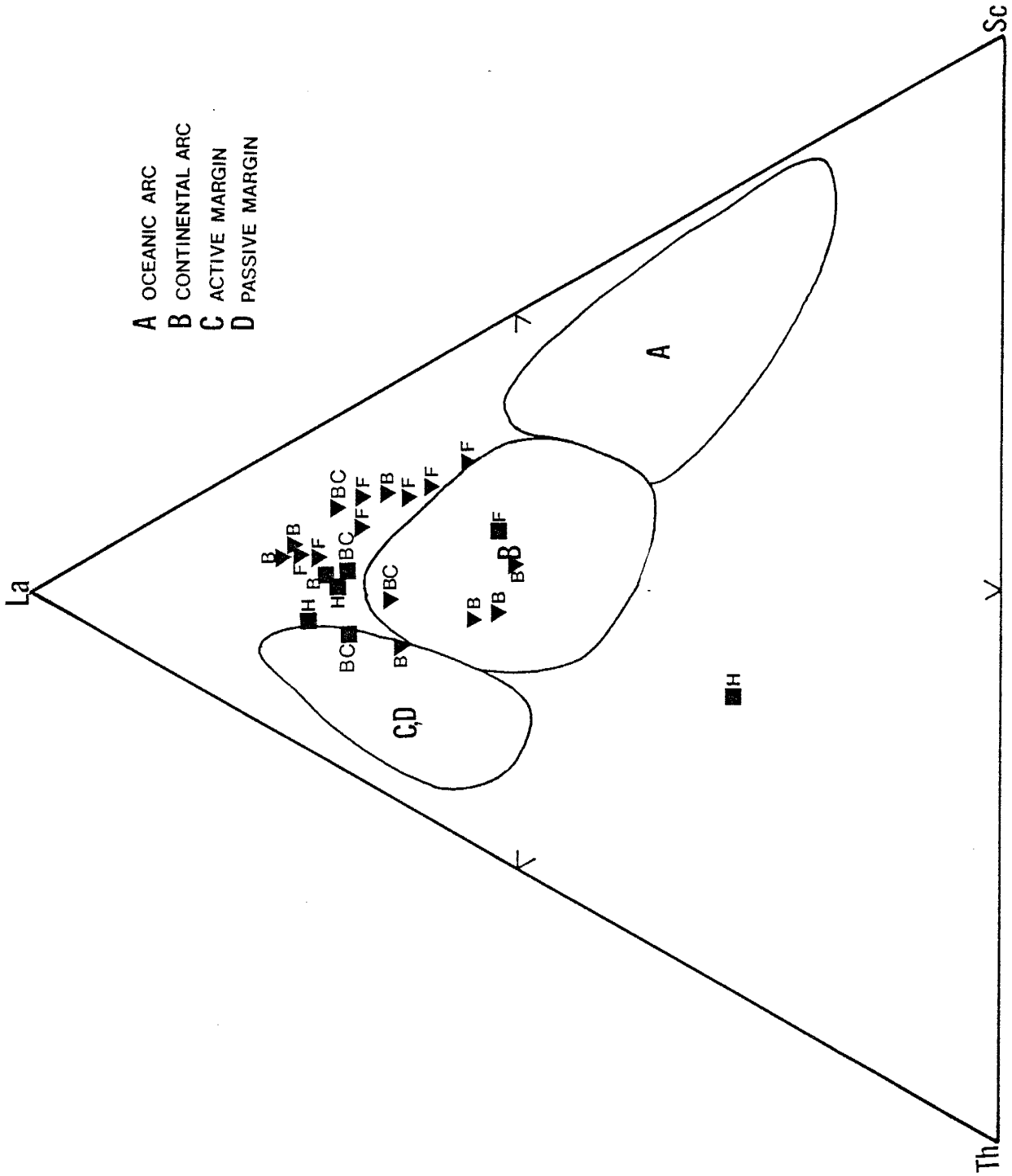

Figure 45. Distribution of Tonto Basin sandstones on the Th-La-Sc tectonic discriminant diagram of Bhatia and Crook (1986). Symbols as in Figure 43.

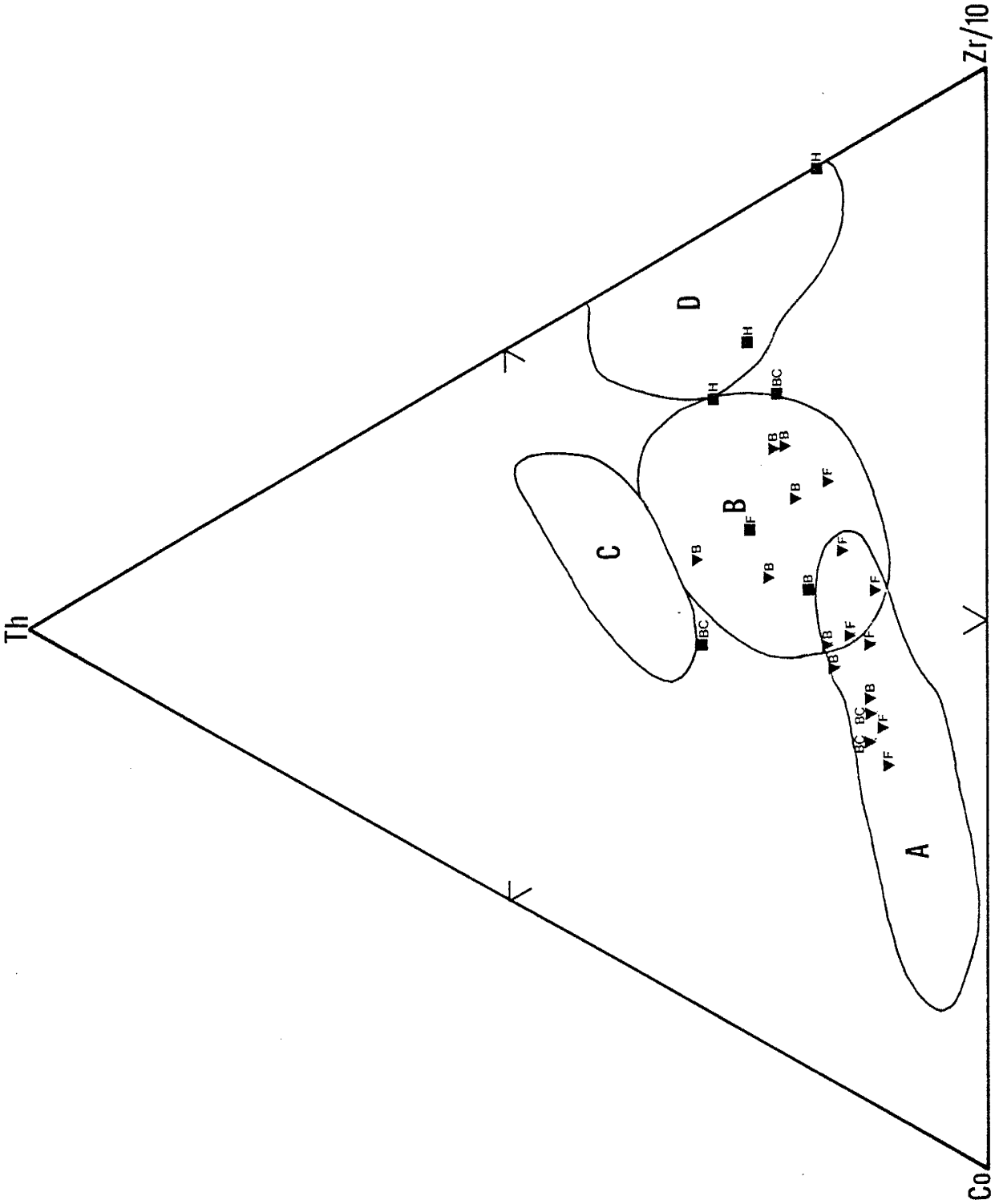

Figure 46. Distribution of Tonto Basin sandstones on the Co-Th-Zr tectonic discriminant diagram of Bhatia and Crook (1986). Symbols as in Figure 43.

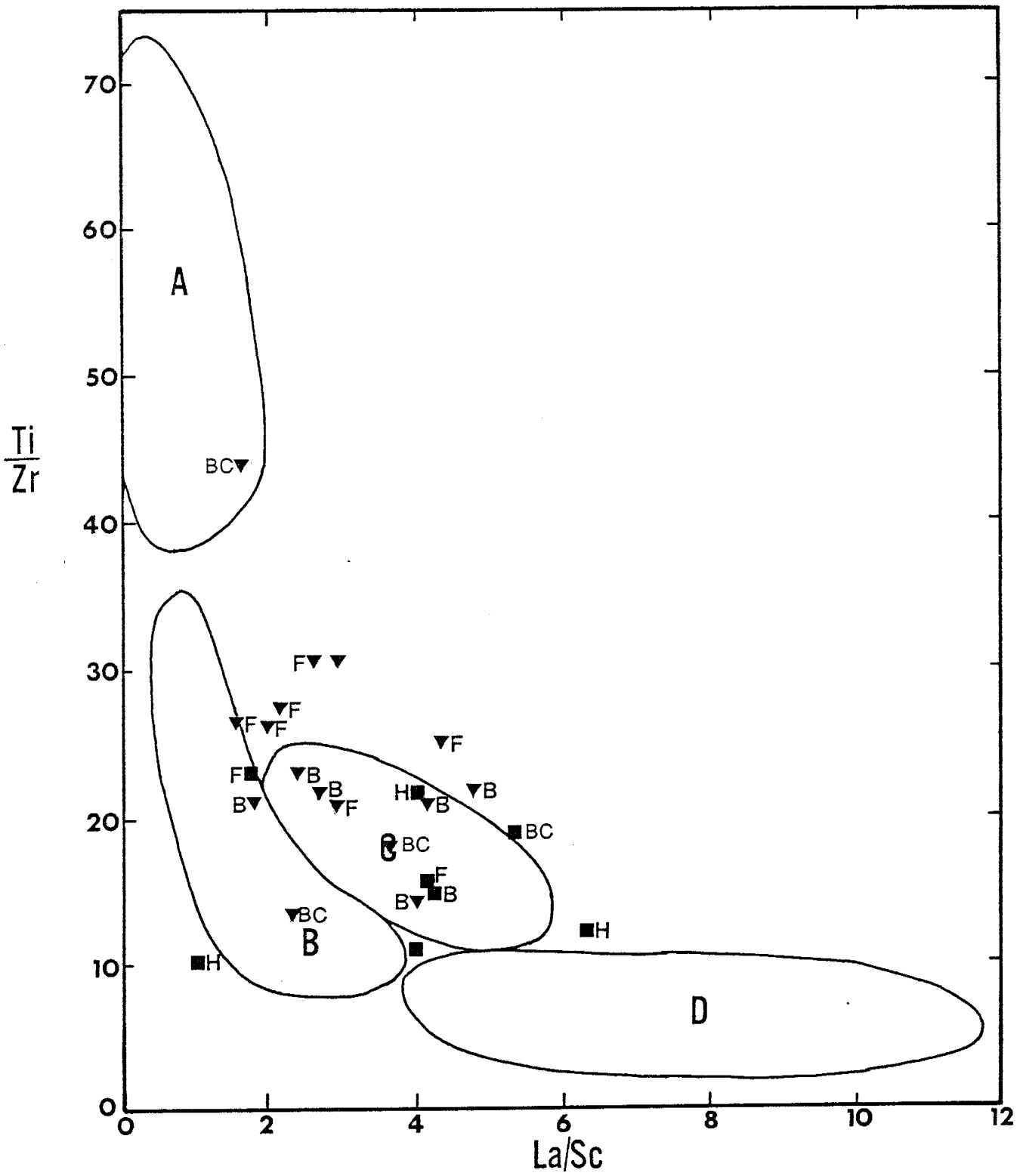

Figure 47. Distribution of the Tonto Basin sandstones on the Ti/Zr vs. La/Sc tectonic discriminant diagram of Bhatia and Crook (1986). Symbols as in Figure 43.

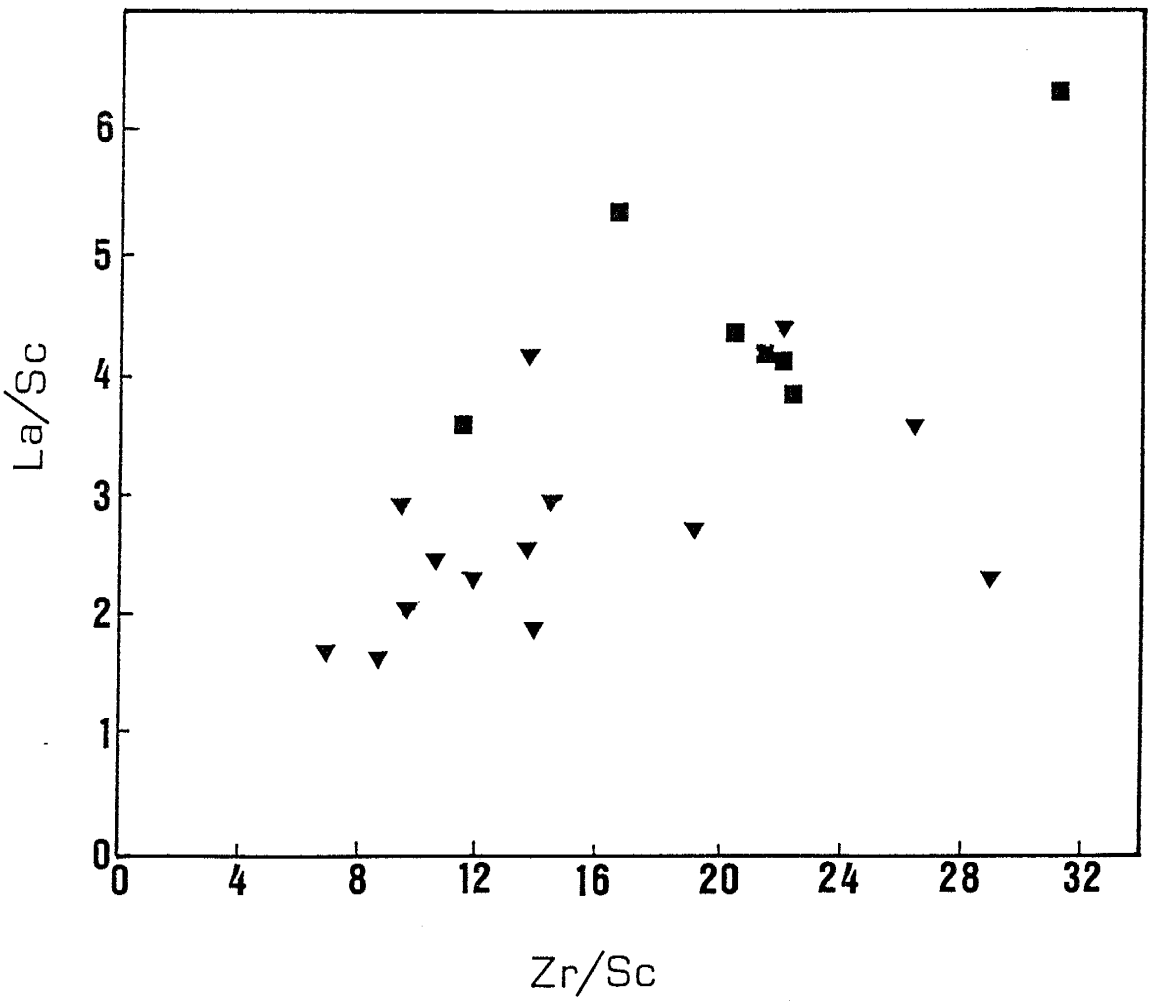

Figure 48. Distribution of Tonto Basin sandstones on the La/Sc vs. Zr/Sc diagram. Symbols as in Figure 43.

high silica pelites may be of cratonic origin. There is no systematic change in major element composition of the pelites with stratigraphic height. All four formations in the Alder Group contain pelites whose SiO_2 contents vary by 20% suggesting that pelites derived from both sources are present in each formation.

LIL element contents of the Tonto Basin pelites are also highly variable. Sr is chiefly low compared to NASC. Cs is consistently high, Rb and Ba are quite variable with both high and low values, U and Th concentrations are similar to NASC. In terms of high SiO_2 pelites versus the low SiO_2 pelites, the LIL elements are highly variable but the high SiO_2 pelites generally have lower LILE contents. Variability may due to mobility of the these elements during weathering, diagenesis, and low-grade metamorphism (Taylor and McLennan, 1985).

REE distributions of the Tonto Basin pelites are represented in Figure 49. High silica pelites have LREE that range from 60-160x chondrites and HREE ranging from 9-20x chondrites. The REE distributions of the low silica pelites overlaps that of the high silica pelites. However, the low silica pelites generally have higher REE contents with LREE ranging from 100-160x chondrites and HREE ranging from 12-20x chondrites. A slight increase in REE content with stratigraphic height is present. Lower Alder Group pelites have LREE contents 60-100x chondrites and HREE 9-18x chondrites. Upper Alder Group pelites have LREE contents 140-160x chondrites and HREE 10-20x chondrites. All Tonto Basin pelites have negative Eu anomalies. According to Taylor and McLennan (1985) this is due to chemical fractionation within the continental crust related to production of K-rich granites by partial melting of the continental crust. This lends evidence to the crustal melting model for the high silica alkali rhyolites of Tonto Basin (see section on geochemical modeling of the Tonto Basin igneous rocks). Overall, the Tonto Basin pelites have REE distributions similar to Phanerozoic shales.

Figures 50 and 51 show the distribution of the Alder Group Pelites on the Th-La-Sc and Hf-Th-Co diagrams. Relative to Phanerozoic shales, the Tonto Basin pelites have more variable distributions. On both diagrams the pelites fall on approximate mixing lines between mafic and felsic end members suggesting a mixed provenance. Low silica pelites

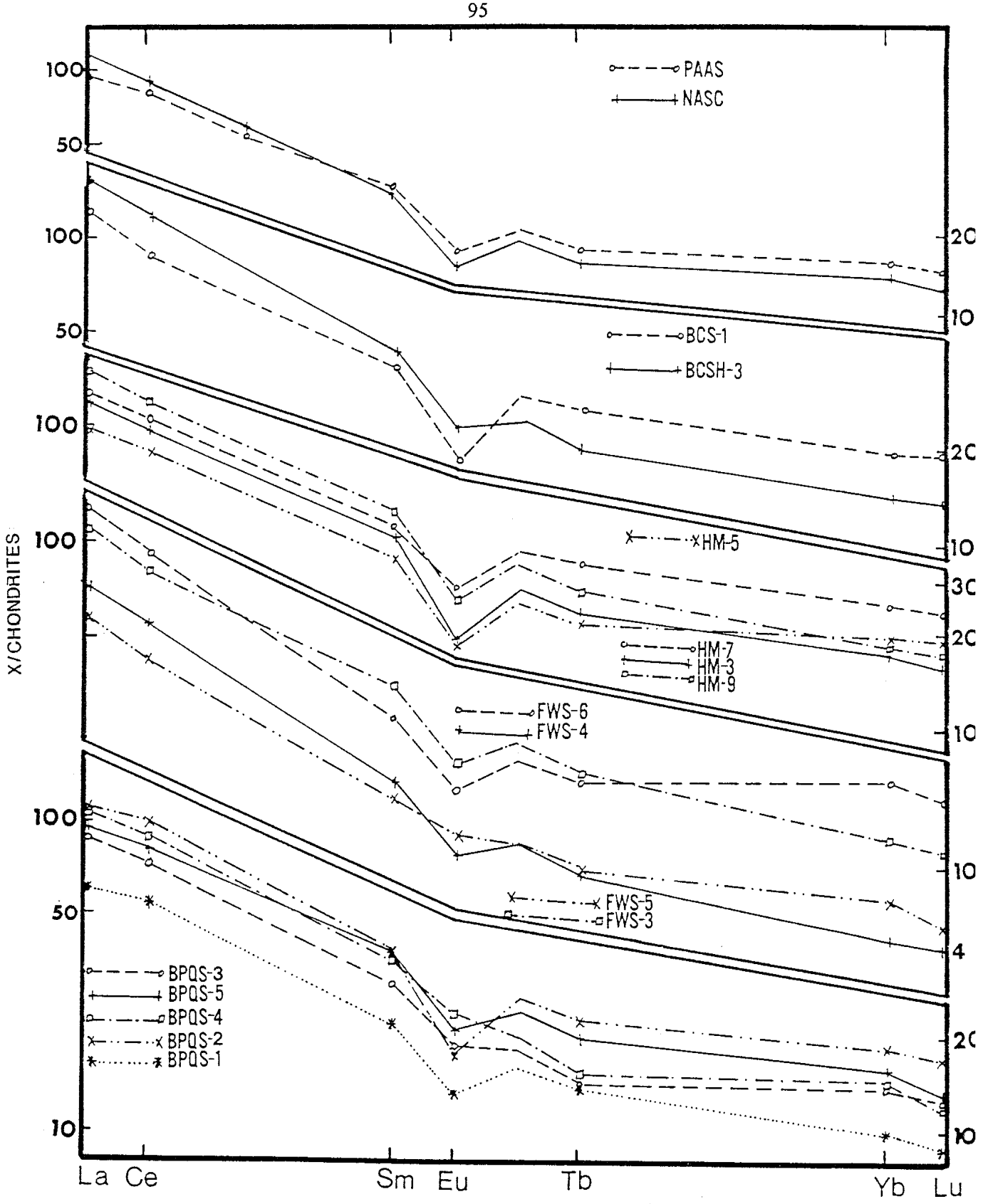

Figure 49. Chondrite-normalized REE plots of Tonto Basin pelites.

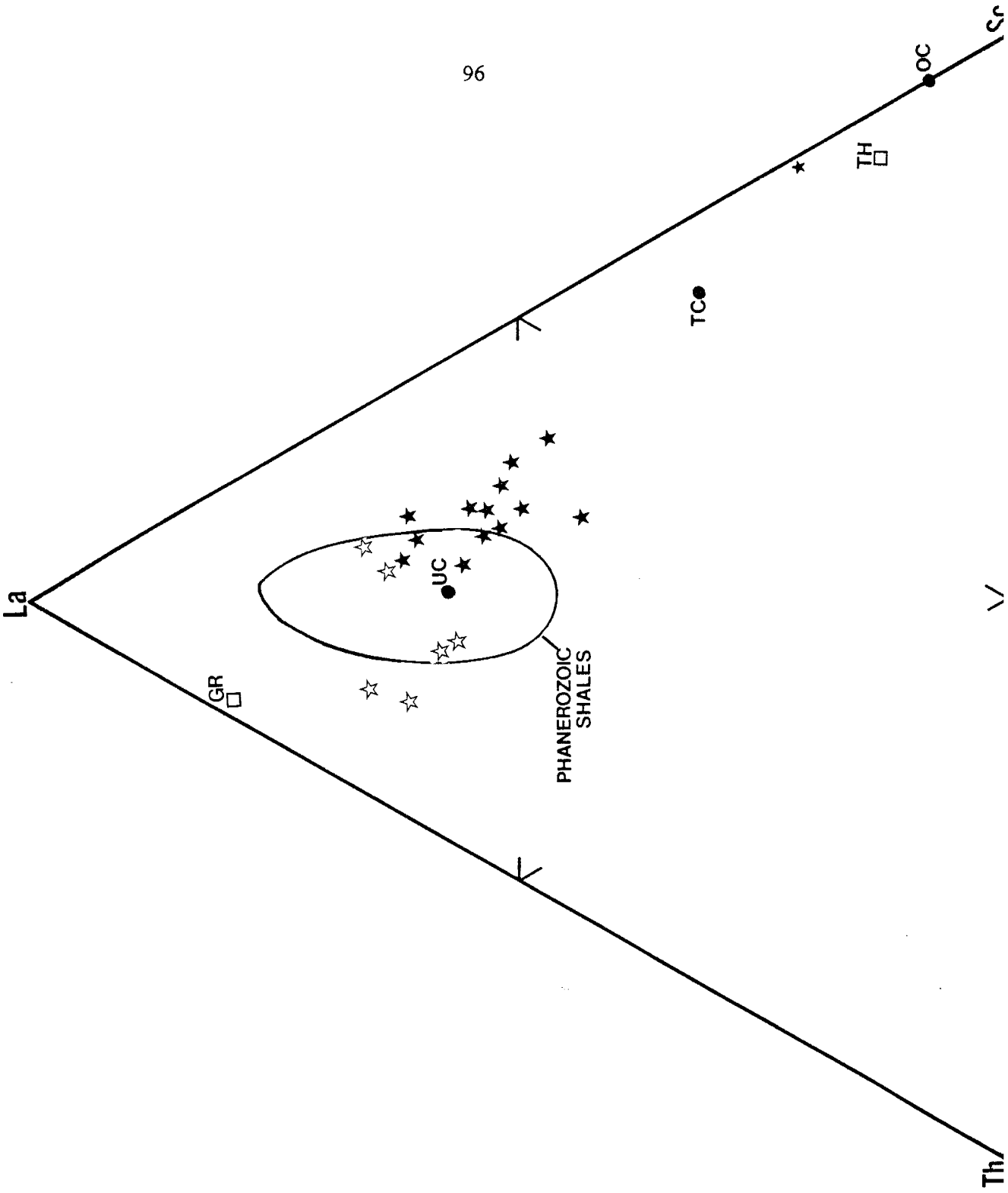

Figure 50. Distribution of Tonto Basin pelites on the Th-La-Sc diagram of Taylor and McLennan (1985). Open stars=high silica pelites. Closed stars=low silica pelites. GR=granite, TH=tholeiite, TC=total crust, OC=ocean crust, UC=upper crust. Estimated crustal compositions from Taylor and McLennan (1985).

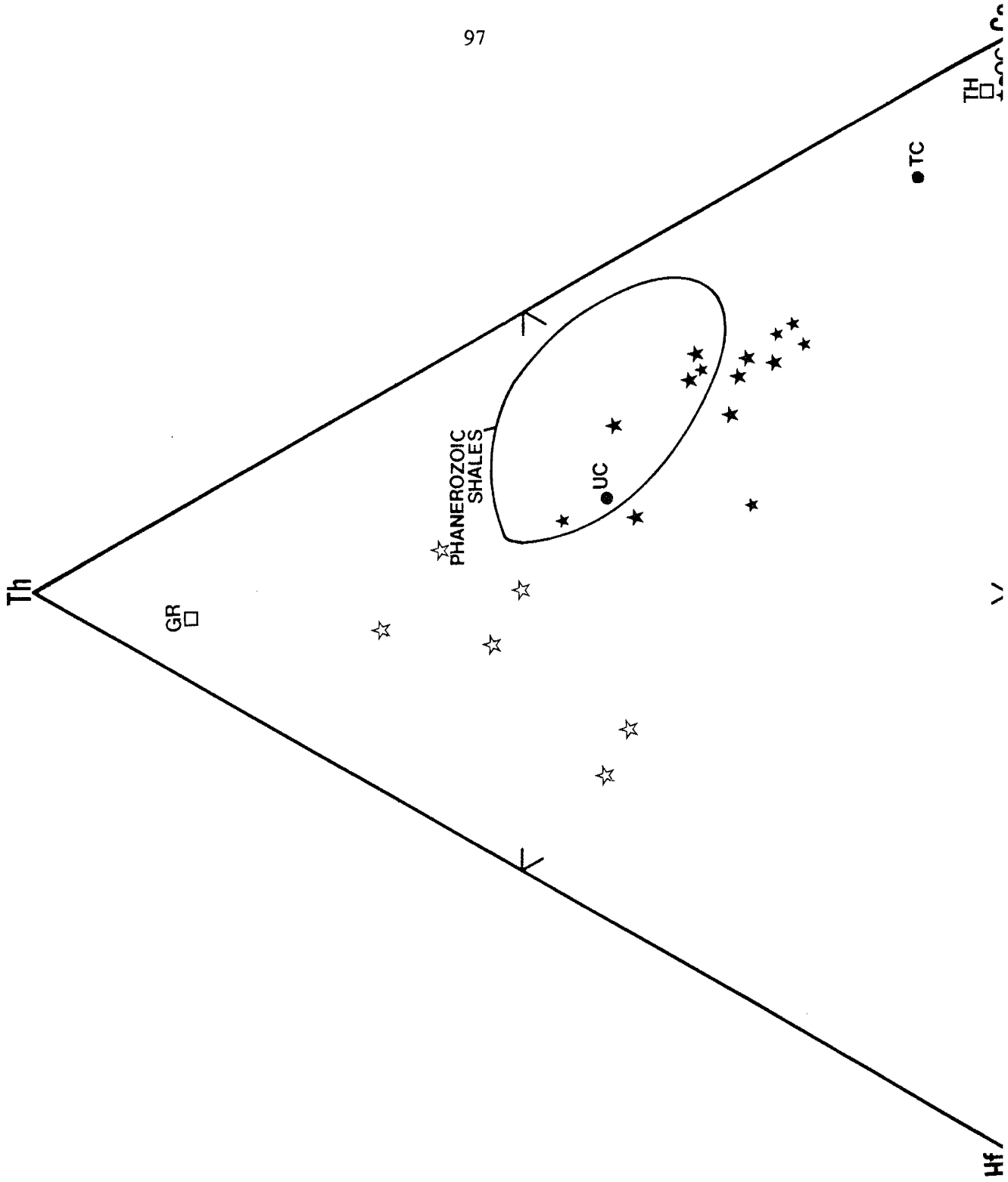

Figure 51. Distribution of Tonto Basin pelites on the Hf-Th-Co diagram of Taylor and McLennan (1985). Open stars=high silica pelites. Closed stars=low silica pelites. GR=granite, TH=tholeiite, TC=total crust, OC=ocean crust, UC=upper crust. Estimated crustal compositions from Taylor and McLennan (1985).

trend towards tholeiite whereas the high silica pelites plot close to granite (Figs. 50 and 51). The pelites with the lowest Co and Sc concentrations are those that plot near the passive margin field on Figure 44. The remainder of the pelites probably have arc affinities.

Provenance

In addition to geochemistry and petrography, field observations allow further characterization of the provenance of the two populations of sediments. Paleocurrent directions were obtained from cross-bedding in sandstones and in one case from asymmetrical ripple marks in a pelite. Although a detailed paleocurrent analysis was not undertaken, general paleocurrent directions for the two populations of sediments were acquired by "rotating" the inclined beds back to horizontal in the field. It must be stressed that this procedure is not quantitative and the results obtained in this manner must be regarded as approximate. The paleocurrent data suggest that the arc related sediments are derived from the southwest. The cratonic sediments, on the other hand, are derived from the northeast. The orientation of the basin of deposition during deposition of the sediments is not known. The important point to note is that the two populations of sediments were derived from opposing sides of a basin. A more detailed paleocurrent analysis of the Alder sandstones undertaken by Reed (1988) reached the same conclusions. A dual provenance for arc and cratonic sediments has also been documented for the Proterozoic Hembrillo Canyon succession south-central New Mexico (Alford, 1987).

From direct paleocurrent measurements and inferences made from petrographic and geochemical data, samples have been assigned a provenance direction (Table VIII). Four samples have contradicting provenance directions. Two samples (FWQ-1 and BPW-5) have paleocurrent directions from the southwest to the northeast (i.e. from the arc to the craton), yet the geochemistry of these two samples suggests that they were derived from the craton-not the arc. Likewise, two samples (HM-5 and BCW-3) have paleocurrent directions from the northeast (craton) but their geochemistry suggests that they are arc-related. One possible explanation for the anomalous behavior of these sediments is that they were subjected to extensive reworking of detritus or mixing of arc and craton end members. Other possibilities

TABLE VIII

Provenance of Tonto Basin Sediments based on paleocurrent and geochemical data.

From Arc (Sw) to Craton (NE)	From Craton (NE) to Arc (SW)
(Based on Paleocurrent Data)	(Based on Paleocurrent Data)
FWQ-1*	HM-5*
BPW-3	H-3*
BPW-4	BCW-3
BPW-5*	HL-1
(Based on Geochemistry)	(Based on Geochemistry)
BPW-1	HL-1
BPW-2	H-3
BPW-3	HL-2
BPW-4	BCSS-1
BPQS-1	BCSS-2
BPQS-2	BSCH-1
BPQS-3	BPW-5*
BPQS-4	FWS-5
BPQS-5	FWS-4
BOQS-7	FWQ-1
BPA-1	BPS-6
BPA-2	
BPQ-5	
BPQ-6	
FWW-1	
FWW-2	
FWW-3	
FWW-4	
FWW-5	
FWW-6	
FWCM-1	
FWS-1	
FWS-3	
FWS-6	
FWCM-1	
FWS-1	
FWS-3	
FWS-6	
HM-1	
HM-3*	
HM-5*	
HM-7	
HM-9	
BCW-3	
BCSH-3	

* indicates conflicting interpretations.

are that the paleocurrent measurement is incorrect or that the predominant current direction was itself anomalous (i.e.during a storm or flooding situation).

Another important field observation is that all formations in the Alder Group contain both arc-related and craton-related sediments. Furthermore, these two sediment types are intimately interbedded within each formation. This interbedding of arc and craton related sediments indicates that the basin of deposition must have been relatively narrow ($\leq$ 150 km across). The absence of pelagic sediments also indicates a narrow basin.

DISCUSSION

The Tonto Basin supracrustal assemblage appears to represent the infilling of a relatively narrow, shallow basin possibly developed on continental crust, at or near a continental margin, along which a volcanic arc was developing. The trend from fine grained chemical-argillaceous sediments to coarse grained conglomerates, indicates a gradual decrease in water depth. The increase in the proportion of volcanic rocks to sedimentary rocks provides evidence for the formation of a volcanic arc, and the increase in the proportion of felsic volcanic rocks to mafic volcanic rocks with increasing stratigraphic height indicates that the arc evolved from an immature arc (mafic volcanism) to a mature arc (rhyolitic volcanism) during Alder through Red Rock time.

Throughout Alder and Red Rock time there were frequent variations in sea level and depositional environment (Gastil, 1958). Evidence for this includes the rapid changes from conglomerates and herring-bone cross-bedded quartzites to pelites, reflecting a change from a shallow water fluvial depositional environment to a deep water oceanic depositional environment, respectively. Earliest Alder Group shales, graywackes, and minor volcanic rocks were apparently deposited in deep water (Conway and Silver, 1986b). The cherts and carbonates found in the earliest Alder (if not Pre-Alder) support this model provided they are not hydrothermal in origin. Sedimentary cherts associated with arc systems can form at depths of hundreds to several thousands of feet (Blatt, et al., 1972). The Flying W Formation reflects a change from a shallow water environment to a subareal environment. The presence of vesicular basalt flows indicates shallow water depths. Moore (1965) showed that with increasing water depth the vesicle content of Kilauea basalts decreases. Vesicles make up less than one percent of the volume of flows at a depth of 200m. Also, hyaloclastic breccias are relatively scarce at deep levels of the ocean floor (Williams and McBirney, 1979). The conglomerates, which contain boulders of the volcanic members upon which they rest, were probably deposited at or above shoreline (Gastil, 1958). Quartz arenite and shale deposition of the Houdon Formation reflects a return to stable shelf conditions. The andesite flows,

some pillowed (Gastil, 1958), and conglomerates of the Board Cabin Formation along with the tremendous volumes of felsic ash flows of the Red Rock Group may reflect the complete infilling of the basin. The pillowed lava flows and conglomerates suggest shallow water and the absence of sediments in the upper Red Rock Group suggests that by the end of Red Rock time, the basin was completely filled in with rhyolite.

Tectonic Setting

Several tectonic settings for the Alder and Red Rock Groups have been proposed (Conway, 1976; Conway and Silver, 1986a, 1986b; Condie, 1982a; Reed et al., 1987; Reed, 1988). These include continental rifts or hotspots, oceanic island arcs, successive development of continental volcanic arcs with repeated closure of back-arc basins, and continental margin arc back-arc basins.

The presence of large amounts of felsic volcanic rocks intimately associated with great thicknesses of quartz arenite (Houdon Formation and Mazatzal Group) seems to require the presence of continental crust (Conway and Silver, 1986a). The increase of the $K_2O/K_2O + Na_2O$ ratio in felsic rocks (Fig. 18) with increasing stratigraphic height (implying continental contamination of the magmas) also implies the presence of continental crust.

Conway and Silver (1986a) state that the Tonto Basin rhyolites are typical of so called alkali rhyolites or high-silica rhyolites which have been documented world wide in Phanerozoic tracts that have formed only on continental crust. In fact, they state that "given the association with quartz arenite, the argument is conclusive that the silicic alkalic magmas of the Tonto Basin-Mazatzal Mountain area are of continental derivation". Whether the argument is conclusive or not, most evidence suggests that the felsic volcanics are of continental derivation.

The presence of continental crust seems to rule out any model for a tectonic setting involving oceanic crust. Volcanic arcs developed on oceanic crust are probably incapable of generating the tremendous volume of felsic rocks seen in Tonto Basin. If the Alder-Red Rock succession were to represent the collision of an oceanic island arc with the stable craton one would expect to see ultramafic rocks (ophiolites) and/or massive sulfide deposits

preserved-neither of which have been described. Also, if the thick succession of sediments and volcanic rocks were deposited on oceanic crust, the crust would be depressed resulting in a basin with deep water. The overlying Mazatzal quartzite has been interpreted as a shallow water fluvial deposit in the northern exposures but to the south becomes more of a tidal and offshore deposit (Trevena, 1979). The Houdon Formation is also interpreted as a shallow water fluvial deposit (as evidenced by herring-bone cross-bedding and ripple marks) and the conglomerates of the upper Alder and Red Rock Groups also imply shallow water.

The continental rift or hotspot model, while consistent with the presence of continental crust, has several problems. Most continental rifts have large volumes of basalt and arkose and bimodal volcanics (Condie, 1982b). The Tonto Basin succession has little or no arkose (in fact, feldspar-rich sediments are rare) and basalts are minor. The volcanic suite in Tonto Basin is not bimodal and there is an abundance of andesites. The alkalinity of volcanics from continental rifts usually decreases with time (Condie, 1982b). The Tonto Basin felsic volcanics increase in alkalinity with time. Volcanics of all compositions from Tonto Basin have subduction zone signatures on NMORB-normalized diagrams. Although some rift volcanics display subduction zone signatures (Rio Grande, Karoo), these signatures are probably inherited. Samples of all compositions plot in arc related fields on numerous tectonic discrimination diagrams. Only a few samples (mostly felsic volcanics) plot in within-plate fields. As of yet, basement to the Tonto Basin succession has not bee identified. The Tonto Basin sedimentary package consists of two populations with distinct provenances. A population of cratonic sediments entered the basin from the NE while an arc related population was introduced from the SW. It is difficult to imagine this sediment distribution occurring in a continental rift. Karlstrom and Puls (1984) and Puls and Karlstrom (1985) have identified a foreland fold-thrust belt in the Mazatzal Group and underlying Red Rock rhyolites in the Mazatzal Mountains and Tonto Basin. The overall structure of the area indicates a NW-SE compressional regime--not an extensional one. The only normal faults identified are late and occur after the main period of thrust and reverse faulting (Conway, 1976).

The Tonto Basin succession has also been compared to the St. Francois Mountains igneous complex of southeastern Missouri (Conway and Silver, 1986b). This complex is an anorogenic felsic plutonic and volcanic complex. Basaltic rocks are rare and occur as small dikes. Intermediate volcanics are present as trachytes and phonolites-much more alkaline than the Tonto Basin suite. Sediments are rare and are limited to volcaniclastic pelites, water laid tuffs, and stromatolitic limestones; all of which have very limited lateral extent and are interpreted as caldera moat sediments. The rocks are generally not folded and the major faults in the area are caldera ring faults. No compressional features are present. Apparently, the large volumes of alkali-rich high silica rhyolite is all the two areas have in common. Obviously they had quite different tectonic settings and geologic histories and the comparison is fortuitous.

The geochemistry of the sedimentary and igneous rocks, along with petrography and field relations indicates that the Tonto Basin rocks formed in an arc setting. The silicic akalic magmatism implies a continental setting and the quartz arenite sedimentation indicates a continental margin setting (Conway and Silver, 1984).

It is herein proposed that the Alder and Red Rock Groups in the Tonto Basin area were deposited in a continental margin arc back-arc basin. Figures 52, 53 and 54 show the configuration of the proposed arc from Alder time through the Mazatzal orogeny. During Alder time sediments were derived from the craton to the northwest and the arc to the southeast and interbedded and mixed in the basin. Escaping volatiles from the descending plate enrich the mantle wedge in LILE relative to HFSE and REE and lower the solidus temperature of the wedge. Partial melting in the wedge gives rise to basaltic magmas that rise and undergo closed system FXL producing the Alder volcanics possibly including the Flying W rhyolites. Fluctuations in volcanic activity cause variations in sea level in the basin resulting in the depositional environments inferred for the Alder Group. During Red Rock time, rifting occurs in the back-arc basin. Subduction slows or ceases and rhyolites are generated by partial melting of the lower crust generating magmas with a within plat geochemical signature. These magmas retain, however, a relict subduction zone signature.

In between pulses of rhyolite magmatism, quartz arenites derived from the northeast are deposited. Felsic magmatism terminates as closure of the basin begins possibly due to collision of another arc to the southwest (see next section). The Alder plus Red Rock succession is buried by the quartz arenites of the Mazatzal Group. Continued SW-NE compression forms the foreland thrust belt and causes the folding, faulting, and metamorphism of the Alder and Red Rock Groups. Uplift and erosion later re-exposes the Alder and Red Rock Groups at the surface. U-Pb zircon ages (Karlstrom, et al., 1987) from the Alder and Red Rock Group rhyolites all cluster around 1695±15 Ma to 1710±20 Ma suggesting that the above scenario took place in a relatively short time period.

Other depositional basins are possible. Many different plate configurations can be contrived that explain the two populations of sediments and many of the geochemical features of the volcanics. However, most of these fail to adequately explain the large volumes of rhyolite and quartz arenite found in Tonto Basin. As such, it appears that a continental margin arc back-arc basin is the most plausible tectonic setting for the Tonto Basin supracrustal assemblage.

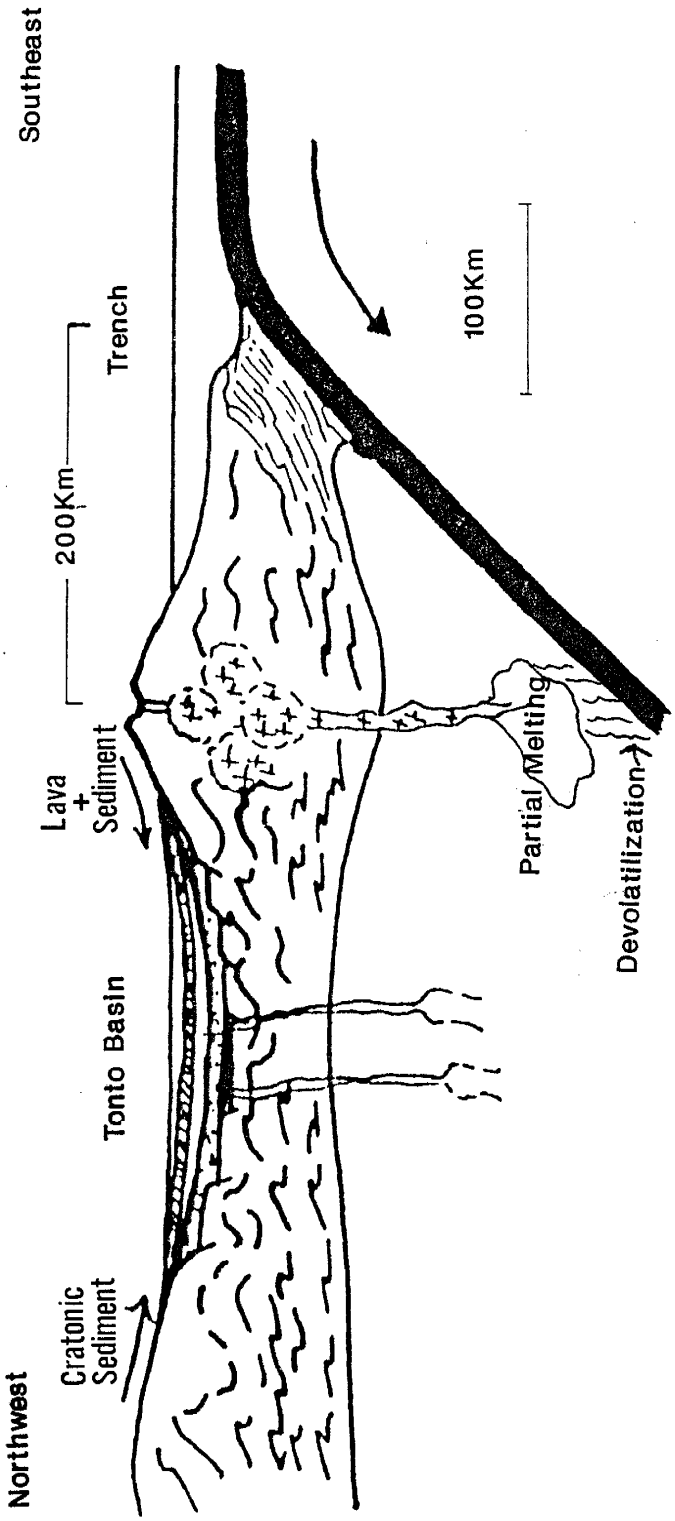

Figure 52. Schematic diagram of proposed arc during Alder time.

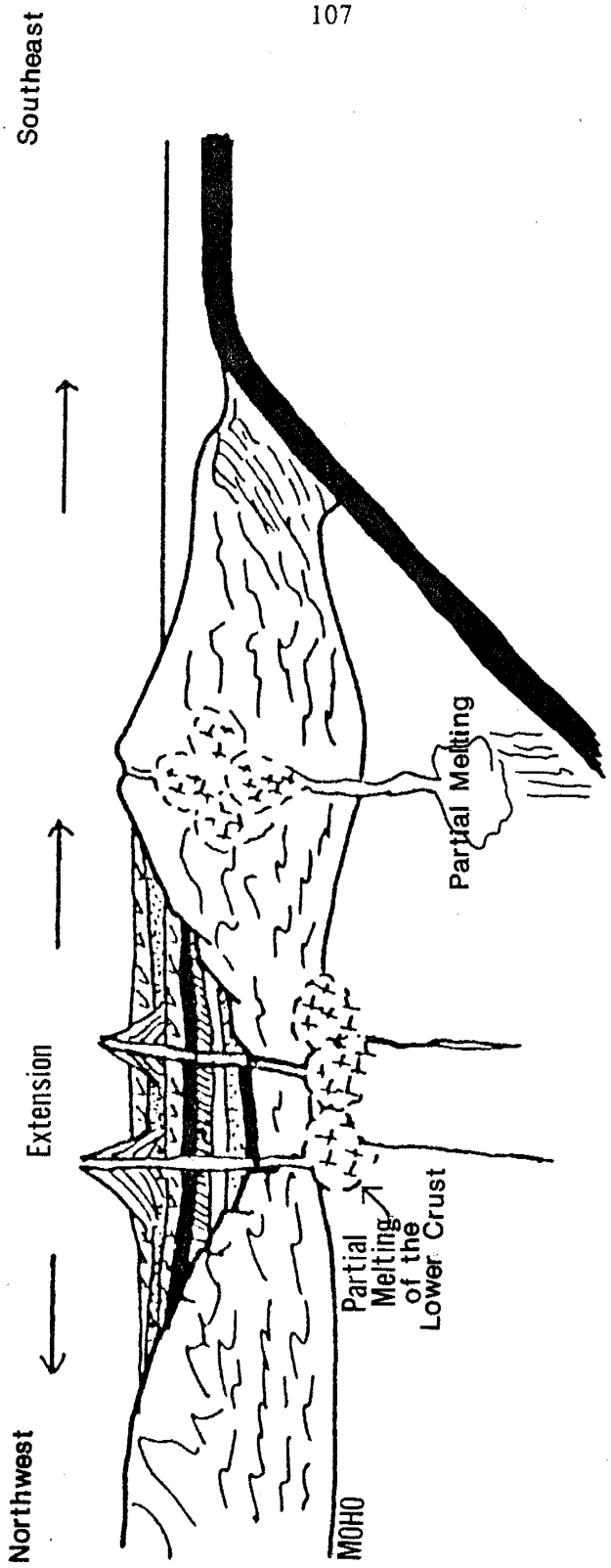

Figure 53. Schematic diagram of proposed arc during Red Rock time.

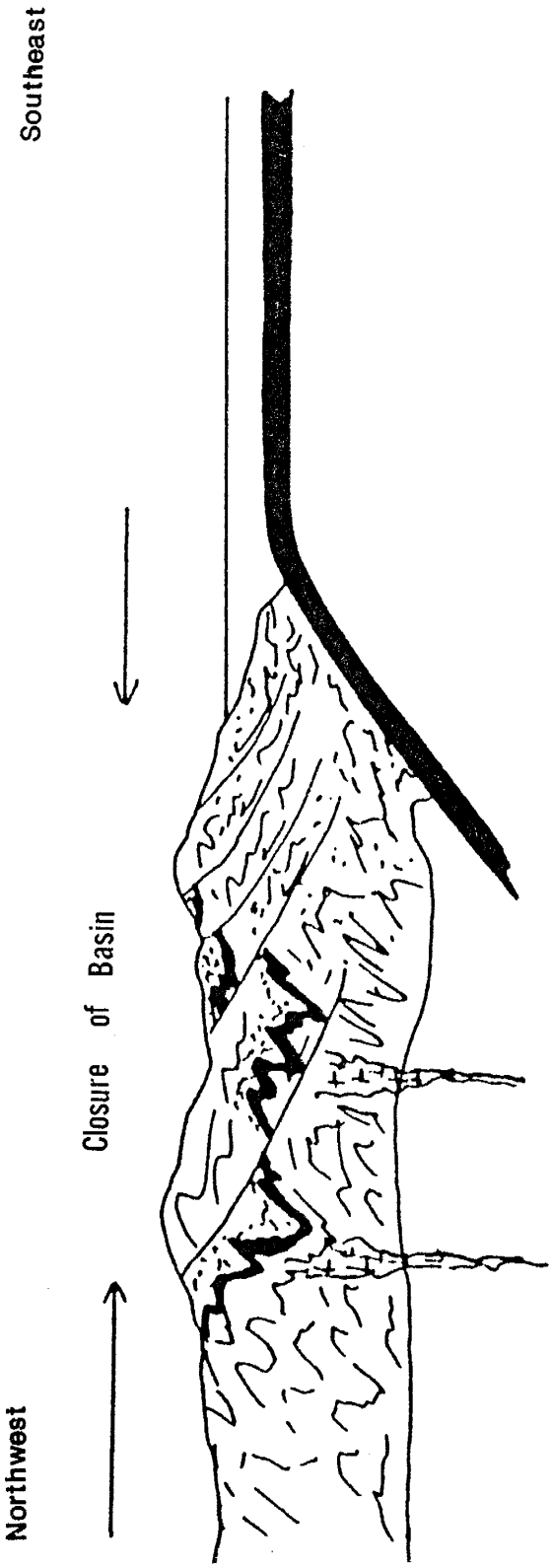

Figure 54. Schematic diagram of proposed arc during the Mazatzal Orogeny.

REGIONAL IMPLICATIONS

Relation of the Mazatzal Terrane to the Yavapai Terrane

Figure 55 shows the geographic relationships of the Mazatzal terrane (including the Tonto Basin area) to the Yavapai and the Pinal-Dos Cabezas terranes. A terrane is defined here as a section of the continental crust that contains a group of rocks which are of the same age and presumably formed within a specific tectonic setting. A recent compilation of U-Pb zircon ages from central Arizona (Karlstrom et al., 1987) indicates the presence of a sub-horizontal two province boundary separating the Yavapai and Mazatzal terranes. The Yavapai terrane has been characterized as an oceanic island arc assemblage (Vance, 1988). It has undergone high temperature multi-phase ductile deformation and peak metamorphism reached conditions of 550°C and 2.5 Kbar (O'Hara, 1980). The 1695 Ma Crazy Basin quartz monzonite intruded syntectonically at depths of 8-10 km. This terrane has been dated at $\geq$1760 Ma (Karlstrom et al., 1987).

In contrast, across the Moore Gultch fault (Fig. 55) to the southeast, the Mazatzal terrane represents a continental margin arc back-arc basin assemblage (Reed, 1988; this study). The Mazatzal terrance has undergone low temperature brittle deformation and the rocks are metamorphosed to the lower greenschist facies.

The contrasting geochemistry, rock packages, and style and degree of deformation suggest that the two terranes evolved independently of each other. While the Mazatzal terrane was being deposited at ≈1700 Ma, the Yavapai terrane was being intruded by the Crazy Basin quartz monzonite at 8-10 km depth and undergoing ductile penetrative deformation. Karlstrom et al. (1987) therefore propose that the Mazatzal terrane may be allochthonous and that its deformation may have been related to its accretion to the Yavapai terrane. This contradicts the proposal by Conway and Silver (1986b) that the Yavapai may be the basement to the Alder-Red Rock succession in Tonto Basin. If it is allochthonous, the Mazatzal terrane may have developed as a microcontinent composed of continental crust on which the Alder and Red Rock Groups were deposited. This microcontinent collided with the Yavapai terrane

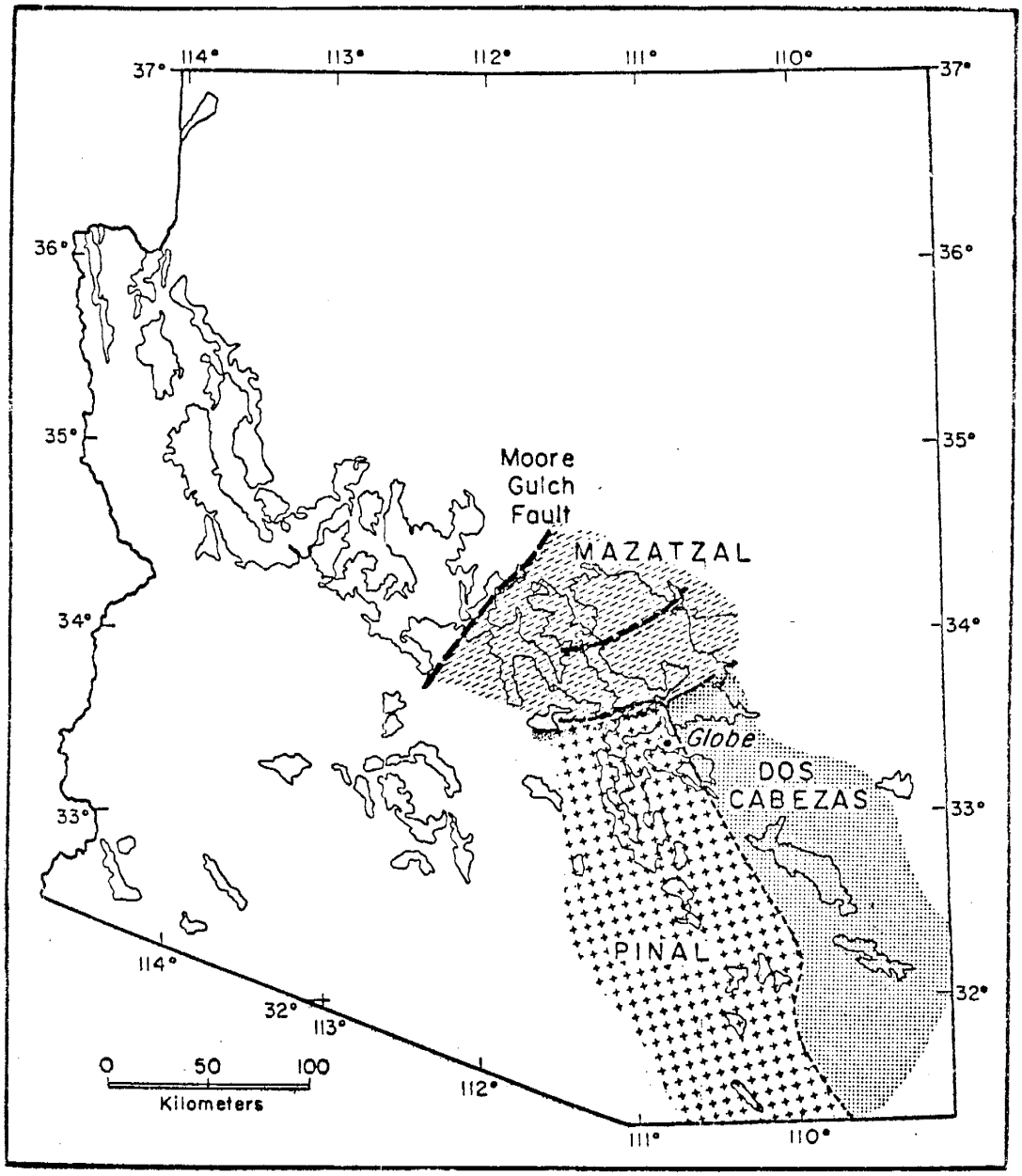

Figure 55. Map of Arizona showing the geographic relationships of the Yavapai, Mazatzal, Pinal, and Dos Cabezas Terranes.

on the stable craton creating the two province boundary (suture?). An alternative, though less probable, interpretation is that the Moore Gulch fault is a normal fault with large components of vertical displacement resulting in mainly "basement" exposed in the Yavapai terrane and principally supracrustal "cover" in the Mazatzal terrane (Karlstrom et al., 1987) preserving the Yavapai Series as basement in the Tonto Basin area.

Relation of the Mazatzal Terrane to the Pinal and Dos Cabezas Terranes

The relation of the Mazatzal terrane to the Pinal-Dos Cabezas terranes to the south is less distinct (Fig. 55). The Pinal terrane consists mainly of quartz wacke turbidites and minor basalts (Condie & De Malas, 1985; Copeland, 1986). It has been proposed that the Pinal terrane represents a back-arc basin that opened wide enough for the basalts erupted within this basin to take on oceanic geochemical signatures. Then the basin closed again (Copeland, 1986). The Dos Cabezas terrane consists of felsic volcanics, feldspathic quartzites, arkose, conglomerates, quartzites, shales, and amphibolites and may reflect either a continental margin arc or a continental rift (Condie et al., 1985).

It is unknown if the Dos Cabezas and Pinal terranes are part of the Mazatzal terrane. The Dos Cabezas terrane does not crop out between the Dos Cabezas Mountains and the Mazatzal terrane. The Pinal terrane is separated from the Mazatzal terrane by a band of 1400 Ma granites obscuring the contact. Field observations near the Mazatzal terrane-Pinal terrane boundary (K.C. Condie, pers. comm., 1988) suggest that as one approaches the boundary from either side the rocks become more sheared. The 1400 Ma granites may have intruded and obscured a major shear zone separating the two provinces, and this shear zone may represent a suture implying that the Pinal-Dos Cabezas terranes are allochthonous. The Pinal-Dos Cabezas terranes are ≈20 Ma younger (though within error) (Karlstrom, et al., 1987) than the Mazatzal terrane and collision of these terranes with the Mazatzal terrane may account for the late strike-slip faulting in Tonto Basin. According to Karlstrom et al. (1987) strike-slip faulting is viewed as a late modification of accreted continent possibly due to oblique convergence to the south.

The relationships of the Pinal-Dos Cabezas terranes to the Mazatzal terrane and of the Mazatzal terrane to the Yavapai terrane suggest that the early Proterozoic North American continent grew by accretion of oceanic and continental arcs. Some of these arcs may have had associated back-arc basins which may have opened and closed several times thus adding additional material to the craton.

CONCLUSIONS

1) Early Proterozoic volcanics of the Alder and Red Rock Groups in the Tonto Basin area exhibit a range of compositions from basalt to rhyolite. Although the rocks show mixed calc-alkaline and tholeiitic affinities they are dominantly tholeiitic.

2) Field observations suggest that no strata older than the Breadpan Formation is preserved in Tonto Basin and that the Slate Creek shear zone is related to high angle reverse and thrust faulting which has resulted in a repeat of the Alder section.

3) The incompatible trace element distributions including low Nb-Ta relative to REE and LILE are similar to volcanics from continental margin arc systems.

4) Basalts of the Alder Group can be derived by variable degrees of batch melting of a chemically and mineralogically heterogeneous garnet lherzolite source. This source was enriched in LILE and REE and is similar to calculated sources of basalts from modern continental margin arcs.

5) Intermediate volcanics of the Alder Group can be derived by shallow, closed-system fractional crystallization of clinopyroxene, orthopyroxene, plagioclase and minor magnetite.

6) The felsic volcanic rocks of the Alder Group can be produced either by partial melting of the lower crust (felsic granulites) or by closed-system fractional crystallization of dacitic liquids.

7) Petrography and geochemistry of Tonto Basin sediments indicates the existence of two populations: one with craton provenance and one with arc provenance.

8) Sediment composition and cross-bedding suggest that the cratonic sediments were derived from the northeast and the arc sediments from the southwest. Both types interfinger in the Tonto Basin succession.

9) Lithologic association and geochemical characteristics of volcanics and sediments from the Alder and Red Rock Groups are consistent with a back-arc basin associated with a continental margin arc as the environment of deposition.

APPENDIX A: SAMPLE LOCATIONS AND ACCESS

The field area covers 7.5 minute quadrangles Diamond Butte and Buzzard Roost Mesa and the Western part of the Young 15 minute quadrangle. Access to the field area is provided by the Globe Highway (from Globe, AZ to Young, AZ) and by forest service roads from Young westward into the Tonto National Forest. A few roads have locked gates but inquiry at the general store in Young usually provides the name of the keyholder. Most samples were taken from National Forest land, a few were taken from the Flying W Ranch propoerty with the kind permission of Mr. Michael Frye. Sample locations are as follows:

Breadpan Formation

PAS-2--NE1/4,SE1/4, SEC.23, T9N, R12E, BRMQ

PAS-3--SW1/4,SW1/4, SEC.24, T9N, R12E, BRMQ

BPQS-1--SW1/4, SEC.13, T9N, R12E, BRMQ

BPQS-2-NW1/4, SEC.24, T9N, R12E, BRMQ

BPQS-3-≈1/4 MILE SOUTH OF CONFLUENCE OF CLOVER CANYON ON ROCK CREEK, BRMQ

BPQS-4-SAME AS BPQS-3

BPQS-5-SAME AS BPQS-3

BPQS-7-IN SPRING CREEK, NW1/4,NE1/4, SEC.23, T9N, R12E, BRMQ

BPS-6--NE1/4,NE1/4, SEC.24, T9N R12E, BRMQ

PALS-1-SE1/4,NW1/4, SEC.24, T9N, R12E, BRMQ

PALS-3-SE1/4,NW1/4,NE1/4, SEC.24, T9N, R12E, BRMQ

BPW-1--SE1/4,NE1/4, SEC.23, T9N, R12E, BRMQ

BPW-2--SAME AS BPW-1

BPW-3--SW1/4,NE1/4, SEC.23, T9N, R12E, BRMQ

BPW-4--SAME AS BPW-3

BPW-5--SW1/4,NW1/4,NE1/4, SEC.23, T9N, R12E, BRMQ

BPA-1--ROCK CREEK, ≈1500' NW OF MINE TANK AND 1000' SOUTH OF CLOVER CANYON

BPA-2--SAME AS BPA-1

BPQ-2--NW1/4, SEC.24, Y9N, R12E, BRMQ

BPQ-5--ROCK CREEK, ≈1200' NW OF MINE TANK, ≈2000' SOUTH OF CLOVER CANYON

BPQ-6--SAME AS BPQ-5

PAV-2--NW1/4,SW1/4,NW1/4, SEC.24, T9N, R12E, BRMQ

PAV-3--SW1/4,SW1/4, SEC.24, T9N, R12E, BRMQ

T-1--NW1/4,SE1/4,NE1/4, SEC.24, T9N, R12E, BRMQ

Flying W Formation

FWS-1--SE1/4,SW1/4,SW1/4, SEC.14, T9N, R12E, BRMQ

FWS-3,4,5,6-SAME AS FWS-1

FWQ-1--CONFLUENCE OF ROCK CREEK AND CLOVER CANYON

FWW-1--SE1/4,SW1/4,SW1/4, SEC.14, T9N, R12E, BRMQ

FWW-2--CONFLUENCE OF ROCK CREEK AND CLOVER CANYON, BRMQ

FWW-3,4,5,6-ROCK, ≈900' NORTH OF CLOVER CANYON, BRMQ

FWCM-1-SE1/4,SW1/4,SW1/4, SEC.14, T9N, R12E, BRMQ

FWBV-2-SW1/4,SW1/4, SEC.13, T9N, R12E, BRMQ

FWC-9,12-SW1/4,SW1/4, SEC.13. T9N, R12E, BRMQ

FWK-2--NW1/4,NW1/4, SEC.23, T9N, R12E, BRMQ

FWC-11-SAME AS FWC-9

FWBV-4,5-ROCK CREEK ≈1000' NORTH OF CLOVER CANYON, BRMQ

FWC-5--SAME AS FWC-9

FWK-3,4-ROCK CREEK ≈900' NORTH OF CLOVER CANYON, BRMQ

FWK-5--SAME AS FWC-9

FWW-7--SAME AS FWK-3

FWR-1--NW1/4,SW1/4, SEC.13, T9N, R12E, BRMQ

FWR-3,4-SE1/4,SW1/4, SEC.14, T9N, R12E, BRMQ

FWC-6,1-SAME AS FWC-9

Houdon Formation

HM-1--NE1/4,NW1/4, SEC.11, T9N, R12E, DBQ

HM-3--CENTER, SEC.7, T9N, R13E, DBQ

HM-5,7-ROCK CREEK, ≈3000' SOUTH OF BRUSHY CANYON, BRMQ

HM-9--SE1/4,NW1/4, SEC.11, T9N, R12E, DBQ

HL-1--NW1/4,SE1/4, SEC.7, T9N, R13E, DBQ

HL-2--SAME AS HM-5

H-2--SAME AS HM-5

H-3--NE1/4,NW1/4, SEC.11, T9N, R12E, DBQ

HC-1--SW1/4,NW1/4, SEC.13, T9N, R12E, BRMQ

Hu-1--SAME AS HM-5

H-1--NW1/4,NE1/4, SEC.31, T9N, R13E, BRMQ

Board Cabin Formation

BCS-1--CENTER, SEC.7, T9N, R13E, DBQ

BCSH-1-NE1/4,SE1/4, SEC.36, T9N, R12E, BRMQ

BCSH-3-NW1/4,NE1/4, SEC.11, T9N, R12E, DBQ

BCSS-1-SAME AS BCSH-1

BCSS-2-SAME AS BCSH-3

BCC-1,2,3,4-SAME AS BCSH-3

BCW-1-SE1/4,NE1/4, SEC.7, T9N, R13E, DBQ

BCW-2-NE1/4,SW1/4, SEC.7, T9N, R13E, DBQ

BCW-3-SAME AS BCSH-3

BCP-1,2,4,5-NW1/4,NE1/4, SEC.11, T9N, R12E, DBQ

BCMV-1-SE1/4,SE1/4, SEC.30, T9N, R13E, BRMQ

BCP-6--SAME AS BCP-1

Winter Camp Formation

WCRD-1,2,4-SE1/4,NE1/4, SEC.2, T9N, R12E, DBQ

Haigler Formation

HBS-1--ONE ROAD TO ELLINWOOD RANCH, SOUTH OF OXBOW MTN., ≈1 MILE DUE EAST OF JAKE TANK, DBQ

HBV-3--ON ROAD TO ELLINWOOD RANCH, ≈1.5 MILES WEST OF THE CHAMBERLAIN TRAIL, YQ

HR-2,5-SE1/4,NE1/4, SEC.27, T10N, R12E, DBQ

Oxbow Mtn. Rhyolite

OX-1--ON ROAD TO ELLINWOOD RANCH, ≈1.5 MILES WEST OF THE CHAMBERLAIN TRAIL, YQ

OX-2,5-ON ROAD TO ELLINWOOD RANCH, ≈0.5 MILE WEST OF CHAMBERLAIN TRAIL, NEAR ALDERWOOD CAMPGROUND, YQ

Intrusive Rocks

HPB-1--SW1/4,SE1/4, SEC.35, T10N, R12E, DBQ

Hd-1--ON ROAD TO ELLINWOOD RANCH, ≈1.75 MILES WEST OF CHAMBERLAIN TRAIL, DBQ

FWD-2--SE1/4,SW1/4, SEC.14, T9N, R12E, BRMQ

FWD-3--ON ROCK CREEK ≈1100' NORTH OF CLOVER CANYON, BRMQ

PYX-2-SW1/4,NE1/4, SEC.24, T9N, R12E, ON WALNUT CREEK, BRMQ

PYX-6--SE1/4,NE1/4, SEC.24, T9N, R12E, ON WALNUT CREEK, BRMQ

D-2--NE1/4,SE1/4, SEC.35, T10N, R12E, DBQ

IR-1--NW CORNER, NE1/4,NE1/4,NW1/4, SEC.29, T9N, R13E, BRMQ

IR-3,4-NE1/4,SW1/4, SEC.36, T9N, R12E, NEAR SPRING CREEK MINE, BRMQ

BI-1--ON ROCK CREEK, ≈1000' SOUTH OF CLOVER CANYON, BRMQ

GR-3--SE1/4,NE1/4, SEC.11, T9N, R12E, DBQ

DBQ=Diamond Butte 7.5 Minute Quadrangle
BRMQ=Buzzard Roost Mesa 7.5 Minute Quadrangle
YQ=Young 15 Minute Quadrangle

Figure A-1
Sample Location Map Indicies

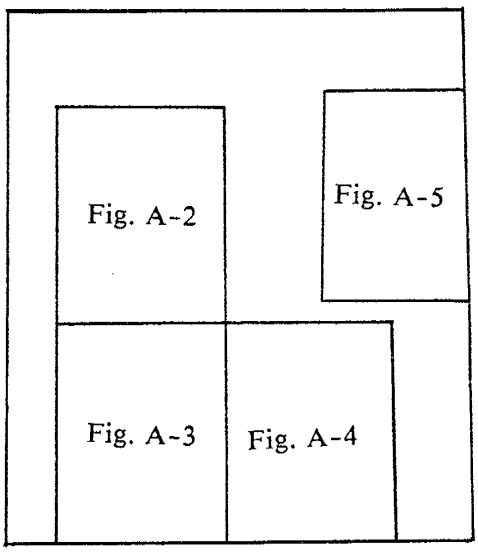

Diamond Butte
7.5 Minute

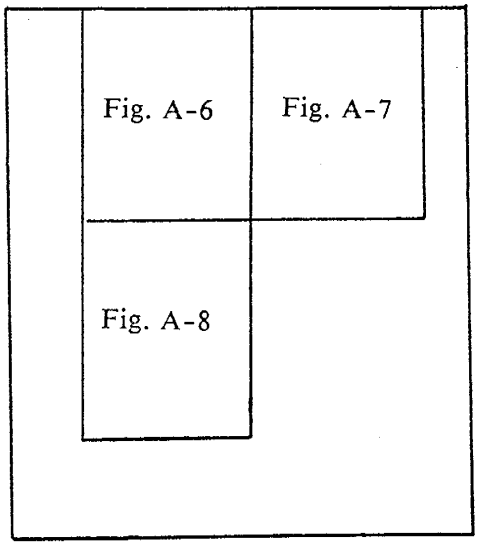

Buzzard Roost Mesa
7.5 Minute

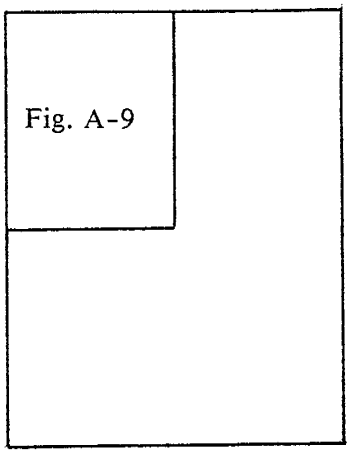

Young
15 Minute

Figure A-2

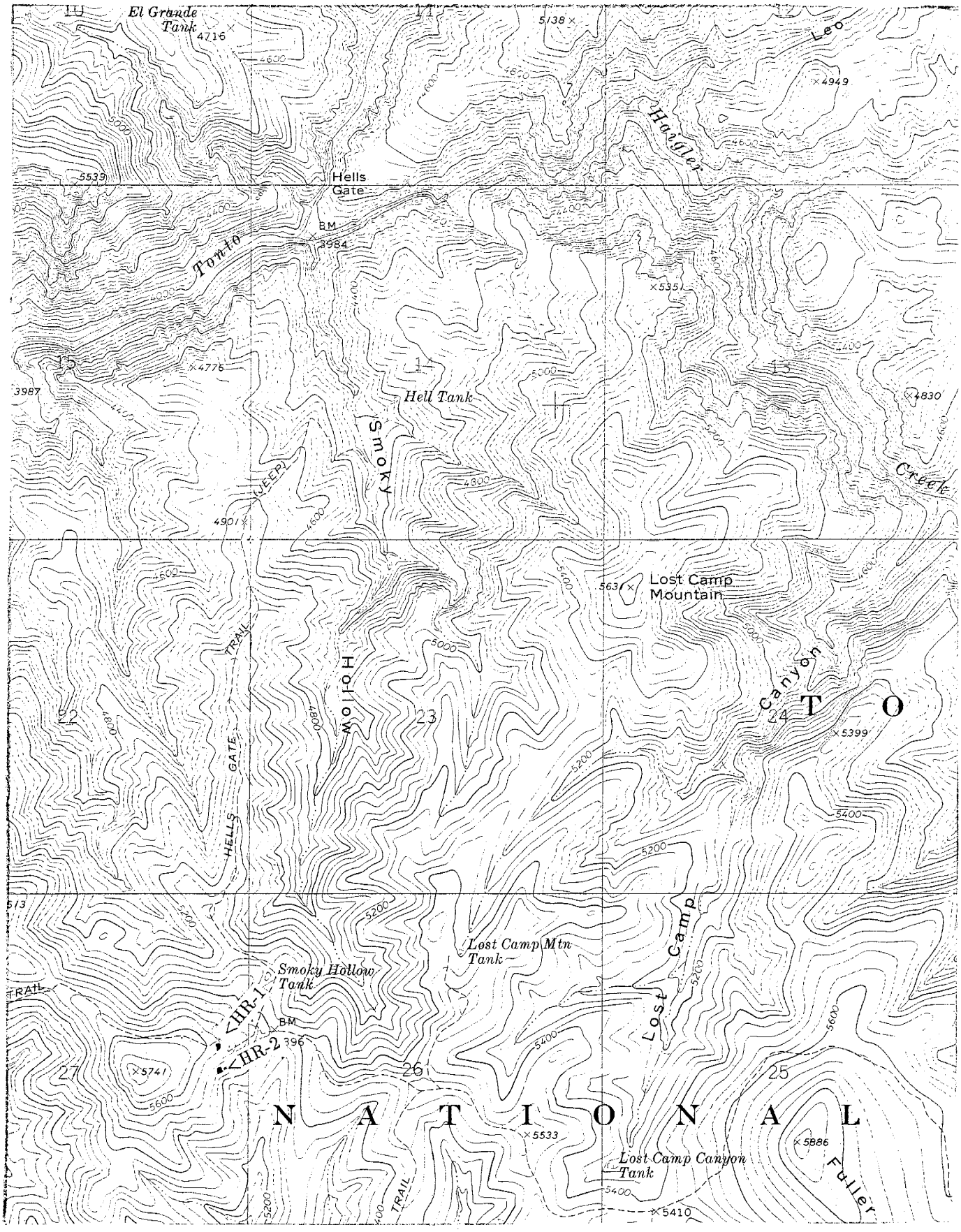
El Grande Tank
4716
Leo
4949
Hayfler
5138
5539
Hells Gate
BM
3984
Tonto
5351
4776
3987
Hell Tank
4830
Smoky
Creek
(JEEP)
4901
Lost Camp Mountain
5631
Hollow
TRAIL
HELLS GATE
Canyon
T O
5399
Lost Camp Mtn Tank
Smoky Hollow Tank
Lost Camp
HR-1
HR-2
BM
396
5741
N A T I O N A L
5533
Lost Camp Canyon Tank
5886
5410
Fuller
TRAIL

Figure A-3

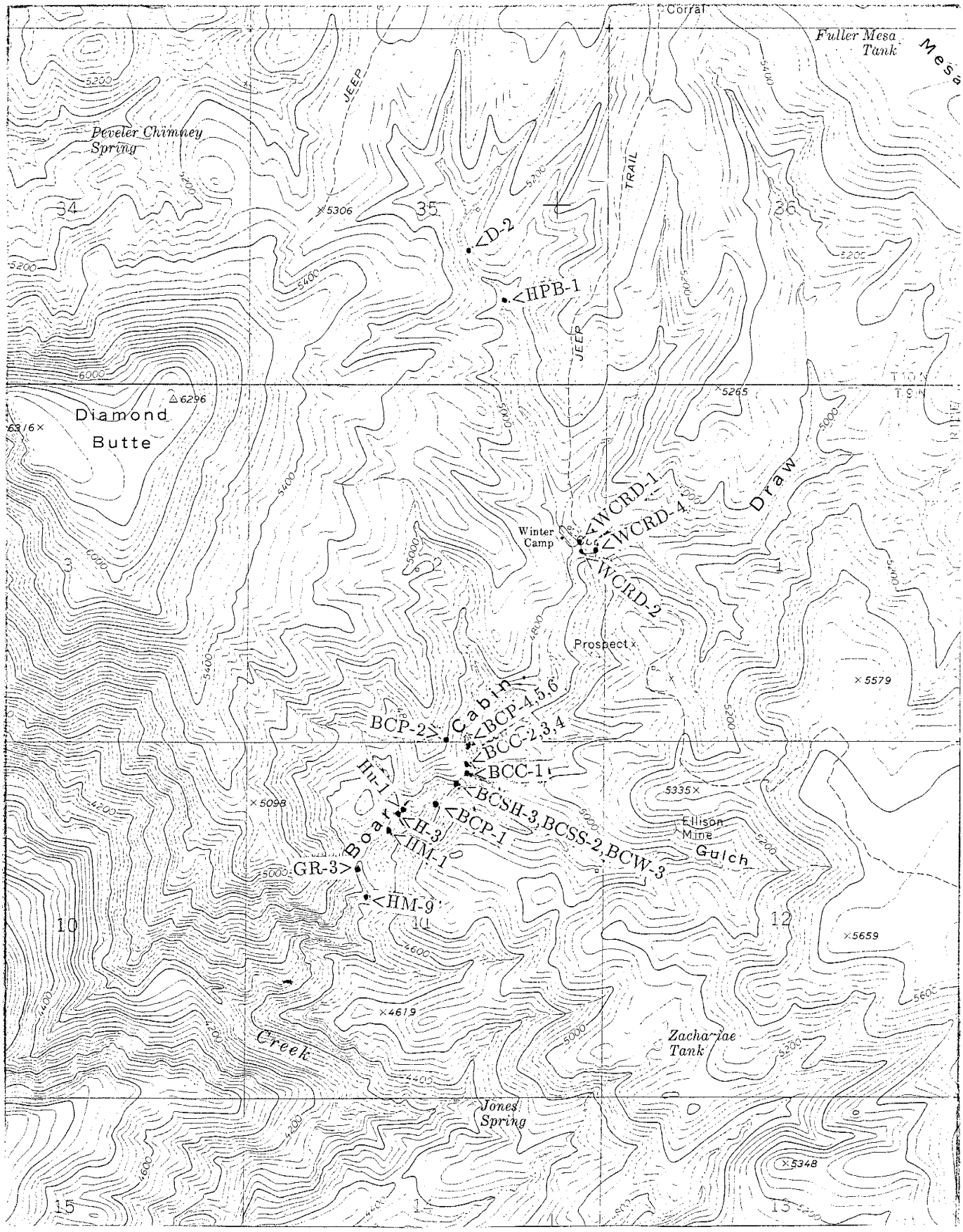
Corral
Fuller Mesa Tank
Mesa
Peveler Chimney Spring
JEEP
TRAIL
JEEP
5306
D-2
HPB-1
5265
Diamond Butte
6296
Winter Camp
WCRD-1
WCRD-4
WCRD-2
Draw
Prospect
5579
Cabin
BCP-2
BCP-4,5,6
BCC-2,3,4
BCC-1
BCSH-3,BCSS-2,BCW-3
BCP-1
Hu-1
H-3
HM-1
HM-9
GR-3
Boar
5098
5335
Ellison Mine
Gulch
5659
4619
Creek
Zachariae Tank
Jones Spring
5348
34
35
36
3
2
1
10
11
12
15
14
13

Figure A-4

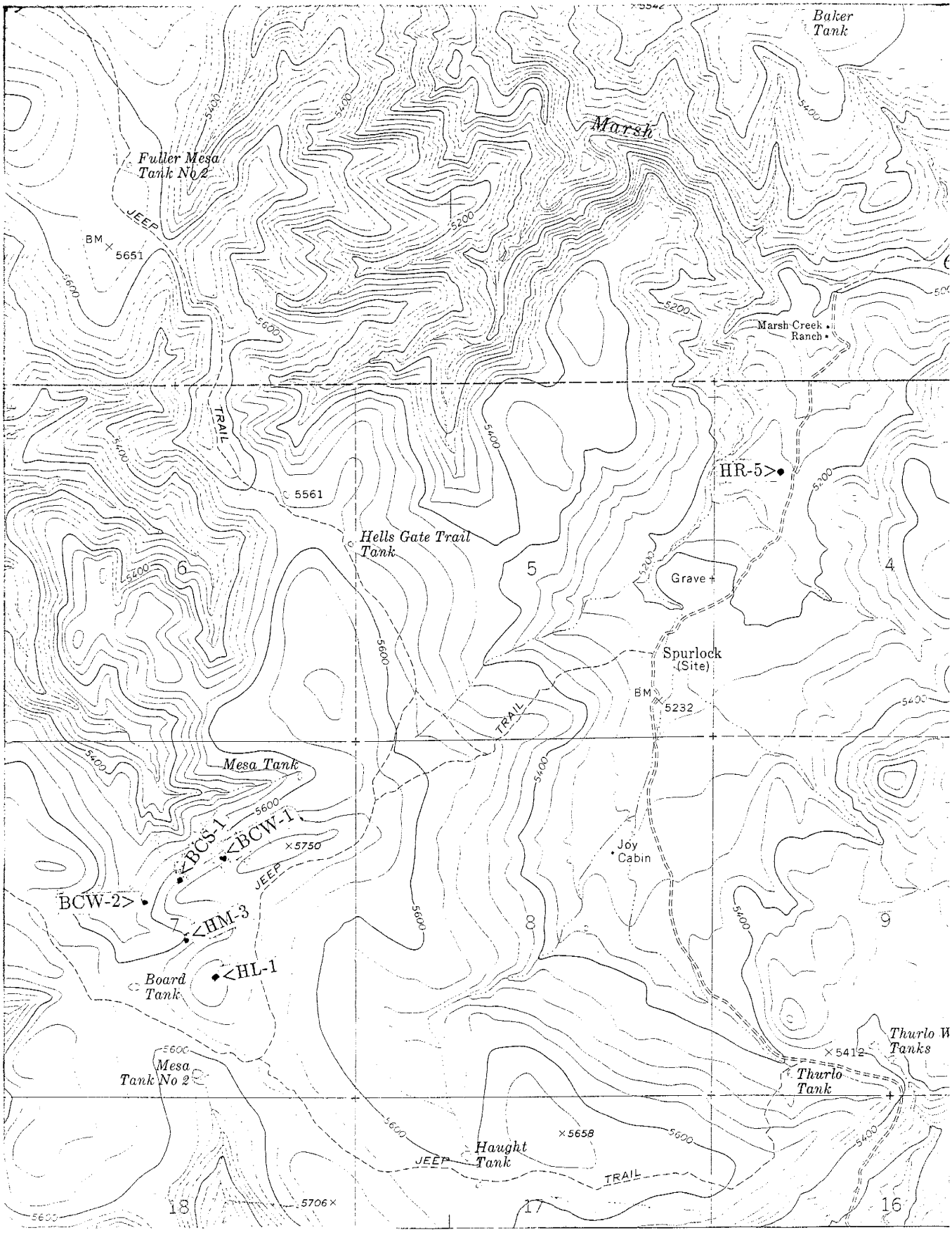
Baker Tank
Marsh
Fuller Mesa Tank No 2
JEEP
BM 5651
Marsh Creek Ranch
TRAIL
5561
Hells Gate Trail Tank
HR-5>
Grave
Spurlock (Site)
BM 5232
Mesa Tank
<BCS-1
<BCW-1
JEEP
BCW-2>
<HM-3
<HL-1
Board Tank
Joy Cabin
Mesa Tank No 2
Thurlo Tanks
Thurlo Tank
Haught Tank
JEEP
TRAIL
5706
5658
5412
18
17
16
6
5
4
8
9

Figure A-5

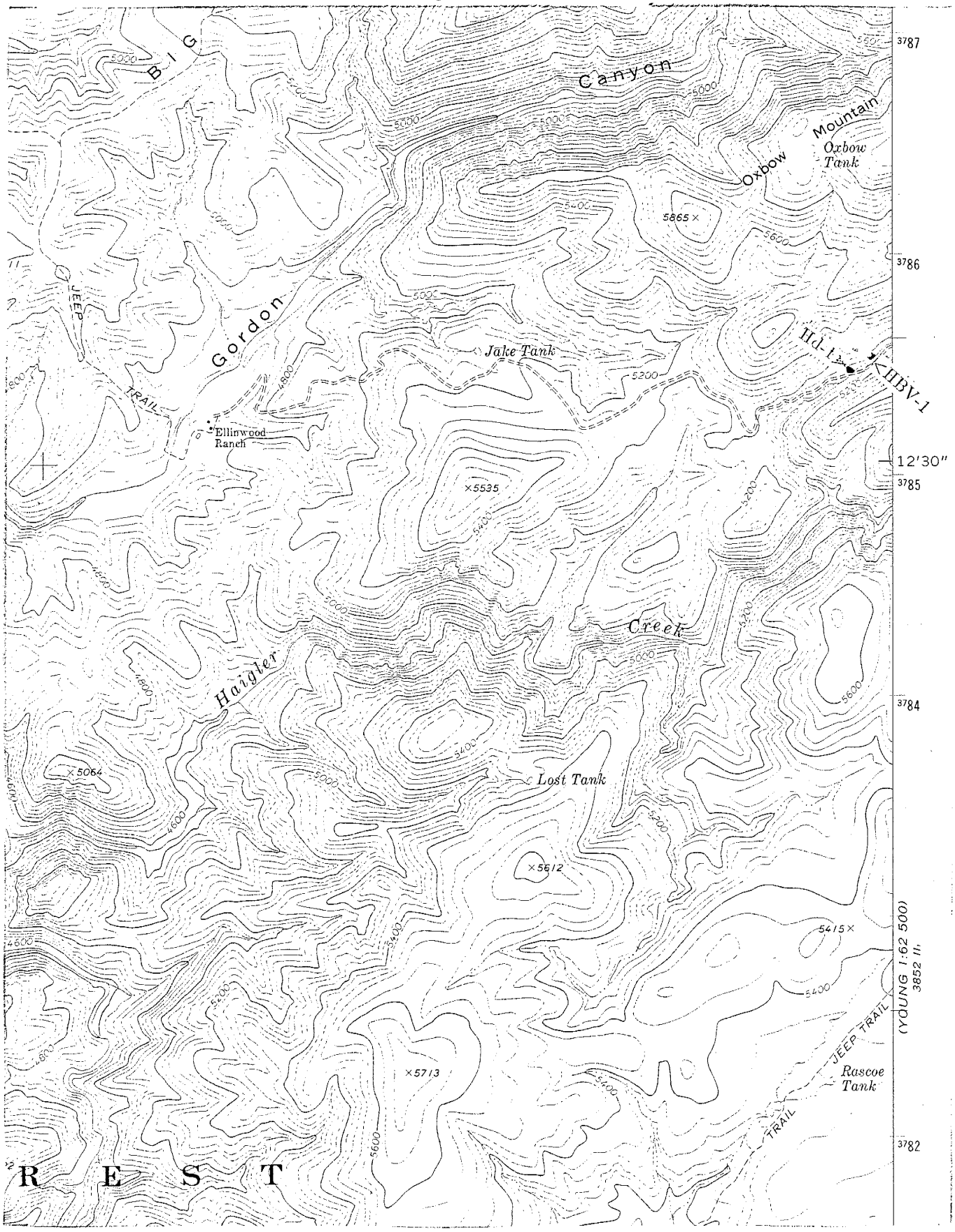
B I G
Canyon
Oxbow
Mountain
Oxbow
Tank
5865×
Gordon
JEEP
TRAIL
Jake Tank
Ellinwood
Ranch
×5535
Haigler
Creek
×5064
Lost Tank
×5612
×5713
5415×
JEEP TRAIL
Rascoe
Tank
TRAIL
R E S T
3787
3786
3785
3784
3782
12'30"
(YOUNG 1:62 500)
3852 II.

Figure A-6

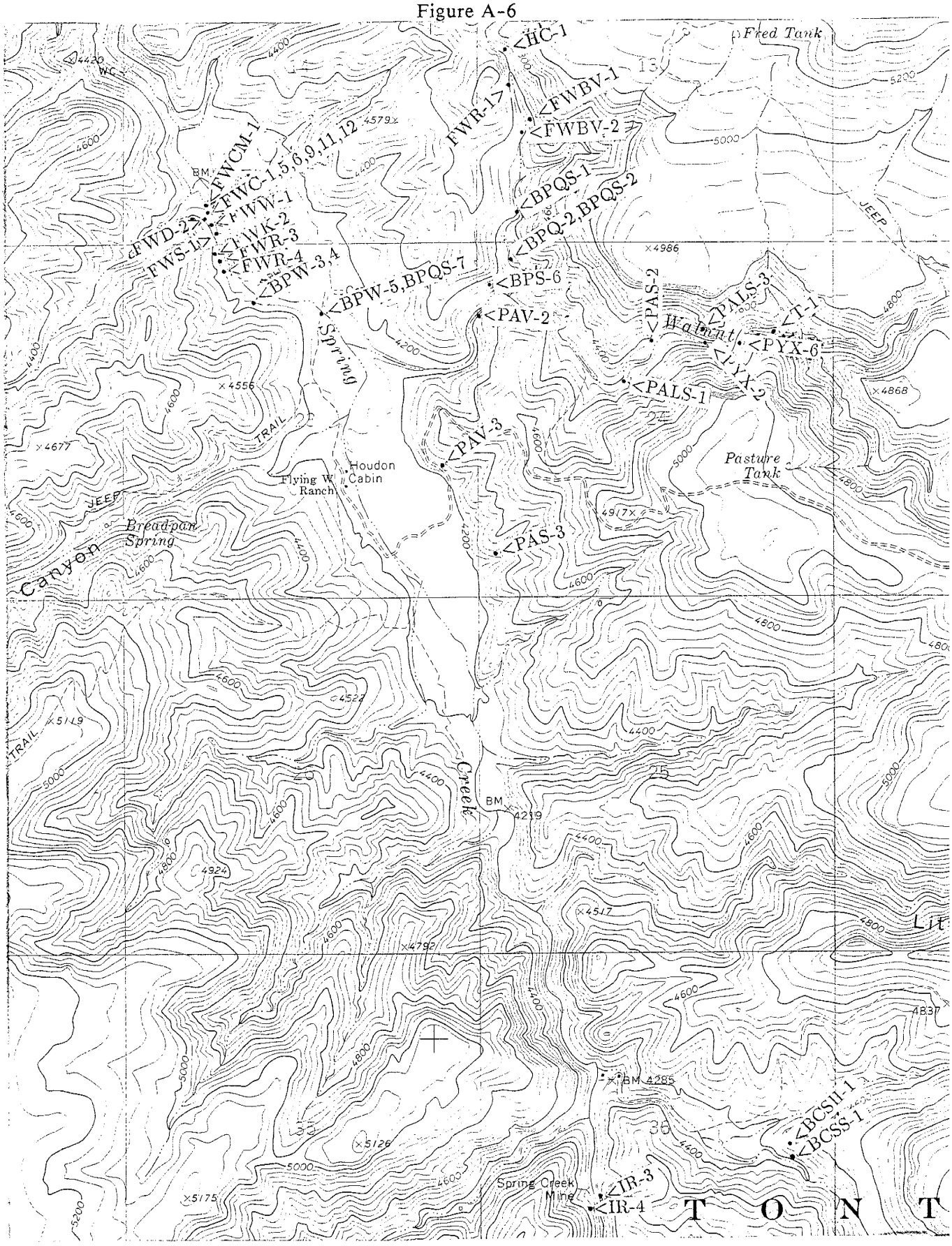
HC-1
Fred Tank
FWR-1
FWBV-1
FWBV-2
FWCM-1
FWC-1,5,6,9,11,12
FWW-1
FWK-2
FWR-3
FWR-4
FWD-2
FWS-1
BPW-3,4
BPW-5,BPQS-7
BPS-6
BPQ-2,BPQS-2
BPQS-1
PAV-2
PAV-3
PAS-2
PAS-3
PALS-1
PALS-2
PALS-3
PYX-1
PYX-2
PYX-6
T-1
Houdon Cabin
Flying W Ranch
Breadpan Spring
Canyon
Spring
Creek
Pasture Tank
Walnut
JEEP
TRAIL
BM 4219
BM 4285
Spring Creek Mine
IR-3
IR-4
BCSII-1
BCSS-1
T O N T

Figure A-7

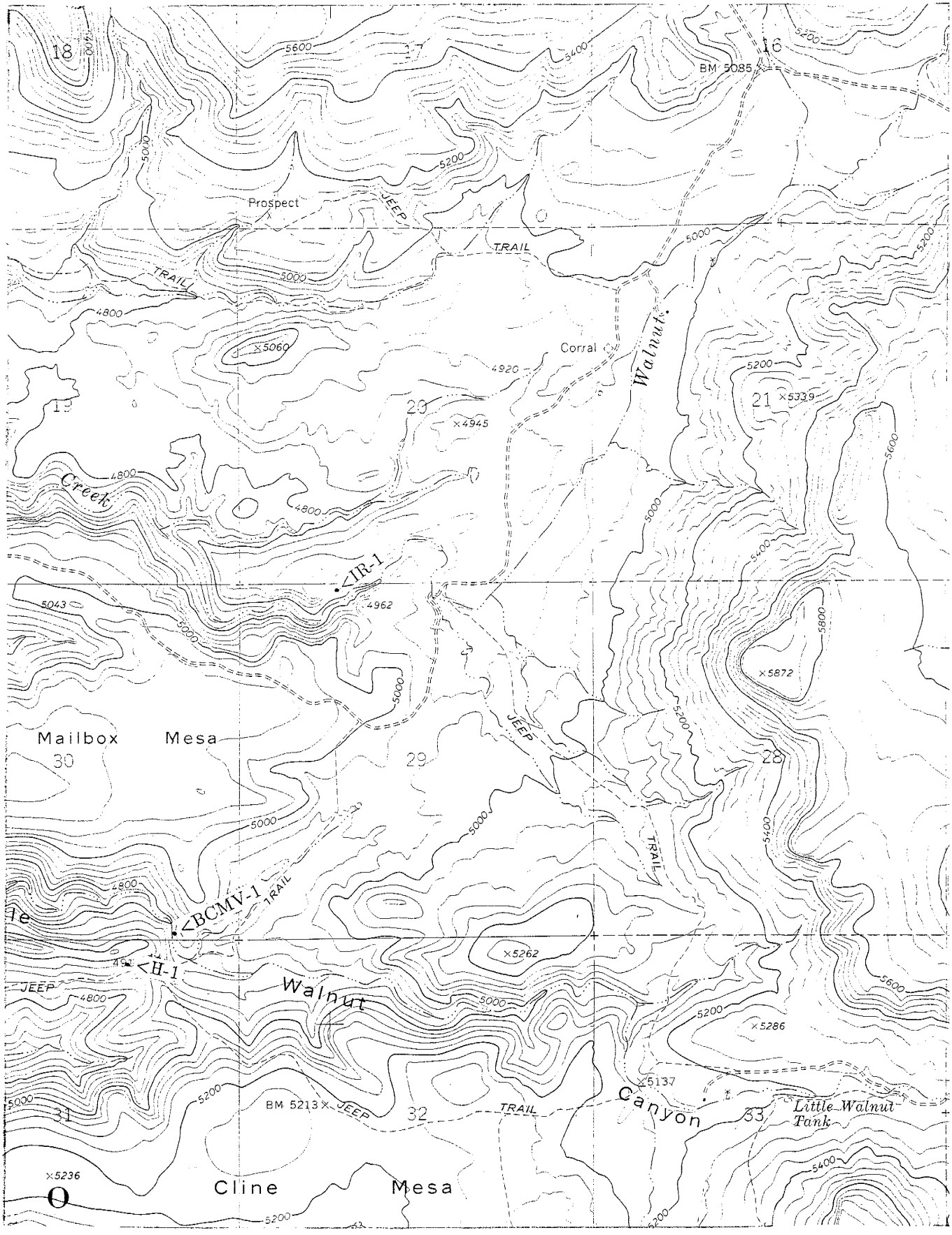
Prospect
JEEP
TRAIL
Corral
Walnut
Creek
Mailbox
Mesa
Cline
Mesa
Canyon
Little Walnut
Tank
BM 5085
BM 5213
IR-1
BCMV-1
H-1
×5060
×4945
×5339
×5872
×5262
×5286
×5137
×5236
4962
5043
4920
18
17
16
19
20
21
30
29
28
31
32
33

Figure A-8

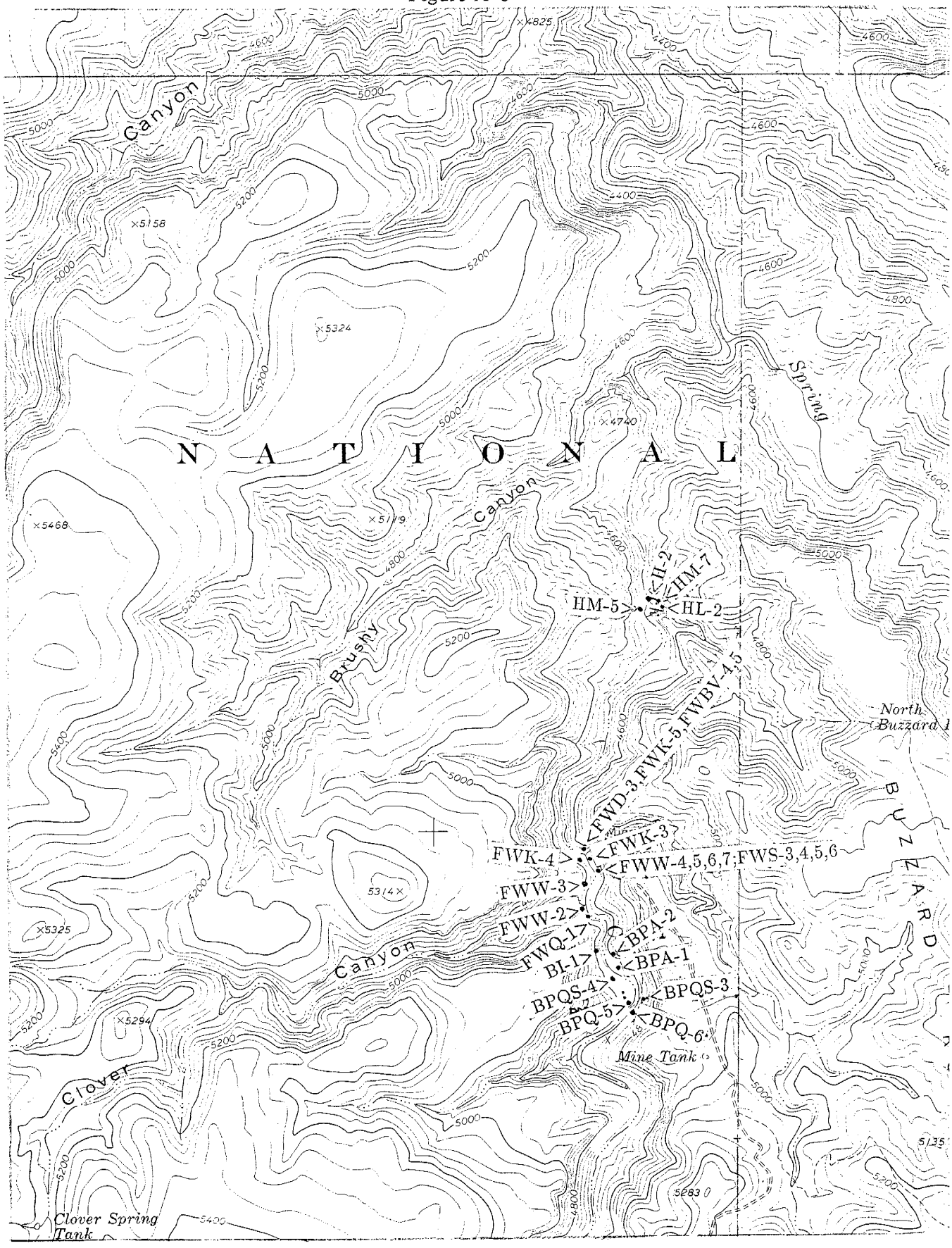
N A T I O N A L
Canyon
Canyon
Canyon
Canyon
Brushy
Spring
Clover
Clover Spring Tank
Mine Tank
North Buzzard
BUZZARD
HM-5
HL-2
HM-7
FWD-3,FWK-3,FWBV-4,5
FWK-4
FWK-3
FWW-4,5,6,7;FWS-3,4,5,6
FWW-3
FWW-2
FWQ-1
BPA-2
BI-1
BPA-1
BPQS-4
BPQS-3
BPQ-5
BPQ-6
×4825
×5158
×5324
×4740
×5468
×5179
×5325
×5294
5314×
5135
5083
4600
4800
5000
5200
5400

Figure A-9

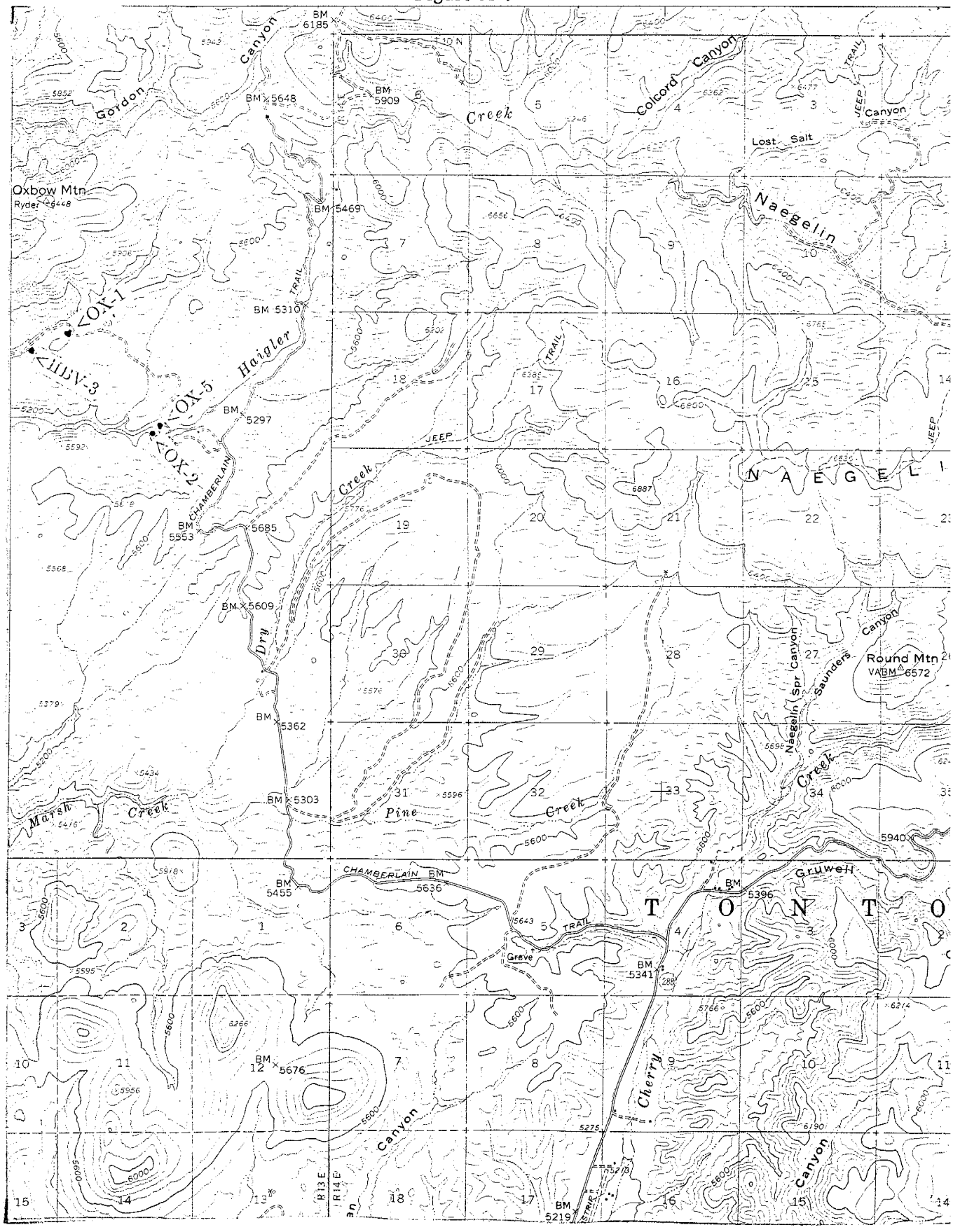
Oxbow Mtn
Ryder 6448
Gordon Canyon
Colcord Canyon
Lost Salt Canyon
Naegelin
Haigler Creek
Dry Creek
Pine Creek
Marsh Creek
Cherry Canyon
Saunders Canyon
Spr Canyon
Round Mtn
VABM 6572
Gruwell
Greve
CHAMBERLAIN
TRAIL
JEEP
BM 6185
BM 5648
BM 5909
BM 5469
BM 5310
BM 5297
BM 5685
BM 5553
BM 5609
BM 5362
BM 5303
BM 5455
BM 5636
BM 5396
BM 5341
BM 5676
BM 5219
OX-1
OX-2
OX-3
OX-5
T 10 N
T O N T O
R 13 E
R 14 E

APPENDIX B: CHEMICAL DATA AND CIPW NORMATIVE MINERALS FOR IGNEOUS ROCKS

Table B-1
Chemical Composition of Igneous Rocks

MAFIC ROCKS	PRE-ALDER	PRE-ALDER	ALDER	ALDER	ALDER
	BAS-AND	BAS-AND	BAS-AND	BASALT	BAS-AND
SAMPLE	*PAV-2	*PAV-3	FWBV-2	*FWC-12	FWC-9
SiO2	49.26	52.50	51.25	50.60	55.13
TiO2	0.90	0.88	2.02	2.05	1.67
Al2O3	14.51	12.65	14.62	13.57	16.85
Fe2O3-T	10.30	8.48	12.30	7.05	11.61
MgO	4.12	2.74	4.40	3.68	1.31
CaO	8.11	9.45	6.16	4.49	3.32
Na2O	1.99	1.32	3.71	5.43	2.81
K2O	0.61	1.03	0.75	0.99	3.35
MnO	0.11	0.15	0.36	0.31	0.14
P2O5	0.22	0.28	0.56	0.86	0.74
LOI	10.38	10.28	4.07	4.73	3.12
TOTAL	100.51	99.76	100.20	99.75	100.05
Rb	47	38	36	58	123
Ba	367	669	350	474	1351
Cs	11	8	8	23	29
Sr	266	200	487	505	328
Pb	13	13	15	27	20
Th	2.4	3.5	3.9	6.6	3.5
U	1.6	1.6	1.7	3.6	3.6
Sc	29	17	44	24	23
V	287	152	6291	133	167
Cr	226	99	4	6	77
Co	31	28	37	81	18
Ni	49	28	6	27	53
Y	17	20	40	44	48
Zr	100	125	175	251	177
Nb	6	8	10	22	10
Hf	2.4	3.2	4.8	5.5	4.0
Ta	0.4	0.6	0.5	1.5	0.5
La	16	21	35	37	37
Ce	36.4	44.5	76.7	90.8	75.9
Sm	4.3	5.0	9.7	10.3	9.9
Eu	1.2	1.4	3.1	2.8	2.6
Tb	0.6	0.6	1.3	0.9	1.8
Yb	1.5	2.0	4.5	2.3	4.5
Lu	0.23	0.30	0.60	0.38	0.64

Table B-1 (continued)
Chemical Composition of Igneous Rocks

Mg Number	47	42	45	54	20
K2O/Na2O	0.31	0.78	0.20	0.18	1.19
Na2O+K2O	2.60	2.35	4.46	6.42	6.16
Al2O3/TiO2	16.1	14.4	7.2	9.6	10.1
CaO/TiO2	9.0	10.7	3.1	2.2	2.0
Zr/TiO2	0.01	0.01	0.01	0.01	0.01
K/Rb	108	225	171	142	226
Ba/Sr	1.4	3.3	0.7	0.9	4.1
Rb/Sr	0.2	0.2	0.1	0.1	0.4
La/Yb	11.0	10.4	7.8	12.8	8.3
La/Sm	3.8	4.1	3.6	3.5	3.7
Sm/Eu	3.6	3.7	3.1	3.7	3.8
Ti/Zr	54.1	42.3	69.2	48.9	56.6
Zr/Nb	17.5	14.9	18.1	11.4	17.5
Nb/Y	0.3	0.4	0.2	0.5	0.2
Zr/Y	5.7	6.4	4.4	5.7	3.7
Nb/Ta	15.9	14.0	18.9	14.8	20.2
Nb/La	0.4	0.4	0.3	0.6	0.3
Ce/Pb	2.9	3.5	5.1	3.4	3.8
Nb/U	3.6	5.1	5.6	6.2	2.8
La/Ta	45	34	69	24	74
La/Th	6.9	5.9	9.0	5.5	10.6
Y/Tb	31.7	31.7	30.5	47.2	26.9
Th/Yb	1.6	1.8	0.9	2.3	0.8
Th/Sc	0.1	0.2	0.1	0.3	0.2
Th/Nb	0.4	0.4	0.4	0.3	0.3
Sc/Ni	0.6	0.6	7.4	0.9	0.9
Hf/Ta	6.8	5.3	9.4	3.7	8.0
Ta/Yb	0.24	0.30	0.11	0.52	0.11
Hf/Th	1.0	0.9	1.2	0.8	1.1
Ti/V	19	35	2	89	60
U/Pb	0.1	0.1	0.1	0.1	0.2
FeO-T/MgO	2.3	2.8	2.5	1.7	8.0
Sm/Yb	2.9	2.5	2.1	3.6	2.2

Table B-1 (continued)
Chemical Composition of Igneous Rocks

MAFIC ROCKS SAMPLE	ALDER BAS-AND BCP-1	GABBRO HPB-1	DIORITE DIKE Hd-1	BASALT DIKE *FWD-2	DIORITE DIKE FWD-3	GABBRO *PYX-2
SiO2	56.08	46.22	50.73	45.61	51.48	42.72
TiO2	1.09	1.12	1.65	1.98	1.07	1.83
Al2O3	18.20	10.48	13.81	15.51	17.43	8.82
Fe2O3-T	7.41	14.14	13.48	14.60	10.81	18.42
MgO	2.47	14.01	5.69	7.61	6.23	10.82
CaO	7.64	5.85	8.75	7.08	8.58	13.23
Na2O	3.07	1.13	2.67	1.90	3.13	0.59
K2O	0.81	0.52	1.66	0.07	1.40	0.02
MnO	0.17	0.22	0.23	0.24	0.25	0.25
P2O5	0.38	0.61	0.24	0.45	0.24	0.02
LOI	2.87	5.54	1.25	4.73	1.34	2.66
TOTAL	100.14	99.84	100.17	99.77	101.96	99.36
Rb	27	18	58	7	44	4
Ba	566	347	302	81	418	1
Cs	4	5	2	4	10	0
Sr	687	292	212	267	644	159
Pb	14	13	20	7	8	9
Th	3.1	1.5	3.0	0.9	2.0	0.0
U	1.5	0.6	1.1	0.6	0.7	0.0
Sc	21	18	29	24	30	59
V	179	168	307	268	280	1247
Cr	35	1482	27	72	47	26
Co	26	82	44	46	38	87
Ni	39	545	68	103	52	92
Y	21	18	42	30	18	11
Zr	140	113	158	135	90	24
Nb	8	10	7	9	5	1
Hf	3.5	2.4	3.9	2.6	2.4	0.4
Ta	0.4	0.4	0.3	0.4	0.2	0.1
La	29	26	14	14	14	1
Ce	64.3	56.3	31.2	35.8	27.3	1.5
Sm	6.5	5.4	5.0	5.1	3.7	1.0
Eu	1.8	1.5	1.3	1.6	1.2	0.3
Tb	0.8	0.6	0.8	0.6	0.5	0.3
Yb	2.2	1.5	3.2	1.9	1.5	0.9
Lu	0.32	0.21	0.49	0.34	0.25	0.15

Table B-1 (continued)
Chemical Composition of Igneous Rocks

Mg Number	43	69	49	54	56	57
K2O/Na2O	0.26	0.46	0.62	0.04	0.44	0.03
Na2O+K2O	3.88	1.65	4.33	1.97	4.59	0.60
Al2O3/TiO2	16.7	9.4	8.4	7.8	16.3	4.8
CaO/TiO2	7.0	5.2	5.3	3.6	8.0	7.2
Zr/TiO2	0.01	0.01	0.01	0.01	0.01	.00
K/Rb	252	243	237	81	264	28
Ba/Sr	0.8	1.2	1.4	0.3	0.6	.0
Rb/Sr	.0	0.1	0.3	.0	0.1	.0
La/Yb	12.9	17.1	4.2	7.2	9.1	0.9
La/Sm	4.4	4.9	2.7	2.7	3.7	0.8
Sm/Eu	3.6	3.5	3.9	3.2	3.1	3.3
Ti/Zr	46.6	59.4	63.0	87.9	71.5	466.0
Zr/Nb	16.7	10.8	22.6	14.9	16.4	19.1
Nb/Y	0.4	0.6	0.2	0.3	0.3	0.1
Zr/Y	6.6	6.2	3.7	4.5	4.9	2.1
Nb/Ta	21.0	24.3	24.0	26.0	27.9	12.3
Nb/La	0.3	0.4	0.5	0.7	0.4	1.5
Ce/Pb	4.6	4.2	1.6	5.0	2.9	0.2
Nb/U	5.5	16.8	6.6	14.4	7.7	ERR
La/Ta	72	60	47	39	71	8
La/Th	9.2	16.7	4.5	14.7	7.2	ERR
Y/Tb	26.7	32.5	54.1	47.9	39.5	40.9
Th/Yb	1.4	1.0	0.9	0.5	1.3	0.0
Th/Sc	0.1	0.1	0.1	.0	0.1	0.0
Th/Nb	0.4	0.1	0.4	0.1	0.4	0.0
Sc/Ni	0.9	.0	0.4	0.2	0.6	0.6
Hf/Ta	8.8	5.5	13.5	7.4	12.4	4.4
Ta/Yb	0.18	0.29	0.09	0.18	0.18	0.11
Hf/Th	1.1	1.5	1.3	2.8	1.2	ERR
Ti/U	37	40	32	44	23	9
U/Pb	0.1	.0	0.1	0.1	0.1	0.0
FeO-T/MgO	2.7	0.9	2.1	1.7	1.6	1.5
Sm/Yb	2.9	3.6	1.6	2.6	2.4	1.1

Table B-1 (continued)
Chemical Composition of Igneous Rocks

MAFIC ROCKS	GABBRO
SAMPLE	*PYX-6
SiO2	47.01
TiO2	0.43
Al2O3	12.33
Fe2O3-T	9.19
MgO	15.25
CaO	6.69
Na2O	2.47
K2O	0.06
MnO	0.15
P2O5	0.15
LOI	7.81
TOTAL	101.56
Rb	1
Ba	20
Cs	1
Sr	77
Pb	3
Th	1.6
U	0.7
Sc	26
V	164
Cr	470
Co	89
Ni	518
Y	11
Zr	62
Nb	4
Hf	1.6
Ta	0.1
La	14
Ce	29.4
Sm	2.8
Eu	0.7
Tb	0.3
Yb	1.1
Lu	0.19

Table B-1 (continued)
Chemical Composition of Igneous Rocks

Mg Number	79
K2O/Na2O	0.02
Na2O+K2O	2.53
Al2O3/TiO2	28.8
CaO/TiO2	15.6
Zr/TiO2	0.01
K/Rb	465
Ba/Sr	0.3
Rb/Sr	.0
La/Yb	12.6
La/Sm	4.9
Sm/Eu	3.8
Ti/Zr	41.5
Zr/Nb	14.0
Nb/Y	0.4
Zr/Y	5.6
Nb/Ta	40.3
Nb/La	0.2
Ce/Pb	10.9
Nb/U	6.8
La/Ta	124
La/Th	8.4
Y/Tb	36.0
Th/Yb	1.5
Th/Sc	0.1
Th/Nb	0.4
Sc/Ni	.0
Hf/Ta	14.2
Ta/Yb	0.10
Hf/Th	1.0
Ti/V	16
U/Pb	0.2
FeO-T/MgO	0.5
Sm/Yb	2.6

Table B-1 (continued)
Chemical Composition of Igneous Rocks

ANDESITE ROCKS SAMPLE	ALDER ANDESITE FWK-2	ALDER ANDESITE FWC-11	ALDER ANDESITE FWBV-4	ALDER ANDESITE *FWBV-5	ALDER ANDESITE *BCP-2
SiO2	56.51	51.85	57.29	56.94	51.22
TiO2	1.19	1.38	1.40	1.42	1.06
Al2O3	17.62	19.60	15.40	15.45	17.16
Fe2O3-T	7.17	10.18	11.65	11.83	7.53
MgO	2.68	1.78	3.31	3.16	3.18
CaO	4.21	4.09	4.28	2.99	7.47
Na2O	3.94	3.50	4.42	7.12	2.48
K2O	2.00	3.46	1.56	0.53	2.61
MnO	0.13	0.16	0.20	0.20	0.15
P2O5	0.51	0.38	0.40	0.42	0.47
LOI	4.14	3.47	0.54	0.78	6.99
TOTAL	100.10	99.87	100.40	100.84	100.52
Rb	89	168	47	14	91
Ba	823	1239	815	269	828
Cs	17	41	8	2	7
Sr	446	484	504	348	548
Pb	19	21	12	10	16
Th	5.7	3.9	3.9	4.0	5.1
U	2.8	2.5	2.0	2.0	2.3
Sc	17	21	24	24	17
V	103	154	205	182	168
Cr	21	66	1	3	57
Co	22	20	25	28	23
Ni	21	41	6	5	55
Y	36	36	45	45	24
Zr	213	182	201	205	164
Nb	13	10	13	13	10
Hf	5.1	4.1	5.2	5.5	3.7
Ta	0.7	0.6	0.9	0.7	0.5
La	38	36	29	27	39
Ce	84.3	75.7	58.6	56.6	86.6
Sm	8.5	7.6	7.0	6.7	7.8
Eu	2.1	2.1	2.3	1.7	1.9
Tb	1.2	1.1	1.1	1.3	0.9
Yb	3.0	3.2	3.8	3.1	2.2
Lu	0.47	0.49	0.59	0.57	0.32

Table B-1 (continued)
Chemical Composition of Igneous Rocks

Mg Number	46	28	39	38	43
K2O/Na2O	0.51	0.99	0.35	0.07	1.13
Na2O+K2O	5.94	6.97	5.98	7.65	5.29
Al2O3/TiO2	14.8	14.2	11.0	10.9	16.2
CaO/TiO2	3.5	3.0	3.0	2.1	7.0
Zr/TiO2	0.02	0.01	0.01	0.01	0.02
K/Rb	188	171	274	306	256
Ba/Sr	1.8	2.6	1.6	0.8	1.5
Rb/Sr	0.2	0.3	0.1	.0	0.2
La/Yb	12.5	11.2	7.6	8.7	17.4
La/Sm	4.4	4.7	4.1	4.0	5.0
Sm/Eu	4.0	3.6	3.0	3.9	4.1
Ti/Zr	33.5	45.6	41.7	41.6	38.8
Zr/Nb	16.7	18.5	15.4	15.6	16.7
Nb/Y	0.4	0.3	0.3	0.3	0.4
Zr/Y	6.0	5.1	4.5	4.5	6.6
Nb/Ta	19.4	15.6	15.1	18.5	18.9
Nb/La	0.3	0.3	0.5	0.5	0.3
Ce/Pb	4.4	3.5	5.0	5.7	5.5
Nb/U	4.6	3.9	6.6	6.6	4.2
La/Ta	57	57	33	38	75
La/Th	6.7	9.2	7.4	6.7	7.6
Y/Tb	29.3	33.2	42.1	35.3	27.2
Th/Yb	1.9	1.2	1.0	1.3	2.3
Th/Sc	0.3	0.2	0.2	0.2	0.3
Th/Nb	0.4	0.4	0.3	0.3	0.5
Sc/Ni	0.3	0.5	3.8	4.8	0.3
Hf/Ta	7.7	6.5	6.1	7.7	7.0
Ta/Yb	0.22	0.20	0.23	0.22	0.23
Hf/Th	0.9	1.1	1.4	1.4	0.7
Ti/V	70	54	41	47	38
U/Pb	0.1	0.1	0.2	0.2	0.1
FeO-T/MgO	2.4	5.1	3.2	3.4	2.1
Sm/Yb	2.8	2.4	1.9	2.2	3.5

Table B-1 (continued)
Chemical Composition of Igneous Rocks

ANDESITE ROCKS	ALDER ANDESITE	ALDER ANDESITE	ALDER ANDESITE	ALDER ANDESITE	ALDER ANDESITE	ALDER ANDESITE
SAMPLE	*BCP-4	BCP-5	BCC-2	*BCC-3	*BCC-4	*BCMV-1
SiO2	48.23	50.37	56.94	51.81	61.22	50.82
TiO2	0.81	0.92	1.01	0.96	1.27	1.17
Al2O3	15.78	16.06	18.84	19.79	15.62	15.73
Fe2O3-T	9.58	10.18	8.47	7.59	8.62	11.90
MgO	6.71	6.13	1.59	4.65	1.26	7.60
CaO	8.38	7.91	4.26	4.88	3.63	4.49
Na2O	3.46	3.73	3.42	3.17	5.53	4.32
K2O	2.45	1.71	3.44	2.34	1.40	1.21
MnO	0.17	0.17	0.09	0.28	0.10	0.15
P2O5	0.22	0.28	0.42	0.39	0.62	0.42
LOI	6.54	3.07	2.09	3.77	1.24	4.29
TOTAL	102.32	100.53	100.58	99.63	100.51	102.07
Rb	76	50	103	65	41	28
Ba	770	730	1363	1255	383	1068
Cs	16	2	5	5	2	1
Sr	501	651	607	583	450	479
Pb	38	13	25	18	18	7
Th	3.3	4.4	5.0	9.3	7.8	2.1
U	0.8	1.0	3.9	4.5	2.8	0.8
Sc	24	26	13	17	13	26
V	207	216	128	148	146	171
Cr	47	36	89	66	4	146
Co	39	41	14	29	10	40
Ni	67	56	37	54	14	101
Y	22	26	34	25	41	28
Zr	105	128	151	222	280	163
Nb	6	7	9	13	16	14
Hf	2.9	3.5	3.6	5.0	4.6	4.4
Ta	0.2	0.3	0.4	0.8	0.6	0.7
La	33	42	47	52	47	33
Ce	70.5	89.6	98.5	114.9	105.7	67.3
Sm	5.3	6.7	8.2	8.4	8.6	6.5
Eu	1.4	1.7	1.9	2.1	1.9	1.8
Tb	0.7	0.7	1.0	0.8	1.1	0.9
Yb	2.1	2.2	3.0	2.1	2.5	2.7
Lu	0.33	0.35	0.47	0.35	0.38	0.40

Table B-1 (continued)
Chemical Composition of Igneous Rocks

Mg Number	61	58	30	58	25	59
K2O/Na2O	0.71	0.46	1.01	0.74	0.25	0.28
Na2O+K2O	5.91	5.44	6.86	5.51	6.33	5.52
Al2O3/TiO2	19.5	17.5	18.6	20.6	12.3	13.5
CaO/TiO2	10.4	8.6	4.2	5.1	2.9	3.8
Zr/TiO2	0.01	0.01	0.01	0.02	0.02	0.01
K/Rb	266	281	276	301	282	355
Ba/Sr	1.5	1.1	2.2	2.2	0.9	2.2
Rb/Sr	0.2	0.1	0.2	0.1	0.1	0.1
La/Yb	16.0	19.4	15.6	24.3	18.8	12.2
La/Sm	6.3	6.3	5.8	6.2	5.4	5.0
Sm/Eu	3.7	4.1	4.3	4.1	4.6	3.5
Ti/Zr	46.0	43.0	40.2	25.9	27.2	43.0
Zr/Nb	17.2	17.5	17.1	17.1	18.0	11.5
Nb/Y	0.3	0.3	0.3	0.5	0.4	0.5
Zr/Y	4.7	4.9	4.5	9.1	6.8	5.9
Nb/Ta	30.7	26.2	20.5	16.1	26.9	20.8
Nb/La	0.2	0.2	0.2	0.3	0.3	0.4
Ce/Pb	1.9	6.8	4.0	6.5	5.9	9.4
Nb/U	8.1	7.5	2.2	2.9	5.5	17.0
La/Ta	167	152	110	64	79	48
La/Th	10.1	9.6	9.5	5.6	6.0	15.6
Y/Tb	31.9	36.0	34.4	29.2	37.7	30.8
Th/Yb	1.6	2.0	1.6	4.4	3.1	0.8
Th/Sc	0.1	0.2	0.3	0.5	0.6	0.1
Th/Nb	0.5	0.6	0.6	0.7	0.5	0.1
Sc/Ni	0.4	0.5	0.5	0.3	0.9	0.3
Hf/Ta	14.3	12.4	8.4	6.1	7.8	6.4
Ta/Yb	0.10	0.13	0.14	0.38	0.24	0.25
Hf/Th	0.9	0.8	0.7	0.5	0.6	2.1
Ti/V	23	25	47	39	52	41
U/Pb	.0	0.1	0.2	0.3	0.2	0.1
FeO-T/MgO	1.3	1.5	4.8	1.5	6.1	1.4
Sm/Yb	2.5	3.1	2.7	4.0	3.5	2.4

Table B-1 (continued)
Chemical Composition of Igneous Rocks

ANDESITE ROCKS SAMPLE	RED ROCK ANDESITE HBV-1	RED ROCK ANDESITE HBV-3	DIORITE DIKE D-2
SiO2	56.51	59.04	50.07
TiO2	1.50	1.36	1.40
Al2O3	17.57	16.46	15.85
Fe2O3-T	10.83	10.18	10.47
MgO	1.00	0.38	6.57
CaO	2.82	3.29	8.40
Na2O	4.13	3.84	3.33
K2O	3.15	2.14	1.25
MnO	0.08	0.12	0.17
P2O5	0.64	0.53	0.50
LOI	1.83	3.65	3.21
TOTAL	100.05	100.99	101.22
Rb	100	61	30
Ba	1140	886	443
Cs	6	3	1
Sr	346	545	774
Pb	14	14	7
Th	6.8	6.1	1.4
U	2.2	2.8	0.7
Sc	20	17	19
V	61	82	229
Cr	4	4	226
Co	14	14	30
Ni	4	6	97
Y	44	41	21
Zr	267	240	143
Nb	15	14	11
Hf	7.1	5.4	2.4
Ta	0.9	0.8	0.5
La	42	41	22
Ce	99.4	96.2	48.9
Sm	11.0	10.1	5.3
Eu	3.0	2.6	1.4
Tb	1.6	1.4	0.5
Yb	4.1	3.6	1.5
Lu	0.57	0.53	0.22

Table B-1 (continued)
Chemical Composition of Igneous Rocks

Mg Number	17	8	59
K2O/Na2O	0.76	0.56	0.38
Na2O+K2O	7.28	5.98	4.58
Al2O3/TiO2	11.7	12.1	11.3
CaO/TiO2	1.9	2.4	6.0
Zr/TiO2	0.02	0.02	0.01
K/Rb	260	292	352
Ba/Sr	3.3	1.6	0.6
Rb/Sr	0.3	0.1	.0
La/Yb	10.2	11.6	14.8
La/Sm	3.8	4.1	4.1
Sm/Eu	3.7	3.9	3.7
Ti/Zr	33.6	34.0	56.6
Zr/Nb	18.1	17.2	13.3
Nb/Y	0.3	0.3	0.5
Zr/Y	6.1	5.9	7.0
Nb/Ta	16.8	17.2	21.5
Nb/La	0.4	0.3	0.5
Ce/Pb	7.3	6.7	7.1
Nb/U	6.7	5.0	16.7
La/Ta	47	51	41
La/Th	6.1	6.8	15.4
Y/Tb	26.8	29.8	44.0
Th/Yb	1.7	1.7	1.0
Th/Sc	0.3	0.4	0.1
Th/Nb	0.5	0.4	0.1
Sc/Ni	4.9	2.3	0.2
Hf/Ta	8.1	6.6	4.6
Ta/Yb	0.21	0.28	0.36
Hf/Th	1.0	0.9	1.7
Ti/V	148	100	37
U/Pb	0.2	0.2	0.1
FeO-T/MgO	9.8	24.1	1.4
Sm/Yb	2.7	2.8	3.6

Table B-1 (continued)
Chemical Composition of Igneous Rocks

DACITIC ROCKS SAMPLE	ALDER DACITE *FWC-5	ALDER DACITE FWK-3	ALDER DACITE FWK-4	ALDER DACITE *FWK-5	ALDER DACITE *FWW-7
SiO2	55.49	63.71	62.74	62.91	52.04
TiO2	0.86	0.98	0.96	0.87	0.86
Al2O3	24.33	15.33	15.37	17.22	15.04
Fe2O3-T	3.00	6.48	6.87	6.86	3.68
MgO	1.20	1.77	1.58	3.63	8.48
CaO	2.48	3.10	3.43	0.43	8.84
Na2O	5.28	5.17	5.85	1.63	2.62
K2O	4.41	2.23	2.00	3.14	2.60
MnO	0.13	0.10	0.11	0.19	0.28
P2O5	0.23	0.33	0.34	0.20	0.24
LOI	3.38	2.36	2.55	3.61	1.49
TOTAL	100.72	101.55	101.79	100.75	102.13
Rb	198	64	54	96	98
Ba	1574	979	990	1003	866
Cs	58	5	5	32	9
Sr	393	368	367	185	325
Pb	18	11	8	9	10
Th	15.4	8.2	8.0	7.4	4.0
U	3.3	3.6	3.5	3.6	1.9
Sc	17	14	14	18	21
V	77	73	77	21	137
Cr	1	7	8	7	575
Co	11	15	16	12	55
Ni	16	10	7	5	348
Y	65	41	41	42	19
Zr	512	258	258	243	148
Nb	35	15	15	14	7
Hf	14.5	7.7	7.8	7.6	4.1
Ta	2.3	1.0	1.0	0.9	0.3
La	35	44	41	35	26
Ce	96.7	98.6	94.9	80.5	53.1
Sm	9.9	8.3	7.9	6.9	5.3
Eu	3.0	2.1	1.9	2.6	1.3
Tb	1.8	1.2	1.2	1.2	0.6
Yb	6.2	4.2	4.0	4.5	1.6
Lu	0.90	0.62	1.25	0.69	0.24

Table B-1 (continued)
Chemical Composition of Igneous Rocks

Mg Number	47	38	34	54	66
K2O/Na2O	0.83	0.43	0.34	1.86	0.99
Na2O+K2O	9.69	7.39	7.85	4.83	5.23
Al2O3/TiO2	28.4	15.7	16.0	19.9	17.6
CaO/TiO2	2.9	3.2	3.6	0.5	10.3
Zr/TiO2	0.06	0.03	0.03	0.03	0.02
K/Rb	184	287	310	271	221
Ba/Sr	4.0	2.7	2.7	5.4	2.7
Rb/Sr	0.5	0.2	0.1	0.5	0.3
La/Yb	5.6	10.4	10.4	7.9	15.7
La/Sm	3.5	5.3	5.2	5.1	4.9
Sm/Eu	3.3	3.9	4.2	2.6	4.0
Ti/Zr	10.0	22.7	22.3	21.3	34.8
Zr/Nb	14.4	17.4	17.8	17.5	20.2
Nb/Y	0.5	0.4	0.4	0.3	0.4
Zr/Y	7.9	6.2	6.4	5.8	7.6
Nb/Ta	15.4	15.2	14.6	15.1	29.1
Nb/La	1.0	0.3	0.4	0.4	0.3
Ce/Pb	5.5	8.8	12.4	3.0	5.1
Nb/U	10.9	4.1	4.1	3.9	3.9
La/Ta	15	45	41	38	103
La/Th	2.2	5.3	5.2	4.8	6.5
Y/Tb	36.8	33.3	34.1	34.1	30.7
Th/Yb	2.5	1.9	2.0	1.6	2.4
Th/Sc	0.9	0.6	0.6	0.4	0.2
Th/Nb	0.4	0.6	0.5	0.5	0.5
Sc/Ni	1.1	1.4	2.1	3.4	0.1
Hf/Ta	6.3	7.9	7.9	8.2	16.2
Ta/Yb	0.37	0.23	0.25	0.21	0.15
Hf/Th	0.9	0.9	1.0	1.0	1.0
Ti/V	67	80	75	247	38
U/Pb	0.2	0.3	0.5	0.4	0.2
FeO-T/MgO	2.3	3.8	3.9	1.7	1.0
Sm/Yb	1.6	2.0	2.0	1.5	3.2

Table B-1 (continued)
Chemical Composition of Igneous Rocks

DACITIC ROCKS SAMPLE	ALDER DACITE BCP-6	RED ROCK DACITE WCRD-1	RED ROCK DACITE WCRD-2	RED ROCK DACITE WCRD-4
SiO2	52.83	61.92	59.01	65.54
TiO2	1.22	1.06	1.16	0.81
Al2O3	18.55	17.16	18.13	15.58
Fe2O3-T	10.19	6.66	7.48	5.91
MgO	3.13	1.29	1.36	0.27
CaO	5.58	4.26	3.61	1.91
Na2O	4.13	5.08	3.74	5.01
K2O	2.89	2.35	3.32	3.87
MnO	0.13	0.17	0.14	0.21
P2O5	0.57	0.40	0.46	0.22
LOI	2.10	1.45	1.98	0.67
TOTAL	101.32	101.79	100.30	99.95
Rb	65	65	108	87
Ba	1158	831	928	1175
Cs	6	4	8	3
Sr	733	547	490	261
Pb	15	22	23	25
Th	7.2	8.9	10.5	8.6
U	4.2	4.3	5.0	4.2
Sc	20	13	16	15
V	182	0	71	22
Cr	72	10	18	3
Co	30	10	13	3
Ni	63	11	18	8
Y	33	39	43	59
Zr	204	307	318	380
Nb	13	16	16	19
Hf	5.3	8.5	8.3	10.2
Ta	0.6	0.9	0.9	1.1
La	49	54	63	55
Ce	113.1	119.5	145.7	117.4
Sm	9.3	9.8	11.5	11.2
Eu	2.3	2.3	2.6	2.7
Tb	1.1	1.3	1.5	2.0
Yb	2.9	3.2	3.8	5.4
Lu	0.42	0.51	0.59	0.85

Table B-1 (continued)
Chemical Composition of Igneous Rocks

Mg Number	41	30	29	9
K2O/Na2O	0.70	0.46	0.89	0.77
Na2O+K2O	7.02	7.43	7.06	8.88
Al2O3/TiO2	15.2	16.3	15.6	19.2
CaO/TiO2	4.6	4.0	3.1	2.4
Zr/TiO2	0.02	0.03	0.03	0.05
K/Rb	370	298	254	370
Ba/Sr	1.6	1.5	1.9	4.5
Rb/Sr	0.1	0.1	0.2	0.3
La/Yb	17.3	16.8	16.7	10.2
La/Sm	5.3	5.6	5.5	4.9
Sm/Eu	4.1	4.2	4.4	4.1
Ti/Zr	36.0	20.7	21.9	12.8
Zr/Nb	15.3	19.4	19.4	19.5
Nb/Y	0.4	0.4	0.4	0.3
Zr/Y	6.1	7.9	7.4	6.4
Nb/Ta	20.6	18.0	17.4	17.1
Nb/La	0.3	0.3	0.3	0.4
Ce/Pb	7.3	5.4	6.5	4.7
Nb/U	3.2	3.7	3.3	4.6
La/Ta	75	62	67	48
La/Th	6.8	6.1	6.0	6.4
Y/Tb	30.6	30.2	28.1	29.2
Th/Yb	2.6	2.8	2.8	1.6
Th/Sc	0.4	0.7	0.7	0.6
Th/Nb	0.5	0.6	0.6	0.4
Sc/Ni	0.3	1.2	0.9	1.3
Hf/Ta	8.1	9.6	9.4	8.3
Ta/Yb	0.23	0.27	0.25	0.21
Hf/Th	0.7	1.0	0.8	1.2
Ti/V	40	ERR	98	222
U/Pb	0.3	0.2	0.2	0.2
FeO-T/MgO	2.9	4.7	4.9	19.7
Sm/Yb	3.3	3.0	3.0	2.1

Table B-1 (continued)
Chemical Composition of Igneous Rocks

DACITIC ROCKS SAMPLE	INTRUSIVE DACITE *IR-1	INTRUSIVE DACITE IR-3	INTRUSIVE DACITE IR-4	INTRUSIVE DACITE BI-1
SiO2	70.07	72.17	73.02	59.66
TiO2	0.51	0.33	0.32	1.26
Al2O3	14.48	13.69	13.59	15.55
Fe2O3-T	2.95	2.47	2.15	8.61
MgO	1.66	1.09	1.32	2.66
CaO	0.31	1.58	1.23	4.28
Na2O	2.04	2.70	3.32	4.80
K2O	7.12	4.68	4.14	1.93
MnO	0.04	0.07	0.11	0.18
P2O5	0.16	0.11	0.12	0.50
LOI	1.22	1.27	1.02	1.48
TOTAL	100.57	100.16	100.93	100.91
Rb	143	200	139	55
Ba	766	915	1149	672
Cs	3	12	7	9
Sr	113	121	116	446
Pb	12	18	14	13
Th	11.3	12.9	12.8	5.3
U	3.1	4.7	3.4	2.5
Sc	11	11	11	17
V	26	13	23	56
Cr	14	9	6	3
Co	4	3	3	13
Ni	15	5	5	3
Y	53	64	57	41
Zr	214	152	150	220
Nb	16	16	15	13
Hf	5.8	6.7	6.3	6.4
Ta	1.0	1.3	1.2	0.8
La	45	44	45	35
Ce	98.7	101.0	103.6	81.8
Sm	10.3	10.2	10.1	8.1
Eu	1.9	2.0	1.9	2.3
Tb	1.4	1.7	1.8	1.3
Yb	4.1	6.3	5.9	3.9
Lu	0.62	1.01	0.92	0.62

Table B-1 (continued)
Chemical Composition of Igneous Rocks

Mg Number	56	50	58	41
K2O/Na2O	3.48	1.73	1.06	0.40
Na2O+K2O	9.17	7.38	8.05	6.73
Al2O3/TiO2	28.2	41.7	42.2	12.4
CaO/TiO2	0.6	4.8	3.8	3.4
Zr/TiO2	0.04	0.05	0.05	0.02
K/Rb	413	194	247	283
Ba/Sr	6.5	7.6	9.9	1.5
Rb/Sr	1.2	1.7	1.2	0.1
La/Yb	10.9	7.0	7.7	9.1
La/Sm	4.4	4.3	4.5	4.3
Sm/Eu	5.3	5.1	5.2	3.5
Ti/Zr	14.4	12.9	12.9	34.3
Zr/Nb	13.0	9.5	10.0	17.2
Nb/Y	0.3	0.3	0.3	0.3
Zr/Y	4.0	2.4	2.6	5.4
Nb/Ta	17.2	12.5	12.4	16.3
Nb/La	0.4	0.4	0.3	0.4
Ce/Pb	8.1	5.6	7.4	6.2
Nb/U	5.3	3.4	4.4	5.2
La/Ta	47	34	37	46
La/Th	4.0	3.4	3.6	6.5
Y/Tb	37.7	36.6	31.7	32.0
Th/Yb	2.8	2.1	2.2	1.4
Th/Sc	1.1	1.1	1.1	0.3
Th/Nb	0.7	0.8	0.8	0.4
Sc/Ni	0.7	2.1	2.1	5.1
Hf/Ta	6.0	5.2	5.2	8.5
Ta/Yb	0.23	0.21	0.20	0.30
Hf/Th	0.5	0.5	0.5	1.2
Ti/V	120	156	83	136
U/Pb	0.3	0.3	0.2	0.2
FeO-T/MgO	1.6	2.0	1.5	2.3
Sm/Yb	2.5	1.6	1.7	2.1

Table B-1 (continued)
Chemical Composition of Igneous Rocks

FELSIC ROCKS SAMPLE	PRE-ALDER RHYOLITE T-1	ALDER RHYOLITE FWR-1	ALDER RHYOLITE FWR-3	ALDER RHYOLITE FWR-4	ALDER RHYOLITE FWC-1
SiO2	72.35	72.66	70.91	72.22	73.45
TiO2	0.24	0.38	0.35	0.33	0.29
Al2O3	13.19	13.20	14.09	14.01	12.82
Fe2O3-T	2.48	3.80	4.25	3.95	4.35
MgO	4.14	0.51	0.71	0.37	1.38
CaO	0.07	0.50	0.15	0.35	1.31
Na2O	0.37	4.42	3.57	3.63	2.61
K2O	4.63	4.05	5.01	4.64	1.93
MnO	0.03	0.09	0.07	0.09	0.11
P2O5	0.02	0.02	0.04	0.03	0.02
LOI	2.68	0.58	0.97	0.36	1.96
TOTAL	100.34	100.15	100.12	100.59	100.22
Rb	90	136	171	198	95
Ba	742	1268	1264	1177	644
Cs	5	13	14	14	32
Sr	12	132	117	125	245
Pb	12	23	20	25	14
Th	8.9	9.9	10.4	9.5	11.1
U	3.6	3.1	2.6	2.8	2.6
Sc	7	8	9	9	10
V		166	202	7	89
Cr	1	2	8	6	5
Co	4	0	1	1	19
Ni	8	9	13	12	11
Y	54	65	81	83	43
Zr	257	413	441	423	383
Nb	20	19	26	24	21
Hf	6.1	12.6	13.0	9.9	13.5
Ta	1.0	1.17	1.20	1.22	1.25
La	31	60	60	60	51
Ce	67.4	134.1	152.7	132.5	103.2
Sm	6.0	13.7	14.3	14.0	8.8
Eu	0.9	3.1	3.3	3.2	1.9
Tb	1.4	3.1	3.1	3.3	1.4
Yb	6.1	7.7	8.3	7.1	5.9
Lu	0.95	1.15	1.23	1.10	0.91

Table B-1 (continued)
Chemical Composition of Igneous Rocks

Mg Number	79	23	27	18	42
K2O/Na2O	12.92	0.92	1.40	1.28	0.74
Na2O+K2O	5.21	8.48	8.58	8.27	4.54
Al2O3/TiO2	56.1	40.2	40.5	41.9	44.2
CaO/TiO2	0.3	1.5	0.4	1.1	4.5
Zr/TiO2	0.11	0.13	0.13	0.13	0.13
K/Rb	448	248	244	194	168
Ba/Sr	62.9	9.6	10.8	9.4	2.6
Rb/Sr	7.6	1.0	1.5	1.6	0.4
La/Yb	5.0	7.8	7.2	8.5	8.5
La/Sm	5.1	4.4	4.2	4.3	5.8
Sm/Eu	6.9	4.4	4.3	4.3	4.6
Ti/Zr	5.5	4.8	4.7	4.7	4.5
Zr/Nb	13.0	21.3	17.1	17.8	18.7
Nb/Y	0.4	0.3	0.3	0.3	0.5
Zr/Y	4.7	6.3	5.4	5.1	8.9
Nb/Ta	19.2	16.6	21.4	19.5	16.4
Nb/La	0.6	0.3	0.4	0.4	0.4
Ce/Pb	5.7	5.8	7.5	5.3	7.5
Nb/U	5.5	6.2	9.7	8.4	7.9
La/Ta	30	51	50	49	41
La/Th	3.4	6.1	5.7	6.3	4.6
Y/Tb	38.3	21.1	26.3	25.4	31.9
Th/Yb	1.5	1.3	1.3	1.3	1.9
Th/Sc	1.2	1.2	1.2	1.1	1.2
Th/Nb	0.4	0.5	0.4	0.4	0.5
Sc/Ni	1.6	1.0	0.7	0.7	0.9
Hf/Ta	5.9	10.8	10.8	8.1	10.8
Ta/Yb	0.17	0.15	0.15	0.17	0.21
Hf/Th	0.7	1.3	1.2	1.0	1.2
Ti/V	ERR	12	10	287	44
U/Pb	0.3	0.1	0.1	0.1	0.2
FeO-T/MgO	0.5	6.7	5.4	9.5	2.8
Sm/Yb	1.0	1.8	1.7	2.0	1.5

Table B-1 (continued)
Chemical Composition of Igneous Rocks

FELSIC ROCKS	ALDER RHYOLITE	RED ROCK RHYOLITE	RED ROCK RHYOLITE	RED ROCK RHYOLITE	RED ROCK RHYOLITE
SAMPLE	FWC-6	HR-2	*HR-5	OX-1	OX-2
SiO2	70.46	75.64	64.52	78.82	72.31
TiO2	0.18	0.23	0.43	0.04	0.24
Al2O3	15.48	12.40	15.91	11.33	13.71
Fe2O3-T	4.01	2.13	2.24	1.25	3.30
MgO	0.09	0.32	0.81	0.00	0.40
CaO	1.29	0.20	0.14	0.35	0.04
Na2O	5.21	2.67	0.28	2.25	2.89
K2O	1.74	5.83	13.84	4.90	6.61
MnO	0.05	0.03	0.04	0.02	0.03
P2O5	0.03	0.01	0.07	0.00	0.01
LOI	1.19	0.73	1.17	0.66	0.65
TOTAL	99.73	100.27	99.51	100.12	100.17
Rb	65	118	161	179	148
Ba	630	1670	614	114	1297
Cs	14	2	1	3	2
Sr	336	77	35	44	28
Pb	17	22	23	16	17
Th	13.8	13.0	14.6	15.7	11.9
U	4.2	6.1	2.5	3.9	2.6
Sc	7	4	5	1	2
V	30	4	22	1	3
Cr	0	1	1	0	0
Co	5	0	3	0	1
Ni	11	7	15	9	11
Y	52	58	49	92	63
Zr	428	356	978	147	450
Nb	31	22	25	34	25
Hf	15.0	10.3	28.2	9.1	12.4
Ta	1.93	1.41	1.60	2.21	1.67
La	105	90	54	48	75
Ce	227.9	167.9	97.8	108.3	114.6
Sm	14.1	14.0	8.6	10.1	15.6
Eu	2.1	2.5	2.2	0.2	2.7
Tb	1.9	2.2	1.3	2.3	2.5
Yb	9.0	5.6	7.8	10.2	6.1
Lu	1.35	0.85	1.26	1.51	0.92

Table B-1 (continued)
Chemical Composition of Igneous Rocks

Mg Number	5	25	45	0	21
K2O/Na2O	0.33	2.22	49.97	2.18	2.28
Na2O+K2O	6.95	8.60	14.12	7.15	9.50
Al2O3/TiO2	86.0	53.7	32.3	283.3	57.6
CaO/TiO2	7.2	0.3	0.3	8.8	0.2
Zr/TiO2	0.24	0.15	0.20	0.37	0.13
K/Rb	224	416	714	228	370
Ba/Sr	1.3	21.7	17.7	2.6	45.1
Rb/Sr	0.2	1.5	4.6	4.1	5.2
La/Yb	11.7	15.3	6.3	4.7	12.3
La/Sm	7.5	6.4	6.3	4.8	4.3
Sm/Eu	6.7	5.6	4.0	63.2	5.8
Ti/Zr	2.5	3.3	3.0	1.6	3.2
Zr/Nb	13.8	16.3	38.2	4.3	18.3
Nb/Y	0.6	0.4	0.5	0.4	0.4
Zr/Y	8.2	6.1	20.0	1.5	7.2
Nb/Ta	16.1	15.5	15.6	15.6	14.8
Nb/La	0.3	0.2	0.5	0.7	0.3
Ce/Pb	13.1	7.6	4.3	6.8	6.9
Nb/U	7.3	3.6	9.8	8.7	9.5
La/Ta	54	64	34	22	45
La/Th	7.6	6.3	3.7	3.1	6.3
Y/Tb	26.7	27.1	36.4	40.6	25.4
Th/Yb	1.5	2.3	1.9	1.5	2.0
Th/Sc	1.9	3.7	2.8	28.0	5.7
Th/Nb	0.4	0.6	0.6	0.3	0.5
Sc/Ni	0.7	0.5	0.3	0.1	0.2
Hf/Ta	7.8	7.3	17.6	4.1	7.4
Ta/Yb	0.21	0.25	0.20	0.22	0.27
Hf/Th	1.1	0.8	1.9	0.6	1.0
Ti/V	36	343	133	220	529
U/Pb	0.2	0.3	0.1	0.2	0.2
FeO-T/MgO	40.1	6.1	2.5	ERR	7.5
Sm/Yb	1.6	2.5	1.1	1.0	2.6

Table B-1 (continued)
Chemical Composition of Igneous Rocks

FELSIC ROCKS	RED ROCK RHYOLITE	INTRUSIVE GRANOPHYRE
SAMPLE	OX-5	GR-3
SiO2	79.47	75.63
TiO2	0.04	0.05
Al2O3	10.68	12.07
Fe2O3-T	1.33	1.40
MgO	0.00	0.43
CaO	0.03	0.41
Na2O	0.00	4.02
K2O	7.47	4.61
MnO	0.01	0.03
P2O5	0.01	0.01
LOI	0.75	0.42
TOTAL	99.79	99.08
Rb	139	194
Ba	318	28
Cs	2	13
Sr	15	5
Pb	13	15
Th	23.0	17.2
U	1.5	10.4
Sc	1	0
V	3	0
Cr	0	2
Co	0	0
Ni	8	5
Y	88	86
Zr	110	195
Nb	25	36
Hf	7.0	10.3
Ta	1.86	3.36
La	46	49
Ce	97.7	89.7
Sm	9.8	9.0
Eu	0.5	0.1
Tb	2.7	1.7
Yb	11.3	10.2
Lu	1.68	1.60

Table B-1 (continued)
Chemical Composition of Igneous Rocks

Mg Number	0	41
K2O/Na2O	ERR	1.15
Na2O+K2O	7.47	8.63
Al2O3/TiO2	267.0	236.6
CaO/TiO2	0.8	7.9
Zr/TiO2	0.27	0.38
K/Rb	446	197
Ba/Sr	20.9	4.9
Rb/Sr	9.1	41.6
La/Yb	4.1	4.8
La/Sm	4.7	5.4
Sm/Eu	21.1	70.3
Ti/Zr	2.2	1.6
Zr/Nb	4.5	5.4
Nb/Y	0.3	0.4
Zr/Y	1.3	2.3
Nb/Ta	13.2	10.8
Nb/La	0.5	0.7
Ce/Pb	7.8	6.0
Nb/U	16.1	8.5
La/Ta	25	15
La/Th	2.0	2.8
Y/Yb	30.6	50.8
Th/Yb	2.0	1.7
Th/Sc	37.0	77.5
Th/Nb	0.9	0.5
Sc/Ni	0.1	.0
Hf/Ta	3.8	3.1
Ta/Yb	0.16	0.33
Hf/Th	0.3	0.6
Ti/V	85	927
U/Pb	0.1	0.7
FeO-T/MgO	ERR	3.0
Sm/Yb	0.9	0.9

Major elements in weight percent.
Trace elements in parts per million.
Fe_2O_{3T}: Total Fe as Fe_2O_{3T}.
LOI: Loss On Ignition.
Mg Number: $(MgO/(MgO + (0.79 \times Fe_2O_{3T}))) \times 100$, molar proportions.
ERR: no value for calculation or division by zero for ratio calculation.
Blank: Not determined.
* Altered sample.

Table B-2
CIPW Norms for Igneous Rocks

MAFIC ROCKS	ALDER BAS-AND	ALDER BAS-AND	ALDER BAS-AND	ALDER BASALT	ALDER BAS-AND
SAMPLE	*PAV-2	*PAV-3	FWBV-2	*FWC-12	FWC-3
Quartz	7.38	14.45	3.67		13.53
Corundum				3.66	4.52
Orthoclase	4.33	7.08	4.67	6.20	20.68
Albite	20.65	18.10	33.04	48.70	24.77
Anorthite	30.57	25.10	22.10	17.64	12.15
Nepheline					
Diopside	10.09	20.21	5.20		
Hypersthene	22.31	10.78	23.70	14.69	17.28
Olivine				1.61	
Magnetite	1.97	1.60	2.23	1.29	2.09
Ilmenite	1.92	1.86	4.04	4.12	3.31
Apatite	0.58	0.73	1.36	2.10	1.78
Total	100.00	99.91	100.00	100.00	100.00

MAFIC ROCKS	ALDER BAS-AND	GABBRO	DIORITE DIKE	BASALT DIKE	DIORITE DIKE
SAMPLE	BCP-1	HBP-1	Hd-1	*FWD-2	FWD-3
Quartz	9.57			1.40	
Corundum				0.55	
Orthoclase	5.03	3.78	10.02	0.45	8.30
Albite	28.34	18.28	28.11	17.15	27.08
Anorthite	33.20	18.28	21.29	34.32	29.20
Nepheline					
Diopside	2.15	7.02	17.85		9.84
Hypersthene	17.10	27.00	20.29	38.34	12.77
Olivine		19.35	1.28		8.35
Magnetite	1.32	2.60	2.37	2.69	1.88
Ilmenite	2.19	2.30	3.21	4.01	2.04
Apatite	0.93	1.40	0.57	1.11	0.55
Total	99.82	100.00	100.00	100.00	100.00

Table B-2 (continued)
CIPW Norms for Igneous Rocks

MAFIC ROCKS	GABBRO	GABBRO
SAMPLE	*PYX-2	*PYX-6
Quartz		
Corundum		
Orthoclase	0.09	0.84
Albite	5.23	29.11
Anorthite	22.48	16.07
Nepheline		3.18
Diopside	38.19	15.15
Hypersthene	9.35	
Olivine	17.03	32.78
Magnetite	3.34	1.66
Ilmenite	3.65	0.88
Apatite	0.04	0.38
Total	100.03	100.00

Table B-2 (continued)
CIPW Norms for Igneous Rocks

ANDESITE ROCKS SAMPLE	ALDER ANDESITE FWK-2	ALDER ANDESITE FWC-11	ALDER ANDESITE FWBV-4	ALDER ANDESITE *FWBV-5	ALDER ANDESITE *BCP-2
Quartz	8.13	2.59	6.65		4.32
Corundum	1.85	3.72			
Orthoclase	12.62	21.41	9.34	3.15	17.85
Albite	37.40	31.04	37.83	60.87	22.67
Anorthite	18.68	18.67	17.78	8.70	29.46
Nepheline					
Diopside			0.68	2.94	5.95
Hypersthene	16.55	17.06	22.07	12.26	15.01
Olivine				6.31	
Magnetite	1.29	1.84	2.04	2.06	1.41
Ilmenite	2.37	2.75	2.68	2.72	2.17
Apatite	1.13	0.92	0.94	0.99	1.16
Total	100.00	100.00	100.00	100.00	100.00

ALDER ANDESITE *BCP-4	ALDER ANDESITE BCP-5	ALDER ANDESITE BCC-2	ALDER ANDESITE *BCC-3	ALDER ANDESITE *BCC-4
		9.23	2.71	11.54
		2.81	4.06	
15.25	10.45	20.82	14.63	8.39
21.18	32.72	29.58	29.25	47.51
21.35	22.79	18.81	22.37	13.86
5.24				
17.09	13.14			0.29
	0.66	14.29	22.77	13.01
15.99	15.97			
1.74	1.82	1.50	1.34	1.50
1.62	1.80	1.96	1.92	2.45
0.54	0.67	1.00	0.95	1.45
100.00	100.00	100.00	100.00	100.00

Table B-2 (continued)
CIPW Norms for Igneous Rocks

ANDESITE ROCKS SAMPLE	ALDER ANDESITE *BCP-4	ALDER ANDESITE BCP-5	ALDER ANDESITE BCC-2	ALDER ANDESITE *BCC-3	ALDER ANDESITE *BCC-4
Quartz			9.23	2.71	11.54
Corundum			2.81	4.06	
Orthoclase	15.25	10.45	20.82	14.63	8.89
Albite	21.18	32.72	29.58	29.25	47.51
Anorthite	21.35	22.79	18.81	22.37	13.86
Nepheline	5.24				
Diopside	17.09	13.14			0.29
Hypersthene		0.66	14.29	22.77	13.01
Olivine	15.98	15.97			
Magnetite	1.74	1.82	1.50	1.34	1.50
Ilmenite	1.62	1.80	1.96	1.92	2.45
Apatite	0.54	0.67	1.00	0.95	1.45
Total	100.00	100.00	100.00	100.00	100.00

ANDESITE ROCKS SAMPLE	ALDER ANDESITE *BCMV-1	ALDER ANDESITE HBV-1	ALDER ANDESITE HBV-3	ALDER ANDESITE D-2
Quartz		9.32	15.27	
Corundum	0.17	3.87	2.84	
Orthoclase	7.36	19.14	13.25	7.61
Albite	37.76	35.88	34.38	29.01
Anorthite	20.17	10.14	12.92	25.34
Nepheline				
Diopside				11.66
Hypersthene	14.26	15.34	14.99	12.06
Olivine	14.86			8.52
Magnetite	2.13	1.92	1.79	1.87
Ilmenite	2.23	2.89	2.66	2.74
Apatite	1.01	1.51	1.29	1.20
Total	100.00	100.00	100.00	100.00

Table B-2 (continued)
CIPW Norms for Igneous Rocks

DACITE ROCKS SAMPLE	ALDER DACITE *FWC-5	ALDER DACITE FWK-3	ALDER DACITE FWK-4	ALDER DACITE *FWK-5	ALDER DACITE *FWW-7
Quartz	0.15	13.89	9.32	32.70	
Corundum	7.12			11.14	
Orthoclase	26.80	13.33	11.99	19.20	
Albite	46.00	44.32	50.17	14.80	
Anorthite	11.14	12.24	9.99	0.83	
Nepheline					
Diopside		0.97	4.36		
Hypersthene	6.05	11.46	9.82	17.91	
Olivine					
Magnetite	0.54	1.13	1.21	1.23	
Ilmenite	1.68	1.88	1.85	1.70	
Apatite	0.54	0.78	0.73	0.49	
Total	100.00	100.00	100.09	100.01	0.00

DACITE ROCKS SAMPLE	ALDER DACITE *FWW-7	ALDER DACITE BCP-6	RED ROCK DACITE WCRD-1	RED ROCK DACITE WCRD-2	RED ROCK DACITE WCRD-4	INTRUSIVE DACITE *IR-1
Quartz			11.75	14.13	13.45	27.63
Corundum				2.98		3.25
Orthoclase		17.38	13.89	20.05	23.08	42.45
Albite		35.52	43.04	32.37	45.35	17.44
Anorthite		24.00	17.11	15.22	6.73	0.53
Nepheline						
Diopside		0.37	1.22		0.94	
Hypersthene		9.46	7.07	8.49	5.70	6.01
Olivine		7.86				
Magnetite		1.78	3.01	3.42	2.64	1.35
Ilmenite		2.36	2.01	2.25	1.57	0.99
Apatite		1.33	0.92	1.09	0.54	0.36
Total	0.00	100.06	100.00	100.00	100.00	100.00

Table B-2 (continued)
CIPW Norms for Igneous Rocks

DACITE ROCKS SAMPLE	INTRUSIVE DACITE IR-3	INTRUSIVE DACITE IR-4	INTRUSIVE DACITE BI-1
Quartz	33.48	29.52	8.80
Corundum	1.60	0.74	
Orthoclase	28.00	24.49	11.53
Albite	23.16	33.21	41.19
Anorthite	7.18	5.30	15.40
Nepheline			
Diopside			2.38
Hypersthene	4.56	4.87	15.63
Olivine		0.97	
Magnetite	1.13	0.61	1.50
Ilmenite	0.63	0.29	2.42
Apatite	0.26		1.17
Total	100.00	100.00	100.00

Table B-2 (continued)
CIPW Norms for Igneous Rocks

FELSIC ROCKS SAMPLE	PRE-ALDER RHYOLITE T-1	ALDER RHYOLITE FWR-1	ALDER RHYOLITE FWR-3	ALDER RHYOLITE FWR-4	ALDER RHYOLITE FWC-1
Quartz	45.75	28.48	28.50	30.95	45.38
Corundum	7.47	0.68	2.64	2.48	4.18
Orthoclase	29.28	24.12	29.95	27.60	11.66
Albite	3.25	37.68	30.58	30.87	22.52
Anorthite	0.19	2.37	0.50	1.53	6.51
Nepheline					
Diopside					
Hypersthene	12.45	4.28	5.14	4.06	7.15
Olivine					
Magnetite	1.12	1.72	1.94	1.80	2.00
Ilmenite	0.46	0.63	0.67	0.64	0.56
Apatite	0.05	0.04	0.09	0.08	0.04
Total	100.00	100.00	100.00	100.00	100.00

FELSIC ROCKS SAMPLE	ALDER RHYOLITE FWC-6	RED ROCK RHYOLITE HR-2	RED ROCK RHYOLITE *HR-5	RED ROCK RHYOLITE OX-1	RED ROCK RHYOLITE OX-2
Quartz	26.55	36.07	8.23	42.57	28.58
Corundum	2.20	1.26	0.40	0.74	1.77
Orthoclase	10.50	35.24	83.31	28.92	39.32
Albite	47.34	22.74	2.39	23.47	24.64
Anorthite	6.15	0.92	0.20	1.62	0.12
Nepheline					
Diopside					
Hypersthene	4.99	2.35	3.32	1.96	3.60
Olivine					
Magnetite	1.80	0.96	1.03	0.56	1.49
Ilmenite	0.41	0.44	0.95	0.15	0.46
Apatite	0.08	0.03	0.18	0.02	0.03
Total	100.00	100.00	100.00	100.00	100.00

Table B-2 (continued)
CIPW Norms for Igneous Rocks

FELSIC ROCKS	RED ROCK RHYOLITE	INTRUSIVE RHYOLITE
SAMPLE	OX-5	GR-8
Quartz	48.69	33.19
Corundum	2.19	
Orthoclase	44.12	27.65
Albite	2.07	34.58
Anorthite		1.27
Nepheline		
Diopside		0.56
Hypersthene	2.16	2.02
Olivine		
Magnetite	0.59	0.65
Ilmenite	0.15	0.10
Apatite	0.11	0.03
Total	100.07	100.00

APPENDIX D: ANALYTICAL PROCEDURES

Sample Preparation

Fresh hand specimens were taken in triplicate--one for geochemistry, one for petrography, and one for a reference sample. Samples used for geochemistry were broken to pebble size on the outcrop to avoid contamination. Samples were further reduced to a coarse sand size using a jaw crusher and then ground to a powder ($\leq$ 200 mesh) in a Bico high speed rotary pulverizer employing high purity porcelain plates. This powder was then split into three aliquots for XRF major and trace element, and INAA analyses.

X-ray Fluorescence (XRF)

Concentrations of the major elements Si, Ti, Al, Fe, Mn, Mg, Ca, Na, K, and P and trace elements Rb, Sr, Pb, V, Ni, Y, Zr, and Nb were determined by XRF. Major elements were analyzed using fused discs made from ≈0.5g of powdered sample and ≈2.7g of lithium borate flux fused in a platinum crucible for 5 to 20 minutes. Discs were quenched and formed to glass by pressing in a mechanically linked platen and mold. Trace elements were analyzed using pressed pellets made from ≈8g of powdered sample (to ensure infinite thickness) and 7-8 drops of polyvinal alcohol as a binder with a boric acid backing. Pellets were pressed under 10 tons in^{-2} for ≈60 seconds.

Analyses were made using an automated Rigaku 3064 XRF spectrometer with associated PDP-11 computer and in-house software at the XRF laboratory at the New Mexico Bureau of Mines and Mineral Resources (New Mexico Inst. of Mining and Tech.) following methods described by Norrish and Hutton (1969) and Norrish and Chappel (1977). Calibration curves were constructed using USGS and international standards. Matrix effects for the major elements were removed by multiple linear regression of the standards used to construct the calibration curves. Mass absorption coefficients for each sample were calculated at the specific wavelength for each element. Examples of analytical error associated with repeat sample runs and precision and accuracy data are shown in Appendix E.

Instrumental Neutron Activation Analysis (INAA)

The trace elements Cs, Ba, Th, U, Sc, Co, Cr, Hf, Ta, La, Ce, Sm, Eu, Tb, Yb, and Lu were analyzed by INAA. Rock powders (≈300mg) were sealed in polyethylene vials and irradiated in the Annular Core Research Reactor at the Sandia National Laboratory, Albuquerque, New Mexico. Counts were made at 7 and 40 days using a liquid N_2 cooled, Ge drifted coaxial intrinsic detector and a Nuclear Data 6600 multichannel analyzer and LSI-11 computer. Data was reduced using a series of programs collectively known as TEABAGS (Trace Element Analysis by Automated Gamma-ray Spectrometry) developed by Lindstrom and Korotev (1982). Sample vials are placed in a container within the core and are blown around with air from an attached hose in order for each sample vial to obtain an equal neutron flux. This is done to try to compensate for the flux gradient within the container. However, problems with this procedure can result in the vials not being properly agitated and thus increase analytical errors. Irradiation time is 2.78 hours and the thermal neutron flux has been estimated at 6.2×10^{12}n $cm^{-2} sec^{-1}$ (M. Knoper, pers. comm., 1988). Coal flyash standard NBS-1633A was used as a reference standard and USGS standards GSP-1 and SCo-1, GIT-IWG standard AN-G, and in-house standard BLCR were used as check standards. Analytical methods are similar to those described by Gordon et al. (1968) and Gibson and Jagam (1980). Analytical precision and accuracy will be discusses in Appendix E.

APPENDIX E: ANALYSTICAL PRECISION AND ACCURACY

Replicate analyses of in-house and international rock standards provided data for precision and accuracy calculations. Table E-1 lists the standards analyzed and the number of repeat analyses performed for each element using XRF. Likewise, Table E-3 lists standards analyzed and the number of repeat analyses for each element using INAA. Tables E-2 (XRF) and E-4 (INNA) list the standards analyzed, the number of analyses, the mean, the standard deviation from the mean, the accepted value for each element, the coefficient of variance (C.V.) (as a measure of precision), and the percent deviation of the mean from the accepted value (as a measure of accuracy).

Equations used for calculating the C.V., mean, standard deviation, and percent error (Levin and Rubin, 1980) include:

$$\mu = \frac{\sum x}{N}$$

$$\sigma = \sqrt{\frac{\sum x^2}{N} - \mu^2}$$

$$C.V. = \frac{\sigma}{\mu}(100)$$

$$\%Error = \frac{\mu - A}{A}(100)$$

x=individual measured value for a given element

N=total number of analyses for a given element

μ=mean

σ=standard deviation

A=accepted value for a given element

As can be seen from Tables E-2 and E-4, the quality of the chemical data obtained in this study varies considerably. In general, good to excellent data is obtained for the elements SiO_2, Al_2O_3, Fe_2O_{3T}, CaO, Ba, Cs, Sr, Sc, V, Co, Ni, Y, Zr, Ta, La, Sm, Eu, Tb, and Yb. Variable data occurs for the elements TiO_2, MgO, Na_2O, K_2O, Rb, Cr, Hf, Ce, and Lu. The least accurate data accompanies the elements MnO, P_2O_5, Pb, Th, U, and Nb.

Table E-1
Number of analyses for standards using XRF

	GIT-IWG AL-I	GIT-IWG AN-G	GIT-IWG BE-N	GIT-IWG MA-N	USGS BIR-1	USGS DR-N
SiO2		10		10		
TiO2		10		10		
Al2O3		10		10		
Fe2O3T		10		10		
MgO		10		10		
CaO		10		10		
Na2O		10		10		
K2O		10		10		
MnO		10		10		
P2O5		10		10		
Rb	6	14	11			16
Sr	6	14	11			16
Pb	6	14	11			16
V		9				
Ni		9	4		5	
Y	6	14	11			16
Zr	6	14	11			16
Nb	6	14	11			16

	USGS SCo-1	USGS SDC-1	USGS W-2	ARNT GS-N	CRPG GA	NMIMT BLCR
SiO2				10	10	8
TiO2				10	10	8
Al2O3				10	10	8
Fe2O3T				10	10	8
MgO				10	10	8
CaO				10	10	8
Na2O				10	10	8
K2O				10	10	8
MnO				10	10	8
P2O5				10	10	8
Rb			11	11		
Sr			11	11		
Pb			11	11		
V				5		8
Ni	5	5		4		
Y			11	11		
Zr			11	11		
Nb			11	11		

Table E-1 (continued)
Number of analyses for standards using XRF

	NMIMT HI31	NMIMT LOSP
SiO2	4	
TiO2	4	
Al2O3	4	
Fe2O3T	4	
MgO	4	
CaO	4	
Na2O	4	
K2O	4	
MnO	4	
P2O5	4	
V	8	9

GIT Groupe International De Travail
IWG International Working Group
USGS United States Geological Survey
ANRT Association National De La Recherche Technique
CRPG Centre De Recherches Petrographiques et Geochimiques
NMIMT New Mexico Institute of Mining and Technology

Table E-2
Summary of Precision and Accuracy
for Standards Analyzed by XRF

NMIMT STANDARD LOSP

	MEAN	STD. DEV.	ACPT. VALUE	C.V. (%)	ERROR (%)
V	5.22	1.73	----	33.11	----

Table E-2 (continued)
Summary of Precision and Accuracy
for Standards Analyzed by XRF

GIT-IWG STANDARD AL-I

	MEAN	STD. DEV.	ACPT. VALUE	C.V. (%)	ERROR (%)
Rb	1.75	0.30	5.80	17.42	69.90
Sr	77.9	0.2	80.0	0.28	2.7
Pb	10.5	0.8	4.5	7.64	132.5
Y	6.7	0.3	7.0	3.69	5.0
Zr	41.4	0.2	43.0	0.53	3.78
Nb	3.2	0.3	4.0	10.54	19.8

GIT-IWG STANDARD AN-G

	MEAN	STD. DEV.	ACPT. VALUE	C.V. (%)	ERROR (%)
SiO2	47.43	0.34	46.3	0.72	2.4
TiO2	0.22	0.02	0.22	8.23	0.8
Al2O3	30.18	0.23	29.8	0.77	1.3
Fe2O3T	3.32	0.02	3.36	0.56	1.2
MgO	1.92	0.3	1.8	15.86	6.8
CaO	16.59	0.04	15.9	0.22	4.4
Na2O	1.2	0.2	1.63	16.33	26.5
K2O	0.07	0.03	0.13	37.76	47.6
MnO	0.05	0.002	0.04	4.84	29.0
P2O5	0.002	0.003	0.01	124.9	79.0
Rb	1.97	0.65	1.0	32.87	96.9
Sr	75.7	0.6	76.0	0.7	0.3
Pb	5.47	2.61	2.0	47.77	173.6
V	71.6	2.5	70.0	3.49	2.2
Ni	36	1.1	35	3.04	1.7
Y	8.1	0.7	8.0	8.67	1.0
Zr	19.8	1.53	15.0	7.74	32.2
Nb	2.8	0.41	2.0	14.64	40.2

GIT-IWG STANDARD BE-N

	MEAN	STD. DEV.	ACPT. VALUE	C.V. (%)	ERROR (%)
Rb	49.8	0.6	47	1.2	6.0
Sr	1412	3.5	1370	0.25	3.1
Pb	2.45	1.24	4	50.5	38.8
Ni	271	1.38	267	0.51	1.6
Y	31.4	0.49	30	1.55	4.5
Zr	274	1.09	265	0.4	3.3
Nb	112	0.41	100	0.37	11.6

Table E-2 (continued)
Summary of Precision and Accuracy
for Standards Analyzed by XRF

GIT-IWG STANDARD MA-N

	MEAN	STD. DEV.	ACPT. VALUE	C.V. (%)	ERROR (%)
SiO2	66.15	0.08	66.6	0.11	0.7
TiO2	0.009	0.004	0.01	43.51	13.3
Al2O3	17.69	0.03	17.62	0.17	0.4
Fe2O3T	0.82	0.002	0.47	0.25	74.6
MgO	0.52	0.24	0.04	45.67	1208.1
CaO	0.58	0.01	0.59	1.14	1.0
Na2O	6.12	0.15	5.84	2.38	4.7
K2O	3.13	0.01	3.18	0.34	1.6
MnO	0.06	0.004	0.04	6.48	39.4
P2O5	1.35	0.01	1.39	0.5	2.6

USGS STANDARD BIR-1

	MEAN	STD. DEV.	ACPT. VALUE	C.V. (%)	ERROR (%)
Ni	163	2.8	144	1.72	2.0

USGS STANDARD DR-N

	MEAN	STD. DEV.	ACPT. VALUE	C.V. (%)	ERROR (%)
Rb	73.1	0.71	70.0	0.97	4.5
Sr	390	5.48	400	1.41	2.5
Pb	53.04	3.02	55.0	5.7	3.6
Y	28.7	0.56	30.0	1.95	4.1
Zr	133	0.72	125	0.54	6.0
Nb	9.03	0.61	6.00	6.77	50.4

USGS STANDARD SCo-1

	MEAN	STD. DEV.	ACPT. VALUE	C.V. (%)	ERROR (%)
Ni	27.3	1.33	30.0	4.87	8.9

Table E-2 (continued)
Summary of Precision and Accuracy
for Standards Analyzed by XRF

USGS STANDARD SDC-1

	MEAN	STD. DEV.	ACPT. VALUE	C.V. (%)	ERROR (%)
Ni	33.6	1.67	36.0	4.95	6.6

USGS STANDARD W-2

	MEAN	STD. DEV.	ACPT. VALUE	C.V. (%)	ERROR (%)
Rb	21.0	0.78	20.9	3.7	0.6
Sr	197	0.64	192	0.33	2.7
Pb	10.0	1.61	----	16.05	----
Y	23.8	0.59	23.0	2.49	3.5
Zr	95.8	0.4	100.0	0.42	4.2
Nb	9.47	0.18	6.75	1.88	44.4

ANRT STANDARD GS-N

	MEAN	STD. DEV.	ACPT. VALUE	C.V. (%)	ERROR (%)
SiO2	66.45	0.09	65.80	0.14	1.0
TiO2	0.67	0.01	0.68	1.12	1.2
Al2O3	14.54	0.02	14.67	0.17	0.9
Fe2O3T	3.52	0.01	3.75	0.42	6.2
MgO	2.56	0.04	2.30	1.74	11.3
CaO	2.53	0.01	2.50	0.48	1.3
Na2O	3.65	0.07	3.77	1.79	3.1
K2O	4.69	0.01	4.63	0.23	1.2
MnO	0.07	0.06	0.06	3.91	9.5
P2O5	0.29	0.28	0.28	0.8	2.2
Rb	186	0.58	185	0.31	0.7
Sr	578	1.13	570	0.2	1.3
Pb	50.1	1.51	53.0	3.02	5.5
V	64.4	1.8	65.0	2.8	0.9
Ni	37.8	0.49	34.0	1.3	11.2
Y	17.5	0.47	19.0	2.69	8.1
Zr	214	0.64	235	0.3	9.1
Nb	23.6	0.26	23.0	1.09	2.5

Table E-2 (continued)
Summary of Precision and Accuracy
for Standards Analyzed by XRF

CRPG STANDARD GA

	MEAN	STD. DEV.	ACPT. VALUE	C.V. (%)	ERROR (%)
SiO2	69.43	0.11	69.90	0.15	0.7
TiO2	0.37	0.01	0.38	1.38	1.6
Al2O3	14.46	0.03	14.50	0.23	0.3
Fe2O3T	2.75	0.01	2.83	0.3	2.8
MgO	1.24	0.05	0.95	3.84	30.6
CaO	2.53	0.004	2.45	0.17	3.2
Na2O	4.00	0.11	3.55	2.87	12.7
K2O	4.14	0.01	4.03	0.15	2.8
MnO	0.009	0.004	0.09	4.91	1.1
P2O5	0.13	0.003	0.12	2.25	10.00

NMIMT STANDARD BLCR

	MEAN	STD. DEV.	ACPT. VALUE	C.V. (%)	ERROR (%)
SiO2	56.96	0.25	55.65	0.44	2.4
TiO2	0.9	0.01	0.87	1.21	3.6
Al2O3	16.93	0.09	16.97	0.52	0.3
Fe2O3T	7.55	0.03	7.43	0.36	1.6
MgO	5.57	0.45	5.86	8.14	4.9
CaO	8.27	0.03	7.9	0.41	4.6
Na2O	3.59	0.15	3.72	4.18	3.5
K2O	3.59	0.15	1.45	4.18	147.6
MnO	0.15	0.004	0.13	2.41	14.1
P2O5	0.16	0.002	0.16	1.56	0.20
V	144	2.94	----	2.05	----

NMIMT STANDARD HI31

	MEAN	STD. DEV.	ACPT. VALUE	C.V. (%)	ERROR (%)
SiO2	60.90	0.08	59.46	0.14	2.4
TiO2	0.85	0.004	0.81	0.51	5.2
Al2O3	17.13	0.03	17.02	0.16	0.6
Fe2O3T	7.15	0.01	7.07	0.12	1.1
MgO	3.11	0.03	2.81	0.86	10.8
CaO	6.57	0.02	6.32	0.25	4
Na2O	3.30	0.15	3.12	4.52	5.7
K2O	2.61	0.004	2.53	0.17	3.1
MnO	0.13	0.01	0.11	5.44	18.2
P2O5	0.4	0.004	0.38	0.91	6.30
V	126	1.84	----	1.45	----

STD. DEV. Standard Deviation
ACPT. VALUE Accepted Value
C.V. Coefficient of Variance

Table E-3
Number of analyses for standards using INAA

	GIT-IWG AN-G	USGS GSP-1	USGS SCo-1	NMIMT BLCR
Ba	3	3	3	3
Cs	3	3	3	3
Th	3	3	3	3
U	3	3	3	3
Sc	3	3	3	3
Cr	3	3	3	3
Co	3	3	3	3
Hf	3	3	3	3
Ta	3	3	3	3
La	3	3	3	3
Ce	3	3	3	3
Sm	3	3	3	3
Eu	3	3	3	3
Tb	3	3	3	3
Yb	3	3	3	3
Lu	3	3	3	3

Table E-4
Summary of Precision and Accuracy
for Standards Analyzed by INAA

GIT-IWG STANDARD AN-G

	MEAN	STD. DEV.	ACPT. VALUE	C.V. (%)	ERROR (%)
Ba	33.3	2.1	34.0	6.16	2.0
Cs	0.05	0.02	----	43.79	----
Th	0.03	0.02	0.2	71.34	84.8
U	0.00	0.00	0.3	----	100.0
Sc	10.6	0.7	10.0	6.55	5.5
Cr	50.8	2.6	50.0	5.06	1.6
Co	26.2	1.7	25.0	6.36	4.6
Hf	0.42	0.07	0.38	15.74	11.0
Ta	0.18	0.03	0.2	14.35	11.2
La	2.4	0.3	2.0	10.56	19.8
Ce	4.9	0.2	4.7	3.68	3.7
Sm	0.79	0.07	0.70	8.76	13.1
Eu	0.38	0.01	0.37	2.78	3.6
Tb	0.18	0.01	0.20	5.51	10.3
Yb	0.87	0.04	0.85	4.09	2.4
Lu	0.13	0.02	0.12	11.53	11.1

Table E-4 (continued)
Summary of Precision and Accuracy
for Standards Analyzed by INAA

USGS STANDARD GSP-1

	MEAN	STD. DEV.	ACPT. VALUE	C.V. (%)	ERROR (%)
Ba	1370	58.7	1300	4.29	5.4
Cs	1.08	0.06	1.0	5.59	7.7
Th	111	6.4	105	6.3	5.2
U	3.90	1.60	2.1	42.5	83.3
Sc	6.3	0.4	6.6	6.98	4.3
Cr	16.5	3.3	12.0	20.0	37.4
Co	6.97	0.39	7.80	5.52	10.6
Hf	17.7	1.09	14.0	6.18	26.3
Ta	0.92	0.05	1.0	5.93	8.3
La	186	9.02	195.0	4.85	4.7
Ce	468	28.7	360	6.13	30.0
Sm	24.0	5.2	25.0	21.7	3.9
Eu	2.3	0.12	2.4	5.08	4.0
Tb	1.4	0.11	1.4	7.85	1.2
Yb	1.8	0.17	1.9	9.18	4.0
Lu	0.3	0.01	0.20	5.09	29.00

USGS STANDARD SCo-1

	MEAN	STD. DEV.	ACPT. VALUE	C.V. (%)	ERROR (%)
Ba	595	20.9	590	3.5	0.8
Cs	8.2	0.4	7.8	4.8	5.1
Th	9.5	0.51	9.6	5.4	1.2
U	3.20	0.19	2.9	5.6	10.0
Sc	12.2	0.6	11.0	4.8	10.2
Cr	74	2.6	71.0	3.5	4.1
Co	12	0.54	11.00	4.6	4.8
Hf	5.14	0.26	4.3	5.1	19.6
Ta	0.85	0.04	0.9	4.4	5.7
La	29.9	1.32	29.0	4.4	2.8
Ce	62.0	4.02	63.0	6.49	1.6
Sm	5.4	0.27	5.1	5.0	5.8
Eu	1.1	0.06	1.2	5.2	6.8
Tb	0.7	0.05	0.8	6.9	7.1
Yb	2.5	0.15	2.2	6.2	11.4
Lu	0.4	0.02	----	4.9	----

Table E-4 (continued)
Summary of Precision and Accuracy
for Standards Analyzed by INAA

NMIMT STANDARD BLCR

	MEAN	STD. DEV.	ACPT. VALUE	C.V. (%)	ERROR (%)
Ba	495	140.0	375	28.3	32.1
Cs	2.24	0.08	2.3	3.59	2.6
Th	4.6	0.68	4.1	15.0	10.9
U	1.60	0.12	1.5	7.3	8.4
Sc	32.5	1.7	32.0	5.1	1.4
Cr	98.0	58.8	160.0	60.0	38.8
Co	33.6	2.10	29.0	6.2	15.7
Hf	4.8	0.18	4.3	3.7	12.3
Ta	0.41	0.02	0.42	4.1	1.6
La	17.1	5.12	11.1	29.9	54.4
Ce	29.2	1.41	26.7	4.81	9.5
Sm	6.4	1.5	3.7	22.7	72.6
Eu	1.3	0.06	1.3	4.9	1.5
Tb	0.9	0.09	0.8	10.1	20.1
Yb	3.6	0.2	3.1	4.5	15.3
Lu	0.6	0.04	0.52	6.42	5.80

APPENDIX F: PETROGRAPHIC DESCRIPTIONS OF SEDIMENTARY ROCKS

HL-1 Houdon Lower Quartzite Unite
Fine grained quartz arenite
Quartz 85%, Rock Fragments 10%, Matrix 2%,
Accessory 3%
No foliation. Herring-bone cross-bedding present.
Degree of Rounding: angular to sub angular
Sorting: moderately well sorted
Matrix: chlorite and sericite, minor grains of zircon
Quartz: up to 0.15mm in diameter, undulatory extinction, polygonization, strain bands, zircon and fluid inclusions present.
Rock Fragments: Chert (recrystallized quartz) and volcanic rock fragments. Volcanic rock fragments highly altered to sericite and chlorite.
Accessory: Zircon, opaques

HU-1 Houdon Upper Quartzite Unit
Fine to medium grained quartz arenite
Quartz 85%, Rock Fragments 10%, Matrix 5%,
Accessory trace.
Quartz grains are stretched and rock shows a faint foliation. Cross-bedding and herring-bone cross-bedding present.
Degree of Rounding: subangular to subrounded
Sorting: moderately well sorted
Matrix: sericite with minor chlorite, zircon
Quartz: up to 3mm long, undulatory extinction on all grains, Strain bands, grains show varying degrees of recrystallization, zircon inclusions
Rock Fragments: siltstone and possibly felsic volcanic, fragments mostly altered to sericite.
Accessory: Zircon opaques

BCW-2 Board Cabin Formation
Fine grained quartz arenite
Quartz 80%, Rock Fragments 10%, Matrix 8%,
Accessory 2%, K-feldspar trace.
No visible foliation. Horizontal bedding present.
Degree of Rounding: subangular to subrounded
Sorting: Moderately well sorted
Matrix: sericite
Quartz: up to 0.8mm in diameter, varying degrees of polygonization, undulatory extinction, zircon inclusions
Rock Fragments: polycrystalline quartz (granite ?), chert, mafic volcanic rocks. Volcanic fragments highly altered to sericite-some small plagioclase phenocrysts present.
Accessory: opaques, zircon.

FWW-3 Flying W Formation
Coarse grained quartz wacke
Quartz 45%, Rock Fragments 37%, Matrix 18%
Accessory trace
No visible foliation, bedding apparent on outcrop scale
Degree of Rounding: subangular to subrounded

Sorting: moderately sorted
Matrix: subequal proportions of sericite and chlorite
Quartz: up to 2.25mm in diameter, undulatory extinction on most grains
Rocks Fragments: volcanic and chert up to 2.25mm in diameter.
Accessory: opaques, calcite

BCSS-2 Board Cabin Formation
Coarse grained quartz wacke
Quartz 40%, Plagioclase <1%, Rock Fragments 47%,
Matrix 8%, Accessory 4%
Late quartz and calcite veins present.
Degree of Rounding: Angular to subrounded
Sorting: moderately well sorted
Matrix: subequal amounts of sericite and chlorite
Quartz: up to 4mm in diameter, some grains are highly fractured.
Rock Fragments: 40% volcanic, 7% sedimentary.
Highly altered to sericite and chlorite.
Accessory: opaques, calcite

BCW-3 Board Cabin Formation
Fine to medium grained lithic arenite
Quartz 5%, Plagioclase 2%, Rock Fragments 75%
Matrix 8%, Accessory 10%
Bedding apparent on outcrop scale.
Degree of Rounding: subangular to subrounded
Sorting: moderately well sorted
Matrix: subequal proportions of chlorite and sericite
Quartz: up to 1.7mm in diameter, mostly monocrystalline.
Rock Fragments: ≈70% volcanic, 5% sedimentary.
Fragments intensely altered to sericite. Sedimentary fragments show bedding and graded bedding. volcanic fragments have phenocrysts of plagioclase (sericite).
Accessory: opaques, epidote

FWQ-1 Flying W Formation
Medium to coarse grained quartz wacke
Quartz 40%, Rock Fragments 50%, Matrix <1%,
Accessory 10%
Foliation parallel to bedding. Layer of opaque subrounded grains present.
Degree of Rounding: subangular to subrounded
Sorting: moderately well sorted.
Matrix: chlorite with minor sericite.
Quartz: 0.1 to 4.5mm in diameter, zircon inclusions, mostly monocrystalline
Rock Fragments: ≈40% volcanic, 10% sedimentary (chert).
Volcanic fragments altered to sericite and chlorite
Accessory: opaques, chlorite, zircon

FWW-6 Flying W Formation
Fine to medium grained lithic arenite
Quartz 7%, Plagioclase 3%, Rock Fragments 74%
Matrix 5%, Accessory 11%
Foliation parallel to bedding

Degree of rounding: angular to subrounded
Sorting: moderately sorted
Matrix: sericite and lesser chlorite
Quartz: 0.1 to 2mm in diameter, mostly monocrystalline
Plagioclase: composition (Michel-Levy) An_6
Rock Fragments: ≈69% volcanic and sedimentary, <5% chert. Volcanic and sedimentary fragments altered to sericite and minor chlorite.
Accessory: chlorite, epidote, opaques

FWW-4 Flying W Formation
Medium to coarse grained lithic arenite
Quartz 10%, Plagioclase <1%, Rock Fragments 75%, Muscovite 5%, Matrix 0%, Accessory 10%
Faint bedding visible.
Degree of Rounding: rounded
Sorting: well sorted
Quartz: up to 2mm in diameter, monocrystalline
Rock Fragments: mostly felsic volcanic rocks altered to sericite and chlorite with quartz.
Accessory: opaques, carbonate, rutile, zircon

BPQ-2 Breadpan Formation
Fine to medium grained lithic wacke
Quartz 10%, Plagioclase <1%, Rock Fragments 60%, Matrix 21%, Accessory 8%
Veins of secondary chlorite and magnetite(?) cut quartz, micro faults present
Degree of Rounding: subangular to subrounded
Sorting: poorly sorted
Matrix: dominantly sericite with minor chlorite
Quartz: up to 1mm in diameter, undulatory extinction on many grains, quartz-quartz contacts are sutured, shattered grains present, some grains remain at extinction, pressure shadows present.
Plagioclase: composition (Michel-Levy) $An_{7.5}$, being replaced by quartz, carlsbad and albite twins
Rock Fragments: siltstone, granitic, volcanic, and chert. Volcanic rocks and siltstones highly altered to chlorite and sericite. Cherts are stained red.
Accessory: opaques, zircon, chlorite

FWW-2 Flying W Formation
Fine grained lithic wacke
Quartz 1%, Plagioclase 1%, Rock Fragments 71%, Matrix 10%, Accessory 17%
Degree of Rounding: subrounded to rounded
Sorting: poorly sorted
Matrix: Dominantly sericite and chlorite with minor calcite, chert and quartz.
Quartz: mostly monocrystalline - some polycrystalline, up to 0.1mm in diameter
Plagioclase: up to 0.05mm long, composition (Michel-Levy) An_{10}
Rock Fragments: volcanic, sedimentary and chert. Some

volcanic fragments are porphyritic. Faint bedding apparent in some sedimentary fragments.
Accessory: calcite, opaques (some cubic)

FWW-5 Flying W Formation
Medium to coarse grained lithic wacke
Quartz 20%, Muscovite 10%, Rock Fragments 55%, Matrix 8%, Accessory 7%
Grains appear to be flattened - especially volcanic rock fragments
Degree of Rounding: subangular to rounded
Sorting: poorly sorted
Matrix: sericite, plagioclase (>1%), chlorite
Quartz: up to 9mm long, mostly monocrystalline - some polycrystalline
Rock Fragments: chert up to 6mm long, volcanic up to 2.5mm long. Volcanic fragments are very fined grained porphyries.
Accessory: chlorite, opaques

HC-1 Houdon Formation
Conglomerate
Quartz 60%, Plagioclase 16%, Matrix 4%,
Rock Fragments 20%, Accessory <1%
Degree of Rounding: subrounded to subangular
Sorting: very poorly sorted
Matrix: subequal sericite and chlorite
Quartz: microcrystalline vein quartz, mono- and polycrystalline quartz
Plagioclase: composition (Michel-Levy) $An_{37.5}$
Rock Fragments: vein quartz, chert (red and white), granite, volcanic, and sedimentary
Accessory: opaques

REFERENCES

Alford, D.E., 1987, **Geology and Geochemistry of the Hembrillo Canyon Succession, San Andres Mountains, Sierra and Doña Ana Counties, New Mexico:** New Mexico Institute of Mining and Technology, Socorro, M.S. Thesis, 153p.

Allegre, C.J., and Minster, J.F., 1978, **Quantitave Models of Trace Element Behavior in Magmatic Processes:** Earth Planet. Sci. Lett., v. **38**, p. 1-25.

Arculus, R.J., 1987, **The Significance of Source Versus Process in the Tectonic Controls of Magma Genesis:** Jour. Volc. Geotherm. Res., v. **32**, p. 1-12.

Best, M.G., 1975, **Migration of Hydrous Fluids in the Upper Mantle and Potassium Variation in Calc-Alkalic Rocks:** Geology, v. 3, p. 429-432.

Blatt, H., Middleton, G., and Murray, R., 1972, **Origin of Sedimentary Rocks:** Englewood Cliffs, New Jersey, Prentice-Hall, Inc., 634p.

Beswick, A.E., and Soucie, G., 1978, **A Correction Procedure For Metasomatism in an Archean Greenstone Belt:** Precambrian Res., v. **6**, p. 235-248.

Bhatia, M.K., 1983, **Plate Tectonics and Geochemical Composition of Sandstones:** Jour. Geol., v. **91**, p. 611-627.

Bhatia, M.K., and Crook, K.W., 1986, **Trace Element Characteristics of Graywackes and Tectonic Setting Discrimination of Sedimentary Basins:** Contrib. Mineral. Petrol., v. **92**, p. 181-193.

Bowling, G.P., 1987, **Geology and Geochemistry of Early Prtoerozoic Supracrustal Rocks From the Western Dos Cabezas Mountains, Cochise County, Arizona:** New Mexico Institute of Mining and Technology, Socorro, M.S. Thesis, 126p.

Campbell, I.I., Lesher, C.M., Coad, P., Franklin, J.M., Gorton, M.P., and Thurston, P.C., 1984, **Rare-Earth Element Mobility in alteration Pipes Below Massive Cu-Zn-Sulfide Deposits:** Chem. Geol., v. **45**, p. 181-202.

Condie, K.C., 1982a, **Plate-tectonics Model for Proterozoic Accretion in the Southwestern United States:** Geology, v. **10**, p. 37-42.

Condie, K.C., 1982b, **Plate Tectonics and Crustal Evolution:** New York, Pergamon Press, 310p.

Condie, K.C., 1984, **Secular Variation in Basalts: An Index to Mantle Evolution:** Jour. Petr., v. 26, p. 545-563.

Condie, K.C., 1986, **Geochemistry and Tectonic Setting of Early Proterozoic Supracrustal Rocks in the Southwestern United States:** Jour. Geol., v. 94, p. 845-864.

Condie, K.C., 1988, **Proterozoic Terranes and Crustal Provinces in Southwestern North America:** Submitted to G.S.A. Bull.

Condie, K.C., and Budding, A.J., 1979, **Geology and Geomchemistry of Precambrian Rocks, Central and South-central New Mexico:** New Mexico Bureau of Mines and Mineral Resources, Memoir 35, 58p.

Condie, K.C., Bowling, G.P., and Vance, R.K., 1985, **Geochemistry and Origin of Early Proterozoic Supracrustal Rocks, Dos Cabezas Mountains, Southeastern Arizona:** G.S.A. Bull., v. 96, p. 655-662.

Condie, K.C. and DeMalas, J.P., 1985, **The Pinal Schist: An Early Proterozoic Quartz-wacke Association in Southeastern Arizona:** Precamb. Res., v.27, p. 337-356.

Conway, C.M., 1973, **Structure and Evolution of a Precambrian Rhyolite Volcanic Complex, Gila County, Arizona:** G.S.A. Abstracts With Programs, v. 5, no. 1, p. 25-26.

Conway, C.M., 1976, **Petrology, Structure, and Evolution of a Precambrian Volcanic and Plutonic Complex, Tonto Basin, Arizona:** California Institute of Technology, Pasadena, Ph.D. Dissertation, 460p.

Conway, C.M., 1985, **Geologic Map of the Hells Gate Roadless Area and Vicinity, Tonto Basin, Gila County, Arizona:** U.S. Geol. Surv. Miscellaneous Field Studies Map, MF-1644-C.

Conway, C.M., and Silver, L.T., 1976, **Rhyolite-Granophyre-Granite Complex, Tonto Basin, Arizona--A Deeply Exposed Precambrian Analog of the Yellowstone Rhyolite Plateau:** G.S.A. Abstracts With Programs, v. 8, no. 5, p 579-580.

Conway, C.M., Silver, L.T., Wrucke, C.T., and Ludwig, K.R., 1981, **Proterozoic Mazatzal Quartzite of Central Arizona:** G.S.A. Abstracts With Programs, v. 13, no. 2, p. 50.

Conway, C.M., Wrucke, C.T., Ludwig, K.R., and Silver, L.T., 1982, **Structures of the Proterozoic Mazatzal Orogeny, Arizona:** G.S.A. Abstracts With Programs, v. 14, no. 4, p. 219.

Conway, C.M., and Silver, L.T., 1984, **Extent and Implications of silicic Alkalic Magmatism and Quartz Arenite Sedimentation in the Proterozoic of Central Arizona**: G.S.A. Abstracts With Programs, v. **16**, no. **4**, p. 219.

Conway, C.M. and Silver, L.T., 1986a, **1700-1610 Ma Proterozoic Rocks in Central to Southeastern Arizona**: Ariz. Geol. Digest, (in press).

Conway, C.M., and Silver, L.T., 1986b, **Early Proterozoic Stratigraphy, Structure, and Geologic History, Tonto Basin, Arizona**: G.S.A. Bull. (in press).

Conway, C.M., Karlstrom, K.E., Silver, L.T., and Wrucke, C.T., 1987, **Tectonic and Magmatic Contrasts Across a Two-Province Boundary in Central Arizona**: Geol. Soc. Am. Field Trip Guide, Ann. Meeting, Phoenix, Arizona.

Copeland, P., 1986, **Geochemistry and Geology of the Pinal Schist, Cochise and Pima Counties Arizona**: New Mexico Institute of Mining and Technology, Socorro, M.S. Thesis, 179p.

Copeland, P., and Condie, K.C., 1986, **Geochemistry and Tectonic Setting of Lower Proterozoic Supracrustal Rocks of the Pinal Schist, Southeastern Arizona**: G.S.A. Bull., v. **97**, p. 1512-1520.

Cox, K.G., Bell, J.D., and Pankhurst, R.J., 1979, **The Interpretation of Igneous Rocks**: London, George Allen and Unwin, Ltd., 450p.

Davies, J.F., and Whitehead, R.E.S., 1979, **Further Immobile Element Data From Altered Volcanic Rocks, Timmins Minings Area, Ontario**: Can. Jour. Earth Sci,. v. **17**, p. 419-423.

Davis, A., Blackburn, W.H., Brown, W.R., and Ehmann, W.D., 1979, **Trace Element Geochemistry and Origin of Late Precambrian-Early Cambrian Catoctin Greenstones of the Appalachain Mountains**: (unpub. ms.).

Dickinson, W.R., and Suzcek, C.A., 1979, **Plate Tectonics and Sandstone Compositions**: A.A.P.G. Bull., v. **63**, p. 2164-2182.

Drury, S.A., 1983, **The Petrogenesis and Setting of Archean Metavolcanics From Karnataka State, South India**: Geochem. Cosmochem. Acta, v. **47**, p. 317-329.

Duncan, A.R., 1987, **The Karoo Igneous Province-A Problem Area For Inferring Tectonic Setting From Basalt Geochemistry**: Jour. volc. Geotherm. Res., v. **32**, p. 13-34.

Finlow-Bates, T. and Stumpfl, E.F., 1981, **The Behaviour of So-Called Immobile Elements in Hydrothermally Altered Rocks Associated With Volcanogenic Submarine-Exhalative Ore Deposits**: Mineralium Deposita, v. 16, p. 319-328.

Floyd, P.A., and Winchester, J.A., 1975, **Magma Type and Tectonic Setting Discrimination Using Immobile Elements**: Earth Planet. Sci. Lett., v. 27, p. 211-218.

Garcia, M.O., 1978, **Criteria for the Identification of Ancient Volcanic Arcs**: Earth Science Reviews, v. 14, p. 147-165.

Gastil, R.G., 1954, **Geology of the Eastern Half of the Diamond Butte Quadrangle, Gila County, Arizona**: University of California, Berkeley, Ph.D. Dissertation.

Gastil, R.G., 1958, **Older Precambrian Rocks of the Diamond Butte Quadrangle, Gila County, Arizona**: G.S.A. Bull., v. 69, p. 1495-1513.

Gibson, I.L., and Jagam, P. 1980, **Instrumental Neutron Activation Analysis of Rocks and Minerals**, in.. Muecke, G.K., ed., **Short Course in Neutron Activation Analysis in the Geosciences**: Min. Assoc. Canada, p. 109-131.

Gill, J.B., 1981, **Orogenic Andesites and Plate Tectonics**: New York, Springer-Verlag, 390p.

Gorden, G.E., Randle, K., Goles, Corliss, J., Beeson, M., and Oxley, S., 1968, **Instrumental Neutron Activation Analysis of Standard Rocks With High Resolution Gamma-ray Detectors**: Geochem. Cosmochem. Acta, v. 32, p. 369-396.

Hall, A., 1987, **Igneous Petrology**: New York, John Wiley and Sons, Inc., 573p.

Harris, N.B.W., Pearce, J.A., and Tindle, A.G., 1986, **Geochemical Characteristics of Collision-Zone Magmatism**, in Coward, M.P. and Ries, A. C., eds., **Collision Tectonics**: Oxford, Blackwell Scientific Publications, p. 67-81.

Hodder, A.P.W., 1985, **Depth of Origin of Basalts Inferred From Ti/V Ratios and a Comparison With the K_2O-Depth Relationship For Island Arc Volcanics**: Chem. Geol., v. 48, p. 3-16.

Hynes, A., 1980, **Carbonatization and Mobility of Ti, Y, and Zr in Ascot Formation Metabasalts, SE Quebec**: Contrib. Mineral. Petrol., v. 75, p. 79-87.

Jaques, A.L. and Green, D.H., 1980, **Anhydrous Melting of Peridotite at 0-15Kb Pressure and the Genesis of Tholeiitic Basalts**: Contr. Min. Petr., v. 73, p. 287-310.

Jensen, L.S., 1976, **A New Cation Plot for Classifying Subalkalic Volcanic Rocks**: Ontario Div. Mines Misc. Paper 66, 22p.

Jolly, W.T., 1975, **Subdivision of the Archean Lavas of the Abitibi Area, Canada, From Fe-Mg-Ni-Cr Relations**: Earth Planet. Sci. Lett., v. 27, p. 200-210.

Karlstrom, K.E., Bowring, S.A., and Conway, C.M., 1987, **Early Proterozoic Two Province Boundary in Central Arizona**: G.S.A. Bull., v. 99, p. 529-538.

Karlstrom, K.E., and O'Hara, P.F., 1984, **Polyphase Folding in Proterozoic Rocks of Central Arizona**: G.S.A. Abstracts With Programs, v. 16, p. 226.

Karlstrom, K.E., and Puls, D.D., 1984, **Geometry of Structures in a Proterozoic Thrust Belt, Mazatzal Mountains, Central Arizona**: G.S.A. Abstracts With Programs, v. 16, p. 554.

Karlstrom, K.E., and Conway, C.M., 1986, **Deformational Styles and Contrasting Lithostratigraphic Sequences Within An Early Proterozoic Orogenic Belt, Central Arizona**, in.. Nations, J.D., Conway, C.M., and Gordon, A.S., eds., **Geology of Central and Northern Arizona**: Geology Dept. Northern Arizona University, Flagstaff, Arizona, 176p.

Karlstrom, K.E., and Bowring, S.A., 1988, **Early Proterozoic Assembly of Tectonostratigraphic Terranes in Southwestern North America**: Jour. Geol., v. 96, p. 561-576.

Knoper, M.W., and Condie, K.C., 1987, **Geochemistry and Petrogenesis of Early Proterozoic Amphibolites West-Central Colorado, U.S.A.**: Chem. Geol., v. 67, p. 209-225.

Knoper, M.W., 1988, **MODULUS: An Igneous Geochemical Spreadsheet Modeling Program Using Lotus**: (ms. in prep.).

Langmuir, C.H., Vocke, Jr., R.D., Hanson, G.N., and Harty, S.R., 1978, **A General Mixing Equation With Applications to Icelandic Basalts**: Earth Planet. Sci. Lett., v. 37, p. 380-392.

Levin, R.I., and Rubin, D.S., 1980, **Applied Elementary Statistics**: Englewood Cliffs, Prentics-Hall, Inc., 322p.

Lindstrom, K.J., and Korotev, R.L., 1982, **TEABAGS: Computer Programs For Instrumental Neutron Activation Analysis**: Jour. Radioanalytical Chem., v. 70, no. 1-2, p. 439-458.

Ludden, J., Gélinas, L., and Trudel, P., 1982, **Archean Metavolcanics From the Rouyn-Noranda District, Abitibi Greenstone Belt, Quebec .2. Mobility of Trace Elements and Petrogenetic Constraints**: Can. Jour. Earth Sci., v. **19**, p. 2276-2287.

Ludwig, K.R., 1973, **Precambrian Geology of the Central Mazatzal Mountains, Arizona**: California Institute of Technology, Pasadena, Ph.D. Dissertation, Part I, 218p.

MacDonald, G.A., 1972, **Volcanoes**: Englewood Cliffs, New Jersey, Prentice-Hall, Inc. 510p.

Marsh, J.S., 1987, **Basalt Geochemistry and Tectonic Discrimination Within Continental Flood Basalt Provinces**: Jour. Volc. Geotherm. Res., v. **32**, p. 35-49.

Meschede, M., 1986, **A Method of Discriminating Between Different Types of Mid-Ocean Ridge Basalts and Continental Tholeiites With the Nb-Zr-Y Diagram**: Chem. Geol., v. **56**, p. 207-218.

Miyashiro, A., 1974, **Classification, Characteristics, and Origin of Ophiolites**: Jour. Geol., v. **83**, p. 249-281.

Moore, J.G., 1975, **Mechanism of Formation of Pillow Lava**: Amer. Sci., v. **63**, p. 269-277.

Mullen, E.D., 1983, **Mno-TiO_2-P_2O_5: A Minor Element Discriminant for Basaltic Rocks of Oceanic Environments and Its Implications for Petrogenesis**: Earth Planet. Sci. Lett., v. **62**, p. 53-62.

Mysen, B.O. and Kushiro, I., 1977, **Compositional Variations of Coexisting Phases With Degree of Melting of Peridotite in the Upper Mantle**: Amer. Min., v. **62**, p. 843-865.

Norrish, K., and Hutton, J.T., 1969, **An Accurate X-ray Spectographic Method for the Analysis of a Wide Range of Geological Samples**: Geochem. Cosmochem. Acta, v. **33**, p. 431-435.

Norrish, K., and Chappel, B.W., 1977, **X-ray Fluoresence**, in.. Zussman, J., ed., **Physical Methods in Determinitive Mineralogy**: Academic Press, p. 235-262.

O'Hara, M.J., 1977, **Geochemical Evolution During Fractional Crystallization of a Periodaclly Refilled Magma Chamber**: Nature, v. **265**, p. 503-507.

O'Hara, P.F., 1980, **Metamorphic and Structural Geology of the Northern Bardshaw Mountains, Yavapai County, Arizona**: Arizona State University, Tempe, Ph.D. Dissertation, 117p.

Pearce, J.A., 1982, **Trace Element Characteristics of Lavas From Destructive Plate Boundaries**, in.. Thorpe, R.S., ed., **Andesites:** New York, Wiley, p. 527-547.

Pearce, J.A., 1983, **Role of the Subcontinental Lithosphere in Magma Genesis at Active Continental Margins**, in.. Hawkesworth, C.J., and Norry, M. J., eds., **Continental Basalts and Mantle Xenoliths:** Cheshire, U.K., Shiva Press, Ltd., p. 230-249.

Pearce, J.A., 1985, **Characteristics and Tectonic Significance of Supra-Subduction Zone Ophiolites**, in.. Hawkesworth, C.J., and Norry, M.J., eds., **Marginal Basin Geology:** Palo Alto, Blackwell, p. 77-94.

Pearce, J.A., and Cann, J.R., 1973, **Tectonic Setting of Basic Volcanic Rocks Using Trace-Element Analysis:** Earth Planet. Sci. Lett., v. **19**, p. 290-300.

Pearce, J.A., and Norry, M.J., 1979, **Petrogenetic Implications of Ti, Zr, Y, and Nb Variations in Volcanic Rocks:** Contr. Mineral. Petrol, v. **69**, p. 33-47.

Pearce, J.A., Harris, N.B.W., and Tindle, A.G., 1984, **Trace Element Discrimination Diagrams for the Tectonic Interpretations of Granitic Rocks:** Jour. Petrol, v. **25**, p. 956-983.

Pearce, T.H., Gorman, B.E., and Birkett, T.C., 1975, **The TiO_2-K_2O-P_2O_5 Diagram; A Method of Discrimination Between Oceanic and Non-Oceanic Basalts:** Earth Planet. Sci. Lett., v. **24**, p. 419-426.

Pharoah, T.C., and Pearce, J.A., 1984, **Geochemical Evidence for the Geotrectonic Settig of Early Proterozoic Metavolcanic Sequences in Lapland:** Precamb. Res., v. **25**, p. 283-308.

Puls, D.D., and Karlstrom, K.E., 1985, **Proterozoic Foreland Thrusting in the Central Mazatzal Mountains in Central Arizona:** G.S.A. Abstracts With Programs, v. **17**, p. 261.

Puls, D.D., and Karlstrom, K.E., 1986, **Proposed Names for Major Thrusts in the Northern Mazatzal Mountains, Central Arizona:** G.S.A. Abstracts With Programs, v. **18**, p. 404.

Reed, J.R., Noll, Jr., P.D., and Condie, K.C., 1987, **Geochemistry and Tectonic Setting of 1700Ma Supracrustal Rocks From Central Arizona:** G.S.A. Abstracts With Programs, v. **19**, p. 533.

Reed, J.R., 1988, **Geology and Geochemistry of the Proterozoic Age Alder Group, Central Mazatzal Mountains, Arizona:** New Mexico Institute of Mining and Technology, Socorro, M.S. Thesis, 191p.

Roller, J.A. and Karlstrom, K.E., 1986, **Structural Geometry of the Upper Alder Group, Mazatzal Mountains, Central Arizona**: G.S.A. Abstracts With Programs, v. 18, no. 5, p. 407.

Roser, B.P., and Korsch, R.J., 1986, **Determination of Tectonic Setting of Sandstone-Mud Suites Using SiO_2 Content and K_2O/Na_2O Ratio**: Jour. Geol., v. 94, p. 635-650.

Saunders, A.D., Tarney, J., and Weaver, S.D., 1980, **Transverse Geochemical Variations Across the Antarctic Peninsula: Implications for the Genesis of Calc-alkaline Magmas:** Earth Planet. Sci. Lett., v.46, p. 344-360.

Tarney, J., Saunders, A.D., Wood, D.A., and Marsh, N.G., 1981, **Geochemical Aspects of Back-Arc Spreading in the Scotia Sea and Western Pacific**: Philos. Trans. R. Soc. London, Sec. A, v. 300, p. 263-285.

Taylor, S.R., and McLennan, S.M., 1985, **The Continental Crust: It's Composition and Evolution**: London, Blackwell Scientific Publications, 312p.

Trevena, A.S., 1979, **Studies in Sandstone Petrology: Origin of the Precambrian Mazatzal Quartzite and Provenance of Detrital Feldspar**: University of Utah, Salt Lake City, Ph.D. Dissertation, 360p.

Trevena, A.S., 1981, **Origin of the Precambrian Mazatzal Quartzite and Related Strata, Central Arizona**: G.S.A. Abstracts With Programs, v. 13, p. 111.

Vance, R.K., 1988, **Geochemistry and Tectonic Setting of the Yavapai Supergroup, West Central Arizona**: New Mexico Institute of Mining and Technology, Socorro, Ph.D. Dissertation.

Vance, R.K., and Condie, K.C., 1987, **Geochemistry of Footwall Alteration Associated With the Early Proterozoic United Verde Massive Sulfide Deposit, Jerome Arizona**: Econ. Geol., v. 82, p. 571-586.

Weaver, B.L, andd Tarney, J., 1984, **Emperical Approach to Estimating the Composition of the Continental Crust**: Nature, v. 310, p. 575-577.

Williams, H. and McBirney, A.R., 1979, **Volcanology**: San Francisco, Freeman, Cooper, and Co., 397p.

Wilson, E.D., 1922, **Proterozoic Mazatzal Quartzite of Central Arizona**: Pan American Geologist, v. 38, p. 299-312.

Winchester, J.A., and Floyd, P.A., 1977, **Geochemical Discrimination of Different Magma Series and Their Differentiation Products Using Immobile Elements:** Chem. Geol., v. 20, p. 325-343.

Wood, D.A., 1979, **A Variably Veined Suboceanic Upper Mantle-Genetic Significance for Mid-Ocean Ridge Basalts From Geochemical Evidence:** Geology v. 7, p. 499-503.

Wood, D.A., 1980, **The Application of the Th-Hf-Ta Diagram to Problems of Tectonomagmatic Classification and to Establishing the Nature of Crustal Contamination of Basaltic Lavas of the British Tertiary Volcanic Province:** Earth Planet, Sci. Lett., v. 50, p. 11-30.

Wood, D.A., Joron, J.L., and Freuil, M., 1979, **A Re-Appraisal of the Use of Trace Elements to Classify and Discriminate Between Magma Series Erupted in Different Tectonic Settings:** Earth Planet. Sci. Lett., v. 45, p. 326-336.

Wronkiewicz, D.J. and Condie, K.C., 1987, **Geochemistry of Archean Shales From the Witwatersrand Supergroup, South Africa: Source-area Weathering and Provenance:** Geochem. Cosmochem. Acta, v.51, p. 2401-2416.

APPENDIX C: CHEMICAL DATA FOR SEDIMENTARY ROCKS

Table C-1
Chemical Compositions of Sedimentary Rocks

CARBONATES	PRE-ALDER	PRE-ALDER
SAMPLE	PALS-1	PALS-3
SiO2	17.03	20.68
TiO2	0.08	0.23
Al2O3	2.64	4.86
Fe2O3-T	1.37	2.25
MgO	3.50	15.26
CaO	41.55	21.60
Na2O	1.84	1.38
K2O	0.12	1.83
MnO	0.22	0.98
P2O5	0.04	0.10
LOI	35.72	33.61
TOTAL	104.10	103.36
Rb	3	22
Ba	28	105
Cs	0	0
Sr	224	21
Pb	25	8
Th	0.6	2.0
U	0.3	0.7
Sc	3	4
V	13	19
Cr	6	42
Co	4	8
Ni	6	11
Y	8	15
Zr	29	53
Nb	6	6
Hf	0.5	1.3
Ta	0.1	0.2
La	5	9
Ce	11.4	20.5
Sm	1.4	3.3
Eu	0.4	0.7
Tb	0.3	0.5
Yb	0.5	1.1
Lu	0.07	0.16
CIA	3.2	9.8
Fe2O3+MgO	4.9	17.5
SiO2/Al2O3	6.5	4.3
Al2O3/SiO2	0.2	0.2
K2O/Na2O	0.1	0.9
CaO/(CaO+Na2O)	1.0	0.9

Table C-1 (continued)
Chemical Compositions of Sedimentary Rocks

$Al_2O_3/(Na_2O+CaO)$	0.1	0.2
$K_2O/(K_2O+Na_2O)$	0.1	0.5
(La/Sm)n	2.3	1.6
(Tb/Yb)n	2.2	1.9
(La/Yb)n	6.5	5.3
Lu/Hf	0.2	0.1
Zr/Hf	60.6	40.7
Th/U	2.2	3.0
K/Rb	363	683
Rb/Sr	.0	1.0
Ba/Rb	10.1	4.7
Ba/Sr	0.1	4.9
Th/Sc	0.2	0.5
La/Sc	1.8	1.9
Zr/Y	3.4	3.5
Ti/Zr	16.1	26.0
Zr/Nb	5.2	9.0
La/Yb	3.9	8.0
La/Th	7.9	4.3
Ni/Co	1.3	1.4
Cr/V	0.5	2.3
V/Ni	2.3	1.7
Cr/Zr	0.2	0.8
Eu/Eu*	0.8	0.6

MAZ.DAT

Table C-1 (continued)
Chemical Compositions of Sedimentary Rocks

all are

PELITES	PRE-ALDER PELITE	PRE-ALDER PELITE	ALDER PELITE	ALDER PELITE	ALDER PELITE
SAMPLE	PAS-2	PAS-3	BPQS-1	BPQS-2	BPQS-3
SiO2	61.20	64.70	77.91	78.45	72.89
TiO2	1.00	0.70	0.74	0.77	0.63
Al2O3	18.45	16.99	9.77	9.77	12.89
Fe2O3-T	8.98	7.73	5.53	5.52	5.57
MgO	1.65	1.31	0.00	0.70	1.04
CaO	0.26	0.82	0.06	0.05	0.26
Na2O	1.72	3.18	0.00	0.41	1.15
K2O	3.28	2.92	3.38	3.40	3.89
MnO	0.03	0.18	0.02	0.03	0.03
P2O5	0.15	0.14	0.05	0.05	0.20
LOI	3.07	3.49	1.53	1.43	1.91
Al/Ti	18.5	24	13.2	12.7	20.5
TOTAL	99.78	102.14	98.99	100.59	100.44
Rb	135	102	118	169	193
Ba	520	890	417	606	638
Cs	14	13	13	16	20
Sr	132	178	27	14	34
Pb	21	22	15	16	6
Th	7.8	7.0	4.9	16.2	10.0
U	2.4	2.7	2.2	5.0	2.7
Sc	25	20	6	10	13
V	130	85	53	0	78
Cr	116	48	83	270	79
Co	22	18	14	7	5
Ni	54	23	53	46	15
Y	39	31	23	38	30
Zr	180	171	116	473 ?	178
Nb	13	12	8	13	12
Hf	5.3	4.4	4.0	17.6	5.2
Ta	0.7	0.7	0.5	1.0	1.1
C/W	86	73	100	93	87
La	30	29	20	36	30
Ce	66.6	63.5	46.8	86.2	65.2
Sm	6.9	6.0	4.0	6.5	5.4
Eu	1.6	1.3	0.9	1.2	1.3
Tb	1.3	1.0	0.7	1.1	0.7
Yb	3.7	3.6	2.0	3.8	2.9
Lu	0.56	0.56	0.30	0.59	0.44
CIA	72.9 74	63.2 64	72.2 73	68.7 69	66.3 68
Fe2O3+MgO	10.6	9.0	5.5	6.2	6.6
SiO2/Al2O3	3.3	3.8	8.0	8.0	5.7
Al2O3/SiO2	0.3	0.3	0.1	0.1	0.2
K2O/Na2O	1.9	0.9	ERR	8.3	3.4
CaO/(CaO+Na2O)	0.1	0.2	1.0	0.1	0.2
~ Cr/Th	15	6.9	17	17	7.9

Table C-1 (continued)
Chemical Compositions of Sedimentary Rocks

Al2O3/(Na2O+CaO)	9.3	4.2	162.8	21.0	9.2
K2O/(K2O+Na2O)	0.7	0.5	1.0	0.9	0.8
(La/Sm)n	2.6	3.0	3.0	3.4	3.3
(Tb/Yb)n	1.5	1.2	1.4	1.2	1.0
(La/Yb)n	5.4	5.4	6.7	6.4	6.8
Lu/Hf	0.1	0.1	0.1	.0	0.1
Zr/Hf	34.0	38.9	28.3	26.9	34.2
Th/U	3.2	2.6	2.3	3.2	3.7
K/Rb	201	238	238	167	167
Rb/Sr	1.0	0.6	4.3	11.7	5.7
Ba/Rb	3.8	8.8	3.5	3.6	3.3
Ba/Sr	4.0	5.0	15.2	42.2	18.8
Th/Sc	0.3	0.3	0.8	1.7	0.8
La/Sc	1.2	1.5	3.1	3.7	2.2
Zr/Y	4.7	5.6	5.1	14.2	6.0
Ti/Zr	33.2	24.5	38.4	9.8	21.2
Zr/Nb	13.8	14.0	15.3	36.4	15.0
La/Yb	8.1	8.2	10.1	9.6	10.3
La/Th	3.8	4.2	4.1	2.2	3.0
Ni/Co	2.5	1.3	3.7	6.4	3.0
Cr/V	0.9	0.6	1.6	ERR	1.0
V/Ni	2.4	3.6	1.0	0.0	5.3
Cr/Zr	0.6	0.3	0.7	0.6	0.4
Eu/Eu*	0.7	0.6	0.7	0.6	0.8
	0.67	0.65	0.66	0.52	0.76
Co/Th	2.8	2.6	2.1	.44	1.5

Table C-1 (continued)
Chemical Compositions of Sedimentary Rocks

PELITES	ALDER PELITE	ALDER PELITE	ALDER PELITE	ALDER PELITE	ALDER PELITE
SAMPLE	BPQS-4	BPQS-5	BPQS-7	BPS-6	FWS-1
SiO2	61.53	59.85	62.93	82.77	52.74
TiO2	0.61	0.66	0.77	0.50	2.03
Al2O3	19.59	19.17	17.36	8.72	20.35
Fe2O3-T	6.85	7.78	7.82	3.49	12.76
MgO	1.33	2.31	1.16	0.01	1.09
CaO	0.17	0.25	0.22	0.12	0.83
Na2O	1.40	2.52	4.15	0.03	1.00
K2O	5.29	4.24	0.20	2.57	5.50
MnO	0.04	0.07	0.05	0.02	0.04
P2O5	0.12	0.13	0.10	0.05	0.53
LOI	3.13	3.40	2.72	1.30	2.98
TOTAL	100.05	100.37	97.46	99.58	99.85
Rb	251	479	23	141	296
Ba	667	556	88	393	1473
Cs	22	170	10	14	49
Sr	93	140	443	24	91
Pb	19	17	14	18	14
Th	10.4	11.1	11.9	8.4	8.6
U	3.5	3.2	4.1	2.8	3.5
Sc	20	18	16	5	28
V	119	112	105	73	1979
Cr	39	93	124	242	20
Co	11	18	24	3	14
Ni	28	45	51	33	22
Y	26	32	27	25	61
Zr	138	173	222	279	357
Nb	13	14	14	9	26
Hf	3.9	4.6	7.5	9.2	9.4
Ta	1.1	0.9	1.0	0.6	1.3
La	35	33	46	19	57
Ce	75.6	71.6	87.7	42.6	118.3
Sm	6.3	6.6	6.9	3.4	12.4
Eu	1.6	1.5	1.3	0.6	3.4
Tb	0.7	1.0	0.8	0.6	2.1
Yb	2.8	3.2	3.2	2.2	5.7
Lu	0.41	0.46	0.51	0.35	0.83
CIA	70.1	67.6	70.0	74.1	69.1
Fe2O3+MgO	8.2	10.1	9.0	3.5	13.9
SiO2/Al2O3	3.1	3.1	3.6	9.5	2.6
Al2O3/SiO2	0.3	0.3	0.3	0.1	0.4
K2O/Na2O	3.8	1.7	.0	85.7	5.5
CaO/(CaO+Na2O)	0.1	0.1	.0	0.8	0.5

Table C-1 (continued)
Chemical Compositions of Sedimentary Rocks

Al2O3/(Na2O+CaO)	12.5	6.9	4.0	58.1	11.1
K2O/(K2O+Na2O)	0.8	0.6	.0	1.0	0.8
(La/Sm)n	3.4	3.0	4.0	3.4	2.8
(Tb/Yb)n	1.1	1.3	1.1	1.1	1.5
(La/Yb)n	8.2	6.8	9.3	5.7	6.6
Lu/Hf	0.1	0.1	0.1	.0	0.1
Zr/Hf	35.2	37.6	29.5	30.3	38.0
Th/U	3.0	3.5	2.8	2.9	2.5
K/Rb	175	73	73	151	154
Rb/Sr	2.7	3.4	0.1	5.9	3.2
Ba/Rb	2.7	1.2	3.9	2.8	5.0
Ba/Sr	7.2	4.0	0.2	16.5	16.2
Th/Sc	0.5	0.6	0.8	1.5	0.3
La/Sc	1.8	1.8	2.9	3.5	2.0
Zr/Y	5.2	5.4	8.1	11.2	5.8
Ti/Zr	26.5	23.1	20.7	10.8	34.0
Zr/Nb	10.9	12.8	15.4	29.4	13.7
La/Yb	12.5	10.3	14.1	8.7	10.0
La/Th	3.4	2.9	3.8	2.3	6.7
Ni/Co	2.5	2.5	2.1	12.3	1.5
Cr/V	0.3	0.8	1.2	3.3	.0
V/Ni	4.2	2.5	2.1	2.2	89.2
Cr/Zr	0.3	0.5	0.6	0.9	0.1
Eu/Eu*	0.8	0.7	0.6	0.6	0.8

Table C-1 (continued)
Chemical Compositions of Sedimentary Rocks

PELITES	ALDER PELITE	ALDER PELITE	ALDER PELITE	ALDER PELITE	ALDER PELITE
SAMPLE	FWS-3	FWS-4	FWS-5	FWS-6	HM-1
SiO2	66.13	75.04	74.23	67.80	40.38
TiO2	0.64	0.16	0.11	0.62	1.25
Al2O3	15.94	13.39	14.18	14.32	15.52
Fe2O3-T	6.67	1.91	1.45	6.74	10.37
MgO	2.27	2.55	1.67	2.08	5.01
CaO	0.21	0.17	0.31	0.56	7.81
Na2O	1.32	1.51	0.80	1.30	0.00
K2O	4.67	3.30	4.05	4.19	4.59
MnO	0.06	0.06	0.04	0.10	0.19
P2O5	0.14	0.05	0.20	0.15	0.20
LOI	2.78	2.89	2.65	2.22	14.21
TOTAL	100.89	101.02	99.68	100.63	99.53
Rb	144	87	100	132	289
Ba	1287	886	963	1032	518
Cs	10	8	9	15	18
Sr	77	56	58	82	224
Pb	10	7	6	13	12
Th	8.5	9.2	8.7	7.5	0.4
U	2.6	3.3	4.4	2.0	0.2
Sc	16	3	3	15	28
V	66	13	8	58	259
Cr	73	14	6	166	98
Co	17	4	2	13	46
Ni	35	12	8	145	136
Y	29	12	17	20	28
Zr	181	91	79	164	85
Nb	13	9	11	11	3
Hf	5.3	3.0	2.9	5.2	2.4
Ta	0.9	0.8	1.2	0.7	0.1
La	45.5*	23	19	36	8.
Ce	79.4	48.6	36.0	71.1	19.2
Sm	4.8	3.0	2.7	6.1	3.5
Eu	1.1	0.7	0.8	1.3	1.3
Tb	0.8	0.4	0.4	0.8	0.7
Yb	3.3	1.0	1.4	2.2	2.3
Lu	0.50	0.17	0.20	0.34	0.30
CIA	67.7	67.8	69.3	62.3	44.7
Fe2O3+MgO	8.9	4.5	3.1	8.8	15.4
SiO2/Al2O3	4.2	5.6	5.2	4.7	2.6
Al2O3/SiO2	0.2	0.2	0.2	0.2	0.4
K2O/Na2O	3.5	2.2	5.0	2.2	ERR
CaO/(CaO+Na2O)	0.1	0.1	0.3	0.2	1.0

Table C-1 (continued)
Chemical Compositions of Sedimentary Rocks

Al2O3/(Na2O+CaO)	10.4	8.0	12.7	5.8	2.0
K2O/(K2O+Na2O)	0.8	0.7	0.8	0.7	1.0
(La/Sm)n	0.0	4.7	4.1	3.6	1.3
(Tb/Yb)n	1.0	1.7	1.2	1.6	1.3
(La/Yb)n	0.0	14.9	8.8	11.0	2.2
Lu/Hf	0.1	0.1	0.1	0.1	0.1
Zr/Hf	34.2	29.9	27.0	31.7	36.2
Th/U	3.3	2.8	2.0	3.9	1.8
K/Rb	269	313	385	263	132
Rb/Sr	1.9	1.6	1.7	1.6	1.3
Ba/Rb	8.9	10.1	9.6	7.8	1.8
Ba/Sr	16.8	15.7	16.3	12.6	2.3
Th/Sc	0.5	3.0	3.0	0.5	.0
La/Sc	0.0	7.6	6.4	2.4	0.3
Zr/Y	6.3	7.4	4.8	8.3	3.1
Ti/Zr	21.4	10.5	8.3	22.8	87.6
Zr/Nb	13.6	10.5	6.8	15.4	24.7
La/Yb	0.0	22.5	13.3	16.6	3.4
La/Th	0.0	2.6	2.1	4.8	18.4
Ni/Co	2.1	3.4	4.4	11.2	3.0
Cr/V	1.1	1.1	0.7	2.8	0.4
V/Ni	1.9	1.1	1.0	0.4	1.9
Cr/Zr	0.4	0.2	0.1	1.0	1.1
Eu/Eu*	0.7	0.7	0.8	0.7	1.0

Table C-1 (continued)
Chemical Compositions of Sedimentary Rocks

PELITES	ALDER PELITE	ALDER PELITE	ALDER PELITE	ALDER PELITE	ALDER PELITE
SAMPLE	HM-3	HM-5	HM-7	HM-9	BCS-1
SiO2	60.96	68.75	61.40	62.11	68.46
TiO2	0.66	0.91	0.86	0.78	0.72
Al2O3	20.70	17.17	19.10	18.84	18.87
Fe2O3-T	7.37	9.00	8.64	7.84	6.25
MgO	0.54	1.56	1.46	2.42	1.57
CaO	0.21	0.26	0.22	0.45	0.38
Na2O	1.17	1.19	1.23	2.03	0.67
K2O	3.74	4.13	4.93	3.51	5.50
MnO	0.06	0.08	0.05	0.14	0.04
P2O5	0.10	0.12	0.15	0.15	0.19
LOI	3.65	2.57	2.83	3.47	3.30
TOTAL	99.16	100.73	100.85	101.80	100.89
Rb	176	163	202	175	186
Ba	717	576	632	710	1425
Cs	12	17	23	12	12
Sr	143	218	239	143	92
Pb	26	18	21	18	16
Th	10.8	8.7	11.1	12.7	13.0
U	3.7	3.4	4.3	4.6	2.7
Sc	20	21	23	20	22
V	110	115	191	111	106
Cr	89	87	115	87	90
Co	18	15	11	21	10
Ni	42	37	30	42	31
Y	37	39	52	39	44
Zr	166	210	213	131	208
Nb	13	18	18	15	15
Hf	4.9	6.3	7.0	5.9	5.9
Ta	0.9	1.2	1.2	1.1	1.0
La	41	32	42	50	41
Ce	97.4	70.8	90.7	105.0	78.8
Sm	7.7	6.7	8.5	9.3	7.1
Eu	1.4	1.4	2.0	1.8	1.3
Tb	1.1	1.1	1.7	1.3	1.3
Yb	3.6	3.9	5.1	3.8	4.0
Lu	0.54	0.64	0.79	0.53	0.65
CIA	76.5	71.3	71.1	70.0	71.1
Fe2O3+MgO	7.9	10.6	10.1	10.3	7.8
SiO2/Al2O3	2.9	3.7	3.2	3.3	3.4
Al2O3/SiO2	0.3	0.3	0.3	0.3	0.3
K2O/Na2O	3.2	3.5	4.0	1.7	8.2
CaO/(CaO+Na2O)	0.2	0.2	0.2	0.2	0.3

Table C-1 (continued)
Chemical Compositions of Sedimentary Rocks

Al2O3/(Na2O+CaO)	15.0	11.9	13.1	7.4	18.8
K2O/(K2O+Na2O)	0.8	0.8	0.8	0.6	0.9
(La/Sm)n	3.2	2.9	3.0	3.3	3.5
(Tb/Yb)n	1.4	1.2	1.4	1.5	1.4
(La/Yb)n	7.5	5.5	5.5	8.9	6.9
Lu/Hf	0.1	0.1	0.1	0.1	0.1
Zr/Hf	33.8	33.5	30.5	32.5	35.5
Th/U	2.9	2.5	2.3	2.8	4.8
K/Rb	176	210	202	167	246
Rb/Sr	1.2	0.7	0.8	1.2	2.0
Ba/Rb	4.1	3.5	3.1	4.1	7.7
Ba/Sr	5.0	2.6	2.6	5.0	15.4
Th/Sc	0.5	0.4	0.5	0.6	0.6
La/Sc	2.0	1.6	1.8	2.5	1.9
Zr/Y	4.5	5.3	4.1	4.9	4.8
Ti/Zr	23.9	25.9	24.3	24.5	20.8
Zr/Nb	12.6	11.4	11.9	12.5	14.3
La/Yb	11.4	8.3	8.3	13.4	10.5
La/Th	3.8	3.7	3.8	4.0	3.2
Ni/Co	2.3	2.4	2.9	2.0	3.3
Cr/V	0.8	0.8	0.6	0.9	0.9
V/Ni	2.6	3.1	6.3	2.7	3.4
Cr/Zr	0.5	0.4	0.5	0.5	0.4
Eu/Eu*	0.5	0.6	0.7	0.6	0.5

Table C-1 (continued)
Chemical Compositions of Sedimentary Rocks

PELITES	ALDER PELITE	ALDER PELITE
SAMPLE	BCSH-1	BCSH-3
SiO2	84.87	61.69
TiO2	0.28	0.94
Al2O3	8.30	16.45
Fe2O3-T	3.56	8.22
MgO	0.61	2.69
CaO	0.11	1.89
Na2O	0.78	2.31
K2O	2.31	4.08
MnO	0.03	0.09
P2O5	0.08	0.16
LOI	1.37	3.42
TOTAL	102.29	101.94
Rb	103	136
Ba	331	937
Cs	10	13
Sr	25	251
Pb	5	10
Th	5.3	9.8
U	0.8	3.7
Sc	9	16
V	33	197
Cr	21	88
Co	2	23
Ni	8	50
Y	20	29
Zr	97	239
Nb	8	14
Hf	2.9	7.2
Ta	0.5	0.8
La	12	52
Ce	25.3	103.1
Sm	2.8	7.7
Eu	0.9	1.7
Tb	0.5	1.0
Yb	2.2	2.8
Lu	0.35	0.45
CIA	67.6	58.5
Fe2O3+MgO	4.2	10.9
SiO2/Al2O3	10.2	3.7
Al2O3/SiO2	0.1	0.3
K2O/Na2O	3.0	1.8
CaO/(CaO+Na2O)	0.1	0.4

Table C-1 (continued)
Chemical Compositions of Sedimentary Rocks

Al2O3/(Na2O+CaO)	9.4	3.9
K2O/(K2O+Na2O)	0.7	0.6
(La/Sm)n	2.6	4.1
(Tb/Yb)n	1.1	1.5
(La/Yb)n	3.6	12.0
Lu/Hf	0.1	0.1
Zr/Hf	33.3	33.0
Th/U	7.1	2.7
K/Rb	186	249
Rb/Sr	4.2	0.5
Ba/Rb	3.2	6.9
Ba/Sr	13.3	3.7
Th/Sc	0.6	0.6
La/Sc	1.3	3.2
Zr/Y	5.0	8.1
Ti/Zr	17.0	23.5
Zr/Nb	12.5	16.7
La/Yb	5.4	18.2
La/Th	2.2	5.2
Ni/Co	4.3	2.2
Cr/V	0.6	0.4
V/Ni	4.4	3.9
Cr/Zr	0.2	0.4
Eu/Eu*	0.9	0.7

Qtz arenite = Q
Qtz wacke = QW
Graywacke = G

Table C-1 (continued)
Chemical Compositions of Sedimentary Rocks

Sandstones	ALDER	ALDER	ALDER	ALDER	ALDER
SAMPLE	BPW-1	BPW-2	BPW-3	BPW-4	BPW-5
	G	G	QW	QW	Qtz arenite
SiO2	59.36	59.93	79.68	79.97	86.44
TiO2	0.78	0.83	0.66	0.67	0.27
Al2O3	14.67	16.06	7.95	8.33	6.09
Fe2O3-T	7.47	7.37	5.36	5.15	3.60
MgO	3.38	2.41	1.74	1.57	1.15
CaO	6.26	3.88	0.25	0.22	0.08
Na2O	3.06	4.25	2.37	2.34	1.78
K2O	1.06	2.45	0.84	1.13	1.05
MnO	0.13	0.10	0.10	0.09	0.06
P2O5	0.90 ?	0.59	0.12	0.11	0.05
LOI	2.65	2.42	1.44	1.62	1.22
TOTAL	99.72	100.29	100.52	101.19	101.79
Rb	47	105	59	67	81
Ba	613	981	213	307	221
Cs	30	10	13	11	11
Sr	1195	760	122	105	51
Pb	25	20	9	9	4
Th	8.8	9.3	11.2	8.7	4.6
U	8.6	4.6	2.9	3.0	1.6
Sc	16	14	7	8	5
V	115	109	86	92	58
Cr	178	130	98	102	96
Co	20	25	11	12	9
Ni	89	74	36	29	30
Y	19	24	22	20	14
Zr	225	223	272	218	108
Nb	12	15	9	9	4
Hf	5.0	5.1	8.8	8.7	3.9
Ta	0.6	0.7	0.9	0.7	0.3
La	66	65	30	29	23
Ce	146.8	144.7	69.1	65.9	43.5
Sm	12.1	11.7	5.5	5.4	3.1
Eu	3.0	3.0	1.3	1.1	0.6
Tb	1.2	1.1	0.7	0.9	0.4
Yb	1.4	1.7	2.4	2.6	1.5
Lu	0.23	0.24	0.37	0.39	0.24
CIA	45.5	49.0	60.2	60.3	59.1
Fe2O3+MgO	10.9	9.8	7.1	6.7	4.8
SiO2/Al2O3	4.0	3.7	10.0	9.6	14.2
Al2O3/SiO2	0.2	0.3	0.1	0.1	0.1
K2O/Na2O	0.3	0.6	0.4	0.5	0.6
CaO/(CaO+Na2O)	0.7	0.5	0.1	0.1	.0
Al2O3/(Na2O+CaO)	1.6	2.0	3.0	3.3	3.3

Table C-1 (continued)
Chemical Compositions of Sedimentary Rocks

K2O/(K2O+Na2O)	0.3	0.4	0.3	0.3	0.4
(La/Sm)n	3.3	3.4	3.4	3.3	4.5
(Tb/Yb)n	3.6	2.8	1.3	1.5	1.1
(La/Yb)n	32.3	25.9	8.3	7.4	9.8
Lu/Hf	.0	.0	.0	.0	0.1
Zr/Hf	45.1	43.7	31.0	25.2	28.1
Th/U	1.0	2.0	3.9	2.9	2.9
K/Rb	189	194	118	140	108
Rb/Sr	.0	0.1	0.5	0.6	1.6
Ba/Rb	13.2	9.4	3.6	4.6	2.7
Ba/Sr	0.5	1.3	1.7	2.9	4.4
Th/Sc	0.6	0.7	1.5	1.1	0.8
La/Sc	4.1	4.7	4.0	3.6	4.2
Zr/Y	11.7	9.5	12.1	10.7	7.8
Ti/Zr	20.8	22.3	14.5	18.5	14.7
Zr/Nb	19.1	15.2	29.3	23.5	26.3
La/Yb	49.0	39.2	12.5	11.3	14.8
La/Th	7.5	7.0	2.7	3.3	4.3
Ni/Co	4.4	3.0	3.1	2.4	3.2
Cr/V	1.5	1.2	1.1	1.1	1.7
V/Ni	1.3	1.5	2.4	3.1	1.9
Cr/Zr	0.8	0.6	0.4	0.5	0.9
Eu/Eu*	0.8	0.9	0.8	0.6	0.6

Table C-1 (continued)
Chemical Compositions of Sedimentary Rocks

Sandstones SAMPLE	ALDER BPC-5	ALDER BPC-6	ALDER BPA-1	ALDER BPA-2	ALDER FWG-1
SiO2	67.80	72.89	74.71	63.71	84.32
TiO2	0.70	0.70	0.60	0.82	0.37
Al2O3	14.88	12.06	10.78	16.78	7.28
Fe2O3-T	5.80	5.53	5.12	7.79	3.82
MgO	2.36	2.26	2.11	2.58	1.16
CaO	0.21	0.49	0.20	0.38	0.11
Na2O	1.21	1.77	1.23	2.66	0.86
K2O	5.48	4.13	3.67	3.11	1.92
MnO	0.06	0.06	0.04	0.09	0.03
P2O5	0.13	0.12	0.10	0.16	0.06
LOI	2.29	1.96	1.92	3.18	1.39
TOTAL	100.69	101.98	100.52	101.26	101.28
Rb	173	116	103	182	56
Ba	841	567	592	768	487
Cs	18	16	15	17	6
Sr	37	63	35	191	28
Pb	6	8	5	10	2
Th	10.7	12.4	10.5	7.2	5.3
U	3.1	3.9	2.4	1.9	1.5
Sc	14	11	8	21	6
V	88	86	110	117	101
Cr	83	93	84	124	40
Co	16	13	7	30	6
Ni	41	34	25	78	20
Y	23	27	27	46	14
Zr	196	311	164	213	95
Nb	14	11	10	14	5
Hf	5.9	10.2	4.8	6.3	3.1
Ta	1.0	0.8	1.0	0.9	0.4
La	25	25	23	49	29.4*
Ce	63.8	61.1	46.6	103.4	54.7
Sm	4.9	5.4	4.6	10.2	2.9
Eu	1.0	1.2	1.3	3.0	0.7
Tb	0.7	0.9	0.6	1.3	0.5
Yb	2.9	2.9	2.7	5.4	1.7
Lu	0.43	0.46	0.38	0.77	0.26
CIA	64.2	59.3	62.6	66.5	66.1
Fe2O3+MgO	8.2	7.8	7.2	10.4	5.0
SiO2/Al2O3	4.6	6.0	6.9	3.8	11.7
Al2O3/SiO2	0.2	0.2	0.1	0.3	0.1
K2O/Na2O	4.5	2.3	2.9	1.2	2.2
CaO/(CaO+Na2O)	0.1	0.2	0.1	0.1	0.1
Al2O3/(Na2O+CaO)	10.5	5.3	7.3	5.5	7.4

Table C-1 (continued)
Chemical Compositions of Sedimentary Rocks

K2O/(K2O+Na2O)	0.8	0.7	0.7	0.5	0.7
(La/Sm)n	3.1	2.8	3.0	2.9	0.0
(Tb/Yb)n	1.1	1.3	0.9	1.0	1.1
(La/Yb)n	5.7	5.7	5.5	6.1	0.0
Lu/Hf	0.1	.0	0.1	0.1	0.1
Zr/Hf	33.2	30.6	34.3	33.6	30.5
Th/U	3.5	3.2	4.3	3.8	3.6
K/Rb	254	296	294	196	287
Rb/Sr	4.9	1.8	2.9	0.7	2.0
Ba/Rb	4.7	4.9	5.7	5.8	8.8
Ba/Sr	23.0	9.0	16.8	4.0	17.7
Th/Sc	0.8	1.2	1.2	0.3	0.7
La/Sc	1.8	2.3	2.7	2.4	0.0
Zr/Y	6.8	11.5	6.1	4.6	7.0
Ti/Zr	21.3	13.4	21.8	23.0	23.1
Zr/Nb	14.4	27.5	16.7	15.6	19.3
La/Yb	8.6	8.6	8.3	9.2	0.0
La/Th	2.3	2.0	2.1	6.9	0.0
Ni/Co	2.6	2.6	3.5	2.6	3.4
Cr/V	0.9	1.1	0.8	1.1	0.4
V/Ni	2.1	2.5	4.4	1.5	4.9
Cr/Zr	0.4	0.3	0.5	0.6	0.4
Eu/Eu*	0.6	0.6	0.9	0.3	0.7

Table C-1 (continued)
Chemical Compositions of Sedimentary Rocks

Sandstones SAMPLE	ALDER FWW-1	ALDER FWW-2	ALDER FWW-3	ALDER FWW-4	ALDER FWW-5
SiO2	52.36	64.35	70.19	59.64	67.91
TiO2	1.81	0.67	0.49	0.99	0.60
Al2O3	19.78	14.75	11.58	17.29	13.29
Fe2O3-T	12.99	7.15	6.74	8.49	6.81
MgO	1.84	3.45	2.93	3.21	2.38
CaO	1.98	3.49	4.55	4.54	3.26
Na2O	1.83	3.22	1.51	3.55	2.71
K2O	4.30	2.46	1.91	3.49	2.74
MnO	0.08	0.15	0.19	0.16	0.13
P2O5	0.35	0.24	0.13	0.33	0.17
LOI	3.22	1.05	1.65	0.78	1.33
TOTAL	100.54	100.98	101.86	102.45	101.34
Rb	321	78	67	115	91
Ba	1235	540	576	1080	843
Cs	47	10	10	12	10
Sr	118	413	293	428	294
Pb	18	23	12	23	17
Th	8.6	5.3	6.0	6.5	6.0
U	6.3	2.3	2.5	2.8	2.0
Sc	25	14	8	18	12
V	127	121	78	131	95
Cr	12	164	27	71	48
Co	31	28	14	23	18
Ni	20	109	27	55	39
Y	69	18	36	28	31
Zr	354	152	187	215	173
Nb	26	9	11	12	9
Hf	10.3	4.0	5.7	5.7	4.8
Ta	1.6	0.5	0.7	0.6	0.5
La	65	29	34	39	35
Ce	128.7	65.8	81.9	88.7	76.7
Sm	14.5	5.3	8.4	7.7	7.2
Eu	3.8	1.4	1.6	1.9	1.7
Tb	2.7	0.6	1.1	0.9	1.0
Yb	6.7	1.6	3.3	2.4	2.7
Lu	0.99	0.24	0.51	0.37	0.44
CIA	66.0	50.8	47.4	49.2	49.9
Fe2O3+MgO	14.8	10.6	9.7	11.7	9.2
SiO2/Al2O3	2.6	4.4	6.1	3.5	5.1
Al2O3/SiO2	0.4	0.2	0.2	0.3	0.2
K2O/Na2O	2.3	0.8	1.3	1.0	1.0
CaO/(CaO+Na2O)	0.4	0.5	0.8	0.6	0.5
Al2O3/(Na2O+CaO)	6.2	2.2	1.9	2.1	2.2

Table C-1 (continued)
Chemical Compositions of Sedimentary Rocks

K2O/(K2O+Na2O)	0.7	0.4	0.6	0.5	0.5
(La/Sm)n	2.7	3.3	2.5	3.1	2.9
(Tb/Yb)n	1.7	1.7	1.5	1.6	1.6
(La/Yb)n	6.4	11.6	6.8	10.6	8.6
Lu/Hf	0.1	0.1	0.1	0.1	0.1
Zr/Hf	34.4	37.7	32.9	37.7	35.9
Th/U	1.4	2.3	2.5	2.4	3.0
K/Rb	111	262	236	252	250
Rb/Sr	2.7	0.2	0.2	0.3	0.3
Ba/Rb	3.8	6.9	8.6	9.4	9.3
Ba/Sr	10.4	1.3	2.0	2.5	2.9
Th/Sc	0.3	0.4	0.7	0.4	0.5
La/Sc	2.6	2.0	4.1	2.2	2.9
Zr/Y	5.1	8.3	5.2	7.8	5.5
Ti/Zr	30.6	26.3	15.7	27.4	20.8
Zr/Nb	13.9	17.1	17.3	17.6	19.0
La/Yb	9.7	17.6	10.3	16.0	13.0
La/Th	7.6	5.4	5.7	6.0	5.8
Ni/Co	0.6	4.0	1.9	2.3	2.1
Cr/V	0.1	1.4	0.8	0.5	0.5
V/Ni	6.4	1.1	2.9	2.4	2.4
Cr/Zr	.0	1.1	0.1	0.3	0.3
Eu/Eu*	0.8	0.8	0.6	0.8	0.7

Table C-1 (continued)
Chemical Compositions of Sedimentary Rocks

Sandstones SAMPLE	ALDER FWN-6	ALDER FWCM-1	ALDER HL-1	ALDER HL-2	ALDER H-3
SiO2	60.64	64.87	90.58	85.04	84.68
TiO2	0.79	1.25	0.16	0.47	0.23
Al2O3	16.02	16.11	3.95	7.16	7.01
Fe2O3-T	7.81	8.02	0.55	4.35	2.43
MgO	4.46	0.96	0.65	0.78	1.71
CaO	5.23	0.72	0.01	0.18	1.47
Na2O	3.70	2.13	0.65	1.20	1.68
K2O	2.05	3.38	1.35	0.92	1.77
MnO	0.22	0.10	0.02	0.03	0.03
P2O5	0.25	0.37	0.02	0.06	0.06
LOI	1.11	2.40	0.31	1.26	1.24
TOTAL	102.27	100.31	98.88	101.40	102.30
Rb	69	139	31	26	105
Ba	820	1509	100	536	366
Cs	8	19	1	5	15
Sr	457	93	12	55	67
Pb	14	14	1	7	8
Th	5.9	8.8	2.0	5.4	5.9
U	2.4	3.8	0.4	2.8	2.1
Sc	18	14	1	6	4
V	118	94	9	90	44
Cr	185	25	23	72	30
Co	28	16	0	3	3
Ni	114	16	1	21	9
Y	20	53	1	30	15
Zr	178	238	91	138	114
Nb	9	22	2	8	5
Hf	4.7	7.0	3.5	4.6	3.6
Ta	0.5	1.3	0.3	0.5	0.4
La	30	59	1	25	24
Ce	67.1	120.3	2.3	50.2	53.2
Sm	6.2	11.7	0.3	5.3	4.1
Eu	1.5	2.8	0.1	1.2	0.8
Tb	0.7	1.8	0.1	0.8	0.5
Yb	1.7	4.7	0.4	2.7	1.7
Lu	0.27	0.69	0.07	0.43	0.25
CIA	47.3	65.5	55.3	69.2	48.8
Fe2O3+MgO	12.3	9.0	1.2	5.1	4.1
SiO2/Al2O3	3.8	4.0	22.9	11.8	12.1
Al2O3/SiO2	0.3	0.2	.0	0.1	0.1
K2O/Na2O	0.6	1.6	3.0	0.8	1.1
CaO/(CaO+Na2O)	0.6	0.3	.0	0.1	0.5
Al2O3/(Na2O+CaO)	1.8	5.7	6.0	5.4	2.2

Table C-1 (continued)
Chemical Compositions of Sedimentary Rocks

K2O/(K2O+Na2O)	0.4	0.6	0.7	0.4	0.5
(La/Sm)n	2.9	3.1	2.9	2.9	3.6
(Tb/Yb)n	1.8	1.6	0.7	1.3	1.4
(La/Yb)n	11.5	8.3	2.3	6.2	9.6
Lu/Hf	0.1	0.1	.0	0.1	0.1
Zr/Hf	37.7	42.6	26.3	29.2	31.9
Th/U	2.5	2.3	5.2	1.9	2.9
K/Rb	248	201	517	291	140
Rb/Sr	0.1	1.5	2.7	0.5	1.6
Ba/Rb	12.0	10.8	3.2	20.5	3.5
Ba/Sr	1.8	16.3	8.6	9.7	5.4
Th/Sc	0.3	0.6	1.7	0.9	1.5
La/Sc	1.6	4.3	1.0	4.1	6.3
Zr/Y	8.8	5.6	71.8	4.5	7.5
Ti/Zr	26.7	25.1	10.2	21.0	12.1
Zr/Nb	19.1	13.5	43.0	17.6	21.4
La/Yb	17.5	12.6	3.5	9.3	14.6
La/Th	5.1	6.7	0.6	4.7	4.1
Ni/Co	4.1	1.0	ERR	8.2	2.8
Cr/V	1.6	0.3	2.6	0.8	0.7
V/Ni	1.0	5.8	7.6	4.4	5.1
Cr/Zr	1.0	0.1	0.3	0.5	0.3
Eu/Eu*	0.8	0.7	1.2	0.7	0.6

Table C-1 (continued)
Chemical Compositions of Sedimentary Rocks

Sandstones	ALDER	ALDER	ALDER	ALDER
SAMPLE	BCSS-1	BCSS-2	BCC-1	BCW-3
SiO2	82.32	84.08	55.93	61.87
TiO2	0.30	0.26	0.94	0.80
Al2O3	7.60	7.00	19.11	16.04
Fe2O3-T	3.52	2.70	8.24	7.31
MgO	0.44	1.38	1.62	3.44
CaO	0.75	1.15	3.25	4.76
Na2O	2.19	1.07	1.10	4.31
K2O	1.47	1.55	3.22	1.09
MnO	0.06	0.06	0.10	0.11
P2O5	0.08	0.08	0.26	0.40
LOI	1.34	1.74	5.40	2.21
TOTAL	100.05	101.00	99.17	102.32
Rb	58	46	120	28
Ba	408	588	820	634
Cs	4	4	11	5
Sr	59	64	335	808
Pb	7	3	10	14
Th	6.2	7.7	4.5	5.4
U	2.1	1.7	1.2	2.2
Sc	7	5	18	16
V	40	34	124	112
Cr	53	17	89	53
Co	5	9	21	23
Ni	18	16	46	48
Y	34	12	19	19
Zr	164	83	128	157
Nb	8	5	8	9
Hf	5.7	2.2	2.9	3.7
Ta	0.6	0.3	0.5	0.5
La	28	26	29	45
Ce	65.2	52.9	57.0	93.4
Sm	6.3	4.8	5.3	7.3
Eu	1.3	1.2	1.4	1.9
Tb	1.0	0.6	0.5	0.7
Yb	3.4	1.4	1.8	1.6
Lu	0.55	0.21	0.25	0.24
CIA	53.7	55.9	63.0	48.7
Fe2O3+MgO	4.0	4.0	9.9	10.7
SiO2/Al2O3	10.8	12.0	2.9	3.9
Al2O3/SiO2	0.1	0.1	0.3	0.3
K2O/Na2O	0.7	1.4	2.9	0.3
CaO/(CaO+Na2O)	0.3	0.5	0.7	0.5
Al2O3/(Na2O+CaO)	2.6	3.2	4.4	1.8

Table C-1 (continued)
Chemical Compositions of Sedimentary Rocks

K2O/(K2O+Na2O)	0.4	0.6	0.7	0.2
(La/Sm)n	2.7	3.3	3.3	3.7
(Tb/Yb)n	1.2	1.8	1.2	1.8
(La/Yb)n	5.4	12.5	10.6	18.0
Lu/Hf	0.1	0.1	0.1	0.1
Zr/Hf	28.8	38.0	44.0	41.9
Th/U	2.9	4.5	3.7	2.4
K/Rb	211	277	224	319
Rb/Sr	1.0	0.7	0.4	.0
Ba/Rb	7.1	12.7	6.9	22.6
Ba/Sr	6.9	9.2	2.4	0.8
Th/Sc	0.9	1.6	0.2	0.3
La/Sc	3.9	5.3	1.6	2.9
Zr/Y	4.9	6.8	6.9	8.3
Ti/Zr	10.9	18.7	44.1	30.7
Zr/Nb	20.0	18.3	15.8	16.9
La/Yb	8.2	18.9	16.0	27.3
La/Th	4.5	3.4	6.3	8.3
Ni/Co	3.6	1.7	2.2	2.1
Cr/V	1.3	0.5	0.3	0.5
V/Ni	2.2	2.2	2.7	2.3
Cr/Zr	0.3	0.2	0.3	0.3
Eu/Eu*	0.6	0.8	0.9	0.9

Major elements in weight percent.
Trace elements in parts per million.
Fe_2O_{3T}: Total Fe as Fe_2O_{3T}.
LOI: Loss on Ignition.
CIA: Chemical Index of alteration
ERR: no value for calculation or division by zero for ratio calculation.
Blank: Not determined.
#: Interpolated from Ce on REE plot.